ROLE OF REDOX SYSTEMS IN DOXORUBICIN METABOLISM AND DOXORUBICIN-MEDIATED CELL SIGNALING: A COMPUTATIONAL ANALYSIS

A Dissertation
Presented to
The Academic Faculty

by

Nnenna Adimora Finn

In Partial Fulfillment
of the Requirements for the Degree
Doctor of Philosophy in Biomedical Engineering

Georgia Institute of Technology
August, 2011

ROLE OF REDOX SYSTEMS IN DOXORUBICIN METABOLISM AND DOXORUBICIN-MEDIATED CELL SIGNALING: A COMPUTATIONAL ANALYSIS

Approved by:

Dr. Melissa L. Kemp, Advisor
Dept of Biomedical Engineering
Georgia Institute of Technology
Emory University

Dr. Dean P. Jones
School of Medicine
Emory University

Dr. Michael E. Davis
Dept of Biomedical Engineering
Georgia Institute of Technology
Emory University

Dr. Eberhard O. Voit
Dept of Biomedical Engineering
Georgia Institute of Technology
Emory University

Dr. Harry W. Findley
School of Medicine
Emory University

Date Approved: June 3 2011

To the Mystery that knew me before I ever was…
To my beautiful husband
To my family

ACKNOWLEDGEMENTS

I would like to thank my advisor, Dr. Melissa L. Kemp, for her guidance, for her support, for her eagerness, and most especially for her patience. I would like to thank all my committee members for their expertise and encouragement. I would like to thank the members of the Kemp lab, past and present, for their camaraderie. I would like to acknowledge the Facilitating Academic Careers in Engineering and Science (FACES), Georgia Tech – Emory Center (GTEC) for Regenerative Medicine, Ford Foundation, and National Science Foundation Fellowship Programs for the funding of this degree.

TABLE OF CONTENTS

LIST OF TABLES

LIST OF FIGURES

NOMENCLATURE

ALL	Acute lymphoblastic leukemia
ATP	Adenosine triphosphate
Cys	Cysteine
CPR	Cytochrome P450 reductase
DHEA	Dehydroepiandrosterone
Dox	Dox
EU1-Res	Dox-resistant ALL cell
EU3-Sens	Dox-sensitive ALL cell
G6PD	Glucose-6-phosphate dehydrogenase
Grx	Glutaredoxin
GSH/GSSG	Glutathione/ glutathione disulfide
GPx	Glutathione peroxidase
GR	Glutathione reductase
$GS^{\bullet}$	Glutathione thiyl radical
H_2O_2	Hydrogen peroxide
$HO_2^{\bullet}$	Hydroperoxyl radical
$OH^{\bullet}$	Hydroxyl radical
HOCl	Hypochlorous acid
IκB / IκB-α	Inhibitor of NF-κB
IKK	Inhibitory κB kinase
IDH	Isocitrate dehydrogenase
NAC	N-acetylcysteine
$NADPH/NADP^+$	Nicotinamide adenine dinucleotide phosphate

NO	Nitric oxide
NOX	NADPH oxidase
NF-κB	Nuclear factor kappa B
$O_2^{\bullet-}$	Superoxide
ODE	Ordinary differential equation
Pgp	P-glycoprotein/MDR1
Prx	Peroxiredoxin
QM / QMB	Quinone methide
Redox	Reduction/oxidation
$RO_2^{\bullet}$	Peroxyl radical
ROS	Reactive oxygen species
$RS^{\bullet}$	Protein thiyl radical
R-SH / Pr-SH	Protein monothiol
$R-(SH)_2$ / $P-(SH)_2$	Protein dithiol
R-SSG / Pr-SSG	S-glutathionylated protein
R-SS-R / Pr-SS-Pr	Protein disulfide
SeOH	Selenic acid
SG	Side group
SOD	Superoxide dismutase
TR	Thioredoxin reductase
Trx	Thioredoxin
XO	Xanthine oxidase

SUMMARY

Insensitivity to chemotherapy is an ongoing issue in cancer treatment, one that appears to be highly dependent on patient-specific variations. It has been shown clinically that while a subset of patients will successfully respond to a particular chemotherapeutic regimen, there exists another subset of patients who when exposed to the same course of therapy will remain resistant to treatment or exhibit signs of relapse after treatment has been administered. This discrepancy raises interesting questions regarding the role that patient-specific variations play in controlling the efficacy of chemotherapy treatment regimens.

Doxorubicin (Dox) is a common chemotherapeutic agent used in the treatment of a variety of solid tumors and leukemias. Even after the extensive and long-standing clinical utilization of Dox, a consensus on the drug's method of action has yet to be reached, thereby suggesting that multiple mechanisms of action may in fact be at work. The diversity of Dox's method(s) of action becomes all the more pertinent considering that resistance to Dox treatment is a major issue in cancer chemotherapy, oftentimes leading to patient relapse. To gain a deeper understanding of the processes that influence Dox resistance, therefore, we must first understand the mechanisms that underlie and contribute to Dox's toxicity. To this end, the metabolic reactions that activate Dox have been implicated as major determinants of Dox cytoxicity and as possible factors that control Dox resistance in cancer cells.

There are several lines of evidence that redox-dependent metabolism plays a large role in Dox toxicity. The Dox bioactivation network is comprised of a system of reduction/oxidation (redox) reactions that lead to the formation of toxic Dox metabolites

and reactive oxygen species (ROS). Moreover, multi-drug resistant acute lymphoblastic leukemia cells derived from relapsed patients have elevated levels of the antioxidant glutathione and show insensitivity to Dox treatment. The redox dependence of Dox bioactivation, the understanding that Dox treatment generates ROS, and the evidence that Dox resistant cells exhibit increased antioxidant capacity, suggest the possibility that redox pathways modulate the efficacy of Dox treatment in cancer cells. The overall objectives of the proposed dissertation, therefore, were to investigate how the redox properties of the Dox bioactivation network influence Dox toxicity in acute lymphoblastic leukemia cells, and to provide evidence that cell-specific variations in the intracellular levels of these redox components influences the degree to which Dox treatment will induce cancer cell death.

The central hypothesis of this dissertation is that the Dox bioactivation network is regulated by intracellular levels of antioxidant components and metabolites that work collectively to generate toxic Dox metabolites or to generate intracellular oxidant signals. More specifically, it is hypothesized that while the generation of toxic Dox metabolites will ultimately promote Dox-induced cell death, the generation of intracellular oxidant signals can either promote cell death or cell viability, depending on the intracellular context in which the oxidant signals are generated. To test this hypothesis, a three step approach was utilized. First, a computational network model of cytosolic Dox bioactivation was developed based upon patient-derived cell line differences in metabolic enzyme levels. Second, a systems-based model of intracellular ROS consumption in lymphocytes was constructed. Third, the consequence of Dox-induced ROS on the

potentially oncogenic nuclear factor kappa B (NF-κB) signal transduction pathway was analyzed.

The significant findings of this study are that the redox reactions involved in Dox metabolism are dual-natured, containing a toxicity-generating module characterized by nicotinamide adenine dinucleotide phosphate (NADPH)-dependent Dox reductive conversion, as well as an ROS signal-generating module characterized by NADPH- and oxygen-dependent Dox redox cycling. This study reveals that balance between the coupled redox reactions that comprise the toxicity- and ROS signal-generating modules of Dox bioactivation determines the sensitivity-phenotype of leukemia cells. This study provides evidence that phenotypic changes in the Dox-sensitivity of leukemia cells can be induced by the successful modulation of the Dox bioactivation network through the pharmacological inhibition of NADPH in a concentration- and cell type-dependent manner.

In addition, this study highlights the importance of the intracellular redox network in controlling chemotherapy-induced ROS. The unequal distribution in antioxidant burden across the various intracellular antioxidant enzymes suggests a significant role for NADPH supply, as controlled by the enzyme glucose-6-phosphate dehydrogenase (G6PD), to the intracellular ROS buffering capacity of cells during instances of oxidative stress. Changes in G6PD activity were shown to promote protein-S-glutathionylation during oxidative stress conditions, thereby implicating G6PD in the modulation of redox-sensitive signal transduction pathways.

Furthermore, this study reveals that intracellular glutathione redox balance, a measure of the intracellular redox environment, can effectively regulate Dox-induced

NF-κB signal transduction in leukemia cells. The systematic modulation of intracellular glutathione redox balance in leukemia cells by N-acetylcysteine (NAC) revealed an important role for protein S-glutathionylation mechanisms in the control of NF-κB signal transduction induced by Dox treatment. These findings identify the glutathione redox network as a potential therapeutic target for the systematic modulation of Dox sensitivity in cancer cells and elucidate the complex role that antioxidants such as NAC can play in modulating the effectiveness of Dox chemotherapy treatment regimens.

Lastly, this study highlights the need for and the capacity of computational models to accurately describe the complex redox-reactions that contribute to Dox metabolism in leukemia cells. This study is groundbreaking in its use of computational modeling to analyze reversible electron transfer events between proteins using mass-action kinetics. The models developed in this study can accurately explain cytosolic doxorubicin bioactivation, intracellular hydrogen peroxide clearance, and kinase-specific S-glutathionylation, thereby showing that the use of comprehensive and/or relatively simple computational models can provide semi-quantitative predictions about the behavior of redox systems in mammalian cells as they relate to Dox-induced toxicity and Dox-induced cell signaling.

CHAPTER 1

INTRODUCTION

Dox, a chemotherapeutic anthracycline, is a well-known cytotoxic drug used in the treatment of a variety of solid tumors, leukemias, and lymphomas (Gewirtz, 1999). While Dox remains one of the most effective drugs to date for treating cancer, there is still some controversy surrounding its mechanism(s) of action (Asmis et al, 2005; Gewirtz, 1999; Gilleron et al, 2009; Kostrzewa-Nowak et al, 2005). Some studies suggest that Dox exerts its toxic effects via its ability to interfere with the biosynthesis of macromolecules, e.g. DNA (Calendi et al, 1965; Di Marco et al, 1965; Supino et al, 1977; Zunino et al, 1972). However, these effects only seem to be evident at high concentrations of Dox. Other studies implicate a major role for free radical generation. However, because most of these experiments were carried out in cell free systems using supraclinical drug concentrations, some level of doubt regarding the importance of free radical generation in Dox-induced toxicity still exists (Bates & Winterbourn, 1982; Eliot et al, 1984; Gutteridge & Quinlan, 1985; Muindi et al, 1984). Other proposed mechanisms for Dox-induced toxicity include DNA adduct formation and DNA crosslinking (Cullinane & Phillips, 1990; Cummings et al, 1991; Sinha & Chignell, 1979; Sinha et al, 1984), interference with DNA strand separation during replication (Bachur et al, 1992; Fornari et al, 1994; Montecucco et al, 1988), and interference with topoisomerase II (Tewey et al, 1984a; Tewey et al, 1984b). The lack of understanding regarding the way in which Dox exerts its antitumor effects is all the more concerning considering that Dox resistance in cancer cells is still an ongoing issue (Akman et al, 1990; Bao et al, 2011; Doroshow et al, 1991; Kievit et al, 2011). Dox resistance in cancer cells has been correlated with a number of different phenomena ranging from aberrant phosphatase activity (Grunwald et al, 2002) and expression of oncogenic proteins like

MDM2 (Gu et al, 2002), to alterations in normal cell signaling (Zhou et al, 2003b) and cell cycle progression (Wang et al, 1999). Although the underlying mechanism of Dox resistance is not fully understood, researchers have determined several factors that influence Dox cytotoxicity, most notably the expression of membrane transporters P-glycoprotein/MDR1 (Pgp) (Dhooge et al, 1999; Fisher & Sikic, 1995; Kostrzewa-Nowak et al, 2005; Ross, 2000) and the generation of ROS and free radicals via Dox redox cycling (Gewirtz, 1999). Because the modulation of Pgp activity *in vivo* (Dhooge et al, 1999; Ross, 2000) and the use of antioxidants (Berggren et al, 2001a; Wang et al, 2004) have failed to demonstrate any long term disease-free survival, alternative mechanisms have been proposed to describe the antitumor effects of Dox and thereby offer plausible explanations for why some cancers are sensitive to Dox treatment while others are not.

Dox Bioactivation and Drug Sensitivity

The reductive conversion of Dox has been implicated as a major determinant of Dox cytotoxicity and has been proposed as an underlying factor controlling drug resistance in cancer cells (Akman et al, 1990; Kostrzewa-Nowak et al, 2005b; Sinha & Chignell, 1979). Reductive conversion of Dox is characterized by the one-electron reduction of the quinone moiety of Dox, via NADPH and cytochrome P450 reductase (CPR), into a semiquinone radical (Kostrzewa-Nowak et al, 2005b; Menna et al, 2007). Once the semiquinone radical has been generated, it can exert direct toxic effects or be oxidized back to the quinone form (i.e. redox cycling) (Ramji et al, 2003). The combination of reductive conversion and redox cycling occurs simultaneously in mammalian cells; this overall process is termed bioactivation. It has been reported that the ability of Dox to undergo reductive conversion is dependent on the availability of molecular oxygen and NADPH, and the activities of several intracellular enzymes such as superoxide dismutase (SOD), glutathione peroxidases (GPx), NADPH oxidases (NOXs), and thioredoxin (Trx) (Akman et al, 1990; Doroshow et al, 1991; Gilleron et al,

2009; Kostrzewa-Nowak et al, 2005), components whose intracellular concentrations and activities may vary from one cancer type to the next, or from patient to patient. This variation may help explain some of the contradictory evidence in the literature that describes the proper intracellular environment or intervention strategy for effectively controlling Dox toxicity *in vivo* (Akman et al, 1990; Berggren et al, 2001a; Ramji et al, 2003). For example, Dox-resistant MCF-7 breast cancer cells showed little change in SOD activity compared to their Dox-sensitive counterparts (Akman et al, 1990); however, in another study Dox-sensitive MCF cells were rescued via the introduction of SOD (Doroshow et al, 1991). Furthermore, despite the central role of CPR in the bioactivation process, the importance of this enzyme in modulating Dox toxicity has been called into question. It is widely accepted that CPR is the primary enzyme for catalyzing the reductive conversion of Dox *in vivo* (Bartoszek, 2002), yet overexpression of CPR does not result in enhanced Dox cytotoxicity (Ramji et al, 2003).

Dox Bioactivation and the Intracellular Redox Environment

Because the overall network structure for cytosolic Dox bioactivation is believed to be conserved across different cell types (Bachur et al, 1979; Cummings et al, 1992; Sinha et al, 1989a), the contradictory behavior described above is most likely the result of differences in the intracellular levels of redox network components (both metabolites and proteins) between cells. *In vitro* studies carried out by Kostrzewa-Nowak et al. support this hypothesis by showing that changes in NADPH concentration and SOD activity had a direct impact on degree of Dox reductive conversion (Kostrzewa-Nowak et al, 2005). This dependence of the drug on [NADPH] becomes very important in light of recent findings that frequently-occurring somatic mutations in gliomas and leukemias can result in a directional change from NADPH production to NADPH consumption by isocitrate dehydrogenases (IDH1/2) resulting in lower intracellular NADPH levels (Dang et al, 2009; Ward et al, 2010). Additionally, several lines of evidence in the literature have

pointed to the involvement of NOX activity in Dox treatment (Gilleron et al, 2009a), providing added relevance to the intracellular levels of NADPH in Dox bioactivation. Thus, the redox context-dependence of Dox metabolism becomes central to accounting for patient variability to anthracycline regimens. Contradictory observations regarding the redox-mediated reactions involved in conferring Dox potency highlight the need for a more in-depth quantitative examination of how the behavior of the Dox bioactivation network is influenced by the initial levels of its system components, its component interactions, and the intracellular redox environment in which the network operates.

Dox-Induced ROS and Signal Transduction

Reactive oxygen species are of great interest to researchers because they are readily diffusible (Antunes & Cadenas, 2000) and can act as signaling molecules due to their second messenger properties (Rhee, 2006). Because the metabolism of Dox results in the generation of ROS such as superoxide ($O_2^{\bullet -}$) and hydrogen peroxide (H_2O_2), Dox treatment has the potential to affect redox-sensitive intracellular signaling networks. One such redox-sensitive signaling network is that which controls the activation of the NF-κB transcription factor. NF-κB is a transcription factor that is known to play a regulatory role in cellular processes such as growth and proliferation (Bharti & Aggarwal, 2002). This ability of NF-κB to regulate cell growth and proliferation becomes all the more important when viewed in the context of cancer biology. Cancer is a hyper-proliferative disorder (Bharti & Aggarwal, 2002) and many malignancies are characterized by abnormalities and irregularities in NF-κB activation (Dolcet et al, 2005). NF-κB is a well-known redox-sensitive protein and the NF-κB pathway is comprised of many redox sensitive steps (Hayashi et al, 1993; Herscovitch et al, 2008; Kamata et al, 2002; Matthews et al, 1992; Oliveira-Marques et al, 2009; Reynaert et al, 2006; Toledano & Leonard, 1991). For this reason, Dox-induced ROS has the potential to regulate NF-κB signal transduction in

cancer cells, and subsequently, NF-κB-dependent transcription of genes that control cell survival.

Research Objectives and Specific Aims

The redox dependence of Dox bioactivation, the ability of Dox to generate ROS, and the ability of ROS to modulate signal transduction, provide substantial evidence to the possibility that redox pathways modulate the efficacy of Dox treatment in cancer cells. **The overall objective of this research, therefore, was to investigate how the redox properties of the Dox bioactivation network influence Dox toxicity in acute lymphoblastic leukemia cells through the generation of toxic Dox metabolites and the induction of ROS**. The *central hypothesis* behind this dissertation was that the Dox bioactivation pathway is regulated by intracellular levels of antioxidant components and metabolites that work collectively to generate toxic Dox metabolites or to generate intracellular ROS signals. More specifically, there was an interest in determining the molecular conditions that would lead to the preferential formation of toxic Dox metabolites at the expense of ROS generation, thereby promoting Dox-induced cell death. Lastly, because ROS can potentially affect redox-sensitive signaling pathways that regulate cell proliferation and growth, it was hypothesized that Dox-induced ROS could either promote cell death or cell viability, depending on the intracellular redox context in which the ROS signals are generated. To test these hypotheses, a three step approach was utilized:

Specific Aim 1: Develop a systems-based model of intracellular Dox bioactivation to examine the role of redox reactions in controlling the formation of toxic Dox metabolites and Dox-induced ROS. The *working rationale* for this aim was that intracellular levels of redox proteins and metabolites control the extent to which Dox reductive conversion occurs in a cancer cell, and ultimately, the sensitivity of the cancer

cell to Dox treatment. An *in vitro* computational model of cytosolic Dox bioactivation was developed and validated with previously determined experimental data of *in vitro* Dox bioactivation (Kostrzewa-Nowak et al, 2005). Previous research had identified most of the components that comprise the Dox bioactivation network; however, adaptation of the network to changes in Dox treatment or to patient-specific changes in network components is much less understood. To investigate the *in vivo* control properties of the coupled redox reactions that comprise the Dox bioactivation network, the metabolic differences between two patient-derived acute lymphoblastic leukemia (ALL) cell lines exhibiting varied Dox sensitivities were analyzed. Cell line-specific computational models were developed and validated to predict Dox bioactivation in the ALL cell lines at different Dox concentrations. Pharmacological inhibitors were administered, simultaneously with Dox, to tease out the rate-limiting properties of the oxygen-dependent redox cycling and NADPH-dependent reductive conversion of Dox. Using these methods, the intracellular conditions necessary to promote Dox reductive conversion or Dox-induced ROS formation in ALL cells were determined.

Specific Aim 2: Develop a comprehensive network model of cellular ROS buffering to predict changes to the intracellular redox environment that occur as a result of oxidative stress. The *working rationale* for this aim was that intracellular levels of redox enzymes control the homeostatic redox potential of the glutathione and thioredoxin redox couples in a manner that affects the overall ROS buffering capacity of individual cells. To elucidate the mechanism by which mammalian cells control intracellular H_2O_2 accumulation during periods of H_2O_2-induced oxidative stress, a computational model was generated. This quantitative model integrated all pertinent components of cellular redox buffering during transient oxidative stress; the model took into account not only the key components of the intracellular redox buffering system, but also the hierarchical interdependence of each component on the other. The network

model incorporated the activity of intracellular protein thiols in ROS buffering and highlighted the importance of protein disulfide formation and protein S-glutathionylation in the cell's ability to cope with transient and sustained conditions of oxidative stress. The use of computational modeling to study peroxide buffering allowed for a detailed investigation of the molecular dynamics of a cell undergoing oxidative stress, one that has not yet been established experimentally.

Specific Aim 3: Characterize the importance of the intracellular redox environment in controlling the degree to which Dox-induced ROS modulates a redox-sensitive signal transduction pathway. The *working hypothesis* for this aim was that the intracellular redox environment, as defined by the intracellular level of the major antioxidant glutathione (GSH), determines the ability of Dox-induced ROS to modulate a redox-sensitive signal transduction pathway. NF-κB is a transcription factor believed to be a key regulator of the initiation and progression of many human cancers (Dolcet et al, 2005). A specific look at the effect of Dox-induced ROS on the NF-κB signal transduction pathway was conducted and the role of the glutathione/glutathione disulfide (GSH/GSSG) redox balance in controlling Dox-induced NF-κB activity in ALL cells was investigated. The examination of Dox-induced NF-κB activation between two ALL cell lines with dissimilar antioxidant capacities, and the use of the antioxidant N-acetylcysteine (NAC) to systematically alter intracellular GSH/GSSG redox potential during Dox treatment, clearly illustrated how intracellular glutathione redox balance can regulate Dox-induced NF-κB signal transduction to potentiate the sensitivity of ALL cells to Dox treatment.

CHAPTER 2

RESEARCH SIGNIFICANCE

In the United States, acute lymphoblastic leukemia (ALL) is the most common form of cancer among children (Bleyer, 1990). While the incidence of childhood leukemia has increased over the past 20 years, the survival rate for children diagnosed with this disease is very promising and resides at approximately 70% (Bleyer, 1990). There are many reasons for this high survival rate but the use of risk-adapted therapy to tailor the intensity of treatment to each patient's risk of relapse is being heralded as the basis for this success (Yeoh et al, 2002). Although the survival rate of childhood leukemia is high, the highly refractory nature of this cancer should not be overlooked (Kearns et al, 2001; Yeoh et al, 2002). Patients who, for unknown reasons, do not respond to therapy have a very low prognostic outcome. Currently, the identification of prognostically important leukemia subtypes is imprecise, labor intensive (Yeoh et al, 2002), and is focused on biomarker identification rather than underlying mechanisms of cancer relapse. There is an obvious need, therefore, for novel methodologies and platforms with which to accurately and efficiently characterize the heterogeneity of ALL subtypes and their ability to respond to chemotherapy. Developing more accessible methods with which to stratify ALL subtypes, methods that rely on protein expression and dynamic intracellular signaling networks, for instance, could result in the development of more efficacious approaches to individualized treatment.

The first step in transitioning from a generalized approach to cancer treatment to a more personalized one is a fundamental understanding of the way in which chemotherapeutic agents achieve their cytotoxicity and an appreciation of how patient-specific variation could affect the efficiency of said mechanism. Currently, the majority of chemotherapeutic drugs are designed to disrupt cytoskeletal dynamics, essential signal

transduction pathways, or DNA replication (Moreno-Sanchez et al, 2010). Most chemotherapeutic agents lack target-specificity and tend to affect or inhibit the normal function of non-transformed cells (Asmis et al, 2005; Gilleron et al, 2009). Dox, for example, is known to have significant and unwanted cardiotoxic effects as a result of its ability to disrupt the mitochondrial respiratory chain and induce oxidative stress (Gewirtz, 1999; Gilleron et al, 2009).

The aim of this work was to improve understanding of the redox-dependent methods by which Dox achieves its cytotoxic actions in cancer cells. Understanding how redox reactions affect Dox bioactivation and how the intracellular redox environment dictates the effect of Dox-induced ROS on redox-sensitive signal transduction pathways provides a framework for the use of patient-specific redox components as predictive markers of patient-sensitivity to Dox treatment. With this knowledge, efficacious pharmacological intervention strategies may be developed for a more controlled manipulation of Dox metabolism to either promote cell viability, as would be desired when protecting non-transformed cells from unwanted Dox toxicity, or to potentiate Dox-induced cytotoxicity in cancerous cells.

CHAPTER 3

LITERATURE REVIEW

3.1. Redox Metabolism in Cell Biology

3.1.1 Reactive Oxygen Species: Intracellular Sources

Cellular respiration is a process by which cells convert biochemical energy from food into adenosine triphosphate (ATP), the main energy currency of the cell. Aerobic respiration is a special type of cellular respiration in that it requires molecular oxygen (O_2) in order for the biochemical conversion process to take place. Mammalian cells primarily utilize aerobic respiration to sustain their energy requirements and a side effect of this process is the generation of ROS (Finkel & Holbrook, 2000). ROS is a term that refers to oxygen radicals (superoxide, $O_2^{\bullet-}$; hydroxyl, $OH^{\bullet}$; peroxyl, $RO_2^{\bullet}$; hydroperoxyl, $HO_2^{\bullet}$) as well as nonradical oxidizing agents (hydrogen peroxide, H_2O_2; nitric oxide, NO) which are formed as a bi-product of aerobic respiration (Nordberg & Arnér, 2001). Althogh ROS have been implicated in a variety of human diseases (Halliwell, 1991), they are also produced as a result of normal metabolism and play a crucial and beneficial role in intracellular signal transduction, activation of transcription factors, and immune defense. There are a variety of different intracellular ROS molecules; the most common ROS found in mammalian cells are superoxide, hydrogen peroxide, and hydroxyl radical (Nordberg & Arnér, 2001). In Figure 3-1, a schematic representation of the step-wise reduction of molecular oxygen to produce these three common ROS molecules is shown.

The common ROS molecules will be discussed in brief to provide a general overview of their intracellular sources. This discussion will begin with the superoxide anion. Although superoxide is considered to be a free radical species, its reactivity with intracellular components is surprisingly limited (Halliwell, 1991; Nordberg & Arnér, 2001). For this reason, $O_2^{\bullet-}$ is considered a very poor signaling molecule (D'Autreaux &

Toledano, 2007). Certain compartments within the mammalian cell that are rich in molecular oxygen and electrons, for example, the inner mitochondrial membrane space, can effectively support the spontaneous production of superoxide. However, because $O_2^{\bullet-}$ is somewhat ineffective at permeating through lipid membranes (D'Autreaux & Toledano, 2007), most of the superoxide produced in the mitochondria is contained within that cellular compartment.

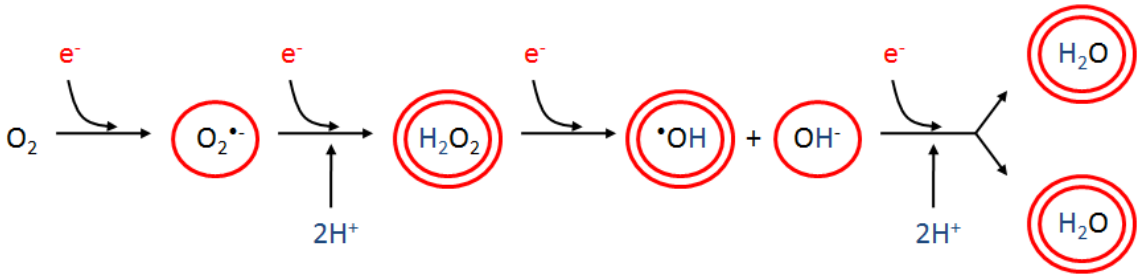

Figure 3-1. Reduction of molecular oxygen to produce ROS. The step-wise reduction of molecular oxygen highlighting the one-electron transfer reactions that produce the common intracellular ROS molecules superoxide ($O_2^{\bullet-}$), hydrogen peroxide (H_2O_2), and hydroxyl radical ($OH^{\bullet}$). Image adapted from the reaction mechanism described by (Nordberg & Arnér, 2001).

Though the majority of endogenous $O_2^{\bullet-}$ stems from processes that take place within the mitochondrion, the mammalian cell contains specialized enzymes that are capable of generating superoxide independent of mitochondrial involvement (Petry et al, 2010). Superoxide can be produced endogenously by the cyclooxygenase enzyme, the lipoxygenase enzyme, or by flavoenzymes (D'Autreaux & Toledano, 2007; Halliwell, 1991; Nordberg & Arnér, 2001). Xanthine oxidase (XO) and NADPH oxidases (NOXs) are well studied superoxide producing flavoenzymes found in mammalian cells (Kuppusamy & Zweier, 1989; Petry et al, 2010). Xanthine oxidase, also known as xanthine oxidoreductase, can be found in most mammalian tissues, but is largely concentrated in epithelial and endothelial cells (Bayir, 2005). In humans, unstimulated

cells have a relatively low basal expression of XO, yet upon cellular activation by cytokines, the transcription of XO is rapidly upregulated and its activity increased (Bayir, 2005). Changes in the oxygen content of the intracellular or extracellular environment, e.g. hypoxia or hyperoxia, can also alter the transcriptional regulation of XO and therefore, the intracellular accumulation of $O_2^{\bullet-}$ (Bayir, 2005; Berry & Hare).

NADPH oxidases are another category of flavoenzymes that are capable of producing $O_2^{\bullet-}$. NOXs are membrane-bound enzymes that catalyze the one electron reduction of molecular oxygen to $O_2^{\bullet-}$ using the electron donor, NADPH (Petry et al, 2010). The NOX family is comprised of 7 distinct enzymes and 6 distinct subunits that form the catalytic core of the NOX enzyme system: NOXs 1-5 and DUOXs 1-2 represent the 7 NOX enzymes (Petry et al, 2010); $p22^{phox}$, $p47^{phox}$, $p67^{phox}$, $p40^{phox}$, NOXO1, and NOXA1 represent the 6 NOX subunits (Bedard & Krause, 2007). While each of the 7 distinct NOX enzymes shares a similar structural domain, they can differ in their cellular location and their need for additional subunits to achieve maximal activation. NOX2, for instance, is a NOX isoform that is found primarily on the plasma membrane of phagocytic cells (Petry et al, 2010). Activation of NOX2 requires the active participation of $p47^{phox}$, $p67^{phox}$, and $p40^{phox}$ (Petry et al, 2010). Alternatively, NOX1, which is believed to associate with plasma membrane caveolae and the nuclear membrane of some cells (Hilenski et al, 2004; Miller et al, 2007), is thought to require the subunits NOXO1 and NOXA1 for cell type- and stimulus-dependent maximal activation (Banfi et al, 2003). There are, however, certain NOXs that are believed to be subunit-independent in their activation. NOX4 is an NADPH oxidase that does not seem to require additional subunits for its activation; regulation of NOX4 activity is achieved primarily through regulation of its transcription (Kawahara et al, 2007; Serrander et al, 2007).

Another common ROS found in mammalian cells is hydrogen peroxide. Although H_2O_2 is not a free radical, its reactivity with intracellular thiols is significant (D'Autreaux & Toledano, 2007). This characteristic, paired with its relatively long half-life, makes

H_2O_2 is a good signaling molecule (Antunes & Cadenas, 2000; Liu et al, 2005). Much like superoxide, hydrogen peroxide is produced primarily by metabolic reactions that take place in the mitochondria (Balaban et al, 2005; Beckman & Ames, 1998; Boveris & Chance, 1973). Within the mitochondria, the electron transport chain generates $O_2^{\bullet-}$ through the one-electron reduction of O_2 (Fig. 3-1). Because $O_2^{\bullet-}$ can be toxic to cells (Marnett, 2000; Mates et al, 1999), it is rapidly detoxified by the mitochondrial enzyme manganese superoxide dismutase (MnSOD) to produce H_2O_2 (Nordberg & Arnér, 2001). Non-mitochondrial generation of $O_2^{\bullet-}$, through the actions of flavin-containing enzymes such as xanthine oxidase and NADPH oxidases, can also result in H_2O_2 generation. Copper and zinc superoxide dismutases (Gray & Carmichael, 1992), located in the cytosol of mammalian cells, are responsible for detoxifying cytotosolic $O_2^{\bullet-}$, producing H_2O_2 as a product (Nordberg & Arnér, 2001). The spontaneous dismutation of $O_2^{\bullet-}$ can also occur, independently of enzyme action, and this spontaneous dismutation is responsible for some of the intracellular H_2O_2 that is evident in cells.

The mammalian cell contains specialized organelles that are capable of producing hydrogen peroxide independently of superoxide generation (Fritz et al, 2007). One such organelle is the peroxisome. Peroxisomes are organelles that play a role in lipid biosynthesis as well as in lipid catabolism and fatty acid breakdown (Angermüller et al, 2009). The breakdown of fatty acids involves the transfer of hydrogen from the fatty acid substrate onto molecular oxygen, a process that results in the production of H_2O_2 (Angermüller et al, 2009). Several notable enzyme-catalyzed processes are thought to be responsible for the generation of H_2O_2 within the peroxisome: the enzyme catalyzed breakdown of uric acid by urate oxidase, the enzyme catalyzed breakdown of xanthine by xanthine oxidase, and the enzyme catalyzed breakdown of fatty acids by acyl-CoA oxidase (Angermüller et al).

Hydroxyl radical is third and final ROS molecule that will be discussed in detail. The hydroxyl radical is an extremely reactive radical capable of interacting with a variety

of biomolecules (Betteridge, 2000; Halliwell, 1991). The hydroxyl radical is formed by the metal ion-catalyzed Fenton reaction of H_2O_2 (Nordberg & Arnér, 2001). In the Fenton reaction, the transition metal ions of copper (Cu^+) and iron (Fe^{2+}), complexed with different proteins or molecules, catalyze the breakdown of H_2O_2 into $^{\bullet}OH$ and OH^- (Fig. 3-1) (Nordberg & Arnér, 2001). Moreover, because $O_2^{\bullet-}$ is capable of replenishing the levels of Cu^+ and Fe^{2+}, through its reaction with intracellular proteins like ferritin and some dehydrogenases (Harris et al, 1994), superoxide and transition metals play an important role in the intracellular formation of hydroxyl radicals. The reaction in which $O_2^{\bullet-}$ generates transition metals via its reaction with intracellular proteins is called the *in vivo* Haber-Weiss reaction (Fridovich, 1997).

3.1.2 Reactive Oxygen Species: Physiological Functions

ROS have many diverse physiological functions within the mammalian cell; the two main functions are phagocyte-dependent defense against infection and redox-regulated signal transduction (Nordberg & Arnér, 2001; Valko et al, 2007). Phagocytes are white blood cells that aid the immune system by ingesting harmful foreign particles, bacteria or dead cells (Steevels & Meyaard, 2011). This phagocytotic process is aided by ROS because most bacteria and foreign microbes are extremely sensitive to ROS exposure. Superoxide is produced within the phagocyte by NADPH oxidase complexes (Babior, 1999; Nauseef, 1999). Superoxide dismutase (SOD) within the phagocyte is able to convert $O_2^{\bullet-}$ into hydrogen peroxide, which when produced, can be further converted into hypochlorous acid (HOCl). The redox enzyme myeloperoxidase is the enzyme responsible for the conversion of H_2O_2 into HOCl (Rossi et al, 1985). Hypochlorous acid can subsequently lead to the production of hydroxyl radical (Valko et al, 2007). Hypochlorous acid and hydroxyl radical are the primary ROS molecules that carryout the antimicrobial effects of ROS within the phagosomes and, as a result, they play an important role in the mammalian defense against infection.

In addition to defense against infection, ROS play an important role in cellular signal transduction. Signal transduction is defined as the process by which cells communicate with one another and with their extracellular environment (Poli et al, 2004). Signal transduction processes, which are triggered by changes in the extracellular or intracellular environment, ultimately lead to the induction of gene expression which induces various cellular processes such as growth, proliferation or even apoptosis (Thannickal & Fanburg, 2000). ROS can regulate signal transduction because they have the ability to modify redox sensitive proteins (Valko et al, 2007). ROS has been shown to affect the structure and thereby the function and activity of many redox sensitive proteins, such as growth factor receptors (Neufeld et al, 1999), protein kinases (Mulder, 2000), and transcription factors (Oliveira-Marques et al, 2009). The oxidation of redox sensitive proteins by ROS can lead to structural changes within the protein, which can promote either protein activation or protein inactivation. This capacity of ROS to modify protein activity is believed to be one reason why many cell types exhibit a small oxidative burst of ROS upon stimulation by extracellular cytokines, growth factors, or hormones (Thannickal & Fanburg, 2000). Additionally, the ability of ROS to modify protein activity helps to explain why the mammalian cell maintains its various intracellular compartments at distinct homeostatic redox potentials (Kemp et al, 2008).

Inspection of the signaling cascade responsible for activating the NF-κB transcription factor, in particular, reveals the extent to which ROS can regulate a particular signal transduction pathway. NF-κB is a transcription factor that is involved in everything from cell proliferation and growth to immune response and inflammation (Ghosh et al, 1998). Although most transcription factors have their effect in the nucleus, the activation of the NF-κB transcription factor begins in the cytosol with the degradation of its inhibitor protein IκB (Ghosh et al, 1998). The degradation of IκB has been shown to be induced by oxidative conditions and is thought to be inhibited by antioxidant action (Dalton et al, 1999; Nakamura et al, 1997). Ironically, S-glutathionylation, an ROS-

dependent protein modification that can serve to inactivate certain redox-sensitive proteins (de Oliveira-Marques et al, 2007; Oliveira-Marques et al, 2009), has been shown to affect IκB; S-glutathionylation of IκB is thought to result in its inhibition (Kil et al, 2008). The kinase responsible for IκB degradation, inhibitory κB kinase (IKK) is also sensitive to protein S-glutathionylation (de Oliveira-Marques et al, 2007; Oliveira-Marques et al, 2009). Previous research has shown that oxidative stress can induce the S-glutathionylation of IKK-β on Cys179 which leads to its inactivation (Korn et al, 2001). The NF-κB molecule itself, irrespective of its protein regulators, has also been shown to be redox-sensitive. The p50 subunit of the NF-κB molecule is susceptible to oxidation (Hayashi et al, 1993; Matthews et al, 1992). This oxidation of the p50 subunit appears to promote NF-κB activation as it is the oxidized form of the NF-κB transcription factor that preferentially translocates to the nucleus (Oliveira-Marques et al, 2009). However, once in the nucleus, it is the reduced form of NF-κB that successfully binds to DNA to promote the transcription of a variety of genes (Kabe et al, 2005). Moreover, recent evidence seems to suggest that this same p50 subunit could be a potential target of protein S-glutathionylation (Pineda-Molina et al, 2001), a modification that would inhibit the DNA-binding activity of the NF-κB transcription factor. These findings provide several examples of how ROS and the intracellular redox environment can effectively regulate intracellular signal transduction.

3.1.3 Reactive Oxygen Species: Oxidative Stress and Disease Induction

Oxidative stress is a condition characterized by an imbalance between the concentration of ROS within a system and the system's ability to consume ROS or repair damage caused by ROS. ROS are likely to cause cellular damage because of their high reactivity with all the major groups of biomolecules within the cell: proteins, lipids and DNA (Nordberg & Arnér, 2001). For this reason, an accumulation of ROS within the cell can be extremely toxic. Reactions of ROS with intracellular proteins can lead to the

oxidation of amino acid side chains, a process that can result in protein-disulfide formation (Gilbert, 1990; Jones, 2008) and protein S-glutathionylation (Gallogly & Mieyal, 2007). Oxidation of proteins by ROS can also lead to peptide bond cleavage as well as protein-protein cross-link formation (Stadtman & Berlett, 1998). These ROS-induced post-translational modifications can cause the detrimental inhibition of enzyme activity and the denaturing and malfunctioning of proteins (Butterfield et al, 1998; Stadtman & Berlett, 1998). Several diseases, such as Alzheimer's (Carney et al, 1994), rheumatoid arthritis (Chapman et al, 1989), and muscular dystrophy (Murphy & Kehrer, 1989), have been associated with ROS-induced protein modifications.

Lipids are another class of biomolecules which are readily susceptible to ROS-mediated damage. The most common form of ROS-induced damage experienced by lipids is lipid peroxidation (Steinberg, 1997; Yla-Herttuala, 1999). Lipids are made up of fatty acids and unsaturated fatty acids are very susceptible to oxidation by free radical species. Free radical oxidation of lipids usually results in oxidative side reactions that potentiate the degree of oxidative damage experienced by the cell (Molavi & Mehta, 2004; Stadtman & Berlett, 1998). Lipid oxidation has the potential to disrupt the organization of the lipid bilayer which could alter the permeability of the lipid membrane to important metabolites and minerals. Because the controlled transport of minerals such as potassium and calcium are important to normal heart function, and because the formation of artherosclerotic plaques involves the oxidation of low-density lipoproteins, lipid oxidation has been implicated in cardiovascular disease (Halliwell, 1991; Valko et al, 2007). Cardiomyocyte hypertrophy, a condition characterized by abnormal cardiac cell growth, can lead to congestive heart failure and other cardiovascular diseases (Molkentin & Dorn, 2001); this process is believed to be mediated by ROS-induced lipid oxidation (Murdoch et al, 2006).

The final class of biomolecules that is susceptible to ROS-mediated damage is nucleic acids. Because deoxyribonucleic acid (Bednarski et al) plays an important role in

cellular replication, damage to DNA can be extremely detrimental to the cell. ROS has the capacity to both cleave and cross-link DNA molecules. Both of these processes will ultimately affect the fidelity with which DNA is replicated. A typical mammalian cell has the machinery to repair DNA damage that is caused by ROS; however, when this machinery is overwhelmed, mutations in DNA can result from erroneous base pairing (Valko et al, 2007). The accumulation of DNA mutations is believed to be one of the main causes of cancer because it can result in aberrant signal transduction, gene transcription, and all around genomic instability (Marnett, 2000; Valko et al, 2006). Correspondingly, there appears to be a high incidence of cancer in individuals who are exposed to high levels of oxidative stress (Marnett, 2000; Mates et al, 1999).

3.1.4 Antioxidant Enzymes

Both radical and non-radical ROS have the potential to cause cellular damage. As a result, mammalian cells have developed a host of antioxidant enzymes that are capable of preventing and repairing ROS-mediated damage. These enzymatic antioxidants include, but are not limited to, superoxide dismutases, catalase, glutathione peroxidases, and peroxiredoxins (Prx). Superoxide dismutases were the first antioxidant enzymes to be discovered (Bannister, 1988). Prior to discussing the specific antioxidant enzyme systems that help maintain normal oxidant levels within the mammalian cell, the NADPH/$NADP^+$ redox couple will be discussed in brief.

$NADP^+$ is the oxidized form of NADPH, the molecule that provides reducing equivalents for a variety of intracellular reactions. Some of these reactions include the anabolic biosynthesis reactions that produce lipids and nucleic acids (Ying, 2008), the redox-dependent reactions that produce and consume ROS (Bedard & Krause, 2007; Nordberg & Arnér, 2001), and the metabolic reactions that activate xenobiotic drugs such as Dox (Kostrzewa-Nowak et al, 2005). The primary source of NADPH in mammalian cells is the pentose phosphate pathway (Ying, 2008). Most mammalian cells have a

homeostatic balance of NADPH/$NADP^+$ that is maintained within the cell at any given time. Unwanted deviations from this homeostatic potential can have detrimental effects on many cellular processes and is associated with several disease states (Ying, 2008).

As mentioned previously, SOD is responsible for catalyzing the dismutation of $O_2^{\bullet-}$ into H_2O_2. In mammals, SOD can be categorized into two metal-containing SOD isoenzymes: mitochondrial Mn-SOD and cytosolic/extracellular Cu,Zn-SOD (Bannister et al, 1987). Although most mammalian cells contain both SOD isoenzymes, the mitochondrial Mn-SOD appears to be more essential than its Cu,Zn-SOD counterpart, as revealed by knockout experiments in mice (Melov et al, 1998).

Catalases are another class of antioxidant enzymes found in mammalian cells. These heme-containing enzymes are found primarily in peroxisomes, where they catalyze the dismutation of hydrogen peroxide into water and molecular oxygen (Aebi, 1984). Catalase has also been shown to play a role in phenol and alcohol detoxification via its ability to catalyze the reaction of these species with H_2O_2 (Nordberg & Arnér, 2001). Other antioxidant roles for catalase include its ability to minimize cellular damage due to the hydroxyl radicals ($OH^{\bullet}$) that are formed via the metal-catalysed Fenton reactions (Nordberg & Arnér, 2001), and its ability to stabilize reduced NADPH, thus allowing the metabolite to effectively carry out its role in supporting many of the intracellular antioxidant enzyme systems (Kirkman & Gaetani, 1984; Kirkman et al, 1999).

Glutathione peroxidases (GPx) are one of the major classes of antioxidant enzymes that depend on NADPH to carry out their antioxidant actions. Glutathione peroxidases are selenocysteine containing enzymes that catalyze the removal of hydrogen peroxide, and other alcohol peroxides, within the mammalian cell (Ursini et al, 1995). There are four classes of GPx in mammals, namely GPx1 – GPx4 (de Haan et al, 1998; Mates et al, 1999). GPx1 and GPx4 are located primarily in the cytosol of mammalian cells; however, recent study has uncovered a specialized role for GPx4 in spermatid development and chromosomal arrangement (Ursini et al, 1999). GPx2 and GPx3 are

found primarily in gastrointestinal cells and kidney cells, respectively (Dreher et al, 1997; Mates et al, 1999). The mechanism by which GPx reduces hydroperoxides appears to be conserved across GPx family members (Epp et al, 1983). Upon oxidation of GPx, the selenoate (Se^-) containing active site is transformed to a selenenic acid (SeOH). This selenenic acid is susceptible to reaction with reduced glutathione (GSH). This reaction forms the Se-SG glutathione adduct, which, upon the addition of a secondary GSH molecule, regenerates the original selenolate active site with the forming glutathione disulfide (GSSG) as a bi-product. Glutathione peroxidases play a substantial part in defending the mammalian cell against H_2O_2-accumulation during instances of oxidative stress (Adimora et al, 2010).

Peroxiredoxins (Prx), also known as thioredoxin peroxidases, are a class of mammalian antioxidant enzymes that are directly responsible for reducing hydroperoxides, e.g., hydrogen peroxides (Shuvaeva et al, 2009). Prx are divided into three classes: typical 2-Cys Prx, atypical 2-Cys Prx, and 1-Cys Prx (Chae et al, 1999). Both the typical and the atypical 2-Cys Prx molecules contain two cysteine subunits: a peroxidatic cysteine subunit, which is responsible for the catalytic peroxidase action of the Prx molecule, and a resolving cysteine subunit (Shuvaeva et al, 2009). The 1-Cys Prx enzyme contains a peroxidatic cysteine subunit with no resolving cysteine to accompany it (Chae et al, 1999). While the different classes of Prx enzymes share the same catalytic mechanism of oxidation, the mechanism by which the oxidatively-inactivated enzymes return to their active form differs between classes. Upon oxidation by a peroxide substrate such as H_2O_2, the peroxidatic cysteine, which is the redox-active cysteine (Cys-SH) located in the active site of the Prx molecule, is transformed to a sulfenic acid (Cys-OH); this oxidation process is conserved across all three Prx enzyme classes (Shuvaeva et al, 2009). For the 2-Cys Prx enzymes, the second step of the catalytic cycle involves the attack of the peroxidatic sulfenic acid by the resolving cysteine to form an inter-subunit disulfide bond, as is the case with the typical 2-Cys Prx, or an intra-chain disulfide bond,

as is the case with the atypical 2-Cys Prx (Chae et al, 1999). In both cases, these disulfide bonds are reduced to their original active cysteine forms by the actions of antioxidant enzymes that specialize in disulfide bond reduction such as the thioredoxins and the glutaredoxins (Chae et al, 1999). Because the 1-Cys Prx conserve only the peroxidatic cysteines, there is no disulfide bond formation, and the peroxidatic sulfenic acid must be reduced back to its active cysteine form be a reductant molecule such as glutathione (Shuvaeva et al, 2009).

3.1.5 The Glutathione Antioxidant System

Glutathione (GSH) is a tripeptide that contains a sulfhydryl group. This amino acid derivative serves several important functions within the mammalian antioxidant system. Glutathione is considered to be the most abundant intracellular thiol-based antioxidant found in mammalian cells, and therefore considered by some as the cell's first line of defense against oxidative stress. It cycles between two forms: the reduced thiol form, GSH, and the oxidized form, GSSG, characterized by the disulfide linkage of two GSH tripeptides (Schafer & Buettner, 2001). Because of its relatively high intracellular level (1 – 10 mM) (Schafer & Buettner, 2001), GSH serves as a sulfhydryl buffer, protecting cells from oxidative damage by reacting with potentially damaging free radicals (Gallogly & Mieyal, 2007; Schafer & Buettner, 2001). When the sulfur atom in GSH reacts with a free radical it produces a GSH thiyl radical ($GS^{\bullet}$) (Gallogly & Mieyal, 2007). Two GSH thiyl radicals can in turn react to produce one GSSG molecule. To be effective as a buffer, therefore, the concentration of reduced GSH must be maintained at a substantially high level compared to the concentration of oxidized GSSG; the ratio of GSH to GSSG in most cells is greater than 500:1 (Schafer & Buettner, 2001). GSSG is reduced by the NADPH-dependent flavoenzyme glutathione reductase (GR), and this enzyme is critical to the maintenance of a proper glutathione redox potential in mammalian cells (Nordberg & Arnér, 2001).

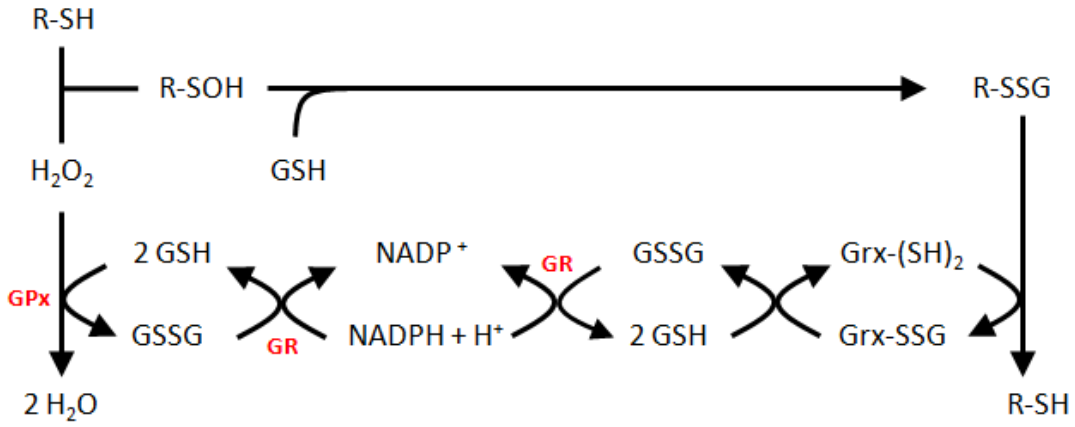

Figure 3-2. Generalized schematic of the mammalian glutathione antioxidant system. Hydrogen peroxide is reduced by the glutathione peroxidase (GPx)-catalyzed oxidation of two molecules of glutathione (GSH) to form glutathione disulfide (GSSG). GSSG is subsequently reduced by the enzymatic actions of glutathione reductase (GR) which depend on the reducing equivalents provided by NADPH. H_2O_2 promotes the oxidation of protein monothiols (R-SH) to protein sulfenic acids (R-SOH); the addition of a glutathione molecule to the protein sulfenic acid generates an S-glutathionylated protein (R-SSG). S-glutathionylated proteins are reduced by glutaredoxins (Grx) via the oxidation of two molecules of glutathione to glutathione disulfide.

Reduced GSH is also an effective sulfhydryl buffer against non-radical ROS. GSH conjugation reactions, catalyzed by glutathione S-transferases (Armstrong, 1997), help protect intracellular protein monothiols from permanent oxidative damage (Schafer & Buettner, 2001) by facilitating the formation of protein mixed disulfides (Pr-SSG). Because the formation of protein mixed disulfides can affect the activity of certain proteins, GSH is believed to play a direct role in redox-dependent cell signaling (Gallogly & Mieyal, 2007; Ghezzi, 2005). As discussed earlier, GSH is an integral contributor to the actions of the GPx and Prx enzyme systems. When GPx reacts with H_2O_2 it becomes oxidized and oxidized GPx relies on subsequent reactions with GSH to return to its active reduced state (Ursini et al, 1995). Moreover, reduced thiols such as GSH are believed to play a direct role in the reduction of the peroxidatic sulfenic acids that are formed upon

the reaction of 1-Cys peroxiredoxins with hydroperoxides (Chae et al, 1999; Shuvaeva et al, 2009).

Glutaredoxins (Grx) are a class of proteins whose function is directly related to GSH (Holmgren, 1976). Four different mammalian Grx proteins have been identified and are categorized into two subgroups: classical dithiol Grxs (Grx1 and Grx2) and classical monothiol Grxs (Grx3 and Grx5) (Holmgren, 1976; Lillig et al, 2008). Grx1 and Grx3 are found primarily in the cytosol of mammalian cells. Grx2 is comprised of three different isoforms which can exist either in the mitochondria, the cytosol, or the nucleus of mammalian cells; however, Grx5 is primarily found in the mitochondria of mammalian cells (Lillig et al, 2008). Glutaredoxins play a role in cellular antioxidant defense by reducing GSH-mixed disulfides and some oxidized protein-disulfide species (Fig. 3-2) (Holmgren, 1976; Lillig et al, 2008; Peltoniemi et al, 2006). In reducing oxidized proteins and GSH-mixed disulfides, Grx itself becomes oxidized and therefore inactivated. To return to its reduced and activated state, Grx proteins depend on reducing equivalents from GSH. The use of GSH as a cofactor in the Grx-catalyzed intracellular enzymatic reactions results in the production of oxidized GSSG. Oxidized GSSG is then reduced by the actions of GR, as described previously (Holmgren, 1976). The Grx proteins, together with GSH and GR, make up the intracellular glutathione antioxidant system.

It is important to note that the activity of the glutathione antioxidant system (Fig. 3-2), as defined by the GSH redox potentials, can vary from one cellular compartment to the next (Kemp et al, 2008; Schafer & Buettner, 2001). The levels of reduced GSH in the cytosol and the mitochondria are significantly higher than those in the endoplasmic reticulum (Hwang et al, 1992). Moreover, although these intracellular compartments may be functionally separated, resulting in compartment-specific redox environments, regulated transport of GSH and GSSG between these compartments is maintained (Kemp et al, 2008).

3.1.6 The Thioredoxin Antioxidant System

The thioredoxin antioxidant system is made up of two antioxidant enzymes working in conjunction with one another: thioredoxin (Trx) and thioredoxin reductase (TR) (Nordberg & Arnér, 2001). Thioredoxins are proteins with oxidoreductase activities that are capable of reducing oxidized proteins via cysteine thiol-disulfide exchange (Holmgren, 1985). When cysteine containing proteins are oxidized by ROS, they have the potential to form protein disulfide bonds; Trx proteins contain a dithiol active site which can be utilized to reduce disulfide-bonded proteins (Holmgren, 1989). Upon reduction of the oxidized protein, the active site of the Trx molecule is transformed from a dithiol state to a disulfide state, thereby inactivating the Trx protein (Fig. 3-3) (Holmgren, 1977). To return to its active dithiol state, Trx depends on the catalytic actions of thioredoxin reductases, which get their reducing equivalents from NADPH (Holmgren, 1977). The manner in which GR reduces oxidized GSSG is very similar to the manner in which TR reduces oxidized Trx. There are two isoforms of TR in the mammalian cell: TR1, which is primarily cytosolic, and TR2, which is primarily mitochondrial (Holmgren & Lu, 2010).

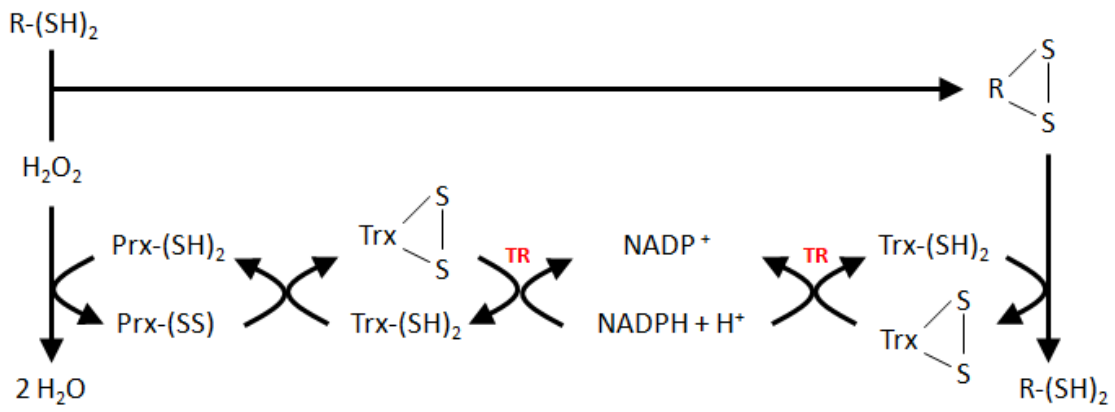

Figure 3-3. Generalized schematic of the mammalian thioredoxin antioxidant system. Hydrogen peroxide is removed by the actions of peroxiredoxins (Prx), which when inactivated by oxidation depend on thioredoxin for their reduction. H_2O_2 also promotes the oxidation of protein dithiols (R-$(SH)_2$) to protein disulfides (R-SS); protein disulfides are reduced back to protein dithiols by thioredoxins which in turn are enzymatically reduced by thioredoxin reductases (TR) using NADPH as reducing equivalents.

There are three known classes of mammalian Trx. The classical Trx-1 protein localizes primarily in the cytosol of mammalian cells (Holmgren & Lu, 2010) while the Trx-2 isoform of Trx localizes to the mitochondria. The third Trx protein, SpTrx, is a Trx variant that is primarily expressed in mammalian spermatozoa (Miranda-Vizuete et al, 2001). Many intracellular proteins depend on Trx for reduction upon their oxidation, most notable of which are the Prx enzymes discussed previously (Rhee et al, 2001). In addition to this well characterized Trx-dependent enzyme, many other intracellular proteins rely on Trx for their reduction, including several transcription factors. The NF-κB transcription factor is an example of a transcription factor whose activity can be modulated by Trx (Schenk et al, 1994). NF-κB activation is inhibited by Trx in the cytosol, whereas in the nucleus, Trx has been shown to activate the DNA-binding of NF-κB (Wei et al, 2000).

The balance between reduced and oxidized Trx is represented by the thioredoxin redox potential (Watson et al, 2003). Much like the GSH antioxidant system, the activity

of the thioredoxin antioxidant system (Fig. 3-3), as defined by the Trx redox potential, can vary from one cellular compartment to the next. The Trx redox potential in the cytosol is more reducing that that of the nucleus, which is in turn more reducing that that of the mitochondria (Kemp et al, 2008). The controlled transport of reduced and oxidized Trx between these intracellular compartments serves to maintain their distinct Trx redox potentials, thereby providing a mechanism for redox-regulated control of signal transduction between compartments (Halvey et al, 2005; Jones et al, 2004; Kabe et al, 2005).

3.2. Redox Chemistry and Anthracycline Drug Toxicity

For over 40 years, anthracycline antibiotics, also known as anthraquinones, have been used to treat a variety of cancers. Microorganisms served as the original source of these molecules (Kovacic & Osuna, 2000) and since then, much attention has been given to the mechanistic understanding of their clinical efficacy against neoplastic growth. The most common anthracycline antibiotics currently in use are Dox (Adriamycin) (Fig. 3-4) and daunorubicin (Daunomycin) (Gewirtz, 1999; Kovacic & Osuna, 2000). While the remainder of this discussion will focus on the Dox anthracycline, most of the conclusions drawn can be applied to other members of the anthracycline family (Abdella & Fisher, 1985). This section will address the redox chemistry of anthracyclines and highlight some of the potential mechanisms of anthracycline toxicity that are attributed to redox-mediated processes.

3.2.1 Redox Chemistry of Anthracyclines

Anthracyclines are molecules that belong to the quinone family of chemicals, more specifically, the quinone methide (QM) family of chemicals (Abdella & Fisher, 1985). The structure of Dox is shown in Figure 3-4. Most anthracyclines share the same

quinone methide backbone (QMB) that is exhibited by Dox, however, changes to the functional group (FG) and side group (Asmis et al) of these molecules separate one anthracycline antibiotic from the other. Anthracyclines are prone to redox modifications, due to the relative reactivity of their respective functional groups (Abdella & Fisher, 1985). The first chemical modification that will be discussed concerns the reactions that lead to semiquinone and hydroquinone formation. Quinones, semiquinones, and hydroquinones differ primarily in the strength of their functional groups to act as leaving groups. In chemistry, leaving groups are defined as molecular fragments that depart from their parent compound upon heterolytic bond cleavage (Broeckaert et al, 2008). Potential leaving groups have been previously characterized in great detail (Broeckaert et al, 2008).

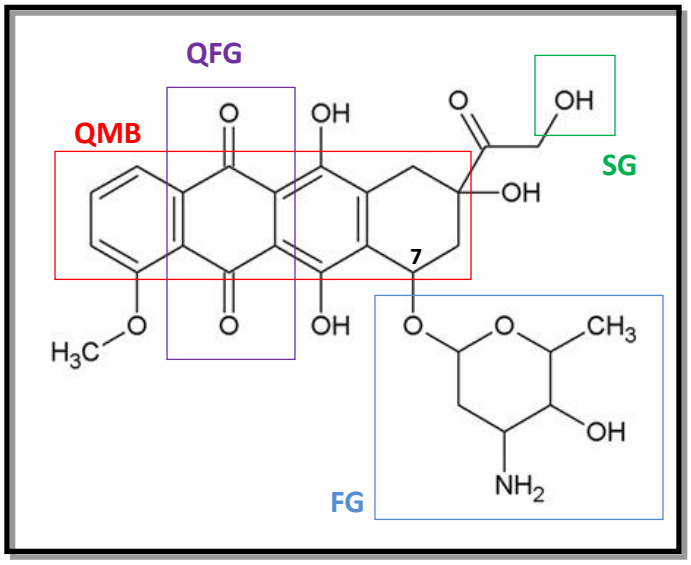

Figure 3-4. Chemical Structure of Dox (Adriamycin). The chemical structure of Dox is offered, highlighting the quinone methide backbone (QMB), the quinone functional group (QFG), the L-daunosamine functional group (FG), and the Dox-specific OH side group (Asmis et al).

Quinones can be transformed into highly reactive semiquinones upon the addition of one electron to the quinone functional group (QFG) (Fisher et al, 1983). Because the

semiquinone molecule is a radical, it has a relatively short lifetime; the semiquinone radical is prone to oxidation by O_2 under aerobic conditions, and its subsequent reaction with O_2 promotes the loss of the carbon-7 glycosidic functional group (Abdella & Fisher, 1985). The resulting aglycon radical is capable of reducing molecular oxygen, abstracting hydrogen atoms, or labeling susceptible nucleophiles, many of which exist in the intracellular milieu (Bachur et al, 1979; Pan et al, 1981; Sinha & Gregory, 1981). Alternatively, quinones can be transformed into highly reactive hydroquinones by the two-electron reduction of the quinone functional group (Fisher et al, 1983). However, because hydroquinones are also extremely susceptible to oxidation by O_2, the hydroquinone structure is not long-lived in aerobic environments; the rapid loss of the glycosidic carbon-7 functional group results in the formation of a non-radical quinone methide product (Fisher et al, 1983). The quinone methide that results from the two-electron reduction of anthracyclines is potentially electrophilic and can take part in the covalent labeling of nucleophilic biomolecules (Lin et al, 1980; Moore, 1977; Moore & Czerniak, 1981).

Both the one-electron and two-electron pathways of quinone reduction are believed to be the primary mechanisms by which flavin-containing intracellular enzymes promote the *in vivo* macromolecular degradation of xenobiotic compounds such as Dox (Bartoszek, 2002; Fisher et al, 1983; Kostrzewa-Nowak et al, 2005). Moreover, the actions of these enzymes promote an intracellular chemical process called redox cycling (Fig. 3-5). Dox and other related anthracyclines can undergo redox cycling in the presence of molecular oxygen. Redox cycling is characterized by the reductive activation of the anthracycline molecule to a semiquinone or hydroquinone, via the one- or two-electron mechanisms previously described (Fisher et al, 1983), followed by the non-enzymatic reoxidation of the semiquinone or hydroquinone compound by molecular oxygen (Kostrzewa-Nowak et al, 2005b).

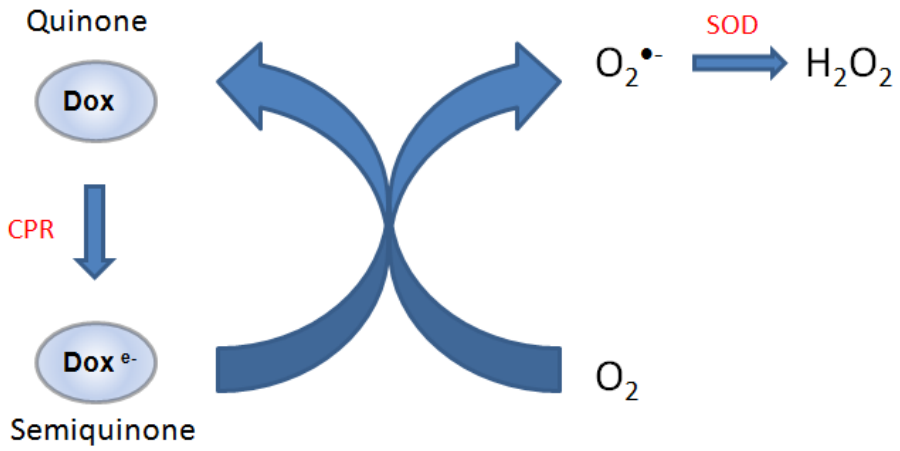

Figure 3-5. Redox Cycling of Dox. Quinone Dox is enzymatically reduced to its semiquinone form by the oxidoreductase cytochrome P450 Reductase (CPR). Semiquinone Dox is rapidly reoxidized to the quinone form by its non-enzymatic reaction with molecular oxygen to form superoxide. Superoxide is subsequently converted to hydrogen peroxide by the actions of the superoxide dismutase enzymes (SOD).

One-electron reduction of quinone anthracyclines is an enzymatic process achieved in biological systems by a range of cellular oxidoreductases, most notably NADH dehydrogenase, NADPH cytochrome P450 reductase (CPR) (Kostrzewa-Nowak et al, 2005), xanthine oxidase (Mordente et al, 2001; Pawlowska et al, 2003), and nitric oxide synthase (Garner et al, 1999; Vasquez-Vivar et al, 1997). The subsequent non-enzymatic oxidation of the semiquinone or hydroquinone radical by molecular oxygen promotes the formation of ROS such as $O_2^{\bullet-}$, $OH^{\bullet}$, and H_2O_2 (Fisher et al, 1983; Kovacic & Osuna, 2000).

3.2.2 Proposed Role of Enzymatic Reduction in Dox Cellular Toxicity

The exact mechanism by which Dox exerts its cytotoxic actions is yet unknown. However, a number of different mechanisms have been proposed, and one of these proposed mechanisms is directly related to the enzymatic reduction of anthracyclines by intracellular oxidoreductases. The one- and two-electron reductions of quinone

anthracyclines leads to the formation of highly reactive semiquinone and hydroquinone intermediates (Abdella & Fisher, 1985; Fisher et al, 1983). These intermediates are regarded as highly electrophilic and can therefore covalently label nucleophilic molecules such as DNA (Lin et al, 1980; Moore, 1977; Moore & Czerniak, 1981). The process by which activated Dox molecules interact with nucleophilic molecules such as DNA is termed bioreductive alkylation (Moore, 1977). There is an increasing body of evidence in the literature that suggests the bioreductive activation of anthracyclines like Dox significantly promote drug retention by facilitating the covalent binding of these drugs to cellular DNA (Cummings et al, 1992). Many cancer cells evade the toxic actions of Dox by actively pumping the drug outside of the cell (Bao et al, 2011), decreasing the intracellular drug retention time. By promoting covalent binding to DNA, the enzymatic reduction of anthracyclines like Dox provides a redox-mediated mechanism that is capable of circumventing multi-drug resistance associated with drug efflux (Kievit et al, 2011). Moreover, the covalent interaction of activated anthracyclines with DNA is believed to promote DNA crosslinking which is thought to contribute to drug-mediated cellular toxicity (Skladanowski & Konopa, 1994).

3.2.3 Proposed Role of ROS in Dox Cellular Toxicity

Another proposed mechanism of Dox toxicity is one which is directly related to free radical generation. It has already been shown in the literature that Dox and other members of the anthracycline family are able to induce ROS production via their ability to be redox cycled (Fisher et al, 1983; Kovacic & Osuna, 2000). However, there appears to be some controversy in the literature regarding the extent to which this ROS contributes to anthracycline-induced cellular toxicity. In fact, although various forms of ROS have been detected by electron spin resonance, including superoxide, peroxides, and hydroxyl radicals, and evidence of lipid peroxidation has been seen in *in vitro* assays of Dox treatment (Kalyanaraman et al, 1980), the question remains as to whether the level

of ROS produced by clinically relevant Dox concentrations is high enough to induce ROS-mediated damage that contributes to cell death (Kovacic & Osuna, 2000). One argument against the role of free radicals in Dox-induced toxicity is that the hypoxic conditions of the tumor microenvironment (Guppy, 2002) do not contain enough oxygen to promote the oxygen-mediated redox cycling of Dox. However, to counter this argument, some researchers claim that the extremely rapid oxidation reaction that occurs between molecular oxygen and the semiquinone/hydroquinone form of Dox does not require large amounts of oxygen to take place; the extremely rapid nature of this reaction is therefore viewed as a clear indicator of the existence of *in vivo* Dox redox cycling and subsequent ROS generation (Taatjes et al, 1998). In fact, the generation of free radicals is accepted as the direct cause of cardiotoxicity that results from Dox treatment (Gewirtz, 1999). Moreover, free radicals generated by Dox redox cycling, if generated in close proximity to essential biomolecules, such as DNA or membrane lipids, can rapidly induce DNA cleavage (Sinha & Gregory, 1981; Taatjes et al, 1998) and lipid peroxidation (Benchekroun & Robert, 1992), two processes that are known to contribute to cell death (Gewirtz, 1999).

3.2.4 Proposed Role of Thiol Signaling in Dox Cellular Toxicity

ROS generated by Dox treatment can induce cellular toxicity by its direct interaction with biomolecules (Abdella & Fisher, 1985; Fisher et al, 1983; Kovacic & Osuna, 2000). However, because ROS can affect redox-sensitive signaling pathways, it is also likely that the ROS generated by Dox treatment could promote cellular toxicity by modulating redox-sensitive signaling pathways that are directly involved in cell survival. The NF-κB signaling pathway is well known as a redox-sensitive pathway that mediates cell survival (Oliveira-Marques et al, 2009). Several proteins in the NF-κB signal activation pathway are susceptible to ROS-mediated protein modifications. Berdnaski and colleagues have shown a direct link between NF-κB activity and Dox induced

apoptosis in osteosarcoma and breast cancer cell lines (Bednarski et al, 2009). The relationship between Dox-induced ROS and NF-κB activity was further clarified in a study by Lin et al. illustrating that inhibition of Dox-induced ROS leads to a correlated inhibition of NF-κB activity in neuroblastoma cells (Lin et al, 2007).

The GSH antioxidant system is the primary determinant of the cellular redox environment and alterations to the redox environment can lead to cell death. Protein S-glutathionylation is a process that is regulated by the glutathione antioxidant system and ROS are known to promote S-glutathionylation of proteins via modulation of GSH, Grx, and GR (Gallogly & Mieyal, 2007; Ghezzi, 2005; Peltoniemi et al, 2006). Recent work by Asmis et al. illustrates the capacity of Dox to alter the glutathione antioxidant system in a way that promotes cell injury in human macrophages, independent of ROS formation (Asmis et al, 2005). The authors report that increased protein S-glutathionylation parallels the GSH oxidation and GSSG accumulation that is induced by Dox treatment (Asmis et al, 2005). The ability of Dox to modify the glutathione antioxidant system in a manner that mediates cellular injury, independent of ROS formation, suggests an alternate pathway of Dox-induced toxicity, one that is that is strongly coupled to intracellular thiol signaling.

CHAPTER 4

THE DYNAMIC REGULATION OF DOX BIOACTIVATION

Introduction

The reductive conversion of Dox has been implicated as a major determinant of Dox cytotoxicity and has been proposed as an underlying factor controlling drug resistance in cancer cells (Akman et al, 1990; Kostrzewa-Nowak et al, 2005; Sinha & Chignell, 1979; Sinha et al, 1989b). Reductive conversion of Dox is characterized by the one-electron reduction of the quinone moiety of Dox, via NADPH and cytochrome P450 reductase (CPR), into a semiquinone radical (Kostrzewa-Nowak et al, 2005; Menna et al, 2007; Ravi & Das, 2004). Once the semiquinone radical has been generated, it can exert direct toxic effects or be oxidized back to the quinone form (i.e. redox cycling) (Ramji et al, 2003). The combination of bioreductive conversion and redox cycling occurs simultaneously in mammalian cells; this overall process is termed bioactivation. It has been reported that the ability of Dox to undergo reductive conversion is dependent on the availability of molecular oxygen and NADPH, and the activities of several intracellular enzymes such as superoxide dismutase (SOD), glutathione peroxidase, NADPH oxidases (NOXs), and thioredoxin (Akman et al, 1990; Berlin & Haseltine, 1981; Doroshow et al, 1991; Gilleron et al, 2009; Kostrzewa-Nowak et al, 2005; Ravi & Das, 2004; Sinha et al, 1989b), components whose intracellular concentrations and activities may vary from one cancer type to the next, or from patient to patient.

---

[*] Modified from Finn NA, Findley HW, Kemp ML "A switching mechanism in Dox bioactivation can be exploited to control Dox toxicity" In press at *Plos Computational Biology*

This variation may help explain some of the contradictory evidence in the literature that describes the proper intracellular environment or intervention strategy for effectively controlling Dox toxicity *in vivo* (Akman et al, 1990; Bartoszek & Wolf, 1992; Berggren et al, 2001; Doroshow et al, 1991; Kim et al, 2001; Ramji et al, 2003; Sinha et al, 1989b).

Because the overall network structure for cytosolic Dox bioactivation is believed to be conserved across different cell types (Bachur et al, 1979; Cummings et al, 1992; Sinha et al, 1989b), differences in cellular Dox sensitivity may result from differences in the intracellular levels of the network components (both metabolites and proteins) that control Dox bioactivation. *In vitro* studies carried out by Kostrzewa-Nowak et al support this hypothesis by showing that changes in NADPH concentration and SOD activity have a direct impact on the degree of Dox reductive conversion experienced by leukemia cells (Kostrzewa-Nowak et al, 2005a). This dependence of the drug on [NADPH] becomes very important in light of recent findings that frequently occurring somatic mutations in gliomas and leukemias can result in a directional change from NADPH production to NADPH consumption by isocitrate dehydrogenases (IDH1/2) resulting in lower intracellular NADPH levels (Dang et al, 2009; Ward et al, 2010). Additionally, there is evidence in the literature that Dox treatment stimulates NOX activity, providing added relevance to the intracellular levels of NADPH in Dox bioactivation (Gilleron et al, 2009). Thus, the redox context-dependence of Dox metabolism becomes central to accounting for patient variability to anthracycline regimens.

Contradictory observations regarding the redox-mediated reactions involved in conferring Dox potency highlight the need for a more in-depth quantitative examination of how the behavior of the Dox bioactivation network is influenced by the initial levels of its system components and its component interactions. The objectives of this study, therefore, were to (a) determine the intracellular factors that control Dox bioactivation for different Dox treatment conditions, (b) develop a mechanistic model of Dox bioactivation in leukemia cells that could be interrogated to predict resistance to Dox treatment prior to

clinical administration of the drug, and (c) test, through simulation, the possible intervention strategies that could be employed to modulate Dox cytotoxic activity in leukemia.

Materials and Methods

Computational modeling

Ordinary differential equation models of *in vitro* and *in vivo* Dox bioactivation were developed based on the scheme proposed by Kostrzewa-Nowak et al (Kostrzewa-Nowak et al, 2005). Here, the term *in vitro* refers to experiments conducted in solution, while the term *in vivo* refers to experiments conducted within living cells. The *in vitro* model, which describes Dox activation in the presence of NADPH and CPR, contains 6 kinetic parameters and 9 ODEs (Table 4-2) that describe the changes in concentration of the 9 compounds (Table 4-1) that comprise the Dox bioactivation network (Dox, metabolites, redox enzymes and reactive oxygen species). The *in vivo* model, which describes Dox activation in the presence of NADPH, CPR, G6PD, SOD1, and NOX4 is an adaptation of the *in vitro* model and contains 10 kinetic parameters and 10 ODEs (Table 4-4). The *in vitro* and *in vivo* mathematical models developed in this study use mass action kinetics of individual redox reactions, in the absence of kinetic regulation, to describe the enzymatic and non-enzymatic reactions that result in the redox cycling and reductive conversion of Dox. The computational models were designed and numerically integrated using MATLAB R2008a (The Mathworks, Inc., Natick, MA, USA).

Major Assumptions of the Computational Model

To accurately describe the effect of NADPH concentration on the mode of Dox bioactivation that takes place, the NADPH molecule was allowed to react slowly with molecular oxygen in the *in vitro* model. Although this reaction is known to take place *in vivo* through the enzymatic actions of NADPH oxidases (Gilleron et al, 2009), due to the high concentration of NADPH contained in the reaction mixture, the non-enzymatic reaction of NADPH with molecular oxygen was assumed to be possible; this reaction was included at a low rate in the network model of *in vitro* Dox bioactivation and was found

to be essential to the accurate description of this process. For the *in vivo* kinetic model of Dox bioactivation, the reaction of NADPH with molecular oxygen was assumed to be primarily catalyzed by NADPH oxidases in a mass action-driven reaction that was dependent on Dox concentration, because it has been shown that Dox treatment can activate NOXs in a Dox concentration-dependent manner (Gilleron et al, 2009). For both the *in vitro* and *in vivo* models, Dox degradation was assumed to be negligible within the time period investigated in the study based on evidence provided in the literature (Ozols et al, 1979).

Table 4-1: Initial concentration values of the nine components that comprise the *in vitro* Dox bioactivation model.

Species	*Abbreviation*	*Initial Condition (M)*	*Reference*
Reduced CPR	CPR_{red}	1.0×10^{-6}	(Kostrzewa-Nowak et al, 2005)
Oxidized CPR	CPR_{ox}	0	Assumption
Quinone Dox	Dox_q	1.0×10^{-4}	(Kostrzewa-Nowak et al, 2005)
Semiquinone Dox	Dox_{sq}	0	(Kostrzewa-Nowak et al, 2005)
NADPH	NADPH	1.0×10^{-4} / 5.0×10^{-4}	(Kostrzewa-Nowak et al, 2005)
$NADP^+$	$NADP^+$	0	Assumption
Molecular Oxygen	O_2	2.7×10^{-4}	(Koshkin et al, 1997)
Superoxide	$O_2^{\bullet-}$	0	Assumption
Hydrogen Peroxide	H_2O_2	0	Assumption

Table 4-2: Rate expressions and rate constants for the six ODEs that comprise the *in vitro* Dox bioactivation model.

Rxn #	*Expression*	*Parameter*	*Reference*
R_1	k_1 ([CPR_{red}]) ([Dox_q])	$k_1 = 1.2 \times 10^4$ $M^{-1}s^{-1}$	Fitted
R_2	k_2 ([CPR_{ox}]) ([NADPH])	$k_2 = k_1$	(Kostrzewa-Nowak et al, 2005)
R_3	k_3 ([O_2]) ([Dox_{sq}])	$k_3 = 3.0 \times 10^8$ $M^{-1}s^{-1}$	(Kalyanaraman et al, 1980)
R_4	k_4 ([NADPH]) ([O_2])	$k_4 = 2.9 \times 10^1$ $M^{-1}s^{-1}$	Fitted
R_5	k_5 ([O_2^-]) ([Dox_q])	$k_5 = 5.5 \times 10^7$ $M^{-1}s^{-1}$	Fitted
R_6	k_6 ([O_2^-]) ([O_2^-])	$k_6 = 6.4 \times 10^9$ $M^{-1}s^{-1}$	(Gray & Carmichael, 1992)

The concentration of intracellular molecular oxygen used in the *in vivo* model was derived from literature reported values of oxygen consumption in the HL-60 human leukemia cell line (Xu et al, 2005). The rate of oxygen consumption in the HL-60 cell line was reported to be significantly lower than the rate of oxygen consumption in the non-transformed murine macrophage cell line J774A (James et al, 1998; Xu et al, 2005). The intracellular oxygen concentration measured for the J774A cell line, in conjunction with the reported oxygen consumption rates for the transformed HL-60 and non-transformed J774A cell lines (James et al, 1998; Xu et al, 2005), were used to estimate the intracellular concentration of oxygen in the two ALL cell lines under investigation: the Dox resistant (EU1-Res) and the Dox sensitive (EU3-Sens). While this may be an inexact estimate of the actual concentration of oxygen in the cell lines being modeled, it does underscore the limited oxygen environment under which cancer cells proliferate (Vaupel et al, 1998).

Dox transport across the cell membrane, as modeled in the *in vivo* models of Dox bioactivation, was described by a concentration gradient multiplied by the permeability constant of Dox. It has been shown previously in the literature that Dox uptake by cells is characterized by a linear diffusive component as well as a saturable, carrier-mediated component (El-Kareh & Secomb, 2005). A simplified version of the Dox uptake

equation, as presented by El-Kareh et al (El-Kareh & Secomb, 2005), was utilized in the description of Dox bioactivation for the EU1-Res and EU3-Sens cell lines at the high Dox concentration condition. It was assumed that at low Dox concentrations, the saturable, carrier-mediated component of Dox uptake was negligible; therefore for the low Dox concentration condition we utilized a simple diffusion-based equation to describe Dox permeation across the cell membrane (Adimora et al, 2010). Additionally, the permeability constant for Dox at the low Dox concentration was fitted to a value that was 10x higher than the permeability constant for Dox at the high Dox concentration. These results are in line with findings by Ghosn et al. that illustrated an inverse relationship between solute concentration and solute permeability coefficient (Ghosn et al, 2008).

Table 4-3: Initial concentration values of the components that comprise the *in vivo* Dox bioactivation model.

Species	*Abbreviation*	*Initial Condition (M)*	*Reference*
Reduced CPR: (EU1-Res)	CPR_{red}	1.3×10^{-6}	(Watanabe et al, 1994)
Reduced CPR: (EU3-Sens)	CPR_{red}	8.9×10^{-7}	Measured[¥]
Oxidized CPR	CPR_{ox}	0	Assigned
EC quinone Dox	Ex_Dox_q	1.0×10^{-5} / 1.0×10^{-7}	Assigned
IC quinone Dox	In_Dox_q	0	Assigned
IC semiquinone Dox	In_Dox_{sq}	0	Assigned
NADPH: (EU1-Res)	NADPH	3.0×10^{-5}	(Martinovich et al, 2005)
NADPH: (EU3-Sens)	NADPH	5.4×10^{-5}	Measured[¥]
NADP: (EU1-Res)	NADP	3.0×10^{-7}	(Schafer & Buettner, 2001)
NADP: (EU3-Res)	NADP	5.4×10^{-7}	(Schafer & Buettner, 2001)
Molecular Oxygen	O_2	1.5×10^{-9}	(James et al, 1998; Xu et al, 2005)
Superoxide	O_2^-	1.5×10^{-11}	Assigned
Hydrogen Peroxide	H_2O_2	1.5×10^{-11}	Assigned

[¥]Measured = Fold change between the resistant and sensitive cell lines (as described in materials and methods) multiplied by the species concentration value for the resistant cell line

Parameter Fitting

Unknown parameters in the *in vitro* Dox activation model were fitted to *in vitro* experimental data generated by Kostrzewa-Nowak et al. (Kostrzewa-Nowak et al, 2005). The fitted parameter values for the *in vitro* model were then used, where applicable, in the *in vivo* Dox bioactivation model and additional parameter fits were made using experimental data generated from Dox-treated ALL cells.

Table 4-4: Rate expressions and rate constants for the ODEs that comprise the *in vitro* Dox bioactivation models.

Rxn No.	*Expression*	*Parameter*	*Reference*
R_1	k_1 ([CPR_{red}]) ([Dox_q])	$k_1 = 1.2 \times 10^4$ $M^{-1}s^{-1}$	*in vitro* model
R_2	k_2 ([CPR_{ox}]) ([NADPH])	$k_2 = k_1$	*in vitro* model
R_3	k_3 ([O_2]) ([Dox_{sq}])	$k_3 = 3.0 \times 10^5$ $M^{-1}s^{-1}$	(Gewirtz, 1999)
R_4: (EU1-Res)	k_4 ([NADPH]) ([O_2])	$k_4 = 4.2 \times 10^4$ $M^{-1}s^{-1}$	(Koshkin et al, 1997)
R_4: (EU3-Sens)	k_4 ([NADPH]) ([O_2])	$k_4 = 9.7 \times 10^3$ $M^{-1}s^{-1}$	Measured[¥]
R_5	k_5 ([O_2^-]) ([Dox_q])	$k_5 = 5.5 \times 10^7$ $M^{-1}s^{-1}$	*in vitro* model
R_6	k_6 ([O_2^-]) ([O_2^-])	$k_6 = 6.4 \times 10^9$ $M^{-1}s^{-1}$	*in vitro* model
R_7: 10 µM	k_7 ([Ex_Dox_q]) (A)[£]	$k_7 = 1.1 \times 10^{-6/-5}$ cms^{-1}	Fitted[F]
R_7: 100 nM	k_7 ([Ex_Dox_q]) (A)[£]	$k_7 = 1.1 \times 10^{-5}$ cms^{-1}	(Ghosn et al, 2008)
R_8: (EU1-Res)	k_8 ([NADP]) /(k_9 + [NADP])	$k_8 = 1.8 \times 10^{-6}$ Ms^{-1}	Fitted
R_8: (EU3-Sens)	k_8 ([NADP]) /(k_9 + [NADP])	$k_8 = 3.3 \times 10^{-6}$ Ms^{-1}	Measured[¥]
R_9	k_8 ([NADP]) /(k_9 + [NADP])	$k_9 = 5.7 \times 10^{-5}$ M	(Yeh et al, 1987)

[£] $A = 10^{-3}$ (L cm^{-3}) $\times$ 6.15 $\times$ 10^{-6} (cm^2) $\times$ 1 $\times$ 10^9 (cells/L)

[¥] Measured = Fold change between the resistant and sensitive cell lines (as determined by basal SOD and G6PD activity) multiplied by the parameter value for the resistant cell line.

[F] The permeability constant for Dox permeation is non-constant for the duration of Dox treatment. See Materials and Methods/Appendix C for detailed description.

The parameter set of the *in vitro* model contains 6 kinetic parameters and 9 initial conditions. Three of the 6 kinetic parameters that make up the *in vitro* model were fitted to experimentally determined data sets (Table 4-2). In the fitting procedure, the experimental data provided by Kostrzewa-Nowak and colleagues describing the *in vitro* redox cycling and reductive conversion of Dox at varied concentrations of NADPH, Dox, cytochrome P450 reductase (CPR), and superoxide dismutase (SOD) (Kostrzewa-Nowak et al, 2005) were used. Because the model is comprised of a simple network with a relatively small number of parameters, parameter fitting was conducted by minimizing the rudimentary cost function, U:

$$U = \sum_{j=1}^{2} \sum_{k=1}^{11} \left[Y_j^{(th)}(t_k) - Y_j^{(\exp)}(t_k) \right]^2 \qquad (4\text{-}1)$$

Where $Y_j^{(\exp)}(t_k)$ and $Y_j^{(th)}(t_k)$ represent the experimental and theoretical (model predicted) data, respectively, of Dox and NADPH (j = 1,2), at time points t_k = 0, 2, 4, … , 20 minutes (k = 1, 2, … , 11). As an initial approximation of the model parameters to be fitted, parameter values estimated from the literature for similar types of enzyme-catalyzed reactions (Gray & Carmichael, 1992; Light et al, 1981) were used. For fitting purposes, $Y_j^{(\exp)}(t_k)$ and $Y_j^{(th)}(t_k)$ were normalized to their maximal values. All the parameters used in the *in vitro* model are shown in Table 4-2.

The catalysis of semiquinone Dox was modeled by a two-step process involving first the reduction of Dox by CPR followed by electron transfer by NADPH to oxidized CPR. The reaction rate of reduced CPR with quinone Dox (Reaction R_1, Table 4-2) was fitted to the data describing the redox cycling of Dox (Kostrzewa-Nowak et al, 2005); the reaction rate for NADPH reacting with molecular oxygen (Reaction R_4, Table 4-2) was fitted to experimental data showing the reductive conversion of Dox (Kostrzewa-Nowak

et al, 2005); the reaction rate for superoxide anion reacting with quinone Dox (Reaction R_5, Table 4-2) was fitted to experimental data showing the SOD-induced redox cycling of Dox (Kostrzewa-Nowak et al, 2005). The cost function, U, was minimized independently for each fitted parameter because the data used in the fitting procedure were generated from three independent experiments with different sets of initial conditions (Kostrzewa-Nowak et al, 2005). The initial conditions for the *in vitro* model were taken directly from the *in vitro* experiments describing redox cycling, reductive conversion, and SOD-induced redox cycling of Dox (Kostrzewa-Nowak et al, 2005).

The *in vivo* kinetic models of Dox bioactivation were based upon the fitted *in vitro* model of Dox bioactivation. The parameter set of the *in vivo* model contains 10 kinetic parameters, six of which were either taken directly or estimated from the fitted *in vitro* model, and 10 initial conditions. Two of the 10 kinetic parameters that make up the *in vivo* model had to be fitted to experimentally determined data (Table 4-4). In the fitting procedure, 10 μM [Dox] NADPH depletion data for the EU1-Res cell line were used to fit k_8, the parameter that describes the rate of NADPH supply by the G6PD enzyme, and 10 μM [Dox] extracellular Dox depletion data for the EU1-Res cell line were used to fit k_7, the parameter that describes the permeability coefficient of Dox. These parameter fits were conducted for the EU1-Res model only. To determine the fitted parameter value, the following cost function, U, was minimized:

$$U = \sum_{k=1}^{7} [Y^{(\exp)}(t_k) - Y^{(th)}(t_k)]^2, \qquad (4\text{-}2)$$

where $Y^{(\exp)}(t_k)$ and $Y^{(th)}(t_k)$ represent the experimental and theoretical (model predicted) data, respectively, of intracellular NADPH or extracellular Dox for the EU1-Res cell line, at time points t_k = 0, 10, …, 60 minutes (k = 1, …, 7). As an initial

approximation of the model parameter to be fitted, parameter values estimated from the literature were used (Adimora et al, 2010). For the fitting of parameter k_8, $Y^{(\exp)}(t_k)$ and $Y^{(th)}(t_k)$ were normalized to their maximal values to allow for the direct comparison of NADPH absorbance readings, generated experimentally using the spectrophotometer, and NADPH concentration values, generated *in silico* using the computational model. Most of the parameters fitted to the EU1-Res experimental data were used unaltered in the EU3-Sens *in vivo* model. However, to model experimentally determined enzymatic differences between the Dox-resistant EU1-Res cell line and the Dox-sensitive EU3-Sens cell line, the experimentally determined fold change values between the EU1-Res and EU3-Sens cell lines were utilized to estimate appropriate parameter values for the EU3-Sens cell line in relation to the EU-Res cell line. This method was used to determine the EU3-Res cell line rate constants for NOX4-dependent superoxide generation (k_4), SOD-dependent superoxide elimination (k_6), as well as G6PD-dependent NADPH reduction (k_8). Tests of pharmacological interventions were conducted *in silico* using the fitted *in vivo* models of Dox bioactivation and assuming 20% inhibition of each target based on previously published data (Tian et al, 1998).

Materials, cell culture and treatment conditions

All reagents were from Sigma-Aldrich unless otherwise specified. Two ALL cell lines representing major phenotypes of childhood acute lymphoblastic leukemia (EU1-Res and EU3-Sens) have been previously characterized (Zhou et al, 2003a; Zhou et al, 1994). Human acute myelogenous leukemia (Arnelle & Stamler) cell lines exhibiting variable PgP expression and Dox resistance (8226/Pgp-, Dox6/Pgp+, and Dox40/PgP++) were donated by Dr. William Dalton, PhD, MD, of the Moffitt Cancer Center (Tampa, FL, USA) (Dalton et al, 1986). ALL and AML cell lines were cultured in RPM1-1640 medium supplemented with 10% FBS and 100 U/ml of penicillin/streptomycin and

grown in a humidified atmosphere of 5% CO_2 at 37°C. For all experiments, unless otherwise stated, ALL cells were resuspended in fresh media (1×10^6 cells/ml) and treated with various concentrations of Dox (Enzo Life Sciences, PA, USA), protected from light and incubated at 37°C. Phenol-red-free medium was comprised of phenol-red-free RPMI-1640 medium supplemented with 10% FBS and 100 U/ml of penicillin/streptomycin.

Cell viability and apoptosis

ALL cells were treated with a range of Dox concentrations for various time periods. After treatment, cell viability was assayed with the cell proliferation reagent WST1 (Roche Applied Science) according to the manufacturer's protocol, using a Synergy 4 hybrid microplate reader (Biotek, Winooski, VT, USA).

Dox accumulation

ALL cells plated in 96-well plate format (1×10^6 cells/ml) were treated with Dox (10 μM or 100 nM) and protected from light at 37°C. Absorbance was read for 1 h, every 10 min, using a Synergy 4 hybrid microplate reader (Absorbance = 480 nm). The absorbance readings of wells containing media and Dox without any cells, and wells containing cells and media without any Dox, were used as controls.

Dox depletion

After ALL cells were treated with 10 μM Dox, phenol-red free media was removed and analyzed for Dox content using the Synergy 4 hybrid microplate reader (Absorbance = 480 nm). The absorption readings of media from wells containing media and Dox without any cells, and wells containing cells and media without any Dox, were used as controls in the extracellular Dox depletion studies.

$DiOC_2$ dye efflux

$DiOC_2$ [3,3'-Diethyloxacarbocyanine iodide] dye (Anaspec Inc.) efflux studies were conducted on ALL and AML cells. 12×10^6 ALL and AML cells were independently resuspended in 12 ml fresh ALL cell media and incubated for 2 h at 37°C in a humidified atmosphere. After incubation, cells were pelleted by centrifugation for 8 min at 300 ×g. Supernatant was discarded and 12 ml of fresh media were used to resuspend the cells. 3 ml of the 12 ml were transferred to a new tube to serve as a negative control. To the remaining 9 ml, $DiOC_2$ was added to a final concentration of 60 ng/ml. All tubes were incubated for 30 min at 37°C in a water bath, gently agitating the tubes every 5 min to ensure adequate mixing. After 30 min incubation, cells were pelleted by centrifugation for 8 min at 300 ×g. Supernatant was discarded and cells were resuspended in fresh media (3 ml and 9 ml, respectively). The control tube was placed on ice immediately and the total volume in the other tube was divided into three equal parts and placed in three separate tubes. The first aliquot was placed on ice immediately; this was used for the baseline measurement of $DiOC_2$ uptake. The cells in the remaining two tubes were pelleted and resuspended in 9 ml of fresh media and incubated for 90 min at 37°C, to measure dye efflux. After 90 min, cells in all tubes were washed with cold PBS and then pelleted. Cell pellets were resuspended in fresh media (4°C) to a final cell concentration of 1×10^6 cells/ml. Propidium Iodide was added at a concentration of 1 µg/ml to exclude dead cells. Intracellular dye content was then analyzed by flow cytometry ($DiOC_2$: Ex = 488 nm, Em = 500 nm).

NADPH Measurement

ALL cells plated in 96-well plate format treated with Dox (10 µM or 100 nM) were protected from light at 37°C. Absorbance was read for 1 h, every 10 min, using a Synergy 4 hybrid microplate reader (Absorbance = 340 nm). The absorption readings of wells containing media and Dox without any cells, and wells containing cells and media

without any Dox, were used as controls. In addition, the absorbance readings of wells containing media and peroxide without any cells, and wells containing media and peroxide with cells, were used as positive controls for NADPH depletion.

Cellular fractionation and ER isolation

Dox-treated and untreated cells were pelleted by centrifugation for 5 min at 300 × g. Cytoplasmic fractions were obtained by lysing in 2% NP-40 buffer containing 50 mM β-glycerophosphate, 10 mM NaPP, 30 mM NaF, 50 mM Tris-HCL, pH 7.5, 150 mM NaCl, 1 nM benzamidine, 2 nM EGTA, 100 µM sodium orthovanadate, 1 mM DTT, 10 µg/ml aprotinin, 10 µg/ml leupeptin, 1 µg/ml pepstatin, 1 µg/ml microcystin-LR, and 1 mM PMSF. Cells were lysed on ice for 1 h, followed by centrifugation for 10 min at 300 ×g. For CPR activity analysis, endoplasmic reticulum (ER) isolation from Dox-treated and untreated cells was conducted using the ER isolation kit (Sigma-Aldrich) according to the manufacturer's protocol.

Enzyme Activity Measurements

Basal G6PD and CPR activities were determined in EU1-Res and EU3-Sens cells using the Glucose-6-Phosphate Dehydrogenase Assay Kit (BioVision, Mountain View, CA, USA), and the Cytochrome c Reductase (NADPH) Assay Kit (Sigma), respectively, according to the manufacturers' protocols. SOD activity was determined using the Superoxide Dismutase Activity Colorimetric Assay Kit according to the manufacturer's protocol (AbCam, MA, USA).

qRT PCR Measurements

RNA was isolated from cells using the RNeasy isolation kit with RNase-free DNase set according to the manufacturer's protocol. 1 µg of RNA was used for reverse transcription. For detection of mRNA levels, a custom RT2 Profiler PCR Array was used,

according to the manufacturer's protocol. The following PCR conditions were used: 10 min at 95°C; 40 cycles of 1 minute at 60°C and 15 seconds at 95°C; melt curve with ramp from 60°C to 95°C. PCR reactions were run using the Applied Biosystems Step One Plus system. Results were normalized to the expression of β-actin. Relative expression levels were calculated using the ΔCT method ($2^{-\Delta CT}$). All arrays were performed with triplicate sets of RNA isolation for each cell line for statistical analysis.

Intracellular ROS determination

For determination of Dox-induced $O_2^{\bullet-}$ formation, cells were plated at a density of 1×10^6 cells/ml and pre-incubated with 50 μM Hydro-Cy5 dye (Kundu et al, 2009) resuspended in DMSO for 15 min. After pre-incubation, 10 μM Dox was added to respective wells and kinetic fluorescence readings were taking with the microplate reader every 10 min for 1 h (Ex = 635 nm, Em = 660 nm). Unstimulated cells, pre-incubated with and without Hydro-Cy5 dye, and phenol red-free media, pre-incubated with and without Hydro-Cy5 dye and Dox, respectively, were used as controls.

Statistical Analysis

All values reported are the average of three or more independent biological replicates +/- standard error. Statistical significance is based upon the criteria of $p < 0.05$ for a Student's t-test (two-tailed, equal variance).

Results

A computational model describes in vitro Dox bioactivation

To investigate the mechanisms that control Dox bioactivation, a kinetic mathematical model of the Dox bioactivation network in a cell free system was developed (Fig. 4-1). From here on, the term *in vitro* shall refer to acellular systems and the term *in vivo* shall refer to cellular systems. The *in vitro* model was used to reproduce previously published *in vitro* data generated by Kostrzewa-Nowak et al on the effect of NADPH concentration on Dox bioactivation (Kostrzewa-Nowak et al, 2005). In the model, the reaction of NADPH with molecular oxygen was allowed; however, it was assumed it to be non-enzymatic since NADPH oxidase was not present in the cell free reaction mixtures. The inclusion of the NADPH / O_2 reaction in the bioactivation network model was particularly important because it provided a mechanistic pathway by which increased NADPH concentration could lead to enhanced Dox reductive conversion. Reductive conversion of Dox is characterized by conservative NADPH depletion and quinone Dox transformation, while redox cycling of Dox is characterized by rapid NADPH depletion and sustained quinone Dox. The *in vitro* model was capable not only of describing the switch in behavior between reductive conversion and redox cycling of Dox (Fig. 4-1 A, B) based upon the high and low NADPH concentrations, but it was also capable of replicating a new experimental condition: upon inclusion of SOD activity in the bioactivation network, the model demonstrated SOD-induced redox cycling of Dox at high NADPH concentration (Fig. 4-1 C) (Kostrzewa-Nowak et al, 2005).

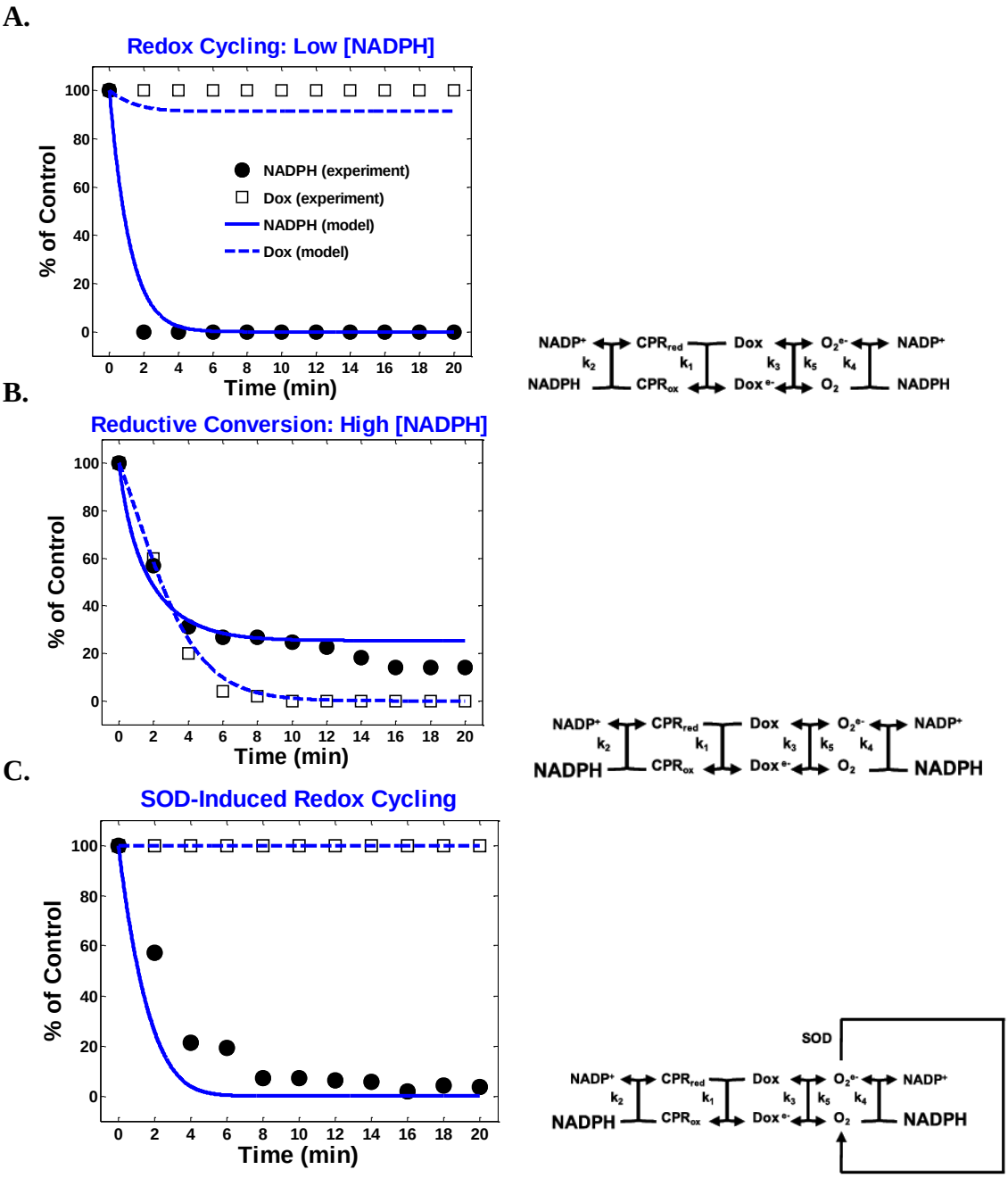

Figure 4-1. Three proposed mechanisms for *in vitro* Dox bioactivation. (A-C) Experimental data (Kostrzewa-Nowak et al, 2005) and model-fitted results for different Dox bioactivation pathways accompanied by a schematic representation of the hypothesized network underlying each pathway. The reaction of NADPH with O_2 (k_4) is a proposed reaction believed to be essential for the accurate description of NADPH-dependent Dox bioactivation. Large fonts denote experimental conditions in which the [NADPH] was increased from 100 µM to 500 µM.

Dox sensitivities and bioactivation network components differ in EU1 and EU3 ALL cells

The validated *in vitro* model of Dox bioactivation emphasizes the importance of the reaction between NADPH and molecular oxygen in the accurate representation of Dox bioactivation. Moreover, the model illustrates how the driving force of [NADPH] and levels of SOD can control the switching between reductive conversion and redox cycling. It was therefore hypothesized that the intrinsic differences in protein expression and redox state between leukemia cells could similarly give rise to shifts in control between these two processes, conferring differences in Dox cytotoxicity. In support of this hypothesis, others have observed that treatment of the HL60 human leukemia cell line with bioactivated Dox led to increased cytotoxic activity compared to treatment with nonactivated, or redox cycled, Dox (Kostrzewa-Nowak et al, 2005). These findings suggest that reductive conversion of Dox may be an important determinant of Dox toxicity in leukemia cells. To further investigate this possibility by computational modeling, the characterization of the Dox sensitivities of two ALL cell lines, EU1 (EU1-Res) and EU3 (EU3-Sens), that were previously reported to have over a 10-fold difference in IC50 to Dox (Zhou et al, 2003a), was conducted. The EU1-Res line displayed limited toxicity to Dox treatment, retaining greater than 100% viability even after exposure to 10 μM Dox for 3 h, whereas the EU3-Sens cell line showed decreased viability after exposure to Dox at concentrations as low as 40 nM for the same treatment duration (Fig. 4-2 B).

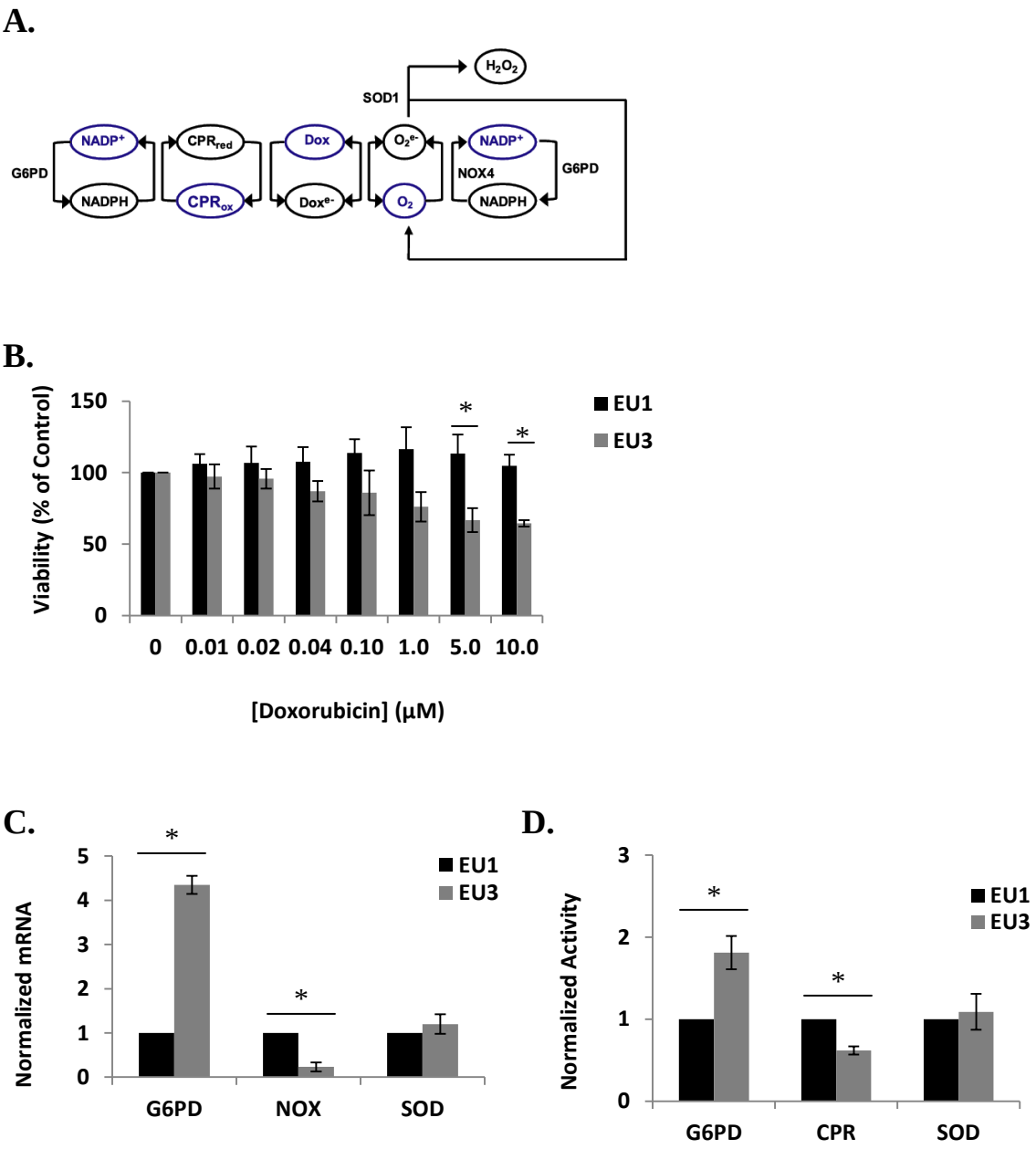

Figure 4-2. Dox sensitivity and bioactivation network components differ in EU1 and EU3 ALL cells. (A) Scheme describing *in vivo* Dox bioactivation. (B) Cell viability for EU1-Res and EU3-Sens cells, determined by WST1 assay, after 3 h Dox treatment at varied concentrations. (C-D) Relative mRNA levels and enzyme activities of enzymes involved in Dox bioactivation in ALL cells. (*$p < 0.05$)

The cellular bioactivation network differs from the *in vitro* one by the inclusion of additional pertinent biochemical reactions (Fig. 4-2 A). The relative mRNA expression levels and activities of the enzymes involved in cytosolic Dox bioactivation were characterized (Fig. 4-2 C-D) for the two cell lines under investigation. G6PD enzymatic activity is the primary source for regenerating reduced NADPH in normal metabolism (Tome et al, 2006) and NADPH oxidases rely on oxygen and NADPH to produce superoxide. It has been previously reported that NOX activity is involved in Dox-induced cell death, implicating NOXs in the cellular Dox bioactivation network (Gilleron et al, 2009). NOX4 is the NADPH oxidase isoform that controls constitutive superoxide production, whereas other isoforms are considered to be activated during signal transduction (Serrander et al, 2007). The EU1-Res cells contain significantly higher NOX4 mRNA levels and CPR activity, compared to the EU3-Sens cells ($p < 0.05$) (Fig. 4-2 D). EU1-Res cells have significantly lower G6PD mRNA levels (Fig. 4-2 C) and activity (Fig. 4-2 D) ($p < 0.05$) compared to the EU3-Sens cells. There was no significant difference in the levels of SOD1 mRNA, or SOD1 activity, between the EU1-Res and EU3-Sens cells (Fig. 4-2 C, 4-2 D). There was a direct correlation between mRNA expression and enzyme activity for the enzymes under consideration.

Cell line specific differences in Dox bioactivation for ALL cells

To examine whether differences in mRNA expression levels and activities of Dox bioactivation enzymes would result in differences in Dox bioactivation between the EU1-Res and EU3-Sens cell lines, intracellular Dox accumulation was measured in the ALL cells for 1 h during a 10 μM Dox treatment. The EU1-Res cells had significantly higher quinone Dox accumulation compared to the EU3-Sens cells, starting at 40 min of treatment and lasting for the remaining treatment duration ($P < 0.05$) (Fig. 4-3 A).

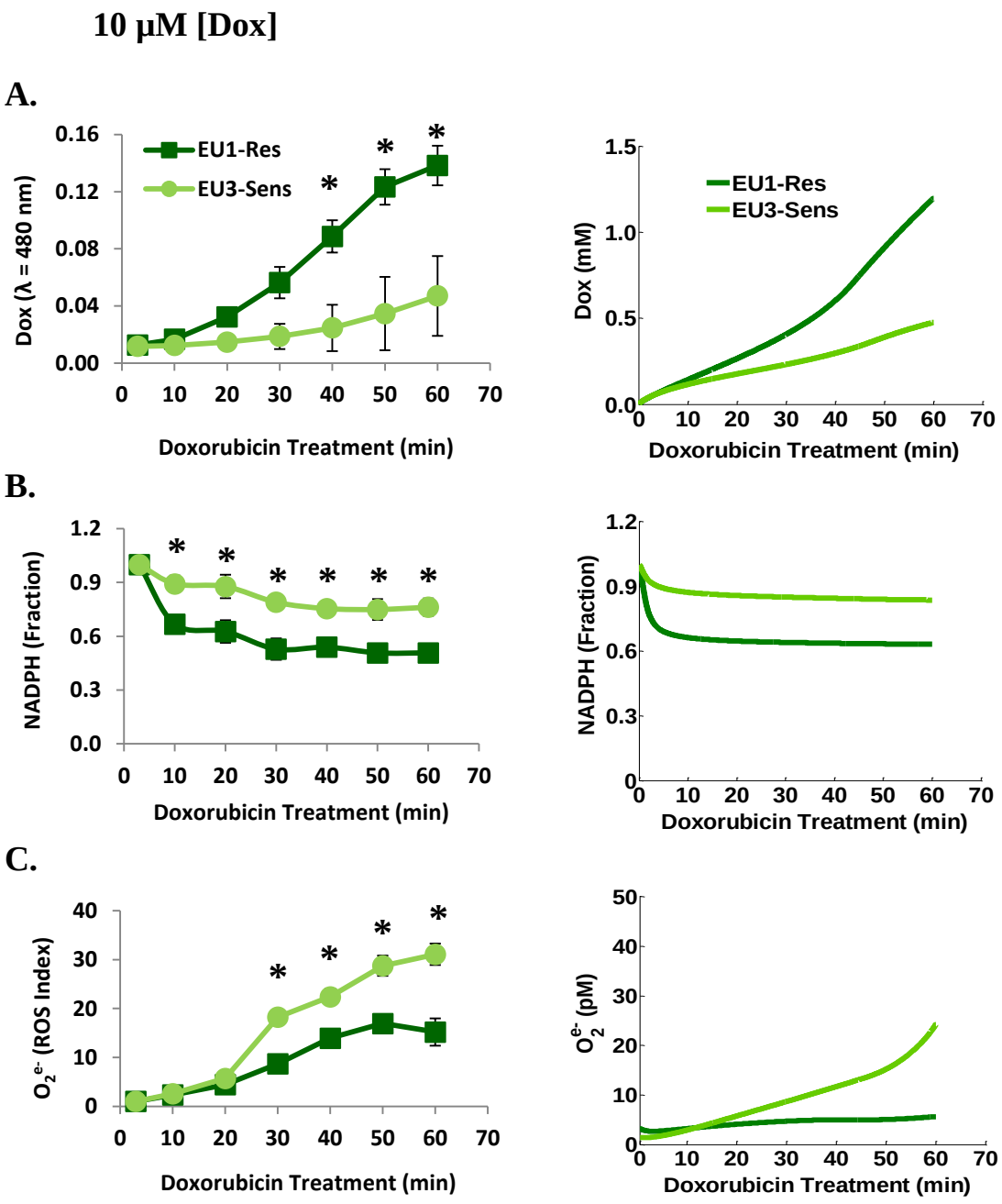

Figure 4-3. Cell-line-dependence of Dox bioactivation. Experimentally-determined and model-predicted quinone Dox accumulation (A), Dox-induced NADPH depletion (B), and Dox-induced superoxide generation (C) in ALL cells treated with 10 µM Dox for 1 h (*$p < 0.05$).

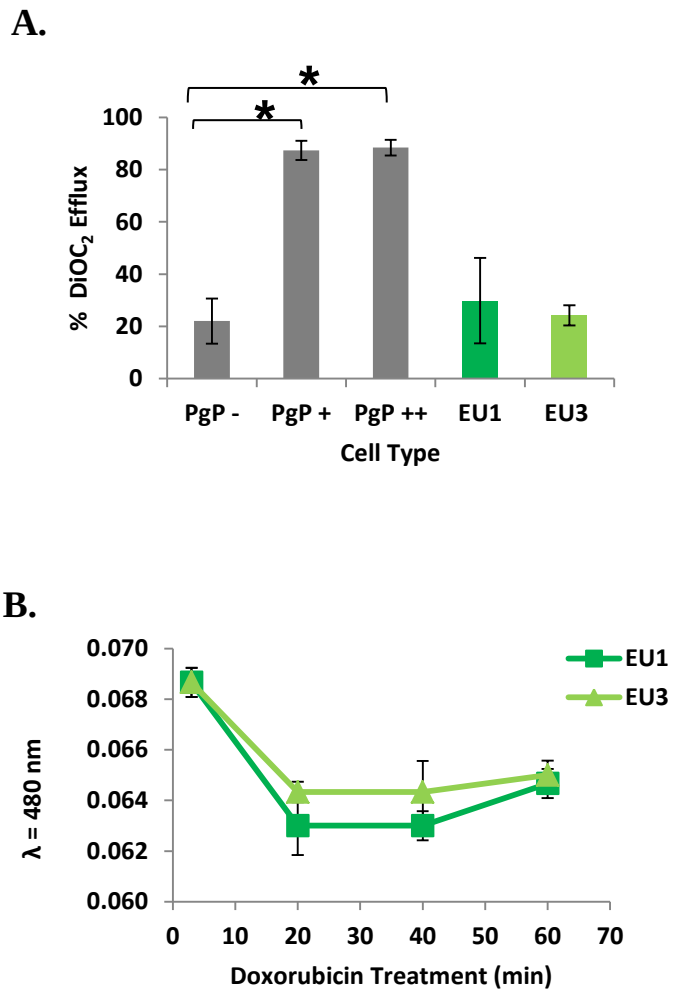

Figure 4-4. Dox transport is equivalent across ALL cell lines. (A) Dye efflux characterization for ALL and AML cell lines indicating that the Dox-resistant EU1 cells and the Dox-sensitive EU3 cells are not significantly different, regarding their PgP activities, from the PgP- AML cell line. (*$p < 0.05$). (B) Extracellular Dox depletion for Dox-resistant EU1 and Dox-sensitive EU3 cells. ([Dox] = 10 µM for 1 h; *$p < 0.05$)

These results were not a function of differential Dox efflux/influx as both the EU1-Res and EU3-Sens cells displayed negligible PgP efflux activity, and the rate of Dox consumption from the cell medium was not significantly different between the cells (Fig. 4-4 A, Fig. 4-4 B). Because NADPH depletion and superoxide production can be indicators for the extent of Dox reductive conversion that has taken place within a cell (Kostrzewa-Nowak et al, 2005), Dox-induced NADPH depletion and superoxide generation were monitored in both cell lines. NADPH depletion due to 10 μM Dox treatment was significantly lower in the EU3-Sens cells compared to the EU1-Res cells, starting as early as 10 min into the treatment regimen and continuing the trend for the duration of the treatment ($p < 0.05$) (Fig. 4-3 B). Dox-induced superoxide generation, measured by HydroCy5, a molecular probe with specificity for $^{\bullet}OH$ and $O_2^{\bullet-}$ (Kundu et al, 2009), was significantly higher in the EU3-Sens cells than in the EU1-Res cells starting 30 min into the treatment regimen and lasting for the remainder of the treatment duration ($p < 0.05$) (Fig. 4-3 C).

Two *in vivo* models were generated for the EU1-Res and EU3-Sens cells based upon the network structure depicted in Figure 4-2 A (See Materials and Methods). The differences in quinone Dox accumulation (Fig. 4-3 A) and superoxide generation (Fig. 4-3 C) between the EU1-Res and EU3-Sens cells were accurately captured by the kinetic model simulations. Although kinetic model simulations of Dox-induced NADPH depletion were able to reproduce the depletion trends seen in both the EU1-Res and the EU3-Sens cells, the magnitude of NADPH-depletion in both cell lines was slightly underestimated compared to experimental results (Fig. 4-3 B). Both experimental measurements and model simulations of Dox-induced intracellular Dox accumulation, NADPH depletion, and superoxide generation suggest that the extent of Dox reductive conversion in EU1-Res and EU3-Sens cells differ significantly. The EU1-Res cells exhibited higher quinone Dox accumulation, more NADPH depletion, and lower superoxide generation, which are all consistent with decreased reductive

conversion/increased redox cycling, as evidenced by the data generated by the validated *in vitro* model. Conversely, the EU3-Sens cells exhibited lower quinone Dox accumulation, lower Dox-induced NADPH depletion, and higher Dox-induced superoxide generation, which are consistent with the *in vitro* conditions that characterize increased Dox reductive conversion (Fig. 4-1 B, Fig. 4-3 A-C). These results suggest an intrinsic mechanistic switch between redox cycling and reductive conversion that takes place in the EU1-Res and EU3-Sens cells, one that is a function of cell-specific levels of intracellular Dox bioactivation components.

Concentration-dependence of Dox bioactivation in ALL cells

Because the apparent switch between redox cycling and reductive conversion appeared to be driven by different catalytic rates within the drug metabolism network, the question was asked as to whether the concentration of Dox would affect the behavior of the coupled redox reactions. To examine whether differences in the Dox concentration applied to the cells could alter the Dox bioactivation profile of the EU1-Res and EU3-Sens cells, intracellular Dox accumulation, Dox-induced NADPH depletion and Dox-induced superoxide generation were again analyzed in the ALL cells for 1 h during a 100 nM Dox treatment regimen. The 100 nM Dox concentration represents a 100-fold change in Dox concentration compared to the 10 μM Dox treatment regimen that had been previously administered to the cells. Experimental results show that the overall shape of the quinone Dox accumulation curve for both ALL cells at the 100 nM Dox treatment level was significantly different that that seen for the 10 μM level. At the 10 μM Dox treatment level, there was a steady increase in the accumulation of quinone Dox in both cell lines as a function of time, although the rate of increase was higher in the EU1-Res cells than the EU3-Sens cells (Fig. 4-3 A). Conversely, at the 100 nM Dox treatment level, there was a rapid increase in quinone Dox accumulation at 10 min, but this increase was followed by a sharp decrease in intracellular quinone Dox which then appeared to

equilibrate to a steady state level that was maintained for the rest of the treatment duration (Fig. 4-5 A). Additionally, for the 100 nM Dox treatment regimen, the intracellular quinone Dox levels in the EU1-Res cells were significantly lower than those seen in the EU3-Sens cells ($p < 0.05$) (Fig. 4-5 A), representing a complete switch in behavior compared to that seen at the 10 μM Dox treatment level (Fig. 4-3 A). Without additional parameter fitting, the kinetic simulation of the low Dox treatment condition was able to capture the decreased amounts of quinone Dox observed in the EU1-Res cells, compared to the EU3-Sens cells, as well as the general shape of the intracellular quinone Dox accumulation curve (Fig. 4-5 A), providing further validation of the quality of the cell-line specific models for explaining the complex responses that were observed experimentally.

The Dox-induced NADPH depletion in the EU1-Res cells was not significantly different from that seen in the EU3-Sens cells (Fig. 4-5 B). While model simulations accurately predicted similar NADPH depletion trends between EU1-Res and EU3-Sens cells, the underestimation of NADPH depletion in the model simulations was still apparent at the 100 nM Dox concentration condition (Fig. 4-5 B). Differences in Dox-induced superoxide generation between the EU1-Res and EU3-Sens cells were negligible (Fig. 4-5 C) and kinetic model simulations of Dox-induced superoxide generation accurately captured this behavior. The lack of sustained accumulation of quinone Dox in both the EU1-Res and EU3-Sens cells, paired with the experimentally determined NADPH depletion and superoxide generation profiles at the 100 nM Dox treatment condition, suggest that both the EU1 and EU3 cells undergo a shift in the control of their Dox metabolism profiles as a result of changes in the Dox treatment condition applied.

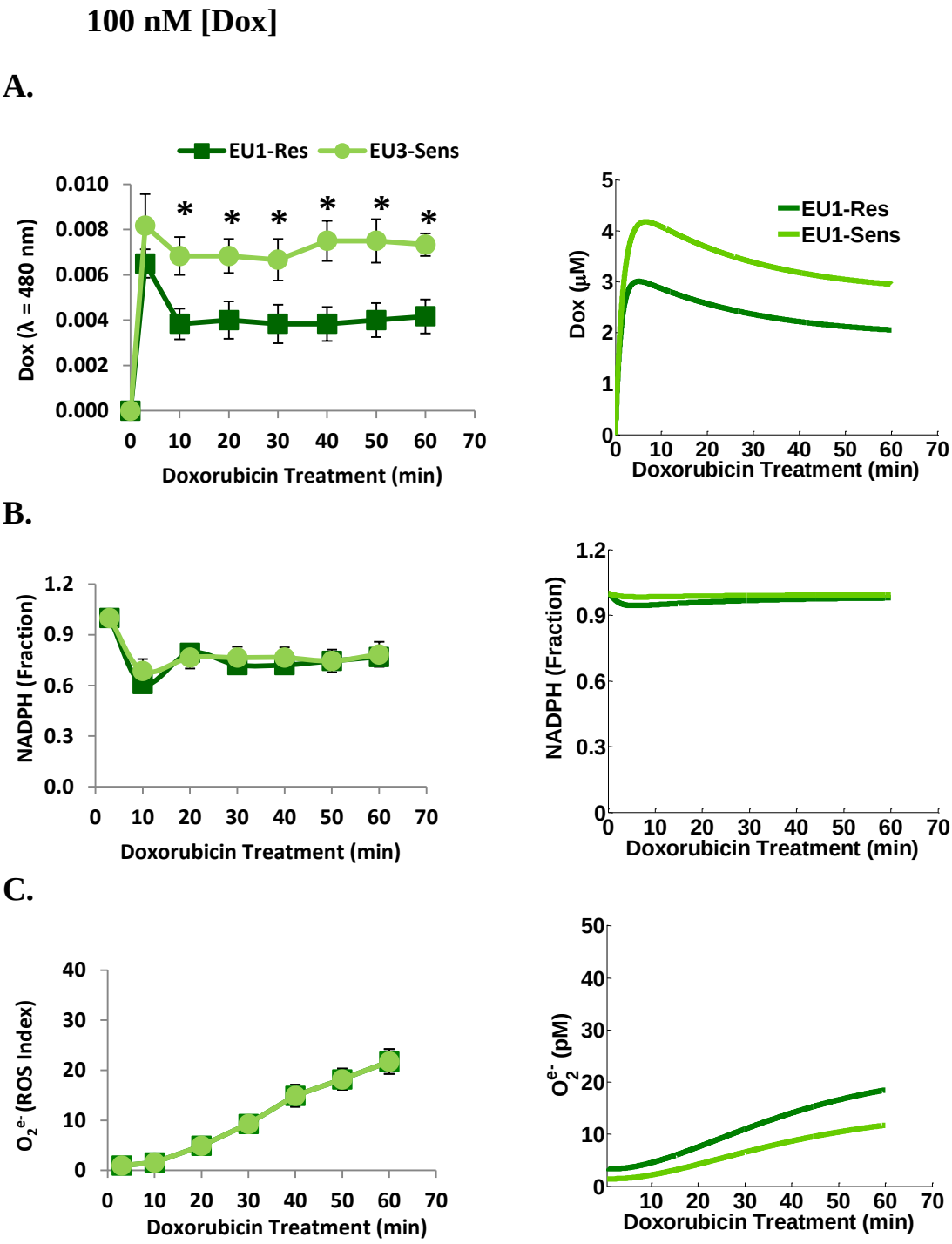

Figure 4-5. Concentration-dependence of Dox bioactivation in ALL cells. Experimentally-determined and model-predicted quinone Dox accumulation (A), Dox-induced NADPH depletion (B), and Dox-induced superoxide generation (C) in ALL cells treated with 100 nM Dox for 1 h (*$p < 0.05$).

Model-generated hypotheses of altered NADPH and quinone Dox dynamics are confirmed by pharmacological intervention in drug-sensitive cells

Concentration-dependent differences in Dox bioactivation exist between the EU1-Res and the EU3-Sens cells (Fig. 4-3, Fig. 4-5). Based on these differences, it was hypothesized that successful intervention strategies for altering the behavior of the Dox bioactivation network within ALL cells would be Dox concentration-dependent. To test this hypothesis in the EU3-Sens cell line, a series of pharmacological intervention strategies was carried out, for both the 10 μM and the 100 nM Dox concentration condition; these strategies were aimed at decreasing the amount of Dox reductive conversion that occurs within the EU3-Sens cells. The capacity for NADPH regeneration (k_8/k_9) was adjusted using the pharmacological G6PD inhibitor, DHEA. NADPH regeneration was modified because NADPH is involved in the CPR- and oxygen-dependent enzymatic reactions that play a role in reductive conversion and redox cycling of Dox, respectively (Fig 4-2). Furthermore, simulations of G6PD inhibition on Dox bioactivation in EU3-Sens cells for the 10 μM Dox concentration condition predicted an appreciably increased accumulation of quinone Dox and an increased depletion of NADPH over one hour (Fig. 4-6 A, B). These processes are indicative of increased redox cycling of Dox, at the expense of Dox reductive conversion, and are similar to the dynamics that occur in the Dox-resistant EU1-Res cells (Fig. 4-3 A). Model predictions were confirmed through pharmacological modification of G6PD activity by the G6PD inhibitor, DHEA, for the 10 μM Dox concentration condition (Fig. 4-6 A, B).

Next, we utilized the kinetic model to simulate the effect of G6PD inhibition on Dox reductive conversion in EU3-Sens cells for the 100 nM Dox concentration condition. The model predicted that inhibition of G6PD activity in the EU3-Sens cells would have no effect on the accumulation of quinone Dox or the depletion of NADPH over one hour (Fig. 4-6 A, B). The *in silico* model predictions of the behavior of the Dox bioactivation

network after pharmacological intervention at the 100 nM Dox concentration condition were also confirmed (Fig. 4-6 A, B).

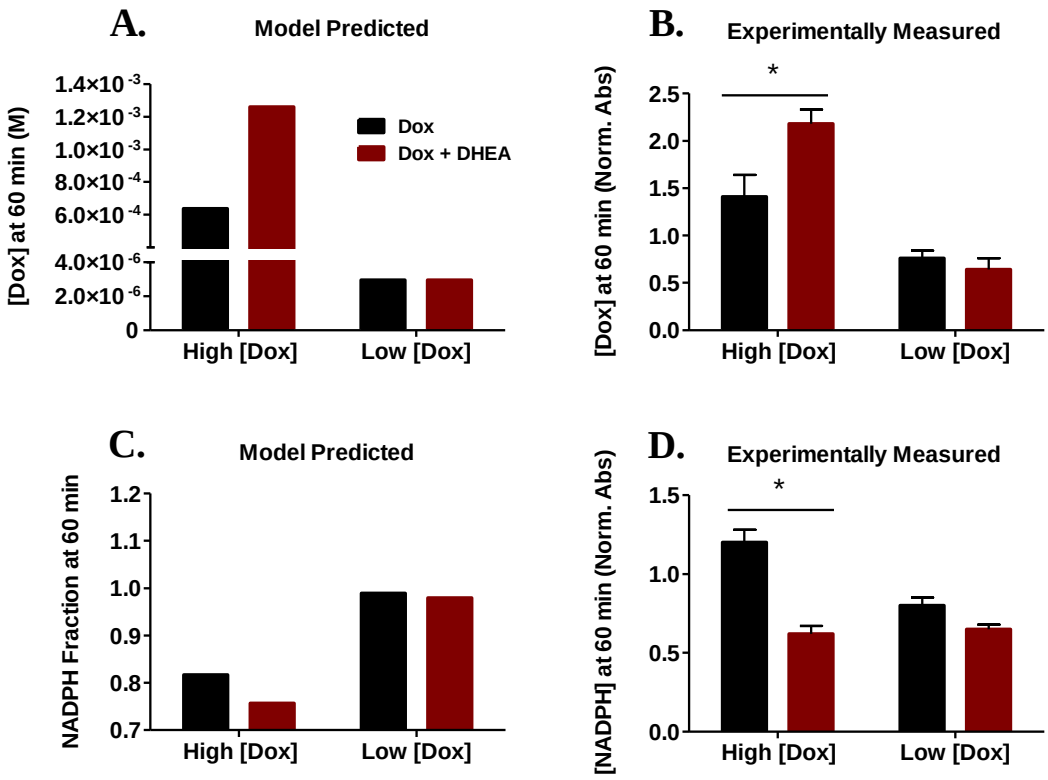

Figure 4-6. Effects of pharmacological intervention on Dox reductive conversion in EU3-Sens cells. (A) Model-predicted and experimentally determined quinone Dox accumulation in EU3-Sens cells, with and without DHEA intervention, at the 10 µM and 100 nM Dox concentration conditions. (B) Model-predicted and experimentally determined NADPH depletion in EU3-Sens cells, with and without DHEA intervention, at the 10 µM and 100 nM Dox concentration conditions. (DHEA = 10 µM, 24 h; *$p < 0.05$)

NADPH supply alters viability of Dox-treated ALL cells by controlling semiquinone Dox formation and superoxide generation in a Dox concentration-dependent manner.

To further explore the concentration-dependent effects of DHEA treatment on Dox bioactivation, the cellular network models of Dox bioactivation were used to quantify the fluxes of semiquinone Dox formation and superoxide generation in both the EU1-Res and EU3-Sens cells with and without DHEA treatment. Analyses indicate that inhibition of NADPH production by G6PD at 10 μM Dox concentration leads to a decrease in the formation of semiquinone Dox in both the EU1-Res and EU3-Sens cells (Fig. 4-7 A), but has no effect on the accumulation of semiquinone Dox in either cell line at the 100 nM Dox condition. Because DHEA will indirectly impact the NADPH-dependent NOX4 by substrate limitations, we also analyzed superoxide fluxes. The models demonstrate that DHEA decreases $O_2^{\bullet-}$ production in all conditions and cell lines except the EU3-Sens cells at the 10 μM Dox treatment condition (Fig. 4-7 B).

To relate the model findings to experimentally determined changes in cell viability, we analyzed both EU1-Res and EU3-Sens cell survival for the different Dox treatment conditions using a WST1 cell viability assay. Corresponding to our model simulated predictions of quinone Dox accumulation (Fig. 4-6 A), NADPH depletion (Fig. 4-6 B) and semiquinone Dox flux (Fig. 4-7 A), we observed that DHEA was able to rescue EU3-Sens cells from Dox-induced cytotoxicity at the 10 μM Dox concentration condition. Conversely, we found that DHEA treatment at the 10 μM Dox concentration condition significantly decreased cell viability of the EU1-Res cells ($p < 0.05$) (Fig. 4-7 C). At the low Dox concentration condition, DHEA treatment still enhanced Dox toxicity in the EU1-Res cells (Fig. 4-7 C), to a similar degree. However, in the EU3-Sens cells, DHEA treatment at the 10 μM Dox concentration condition enhanced Dox toxicity (Fig. 4-7 C), rather than prevent it.

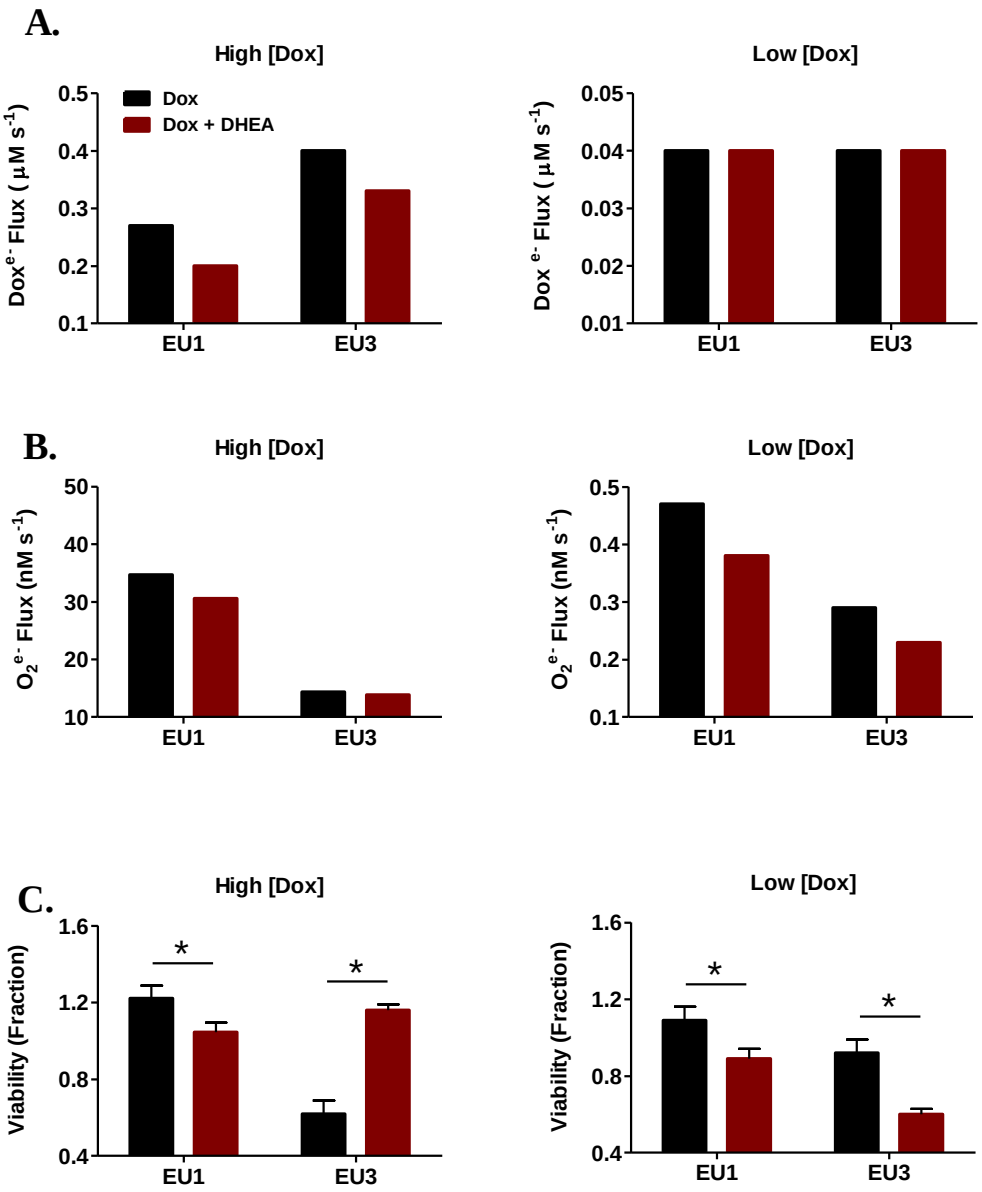

Figure 4-7. NADPH supply alters Dox sensitivity in ALL cells in a concentration- and cell-dependent manner. (A) *in silico* model predictions of NADPH-dependent semiquinone Dox flux in ALL cells, with and without DHEA intervention, at the 10 µM and 100 nM Dox concentration conditions. (B) *in silico* model predictions of NADPH-dependent superoxide flux in ALL cells, with and without DHEA intervention, at the 10 µM and 100 nM Dox concentration conditions. (C) Experimentally determined (WST1 assay) cell viability for ALL cells after 3 h Dox treatment, at the 10 µM and 100 nM Dox concentration conditions. (DHEA = 10 µM, 24 h; *$p < 0.05$)

Discussion

Although the anthracycline drug Dox is used clinically for the treatment of leukemias and solid tumors (Berlin & Haseltine, 1981; Gilleron et al, 2009; Kostrzewa-Nowak et al, 2005), the efficacy of Dox treatment is limited by the development of drug resistance (Akman et al, 1990; Doroshow et al, 1991; Sinha et al, 1989b). Evidence points to the reductive conversion of Dox as an important 'first step' in the regulation of Dox toxicity (Akman et al, 1990; Gilleron et al, 2009; Kostrzewa-Nowak et al, 2005; Sinha & Chignell, 1979; Sinha et al, 1989b). While the Dox bioactivation network has been studied extensively, with the overall network structure for cytosolic Dox bioactivation having been deciphered and believed to be conserved across different cell types (Bachur et al, 1979; Cummings et al, 1992; Sinha et al, 1989b), the adaptation of the bioactivation network to changes in the levels of system components or changes in Dox concentration is much less well understood. This study illustrated the dynamic nature of the Dox bioactivation network and revealed the sensitivity of the Dox bioactivation network to network component levels and Dox concentrations. This study illustrated how the intracellular Dox bioactivation network is capable of executing multiple modes of Dox metabolism; the network contains toxicity-generating and ROS-generating reactions that control Dox metabolism via reductive conversion or redox cycling. Finally, this study illustrated how the reactions that comprise the Dox bioactivation network can be modulated by pharmacological intervention strategies to either enhance or hinder Dox toxicity in a concentration-dependent manner.

Validation of an *in vitro* Dox bioactivation model suggested that the reaction of molecular oxygen with NADPH is a necessary and significant component of the overall Dox bioactivation network. By analyzing the *in vitro* Dox bioactivation network under the distinctively different conditions described by Kostrezewa-Nowak et al (Kostrzewa-Nowak et al, 2005), three distinct pathways of Dox metabolic conversion were revealed:

CPR-independent redox cycling, CPR-dependent redox cycling, and reductive conversion.

The CPR-independent redox cycling of quinone Dox is the first method by which Dox can be metabolically altered (Fig. 4-1 A). This form of redox cycling of Dox dominates when NADPH is limited. The *in vitro* system has no way of recycling oxidized NADPH once it has reacted with oxidized CPR; the result of this limitation is that when reduced NADPH has been fully consumed, the reduction of quinone Dox by CPR can no longer take place. At this point, the only reactions that can occur are the oxygen-dependent redox cycling reactions of Dox (k_3 / k_5), which result in a zero net transformation of the quinone Dox molecule and the generation of superoxide.

The second Dox metabolic pathway to consider is the CPR-dependent redox cycling of Dox. CPR-dependent redox cycling of Dox is very similar to CPR-independent redox cycling of Dox in that there is a zero net transformation of quinone Dox into its semiquinone form (Fig. 4-1 C). However, whereas CPR-independent redox cycling takes place at low [NADPH] conditions, CPR-dependent redox cycling takes place when high concentrations of NADPH and molecular oxygen are present simultaneously. When these two conditions are met, the rapid reduction of quinone Dox via CPR occurs, maintained by the high levels of NADPH in the system; the rapid reoxidation of semiquinone Dox by molecular oxygen also occurs, maintained by the SOD-dependent regeneration of molecular oxygen. The analogous *in vivo* scenario was observed in both the EU1-Res and EU3-Sens cells at the low Dox concentration condition (Fig. 4-5 A-C). The NADPH fraction for both cell lines was maintained at a nearly constant level due to the non-enzymatic reactions defined by k_3 / k_5. Superoxide is produced as a byproduct to a significant degree for a 100-fold lower Dox treatment due to CPR-dependent redox cycling.

The third and final Dox metabolic pathway to consider is the reductive conversion of Dox. When the flux of Dox semiquinone production exceeds the flux of Dox

semiquinone consumption, there is a net transformation of quinone Dox into its semiquinone form (Fig. 4-1 B). Dox reductive conversion dominates at the *in vitro* high [NADPH] condition because there is enough NADPH to support the CPR-mediated reduction of quinone Dox, forcing Dox semiquinone production to overwhelm Dox semiquinone consumption by molecular oxygen. Furthermore, the increased NADPH level diminishes oxygen-dependent semiquinone Dox consumption (k_5) because NADPH effectively competes with semiquinone Dox for molecular oxygen. The dominance of reductive conversion, *in vivo*, was observed with the EU3-Sens cells during the 10 μM Dox treatment regimen (Fig. 4-3 A). This behavior occurred because as the EU3-Sens cells have an increased capacity to reduce oxidized NADPH, evidenced by their higher G6PD mRNA and activity levels, they can drive a stronger flux through CPR than their EU1-Res counterparts (Fig. 4-3 A).

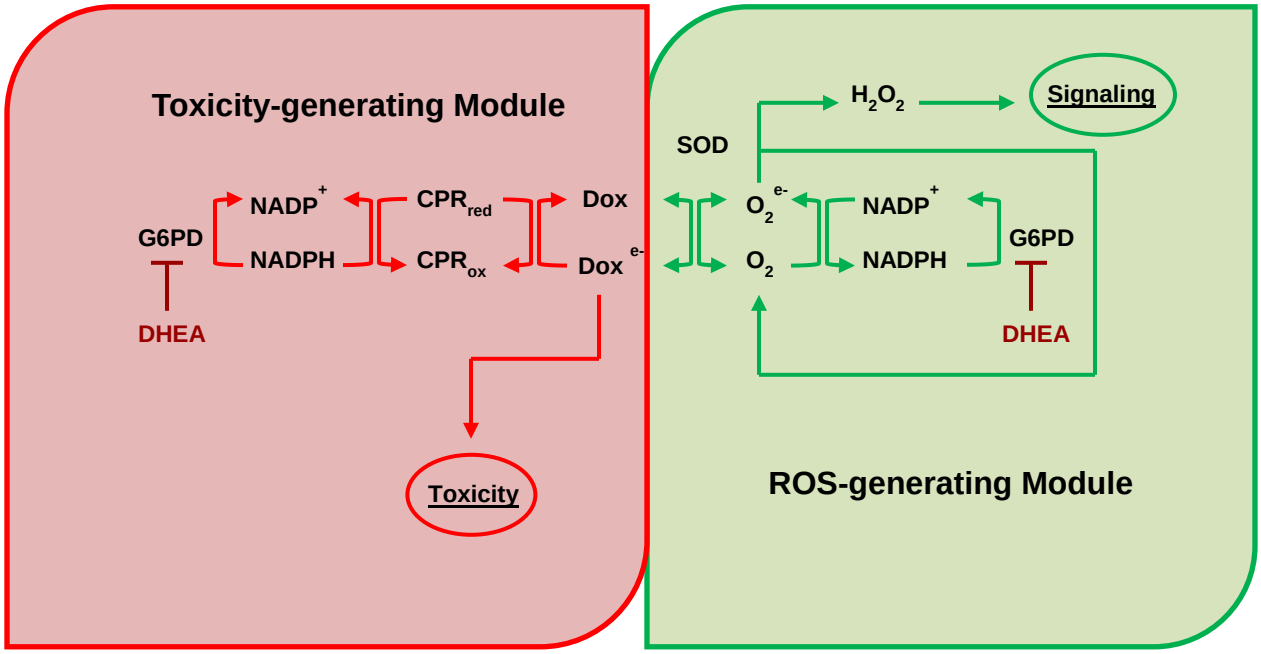

Figure 4-8. Proposed model of Dox metabolism in ALL cells that emphasizes the toxicity-generating and signal-generating modules that comprise the network. The toxicity-generating module is NADPH-limited at the high Dox condition, allowing DHEA administration to decrease NADPH-dependent semiquinone Dox formation. The signal-generating module is NADPH-limited at the low Dox condition, allowing DHEA administration to decrease NADPH-dependent superoxide formation. (DHEA = 10 µM, 24 h; *$p < 0.05$)

After investigating the NADPH-dependent Dox semiquinone and superoxide fluxes that occur during Dox treatment of EU1-Res and EU3-Sens cells, at both the high and the low Dox concentration conditions, and comparing these model generated fluxes to experimental viability studies (Fig. 4-7 C), it was concluded that the Dox bioactivation network is comprised of a toxicity-generating module and a ROS-generating module that likely is implicated in additional signaling (Fig. 4-8). The models suggest that at different Dox concentrations, certain components become limiting in either the toxicity-generating module or the ROS-generating module, and these limiting components effectively determine the extent of Dox toxicity that a cell will experience.

Prior *in vitro* biochemical studies have established a minimal concentration of NADPH that is required to promote the reductive conversion of Dox *in vitro* (Kostrzewa-Nowak et al, 2005). Here it is proposed that a cell-specific set-point of intracellular NADPH availability exists, controlled in part by G6PD activity, above which the modulation of NADPH concentration will have little effect on the ROS-generating module of Dox bioactivation within a particular cell. At the high Dox concentration condition, DHEA promoted decreased superoxide flux in the EU1-Res cells, whereas it had little effect on the EU3-Sens cells (Fig. 4-7 B). This is most likely due to the fact that the basal level of NADPH in the EU1-Res cell is already below the threshold level at which the ROS-generating module of Dox bioactivation can be affected by changes in G6PD activity. It was shown experimentally that the basal level of NADPH in the EU1-Res cell is significantly lower than that of the EU3-Sens cell (Fig. 4-9) making it more susceptible to the effects of DHEA at the high Dox concentration condition, as evidenced by the strong effect of DHEA on cell viability (Fig. 4-7 C). The inhibition of G6PD activity by DHEA at the high Dox concentration condition was able to rescue EU3-Sens cells from Dox induced toxicity because it selectively hindered CPR-dependent Dox reductive conversion (Fig. 4-7 A-C) without affecting the ROS-generating module of

Dox bioactivation; the threshold of NADPH below which the ROS-generating module becomes compromised had not yet been reached in the EU3-Sens cells.

Inhibition of G6PD at the low Dox concentration condition did not rescue any of the ALL cells from Dox toxicity, but rather promoted Dox-induced cell death. Because Dox has been shown to activate NOXs *in vivo* (Gilleron et al, 2009), NOX activity can be thought of as being dependent on [NADPH], [O_2], and [Dox]. Therefore, at the low Dox concentration, compared to the high Dox concentration, more NADPH is needed to maintain the same level of NOX activity; this effectively lowers the NADPH threshold of the signal generating module. The NOX reaction becomes more sensitive to [NADPH] at the low Dox condition and DHEA can effectively decrease NOX-induced superoxide flux for both cell lines (Fig. 4-7 C). Inspection of the trends between the model fluxes (Fig. 4-7 A-B) and the resultant cytotoxicity (Fig. 4-7 C) suggests that perturbation of the bioactivation network by DHEA affects the CPR-driven reductive conversion component (red module, Fig. 4-8) at 10 μM Dox and the ROS-producing redox cycling component (green module, Fig. 4-8) at 100 nM Dox.

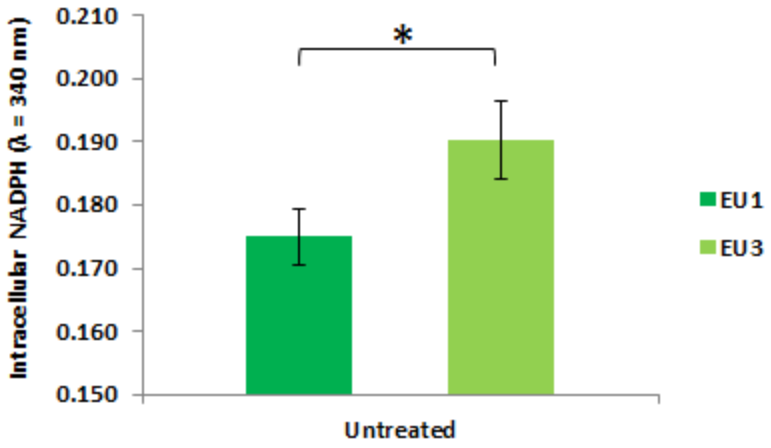

Figure 4-9. Basal NADPH levels are significantly different between the EU1 and EU3 cells. Relative basal intracellular [NADPH] in Dox-resistant EU1 and Dox-sensitive EU3 cells determined by absorbance readings. (340 nm; *$p < 0.05$)

It has already been shown in the literature that Dox reductive conversion increases Dox toxicity in cancer cells (Bartoszek & Wolf, 1992; Kostrzewa-Nowak et al, 2005a) and our findings corroborate this understanding. When we related our experimental viability studies with our model-simulated flux analyses for the EU1-Res and EU3-Sens cells, a distinct pattern emerged: conditions that hindered the toxicity-generating module of Dox bioactivation decreased Dox-sensitivity, while conditions that hindered the ROS-generating module of Dox bioactivation increased Dox-sensitivity. Moreover, cell-specific levels of NADPH, and to some extent the cell-specific activities of G6PD, determined the ultimate effect of G6PD pharmaceutical perturbation on cell viability at each Dox condition investigated. Therefore, during Dox treatment, one can assume that both the toxicity- and the ROS-generating modules of Dox bioactivation are functioning within a given cancer cell. It is the relative dominance of either the toxicity- or the ROS-generating modules of Dox bioactivation that will ultimately determine cell sensitivity to Dox treatment. A systemic approach to understanding how variability in enzyme activity

and concentration control both the toxicity- and the ROS-generating modules of the Dox bioactivation network may provide more efficacious strategies for cancer chemotherapy.

This study showed that by limiting the influence of the ROS-generating module of Dox bioactivation, one can effectively promote Dox-induced toxicity in a Dox-resistant cell line (Fig. 4-7). Based on these results, it is possible that Dox-induced NOX-dependent ROS generation in the ALL lines serves as a second messenger for downstream signaling pathways that contribute to cell viability. The idea of ROS modulating cell viability is not unprecedented as several intracellular signaling pathways are known to be redox sensitive, the most notable being the NF-κB pathway (Oliveira-Marques et al, 2009). The transcription factor NF-κB itself is a redox-sensitive protein (Liao et al, 2010; Loukili et al, 2010; Maioli et al, 2009) known to potentiate cell survival during chemotherapy treatment (Annunziata et al, 2010; Ban et al, 2010; Jani et al, 2010; Pham et al, 2010). Thus, the resulting effect of ROS generation on cell viability most likely involves other downstream signaling pathways.

This study has revealed the concentration-dependence of Dox bioactivation that exists in leukemia cells. The study proposes that oxygen-dependent, ROS-generating reactions have greater influence over Dox toxicity at low Dox concentrations. If this concentration-dependence is exhibited by a variety of other transformed or non-transformed cells, it could help explain the conflicting evidence in the literature regarding the importance of different enzymatic systems in conferring Dox sensitivity (Akman et al, 1990; Bartoszek & Wolf, 1992; Berggren et al, 2001; Doroshow et al, 1991; Kim et al, 2001; Ramji et al, 2003; Sinha et al, 1989b). Work conducted by Asmis et al seems to support the universality of these findings. They observed in macrophages that at low Dox concentrations (0 – 2 μM) there is a concentration-dependent decrease in the ratio of GSH/GSSG, a marker of increased oxidative stress; however, when Dox concentrations were increased from 2 μM to 5 μM, the GSH/GSSG ratio was recovered (Asmis et al, 2005). This finding appears to be in line with the proposed theory that at low Dox

concentrations, the ROS-generating module of Dox bioactivation is more significant than it is at high Dox concentrations, where it gives way to the toxicity-generating module. The ROS-generating module, however, may also be capable of promoting cell injury in some cell lines. In the same study, Asmis reports, that Dox-induced ROS modified glutathione-dependent thiol oxidation in macrophage cells to promote increased cell injury, implicating the glutathione antioxidant system in the management of Dox-induced cell injury (Asmis et al, 2005). This result suggests that cell-specific antioxidant capacity may ultimately determine whether Dox-induced ROS promotes cell viability, by modifying signaling pathways, or whether it promotes cell death, by inducing cellular damage via a thiol oxidation-based mechanism.

The two cell-line specific models of Dox bioactivation have demonstrated predictive power and have recapitulated the dynamics of the Dox bioactivation network for multiple conditions. The model behavior, however, falls short in explaining the delayed onset of $O2^{\bullet -}$ or the initial drop in NADPH upon Dox treatment. One reason for this model limitation could be our description of the NADPH-dependent NOX4 enzymatic reaction that utilizes NADPH and molecular oxygen to produce superoxide. The reaction of NADPH with molecular oxygen, as a result of NOX4 activity, was modeled as a function of the concentrations of NADPH, molecular oxygen, and intracellular quinone Dox because it has been shown previously in the literature that Dox treatment promotes intracellular NOX activity in other cell types (Gilleron et al, 2009). Although the cell-specific ALL computational models incorporated the Dox-dependence of NOX activity, the lack of knowledge on the exact mechanism by which this dependence is executed introduces some uncertainty into the mathematical formulation that was utilized to describe the reaction. However, it should be noted that the computational modeling analyses do support the idea that without Dox-dependent NOX activation both the *in vitro* and the *in vivo* descriptions of Dox bioactivation were limited in their ability to recapitulate experimental results. Perhaps, testing the effect of time

delays in various processes involved in the Dox bioactivation network would reveal additional aspects of kinetic regulation that could increase the robustness of the model.

An additional limitation of the *in vivo* models is that they are incomplete in scope and complexity. There are multiple mechanisms for anthracycline bioactivation in mammalian cells: the mitochondria-dependent bioactivation of Dox by mitochondrial complex I and NADH (Davies & Doroshow, 1986; Doroshow & Davies, 1986), and the mitochondria-independent mechanisms of Dox bioactivation by CPR and NADPH (Bartoszek, 2002). Some studies have even placed the cytotoxic action of Dox in the nuclear compartment of mammalian cells (Egorin et al, 1974). As it currently stands, the cell-specific models of Dox bioactivation only consider cytosolic Dox bioactivation, and are therefore inherently limited. Additionally, the *in vivo* Dox bioactivation network includes species that are involved in a variety of other intracellular reactions which are independent of Dox bioactivation, such as NADPH. NADPH is a metabolite that is used ubiquitously in cells for a variety of redox dependent reactions (Adimora et al, 2010). Moreover, NADPH-dependent thiol oxidation-based mechanisms may actually contribute to Dox-induced cell injury in some cells (Asmis et al, 2005), thereby providing a link between intracellular thiol-disulfide status and Dox-induced toxicity; a link that was unaccounted for by the model because of the qualitative nature of the findings.

In summary, examining the cytosolic Dox bioactivation pathway from a systems biology perspective has provided insight into the redox-dependent mechanisms that may be responsible for conferring Dox sensitivity in cancer cells. Kinetic modeling of the electron transfer mechanisms demonstrates that the Dox bioactivation pathway is dual natured and dynamic, exhibiting sensitivity to initial levels of system components, as defined by cell specific enzyme levels, as well as Dox concentration conditions. This study has shown, through mathematical modeling and experimental analysis, that the toxicity-generating module of Dox bioactivation overwhelms the ROS-generating module in the EU3-Sens cell line, whereas the ROS-generating module of Dox bioactivation

overwhelms the toxicity-generating module in the EU1-Res cell line. This discrepancy in Dox metabolism between the EU1-Res and EU3-Sens cells determines the effectiveness of pharmacological intervention strategies that are aimed at modifying Dox induced toxicity. The model elucidates an important role for NAPDH supply, as modulated by G6PD activity, in controlling concentration-dependent Dox cytotoxicity in tumor cells. This work demonstrated the feasibility of enhancing Dox cytotoxicity via the pharmacological modification of G6PD activity in both the EU1-Res and EU3-Sens leukemia cell lines. Moreover, the work has demonstrated how this same intervention strategy can be used in concert with a high dose of Dox, or within a cell containing protein expression levels that promote reductive conversion, to promote cell viability rather than impede it. The dynamic nature of the Dox bioactivation network, and its ability to metabolize Dox via distinctively different modes, allows for the controlled manipulation of the system to either promote cell viability, as would be desired when protecting non-transformed cells from unwanted Dox toxicity, or to promote Dox-induced transformed-cell death. Finally, because the quinone structure of Dox is conserved across the anthracycline drug family, future studies may elucidate similar control mechanisms in the metabolism of other anthracyclines by cancer cells.

CHAPTER 5

KINETIC MODEL OF HYDROGEN PEROXIDE CLEARANCE

Introduction

An accumulation of reactive oxygen species within the cell can lead to oxidative stress, resulting in changes in the redox state of many proteins (Watson & Jones, 2003). Although cellular processes such as growth, proliferation and apoptosis are controlled by the overall redox state of the cell (Schafer & Buettner, 2001), high levels of ROS can be toxic (Liu et al, 2005; Seaver & Imlay, 2001). The oxidant hydrogen peroxide (H_2O_2) is of great interest to researchers because it is continuously produced as a result of cellular metabolism, diffuses across cellular membranes, has a longer half-life than other oxidative species, and reversibly oxidizes protein thiols (Antunes & Cadenas, 2000; D'Autreaux & Toledano, 2007; Liu et al, 2005).

The apparent paradox between the role of H_2O_2 as a cellular signaling molecule and its role as a cellular toxin appears to be highly dependent on its intracellular concentration, and the resolution of several key questions regarding how mammalian cells handle peroxide levels will facilitate our understanding of this paradox: Which antioxidant mechanisms exert the most control over the removal of hydrogen peroxide from the cell, and how could this be impacted by intervention? How independent are the redox couples from one another during oxidative stress? What role does the global protein thiol pool play in antioxidant defense? In order to accurately address these questions, quantitative computational modeling that integrates the known mechanisms by which mammalian cells control intracellular H_2O_2 accumulation during periods of oxidative stress is necessary.

[*] Modified from Adimora NJ, Jones DP, Kemp ML "A model of redox kinetics implicates thiol proteome in cellular hydrogen peroxide responses" *Antioxid Redox Signal*, 2010 13(6): 731-43

This form of analysis addresses whether current knowledge can quantitatively account for observed cellular behavior. Ultimately, modeling can provide additional insight regarding the discrimination of the physiological function of H_2O_2 from its pathological role.

Researchers have a general understanding of the key players involved in a cell's ability to maintain its intracellular redox state and most models of H_2O_2 depletion can accurately describe one or two aspects of this system (Antunes & Cadenas, 2000; Makino et al, 2004; Sasaki et al, 1998; Seaver & Imlay, 2001). A previous mathematical model developed by Antunes and Cadenas (Antunes & Cadenas, 2000), for example, offered great insight into the enzymatic contributions of glutathione peroxidase (GPx) and catalase to the development of peroxide gradients across cellular membranes. Antunes' model provided a new quantitative estimate for the H_2O_2 membrane permeability coefficient, one that was an order of magnitude smaller than what was cited in the literature (Makino et al, 2004; Seaver & Imlay, 2001). Although Antunes' model provided novel findings, the model did not consider the enzymatic contribution of peroxiredoxins and the non-enzymatic contributions of protein thiols. Since the publication of Antunes' model, multiple studies have revealed that the previously accepted reaction rate of peroxiredoxin with H_2O_2 grossly underestimated its true value (Manta et al, 2009; Peskin et al, 2007). Increased rates of H_2O_2 consumption, therefore, may suggest a H_2O_2 permeability coefficient that is even smaller than that predicted by Antunes and coworkers. As researchers gain a more thorough understanding of the different components that play a role in intracellular H_2O_2 consumption, the accepted kinetic reactions rates of particular species with H_2O_2 will have to be amended.

Over the past few years, knowledge of the varied intracellular antioxidant systems has increased and the need for a comprehensive model that incorporates these new findings is evident. The highly complex nature of the system in question, which results from the interconnectivity between protein thiol oxidation and redox couples during transient oxidative stress, has made development of integrative models difficult. For instance, the

anti-oxidative roles of glutathione peroxidase (GPx) and peroxiredoxins (Prx) depend directly on the reducing capacities of their respective co-substrate molecules, glutathione (GSH) and thioredoxin (Trx). In order to maintain their reducing capacities, GSH and Trx depend on the enzymes glutathione reductase (GR) and thioredoxin reductase (TR), respectively, in addition to NADPH. Moreover, the co-dependence of both the GSH and Trx thiol/disulfide redox couples on NADPH regeneration does not readily explain their maintenance at dissimilar non-equilibrium redox potentials (Jones et al, 2004; Kemp et al, 2008).

In this study, a network model of the major redox reactions and cellular thiol modifications involved in H_2O_2 metabolism is generated in order to improve understanding of the processes by which a cell deals with H_2O_2-induced oxidative stress. At this point, the use of the term "buffering" as it applies to the redox systems that are described will be clarified. Here, the term buffering is not used to describe a system at equilibrium; rather, it is used to describe the process by which the intracellular redox network, as a whole, protects against deviations in the redox states of the individual components that make up the network. This model, therefore, takes into account not only the key components of the network, but also the hierarchical interdependence of each component on the other. It builds in scope upon prior modeling studies (Antunes & Cadenas, 2000; Makino et al, 2004; Sasaki et al, 1998; Seaver & Imlay, 2001) to explore the collective features of an intact redox system by accounting for all the major enzymes known to consume hydrogen peroxide in the cytosol as well as the pseudo-enzymatic oxidative turnover of protein thiols. The use of computational modeling to study peroxide buffering allows for a detailed investigation of the cellular dynamics of oxidative stress.

Materials and Methods

Overview of model structure

A computational model, based upon ordinary differential equations, was developed using mass action and Michaelis-Menten kinetics to describe the changes in concentration of cellular redox-buffering components upon exposure to extracellular H_2O_2. Figure 5-1 is an illustration of the reactions included in the model. Organellar compartmentation provides additional regulatory control in redox mechanisms by maintenance of non-equilibrium redox potentials (Hansen et al, 2006); this model was simplified in description to the extracellular medium, intracellular cytosol and the peroxisomes. Intracellular generation of hydrogen peroxide by the mitochondria was described by a zero-order production term, and the more rapid oxidation rate of Trx2 (Hansen et al, 2006) was excluded from the model.

In this model, the anti-oxidative capacity of the cell is divided into several branches, with each branch describing a particular mode of H_2O_2 elimination. The first branch describes H_2O_2 elimination by the catalase enzyme. An average of 2 peroxisomes per cell has been measured in Jurkat cells (Ishizuka et al, 2004) and all the catalase activity within the cell is assumed to occur inside the peroxisomes.

The second branch of H_2O_2 elimination describes the glutathione peroxidase enzymes (GPx). While multiple GPx isozymes are present in cells, and some glutathione S-transferases have GPx activity, a reliable value for the cytosolic concentration of GPx in Jurkat cells is unknown (Antunes & Cadenas, 2000). For the purpose of modeling this system, this description was simplified by considering the predominant glutathione peroxidase, GPx1, and implementing the literature-reported estimate of its intracellular concentration as predicted by a previous generalized mathematical model (Ng et al, 2007). GPx catalyzes the reaction of hydrogen peroxide with GSH to produce glutathione disulfide (GSSG). Glutathione disulfide is subsequently reduced through the actions of GR and NADPH (Antunes & Cadenas, 2000; Makino et al, 2004).

The third branch of H_2O_2 elimination accounts for the peroxiredoxin (Prx) enzymes in conjunction with Trx, TR, and NADPH. Mammalian cells have several members of the peroxiredoxin family but the predominant mammalian cytoplasmic Prxs are peroxiredoxin 1 and 2 (Moore et al, 1991; Peskin et al, 2007); the combined contribution of these two isoforms are described in the model. The total concentration of cytosolic Prx in Jurkat cells was estimated from the literature (Chae et al, 1999; Moore et al, 1991). The total concentrations of reduced and oxidized NADPH were estimated from values reported in the literature (Martinovich et al, 2005; Schafer & Buettner, 2001). Cytosolic Trx1, at a concentration of 0.5 μM (Watson et al, 2004), was distributed between its reduced and oxidized forms as experimentally determined for this study by redox western blot.

The fourth branch of H_2O_2 elimination involved the oxidation of cysteine residues of intracellular proteins (Pr-SH/Pr-$(SH)_2$). Cysteine (Cys) residues of intracellular proteins contain redox-sensitive thiols that are susceptible to oxidation (Watson & Jones, 2003). Upon oxidation, the Cys residues of proteins can be reduced, with different characteristics depending on the microenvironment, via a system of reactions involving GSH or Trx (D'Autreaux & Toledano, 2007; Peltoniemi et al, 2006; Watson & Jones, 2003); vicinal dithiols are considered to form protein disulfides (P-SS-P) that are reduced by Trx1. Other thiols are oxidized to protein sulfenic acids (P-SOH) which undergo protein S-glutathionylation (P-SSG). The model reserves protein disulfide reduction exclusively for Trx, while protein sulfenic acids are reduced exclusively by GSH-dependent reactions (Fig. 5-1) (D'Autreaux & Toledano, 2007). Methionine residues are also subject to oxidation but the rates are not known. Because methionine sulfoxide reductases are thioredoxin-dependent, the model, as described, can be considered to have methionine oxidation grouped with Trx-dependent reductions (Jones, 2008).

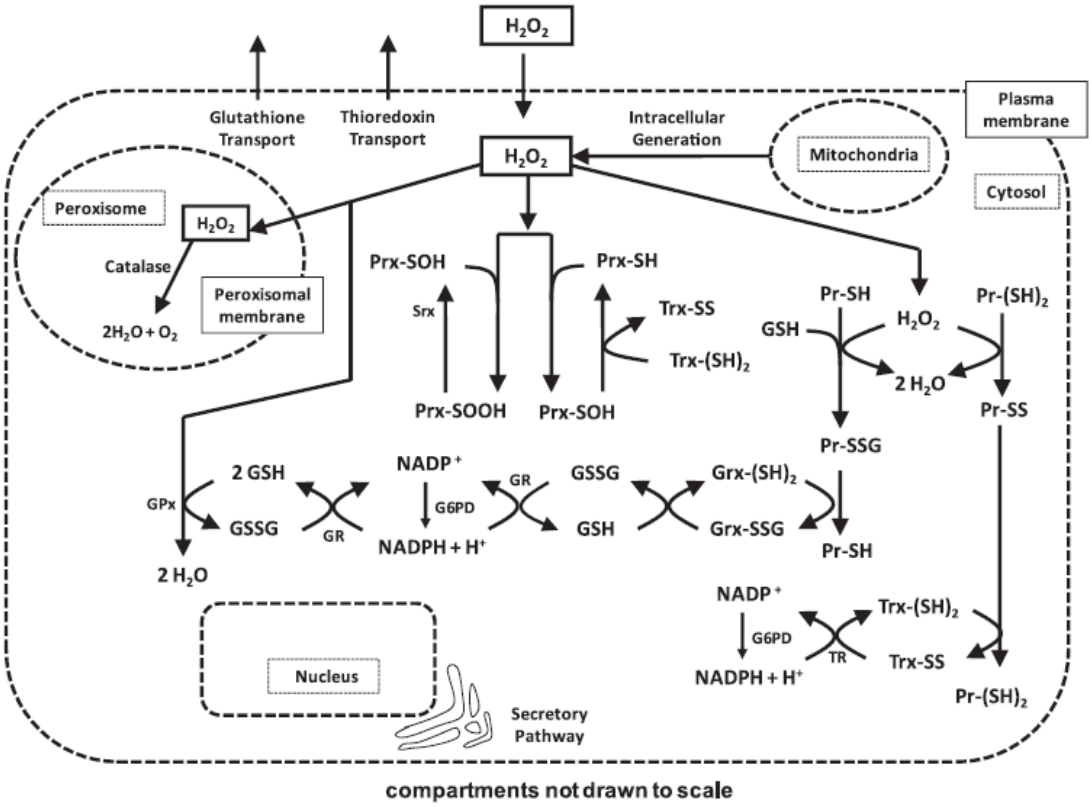

Figure 5-1. Model of hydrogen peroxide (H_2O_2) elimination by Jurkat T-cells. The modeled system was that of an individual cell with three compartments being considered: the extracellular medium, the intracellular cytosol, and the peroxisomes. H_2O_2 is allowed to move freely between compartments by permeating through the cytoplasmic and peroxisomal membranes. A constant intracellular H_2O_2 production rate was defined by a mitochondrial source. Within the intracellular cytosol, H_2O_2 was metabolized by a series of reactions (denoted by arrows) each with a given reaction rate constant (Table 1). There were four main pathways by which H_2O_2 was metabolized by the simulated cell. The first was controlled by catalase and the second was controlled by glutathione peroxidase (GPx) enzymes working in conjunction with GSH, GR, and NADPH. The third was controlled by the peroxiredoxin enzymes (Prx) working in conjunction with Trx, TR, and NADPH. The fourth and final pathway described the non-enzymatic elimination of H_2O_2 through the oxidation of cysteine residues on intracellular proteins. This can occur at single Cys residues resulting in sulfenic acids which react with GSH to form glutathionylated intermediates. Alternatively, this can occur at dithiols resulting in the formation of an internal disulfide.

Table 5-1: Rate expressions and rate constants for the ODEs that comprise the intracellular peroxide clearance model.

Rxn #	*Expression*	*Parameter*	*Reference*
R_1	k_1 ($[H_2O_2]_{media}$) (A) ‡	k_1 = 1.0 x 10^{-5} cm s^{-1}	Fitted
R_2	H_2O_2 Intracellular Generation	k_2 = 1.1 x 10^{-7} M s^{-1}	(Jones, 2008)
R_3	k_3 ($[H_2O_2]_{cytosol}$) ($[GPx_{red}]$)	k_3 = 2.1 x 10^7 M^{-1} s^{-1}	(Ng et al, 2007)
R_4	k_4 ([GSH]) ($[GPx_{ox}]$)	k_4 = 4 x 10^4 M^{-1} s^{-1}	(Ng et al, 2007)
R_5	k_5 ([GSH]) ([GPx-SSG])	k_5 = 1 x 10^7 M^{-1} s^{-1}	(Ng et al, 2007)
R_6	k_6 ($[H_2O_2]_{cytosol}$) ([Catalase])	k_6 = 3.4 x 10^7 M^{-1} s^{-1}	(Aebi, 1984; Peskin et al, 2007)
R_7	k_{22} ($[NADP^+] - [NADP^+]_i$)/(k_7 + $[NADP^+]$)	k_7 = 5.7 x 10^{-5} M	(Yeh et al, 1987)
R_8	k_8 ($[H_2O_2]_{cytosol}$) ($[Prx\text{-}(SH)_2]$)	k_8 = 4 x 10^7 M^{-1} s^{-1}	(Winterbourn & Hampton, 2008)
R_9	k_9 ($[H_2O_2]_{cytosol}$) ([Prx-SOH])	k_9 = 7.2 x 10^4 M^{-1} s^{-1}	(Yang et al, 2002)
R_{10}	k_{10} ($[Prx\text{-}SO_2H]$)	k_{10} = 3 x 10^{-3} s^{-1}	(Chang et al, 2004)
R_{11}	k_{11} ([Prx-SOH])	k_{11} = 15 s^{-1}	(Trujillo et al, 2007)
R_{12}	k_{12} ([Prx-SS]) ($[Trx_{red}]$)	k_{12} = 2.1 x 10^6 M^{-1} s^{-1}	(Low et al, 2007)
R_{13}	k_{13} ([GSH]) ([GSH])	k_{13} = 7.4 x 10^{-5} s^{-1}	(Sasaki et al, 1998)
R_{14}	k_{14} ([Pr-(SH)]) ($[H_2O_2]_{cytosol}$)	k_{14} = 1 x 10^4 M^{-1} s^{-1}	Fitted
R_{15}	k_{15} ([GSH]) ([Pr-SOH] – $[Pr\text{-}SOH]_i$)	k_{15} = 1.2 x 10^5 M^{-1} s^{-1}	(Gallogly & Mieyal, 2007; Lo et al, 2004)
R_{16}	k_{16} ([Grx-SH]) ([Pr-SSG] – $[Pr\text{-}SSG]_i$)	k_{16} = 9.1 x 10^4 M^{-1} s^{-1}	(Peltoniemi et al, 2006)
R_{17}	k_{17} ([Grx-SSG] – $[Grx\text{-}SSG]_i$) ([GSH])	k_{17} = 3.7 x 10^4 M^{-1} s^{-1}	(Srinivasan et al, 1997)
R_{18}	k_{18} ($[Pr\text{-}(SH)_2]$) ($[H_2O_2]_{cytosol}$)	k_{18} = 5 x 10^5 M^{-1} s^{-1}	Fitted
R_{19}	k_{19} ($[Trx_{red}]$) ([Pr-SS] - $[Pr\text{-}SS]_i$)	k_{19} = 1 x 10^5 M^{-1} s^{-1}	(Holmgren, 1985)
R_{20}	k_{20} ([GSSG] – $[GSSG]_i$) ([NADPH])	k_{20} = 3.2 x 10^6 M^{-1} s^{-1}	(Henderson et al, 1991)
R_{21}	k_{21} ($[Trx_{ox}] - [Trx_{ox}]_i$) ([NADPH])	k_{21} = 2 x 10^7 M^{-1} s^{-1}	(Arner et al, 1999)
R_{22}	k_{22} ($[NADP^+] - [NADP^+]_i$)/(k_7 + $[NADP^+]$)	k_{22} = 3.75 x 10^{-4} M s^{-1}	(Yeh et al, 1987)
R_{23}	k_{23}($[H_2O_2]_{cytosol}$)(B) ¥	k_{23} = 3 x 10^{-3} cm s^{-1}	(Poole, 1975)
R_{24}	GSH synthesis	k_{24} = 4.1 x 10^{-7} M s^{-1}	(Kemp et al, 2008)
R_{25}	GSSG efflux	k_{25} = 1.2 x 10^{-8} M s^{-1}	(Akerboom et al, 1982)
R_{26}	GSH + GSSG efflux	k_{26} = 1.2 x 10^{-7} M s^{-1}	(Lee et al, 2001)
R_{27}	Trx efflux	k_{27} = 7.5 x 10^{-10} M s^{-1}	(Kondo et al, 2004)
R_{28}	Trx synthesis	k_{28} = 7.0 x 10^{-10} M s^{-1}	(Kondo et al, 2004)

‡A = 10^{-3} (L cm^{-3}) x 6.5 x 10^{-5} (cm^2) x 1 x 10^9 (cells L^{-1})
¥B = 10^{-3} (L cm^{-3}) x 3.0 x 10^{-9} (cm^2) x 1.5 x 10^{14} (L^{-1})

Parameter and species fitting

For this global model which encompassed 28 kinetic parameters and 24 species, there existed several values that had yet to be appropriately defined in the literature: the H_2O_2 permeability constant, the rate of protein thiol oxidation, and the concentration of protein thiols dependent on GSH and Trx1, respectively, for reduction (Tables 5-1 and 5-2). Experimentally determined dynamics, therefore, were used for model fitting in order to arrive at acceptable estimates for these parameters and species (Fig. 5-2). The first experimental data set used for parameter fitting was digitized from the results of Antunes and Cadenas describing the consumption of a bolus addition of extracellular H_2O_2 by intact Jurkat cells (Antunes & Cadenas, 2000) (Fig. 5-2 B). Four additional data sets were generated under identical experimental conditions and quantified using HPLC techniques and redox western blots. These results describe the changes in distribution of GSH and GSSG as well as reduced and oxidized cytosolic Trx1 that occur as a result of H_2O_2 treatment (Fig. 5-2 C, D). Parameters were estimated by minimizing an objective function, comprising the normalized root mean square deviation (RMSD) between experimentally observed time course data and computed model predictions (Chen et al, 2009).

Table 5-2: Initial concentration values of the components that comprise the intracellular peroxide clearance model.

Species	*Initial Condition (M)*	*Reference*
$[H_2O_2]_{media}$	1×10^{-4}	Assigned
$[H_2O_2]_{cytosol}$	1×10^{-9}	(Oliveira-Marques et al, 2009)
$[GPx_{red}]$	5×10^{-5}	(Ng et al, 2007)
$[GPx_{ox}]$	1×10^{-14} ‡	Assigned
[GPx-SSG]	1×10^{-14} ‡	Assigned
[GSH]	3.68×10^{-4}	Measured
[GSSG]	1.78×10^{-6}	Measured
[Catalase]	9×10^{-7}	(Mueller et al, 1997; Poole, 1975)
$[H_2O_2]_{peroxisome}$	1×10^{-10} ‡	Assigned
$[Prx\text{-}(SH)_2]$	1.9×10^{-5}	(Hansen et al, 2006; Rhee et al, 2001)
[Prx-(SOH)]	1×10^{-14} ‡	Assigned
[Prx-(SOOH)]	1×10^{-14} ‡	Assigned
[Prx-SS]	9.6×10^{-8} †	(Jones, 2008)
$[Trx_{red}]$	4.3×10^{-7}	Measured
$[Trx_{ox}]$	7.5×10^{-8}	Measured
[Pr-SH]]	1.22×10^{-4}	Fitted
[Pr-SOH]	6.1×10^{-7} †	(Jones, 2008)
[Pr-SSG]	6.1×10^{-7} †	(Jones, 2008)
[Grx-SH]	1.2×10^{-6}	(Lundberg et al, 2004)
[Grx-SSG]	6.0×10^{-9} †	(Jones, 2008)
$[Pr\text{-}(SH)_2]$	1.0×10^{-3}	Fitted
[Pr-(SS)]	5.5×10^{-6} †	(Jones, 2008)
[NADPH]	3.0×10^{-5}	(Martinovich et al, 2005)
$[NADP^+]$	3.0×10^{-7}	(Schafer & Buettner, 2001)

‡Baseline assignment to highlight the effects of exogenously applied H_2O_2 only
†Estimate of 0.5% [protein] in the glutathionylated form (Jones, 2008)

Two models of protein oxidation

Accurate modeling of the contribution of protein thiols to the overall redox network requires knowledge of the concentration of protein thiols that are susceptible to hydrogen peroxide oxidation as well as the rates at which these oxidation reactions occur. In order to determine the proper description of intracellular protein oxidation, two distinct models of protein thiol oxidation, a "slow" model and a "fast" model, were postulated and tested for their ability to recapitulate experimental data (Fig. 2). The slow model was constructed by assuming the total available protein thiol pool, as estimated by Jones (Jones, 2008), would react with intracellular hydrogen peroxide with the pre-established rate constant of 5×10^2 $M^{-1}s^{-1}$, the rate at which GAPDH is estimated to react with hydrogen peroxide (Winterbourn & Hampton, 2008). In this model, the available protein thiol pool was further divided into two subgoups: the protein monothiol pool (Pr-SH), which contained 50% of the total available protein thiols, and the protein dithiol pool (Pr-$(SH)_2$), which contained the remaining 50% of the total protein thiol pool (Figure 5-2 A, left panel).

The fast model, on the other hand, was constructed by assuming that there existed a smaller subset of protein thiols, approximately 20% of the total available protein thiol pool, which reacted with hydrogen peroxide at an appreciably faster rate than what was estimated for GAPDH oxidation. The remaining 80% of the total protein thiol pool was divided equally between the protein monothiol group and the protein dithiol group and was allowed to react with hydrogen peroxide at the slower rate constant of 5×10^2 $M^{-1}s^{-1}$. The purpose of the fast model was to determine the percentage of the highly reactive protein thiols that belonged to the protein monothiol group and the protein dithiol group, respectively, and to predict the rates of reactions of these fast reacting thiols with intracellular hydrogen peroxide (Fig. 5-2 A, right panel).

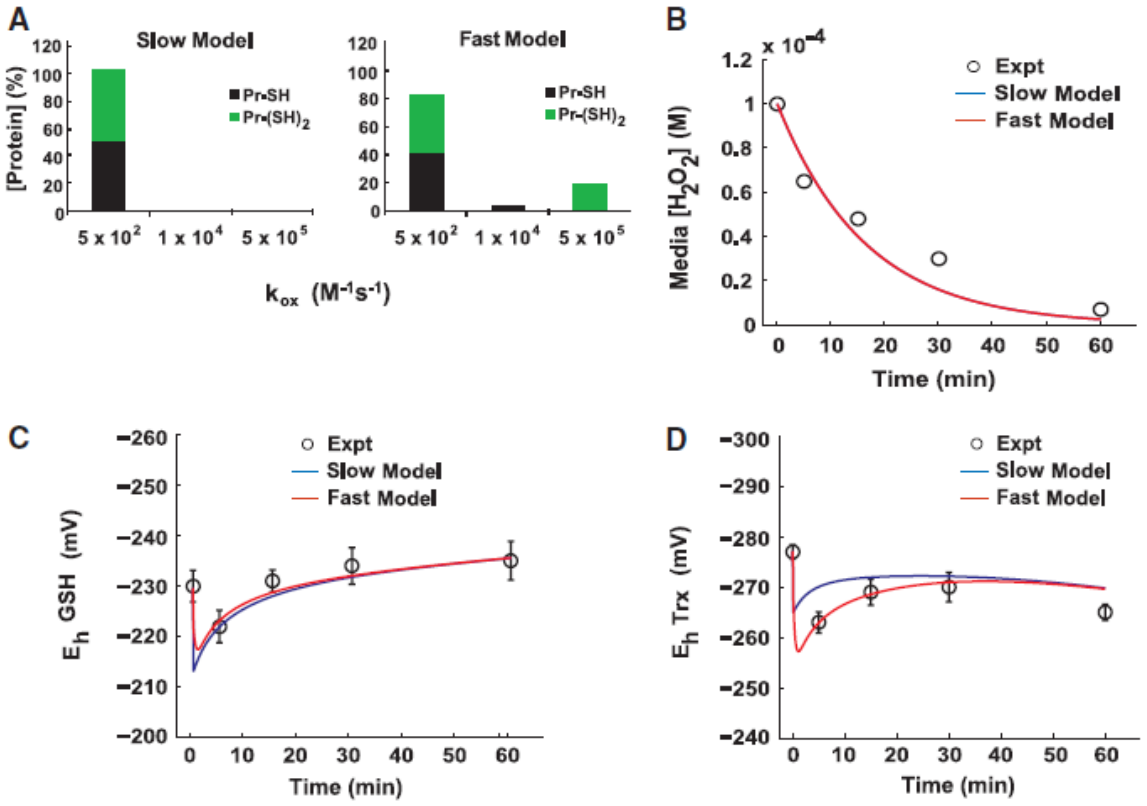

Figure 5-2. A model with rapid protein dithiol oxidation accurately describes hydrogen peroxide consumption. (A) Assignment of the distribution of protein thiol pools and rate constants for the slow and fast protein thiol oxidation models. (B) Experimental data (Antunes & Cadenas, 2000) and model fitted results for the slow and fast protein thiol oxidation models showing the consumption of H_2O_2 by intact Jurkat T-cells at a density of a 1×10^6 cells/ml after being exposed to a bolus addition of 100 µM extracellular H_2O_2. (C) Redox states of the glutathione redox couple as experimentally determined and model fitted for the slow and fast models. Experimental values represent the mean ± S.E.M. of three separate experiments. (D) Redox states of the thioredoxin redox couple as experimentally determined and model fitted for the slow and fast protein thiol oxidation models. Experimental values represent the mean ± S.E.M. of three separate experiments.

Parameter estimation

The parameters predicted by the model were i) the concentration of fast reacting protein monothiols (Pr-(SH)), ii) the reaction rate constant for the fast reacting protein monothiols with hydrogen peroxide, iii) the concentration of fast reacting protein dithiols (Pr-$(SH)_2$), iv) the reaction rate constant for the fast reacting protein dithiols with hydrogen peroxide and v) the permeability coefficient of the cytoplasmic membrane. The protein oxidation parameters to be fitted were initialized to randomized values that lay within the literature-reported estimates of their upper and lower bounds (D'Autreaux & Toledano, 2007; Winterbourn & Hampton, 2008; Winterbourn & Metodiewa, 1999). Due to conflicting estimates of the lower bound of the permeability coefficient (Antunes & Cadenas, 2000; Makino et al, 2004; Seaver & Imlay, 2001), it was deemed appropriate to expand the lower bound of the explored parameter space for this parameter by one order of magnitude. Multiple simulations were conducted for each condition (n = 2000 runs) in which each of the three unknown parameters was simultaneously assigned a random initial value from its allowable parameter space and the objective function calculated. The parameter set that resulted in the minimization of the objective function was selected as the optimal model description.

Membrane H_2O_2 transport

The rate of movement of H_2O_2 across the cytoplasmic membrane has been described previously by the following (Seaver & Imlay, 2001):

$$\frac{d[H_2O_2]_{media}}{dt} = -\left([H_2O_2]_{cytosol} - [H_2O_2]_{media}\right) \times 10^{-3}\left(\frac{L}{cm^3}\right) \times P\left(\frac{cm}{s}\right) \times A\left(cm^2\right) \times \frac{cells}{L} \qquad (5\text{-}1)$$

where $[H_2O_2]_{media}$ and $[H_2O_2]_{cytosol}$ represented the concentration of peroxide in the extracellular media and the intracellular cytosol, respectively, at time t. H_2O_2 flux across the cytoplasmic membrane is a function of the intra- and extra-cellular concentration of

H_2O_2, the permeability coefficient of H_2O_2 through the cytoplasmic membrane, *P*, and the surface area of the cell, *A*, approximately 1.0×10^{-5} cm^2 as calculated from the average diameter of the Jurkat cell, 20 μm (ViCell Viability Counter, Beckman Coulter). The volume of the cytoplasmic compartment was calculated assuming the Jurkat cell to be a perfect sphere of diameter 20 μm. The concentration of H_2O_2 in a cell has been described previously as a sum of the influx, production, efflux and scavenging of H_2O_2 within a particular cellular compartment (Bienert et al, 2006). H_2O_2 flux across the peroxisomal membrane was modeled in a similar fashion using the concentration of peroxide in the cytosol and the concentration of peroxide in the peroxisome to generate the gradient force for diffusion. The permeability coefficient of H_2O_2 through the peroxisomal membrane, *P*, was obtained from the literature (Poole, 1975), assuming a uniform concentration of H_2O_2 within a particular compartment.

Parameter values

The majority of the rate constants and initial species concentrations used in this model were derived from published data (Tables 5-1 and 5-2, respectively). Where possible, values reported specifically for Jurkat cells were used; there were reactions and species, however, for which Jurkat cell line specific values were undefined. For these types of reactions, published data for other cell lines were used as appropriate estimates. The fractional cytosolic volume used for concentration calculations was defined as 30% of total cell volume by estimation from images of Hoescht nuclear-stained Jurkat cells.

Description of reaction kinetics

The series of differential equations were solved using Matlab R2008a (Mathworks, Natick, MA). The generalized equation for a particular species constituted the sum of all reactions that produced the species minus the sum of all reactions that

consumed it. Several components in the model, however, deviated from the generalized equation form as described below.

Ideally, if the law of mass action was used to describe the reduction of GSSG by GR to produce GSH the resulting equations would resemble the following:

$$GSSG + NADPH + H^+ \rightarrow 2GSH + NADP^+ \quad (5\text{-}2)$$

$$\frac{d[GSH]}{dt} = 2 \times k_{20} \times [GSSG] \times [NADPH] \times [H^+] \quad (5\text{-}3)$$

where [GSH], [GSSG], and [NADPH] represent the intracellular concentrations of reduced glutathione, glutathione disulfide, and NADPH, respectively, at time t, and k_{20} represents the rate constant for the reduction reaction. Instead of equation 3, the change in concentration of GSH as a result of the reduction of GSSG by GR was described in the model by the following:

$$\frac{d[GSH]}{dt} = 2 \times k_{20} \times ([GSSG] - [GSSG]_i) \times [NADPH] \quad (5\text{-}4)$$

where $[GSSG]_i$ represents the initial concentration of glutathione disulfide in the cell. Because the cell maintains a fixed non-equilibrium ratio of [GSH]:[GSSG] under normal oxidative conditions (Kemp et al, 2008), the spontaneous reduction of GSSG in the absence of oxidants could not be allowed. To prevent this behavior, the reduction of GSSG was modeled as a function of the difference between [GSSG] and $[GSSG]_i$. While this model description correctly captures oxidant-induced changes to the glutathione disulfide reduction rate, the absolute GSSG reduction rate in the model may be somewhat underestimated by the endogenous rate at baseline because the K_m of GR is high relative to concentrations of GSSG achieved in cells (Gilbert, 1990). The same basic principles and assumptions were applied to the reactions involving the Trx redox couple. The

complete list of rate expressions governing the change in concentration of each species of the model is listed in Table 5-1.

Objective function for parameter estimation

Parameters were estimated by minimizing a modified version of a previously described objective function, U, comprising the normalized root mean square deviation (RMSD) between experimentally observed time course data and computed model predictions (Chen et al, 2009):

$$U = \sum_{i=1}^{N_{expt}} \sum_{j=1}^{N_{obs}} \sum_{k=1}^{N_t} \frac{(x_{ij}(t_k) - x_{ij}^e(t_k))^2}{\sqrt[2]{((x_{ij}^e(t_k))^2)}} \tag{5-5}$$

where x is the concentration of some particular species in the model, x^e is the experimentally observed concentration of the same species, N_{obs} is the number of experimentally observed species, N_{expt} is the number of experimental conditions, as defined by the relative percentage of proteins assigned to the monothiol and dithiol protein pools, and N_t is the number of time points sampled.

Sensitivity analysis

The finite difference approximation (FDM) method was used to calculate the sensitivity coefficient, $s_{i,j}$, which defined the difference between the nominal and perturbed solutions offered by the model according to the equation (Yue et al, 2006):

$$s_{i,j}(t) = \frac{\partial x_i(t)}{\partial \theta_j} = \frac{x_i(\theta_j + \Delta\theta_j, t) - x_i(\theta_j, t)}{\Delta\theta_j} \tag{5-6}$$

where $x_i(\theta_j, t)$ represents a measured model output at time t, when a particular parameter has the value θ_j; subsequently, $x_i(\theta_j + \Delta\theta_j, t)$ represents the value of the same model output when the same parameter is perturbed by the value $\Delta\theta_j$. For the purposes of this model, all parameters were perturbed by ±10% of their initial values. As a result of the difference in magnitude between parameters, the absolute sensitivity values obtained from Equation 6 were not accurate measures of relative sensitivity. To calculate the relative sensitivities, for a more direct comparison of model response at different states across different parameters, a previously described normalization method was employed (Yue et al, 2006):

$$\bar{s}_{i,j}(t) = \frac{\partial x_i / x_i}{\partial \theta_j / \theta_j} \tag{5-7}$$

From this equation, the normalized sensitivity of a particular model output to perturbations in a particular parameter at time, t, could be determined. All sensitivity analysis calculations were done at t = 5 min and parameter sensitivities were calculated with respect to the concentrations of the experimentally determined model species (extracellular peroxide, intracellular GSH, intracellular GSSG, intracellular reduced Trx1, and intracellular oxidized Trx1).

Materials cell culture and stimulation conditions

All reagents were from Sigma-Aldrich, St. Louis, MO unless specified otherwise. Jurkat cells (clone E6-1) were obtained from American Type Culture Collection (ATCC, Manassas, VA). Cells were cultured in supplemented RPMI-1640 medium (glutamine, non-essential amino acids, 100 U/ml penicillin/streptomycin, 1 mM sodium pyruvate, 10 mM HEPES, 10% FBS). For stimulation, cells were resuspended in fresh media (1×10^6 cells/ml) and treated with H_2O_2 for various times at 37°C before lysing. Pyruvate is

known to undergo oxidative decarboxylation in the presence of H_2O_2 so a control experiment was performed to determine the rate of H_2O_2 removal by the culture media alone. An Amplex Red assay (Invitrogen, Carlsbad, CA) showed that the background oxidation of sodium pyruvate in the media by H_2O_2 was not detectable for the duration of the treatment conditions used throughout the study.

Cellular fractionation and derivatization of protein thiols

After treatment, cells were pelleted by centrifugation at 300 × g. The cell pellet was immediately resuspended in guanidine-Tris solution (50 mM Tris-HCL, pH 8.3, 3 mM EDTA, 6 M guanidine-HCL, 0.5% Triton X-100) supplemented with 50 mM iodoacetic acid (IAA, pH 8.3) and incubated at 37°C in the dark for 45 min (Watson & Jones, 2003). This procedure was carried out to simultaneously lyse the cells and derivatize reduced protein thiols. After incubation, the samples were run through Microspin G-25 columns (GE Healthcare, Buckinghamshire, U.K.) to remove excess IAA.

Redox western blot analysis

To analyze the redox state of cytosolic Trx1, derivatized proteins were separated by native polyacrylamide gel electrophoresis as previously described (Watson & Jones, 2003). PVDF membranes were probed with antibody to human Trx1 (American Diagnostica, Stamford, CT) and a goat IgG-IRDye 800 CW conjugated antibody (Rockland Immunochemicals, Gilbertsville, PA). Trx1 bands were visualized and quantified using the LI-COR Odyssey scanner 2.1 (Lincoln, NE) and the LI-COR Odyssey 2.1 gel analysis software, respectively.

Measurement of intracellular GSH and GSSG

GSH and GSSG were measured by high-performance liquid chromatography (HPLC) as S-carboxmethyl N-dansyl derivatives using γ-glutamylglutamate as an internal standard (Jones, 2002).

Calculation of E_h values

The redox potentials of GSH and Trx1 were calculated using the Nernst equation. To convert total values for GSH and GSSG into intracellular concentrations, measured intracellular protein concentrations were used and a constant cellular water volume (5µl/mg protein) was assumed. The integrated band intensities of reduced and oxidized Trx1, as quantified by the LI-COR Odyssey 2.1 gel analysis software, were assumed to be directly proportional to the normalized intracellular concentrations of these species (Watson et al, 2003). The intracellular pH was assumed to be 7.4 (Nordstrom et al, 1992) and to be unaffected by H_2O_2 treatment. E_0 values used for pH 7.4 were as follows: GSH/GSSG redox couple, -264 mV; and for the active site dithiol/disulfide of Trx1, -254 mV (Watson & Jones, 2003).

Results

Parameter and species fitting

Table 5-1 lists the kinetic parameter values obtained from the literature and the fitted values determined for the unknown parameters in the fast model. While the slow model (Fig. 5-2 A, left panel) was able to accurately represent the dynamics of peroxide consumption and the oxidation dynamics of the glutathione redox couple, it was unable to accurately capture the oxidation dynamics of the thioredoxin redox couple, Figure 5-2D. The fast model (Fig. 5-2 A, right panel), on the other hand, was able to capture the entire dynamic dataset. The fitted values in the fast model for the rates of protein oxidation for Pr-SH and Pr-$(SH)_2$ (k_{14} and k_{18}, respectively) were 1 x 10^4 $M^{-1}s^{-1}$ and 5 x 10^5 $M^{-1}s^{-1}$. These values were within the order of magnitude range of predicted reaction rates for protein thiols with H_2O_2 (10 to 10^6 $M^{-1}s^{-1}$) (D'Autreaux & Toledano, 2007). Because the fast model was able to better replicate the experimental data, we used this model to generate all subsequent parameter estimates and model predictions. The permeability constant (Eq. 5-1) that describes the movement of peroxide through the plasma membrane, k_1, was fitted to a value of 1.0×10^{-5} cm s^{-1}. This value was approximately 1 order of magnitude smaller than the value estimated by Antunes and Cadenas (Antunes & Cadenas, 2000).

Table 5-2 lists the initial species concentrations obtained from the literature and the fitted values determined for the concentration of protein thiols dependent on GSH and Trx1, respectively, for reduction. The protein thiol distribution that resulted in the minimization of the objective function was 42% GSH-dependent protein thiols and 58% Trx1-dependent protein thiols.

Consumption of H_2O_2 by intact Jurkat cells

The rate at which Jurkat cells clear the extracellular environment of H_2O_2 is an effective measure of their internal anti-oxidative response system. The model was fitted

to the condition of a bolus addition of 100 µM extracellular H_2O_2 being consumed by 1×10^6 Jurkat cells per ml. The model-predicted rate of extracellular H_2O_2 decay was 9.4×10^{-4} s^{-1} per 10^6 cells. This decay rate was very close to the experimentally determined $1.0 \pm 0.1\times10^{-3}$ s^{-1} per 10^6 cells reported by Antunes and Cadenas (Antunes & Cadenas, 2000).

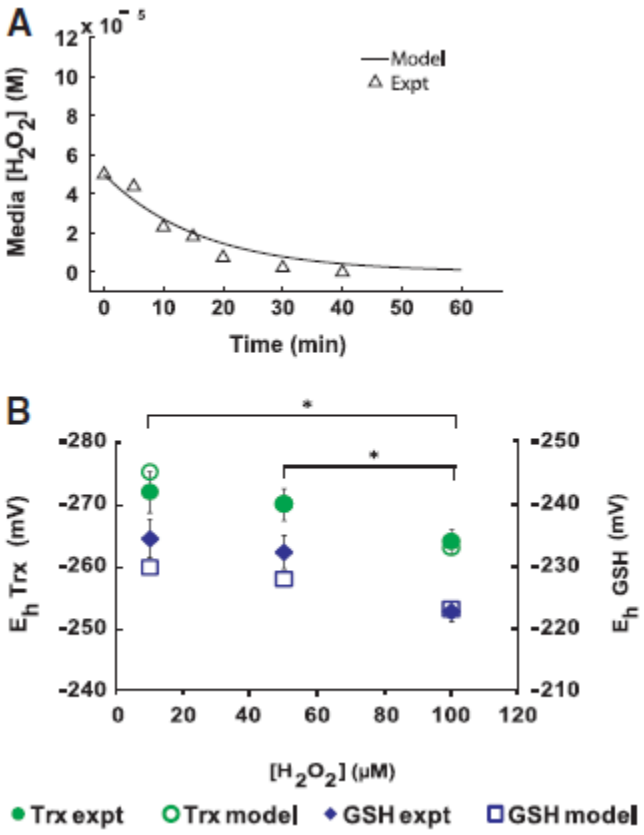

Figure 5-3. Model validation for varied initial extracellular peroxide concentrations. (A) Model-simulated and experimentally determined (Hampton & Orrenius, 1997) consumption of H_2O_2 by intact Jurkat T-cells (cell density = 1×10^6 cells/ml) after being exposed to a bolus addition of 50 µM extracellular H_2O_2. (B) Model-simulated and experimentally determined glutathione and thioredoxin redox potentials for a varying initial extracellular [H_2O_2] (Jurkat T-cell density = 1×10^6 cells/ml).

After the model parameters and protein thiol distributions were optimized based upon the bolus condition, the ability of the model to describe hydrogen peroxide consumption by Jurkat cells at varied extracellular peroxide conditions was investigated. Without any additional parameter optimization, the fitted model accurately simulated the extracellular decay of 50 μM hydrogen peroxide at a cell density of 1 x 10^6 cells/ml from another published dataset (Hampton & Orrenius, 1997). This new peroxide concentration was 50% less than what was used in the model fitting exercises (Fig. 5-3 A). Simulations of peroxide consumption dynamics of a population of Jurkat cells exposed to low steady state levels of extracellular H_2O_2 were carried out. Since the steady state consumption behavior of Jurkat cells was not used to fit any of the parameters contained in the model, the steady state consumption experiment, previously carried out by Antunes and Cadenas (Antunes & Cadenas, 2000), served as additional validation for the model. In this experiment, cells at a concentration of 1×10^6 cells/ml were incubated simultaneously with a low concentration of H_2O_2 and glucose oxidase to generate a steady state extracellular H_2O_2 concentration of approximately 9 μM (Antunes & Cadenas, 2000). The model simulation for this condition accurately predicted that Jurkat cells (1×10^6 cells/ml) would be able to maintain, at a constant level, the low concentration of H_2O_2 in their extracellular environment for at least one hour after exposure.

The intracellular GSH/GSSG pool is transiently oxidized by H_2O_2 treatment

Glutathione disulfide (GSSG) was quantified as approximately 0.5% of the total glutathione pool in resting Jurkat cells (E_h value of cytosolic GSH/GSSG = -230 ± 3 mV). At 5 min post-H_2O_2 addition, the intracellular GSH/GSSG redox potential had been oxidized by approximately 8 mV (Fig. 5-2 C). Within 30 min of treatment, the concentration of GSSG was approaching its baseline level. In contrast, the intracellular GSH concentration increased slightly; therefore, a net change in total glutathione was

occurring over the experimental window of observation. At 60 min of exposure, the E_h value of the GSH/GSSG pool was -235 ± 4 mV.

Using the measured baseline values of oxidized and reduced glutathione as initial conditions for GSH and GSSG, the model simulated the changing glutathione redox potential due to H_2O_2 treatment as a function of time (Fig. 5-2 C). A rapid oxidation of the GSH/GSSG pool upon H_2O_2 treatment resulted in an E_h value of -224 mV at 5 min post-treatment, very close to the 8 mV magnitude oxidation measured. The model curve showed a return to baseline redox potential after 60 minutes and, as a result of the incorporation of glutathione transport and synthesis, the model was capable of capturing the slight overshoot seen experimentally.

Cytosolic Trx1 oxidation is sustained after H_2O_2 treatment

Cytosolic Trx1 was measured in resting Jurkat cells and found to be approximately 85% reduced, corresponding to an E_h value for cytosolic Trx1 of -277 ± 1.4 mV (Fig. 5-2 D), a value that is in agreement with previous reports of the steady state redox potential of cytosolic Trx1 (Kemp et al, 2008). The potential of the Trx1 redox couple at 5 min of treatment was approximately -263 mV, reflecting 14 mV oxidation. From 5 min to 30 min of treatment, the percentage of oxidized Trx1 began to decline towards its baseline value. At 60 minutes of treatment, however, the redox potential of the cytosolic Trx1 redox couple was re-oxidized. The 60 minute Trx E_h value of -265 ± 1.6 mV was very similar to the level of Trx1 oxidation seen at 5 min of treatment (Fig. 5-2 D).

The fitted model was capable of simulating transient E_h values for cytosolic Trx1 following exposure to 100 μM H_2O_2 (Fig. 5-2 D). The baseline distributions of oxidized and reduced Trx1 were used as the initial conditions for the Trx1 species in the simulation. An appropriate degree of Trx1 oxidation upon exposure to H_2O_2 was

reproduced by the model and the model was capable of simulating the re-oxidation observed at the 60 minute time point.

Model sensitivity analysis

Sensitivity analysis was conducted on the model to identify the parameters with the greatest influence on model simulation results. Sensitivity analysis was conducted at 5 min because the maximum effect of peroxide treatment was seen at or close to that time point. The parameter to which a majority of the species investigated was most sensitive was k_1, the permeability constant of the cytoplasmic membrane. Reduced and oxidized Trx1 showed the highest sensitivity to the parameters k_1, k_{12} and k_{21}, where k_{12} and k_{21} represented the rate constant for the reduction of oxidized peroxiredoxin (Prx-SS) by reduced Trx1 and the rate constant for the reduction of oxidized Trx1 by TR and NADPH, respectively. GSH showed the highest sensitivity to k_1 and k_3, where k_3 represented the rate constant for the GPx-catalyzed removal of hydrogen peroxide. GSSG showed the highest sensitivity to k_3 and k_{20}, where k_{20} represented the reduction of GSSG by GR and NADPH. While both the glutathione and thioredoxin redox couples showed relatively high sensitivity to k_{22}, the rate constant describing the rate of NADPH resupply by the G6PDH enzyme, the Trx redox couple was more sensitive to perturbations in this parameter than the GSH redox couple. Experimental studies showing the effect of G6PD inhibition on peroxide-induced protein S-glutathionylation in Jurkat cells corroborate the model-predicted sensitivity of G6PD-dependent NADPH resupply to the intracellular ROS buffering capacity of Jurkat cells (Appendix A). Model components, in general, were "insular" in their sensitivities (i.e. affected by rate constants of reactions in which they played either a direct or very nearly direct role) with very few enzymatic parameters, such as k_{22} (NADPH supply), affecting both the thioredoxin and glutathione couples.

Model predicts oxidation profiles of glutathione and thioredoxin redox couples for varied initial extracellular [H_2O_2]

The anti-oxidative properties of the model were capable of replicating *in vivo* Jurkat dynamics for particular instances of both the transient and steady state condition of oxidative stress. To further interrogate the system, we explored the model's ability to predict these dynamic responses for a variety of oxidation levels. We simulated a bolus extracellular H_2O_2 addition of 10 μM and 50 μM at a cell density of 1×10^6 cells/ml, and compared the results to the redox potential of the glutathione and thioredoxin redox couples experimentally measured 5 minutes post-treatment (Fig. 5-3 B). There were significant statistical differences (alpha = 0.05) between the experimentally determined redox potentials of the glutathione and thioredoxin redox couples at 5 min of 10 μM peroxide treatment compared to the 100 μM peroxide treatment. Statistically significant differences were also seen between the 50 μM and the 100 μM extracellular peroxide treatments. Model simulations of the redox potential of the glutathione and thioredoxin redox couples for the 10 μM, 50 μM, and 100 μM peroxide treatments deviated slightly from the experimental values but accurately captured the oxidative change between the redox potentials of both redox couples for all peroxide treatment conditions examined (Fig. 5-3 B).

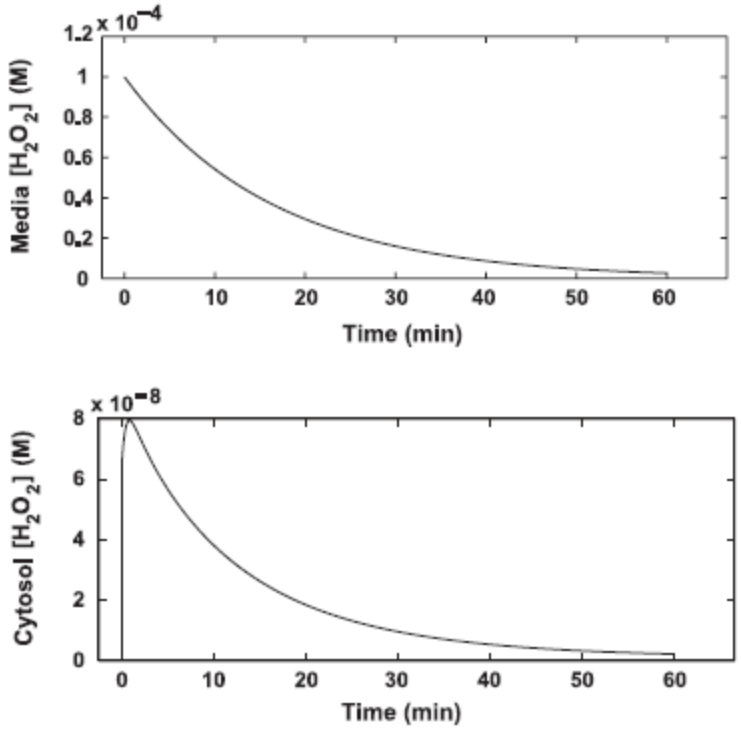

Figure 5-4. Model predicted intracellular [H_2O_2]. Dynamic model-simulated extracellular (top) and intracellular (bottom) peroxide concentration as a result of 100 µM H_2O_2. (Jurkat T-cell density = 1×10^6 cells/ml).

Model predicts intracellular peroxide concentrations and levels of protein thiol oxidation resulting from exogenous hydrogen peroxide

One benefit of the model is the ability to offer quantitative estimates for the intracellular [H_2O_2] resulting from an external source of hydrogen peroxide. The model predicts that a concentration of about 8×10^{-8} M of hydrogen peroxide develops within the cell when it is exposed to 100 µM of extracellular peroxide at a cell density of 1×10^6 cells/ml (Fig. 5-4); thereby representing a gradient of about 1000 that develops between the extracellular environment and the intracellular cytosol.

A.

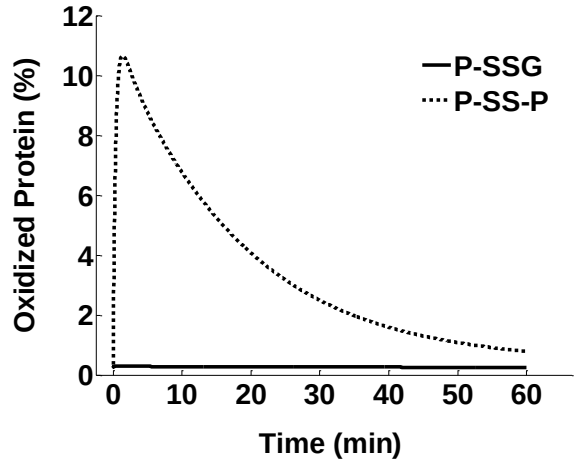

B.

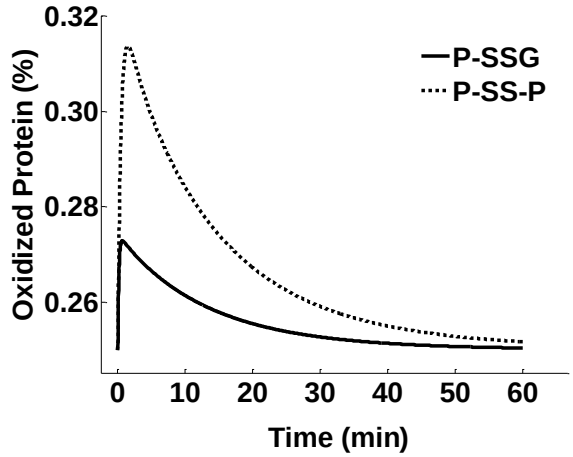

Figure 5-5. Model predicted protein oxidation profiles. Simulated percentages of S-glutathionylated proteins and protein disulfides that form as a result of oxidative stress (100 μM H_2O_2; Jurkat T-cell density = 1×10^6 cells/ml) for the fast (A) and slow (B) models.

In addition to offering quantitative estimates of the intracellular peroxide concentration, the model is capable of providing predictions of protein thiol oxidation. The protein thiol pool may significantly contribute to the cellular antioxidant defense due to the substantial concentration of protein thiols in the cell (Jones, 2008). To investigate the independent roles of monothiol and dithiol proteins during dynamic oxidative conditions, the model was used to predict the level of peroxide-induced protein oxidation as a function of initial extracellular [H_2O_2] (Fig. 5-5). For this *in silico* experiment, protein oxidation was quantified by the concentration of protein disulfides ([Pr-SS-Pr]) and S-glutathione adducts ([Pr-SSG]) observed at 5 min of 100 μM H_2O_2 treatment for the slow and the fast model of peroxide consumption. The slow model, which was unable to fit all the experimental data (Fig. 5-2), showed very little protein oxidation, with the maximum concentration of protein S-glutathione adducts and protein disulfides not exceeding 1% of the total thiol pool (Fig. 5-5, bottom). The fast model, on the other hand, which was capable of fitting all the experimental data, predicted a significant increase in the concentration of protein disulfides, approximately 10% of the total protein thiol pool (Fig. 5-5, top).

Discussion

The development of kinetic computational models of redox enzyme systems presents unique challenges in comparison to other biochemical networks. The non-equilibrium condition of intracellular thiol based-redox couples provides for a rapid and highly sensitive switching mechanism in response to changes in intracellular redox state (Kemp et al, 2008). Because many thiol-based redox couples are set at different potentials, the model species tend to equilibrate even in the absence of oxidative stress. The spontaneous change in redox potential that is due to this inherent non-equilibrium condition must be filtered out in order to focus entirely on those changes that are the result of oxidative stress alone. One modeling approach is to define the driving force for electron transfer to be the function of the difference between the homeostatic potential and the actual potential of the system as defined by the redox couple of interest (Kemp et al, 2008). With this approach, the defined system can describe the dynamic response to changes in intracellular [H_2O_2] without having to explicitly include the numerous steady-state fluxes that must occur across cellular membranes in order to maintain the redox couples out of equilibrium.

Importance of membrane permeability in cellular antioxidant defense

The model highlights the sensitivity of the entire redox enzyme network to the membrane permeability constant for hydrogen peroxide and revises estimates for this constant. The first barrier to extracellular hydrogen peroxide consumption is the cytoplasmic membrane. Transmembrane diffusion of H_2O_2 is an important factor in the maintenance of peroxide gradients between the extracellular environment and the intracellular cytosol (Bienert et al, 2006). The model recapitulated this experimental observation by highlighting k_1, the model parameter describing the permeability coefficient of the cytoplasmic membrane, as the parameter to which most model components were the most sensitive. The optimized permeability coefficient was

approximately 1 order of magnitude smaller than what was previously estimated by Antunes and Cadenas (Antunes & Cadenas, 2000). The literature-reported estimate calculated by Antunes and Cadenas was based on the assumption that the GPx and catalase pathways were the only pathways working towards H_2O_2 removal. Realistically, however, the cell has several additional enzymatic and non-enzymatic methods of H_2O_2 clearance, most of which have been integrated into this present model. Without the incorporation of all redox reactions that take place *in vivo*, an overestimated value for the permeability coefficient is expected. From a systems perspective, therefore, it would be beneficial if the cell could control its cytoplasmic membrane permeability in order to control the amount of transmembrane H_2O_2 diffusion it experiences. Indeed, recent studies have shown that some membranes are poorly permeable to H_2O_2, compared to other membranes, implying that transport of H_2O_2 could in fact be regulated (Bienert et al, 2006). Differences in membrane permeability could be attributed to changes in membrane lipid composition or changes in the number of membrane-bound diffusion-facilitating channel proteins, all of which can be controlled by the cell. The importance of the membrane permeability coefficient, as dictated by the model sensitivity analysis, suggests that the cytoplasmic membrane permeability is a parameter capable of being tuned by the cell in order to control H_2O_2 transport and, ultimately, the concentration of H_2O_2 inside the cell. Whether such transport could be actively controlled by aquaporins is presently unknown.

Precise modeling of the intracellular peroxide consumption dynamics and membrane permeability provides a more accurate description of intracellular peroxide levels. The model-predicted peak intracellular concentration of hydrogen peroxide that is induced by 100 μM is about 100 nM. The model is the most comprehensive model to date to offer quantitative and dynamic estimates of the intracellular concentration of hydrogen peroxide resulting from external peroxide assault.

Unequal anti-oxidative burden of intracellular redox enzymes and thiol containing compounds

The model addresses which redox enzymes and thiol containing compounds are primarily responsible for the antioxidant capacity of the cell. The Trx1 and GSH redox couples are often used as measures of the overall redox state of the cell (Schafer & Buettner, 2001). We utilized the model to describe the dynamics of these two redox couples under conditions of oxidative stress. Experimental results showed the E_h value of the Trx1 redox couple to be oxidized by a maximum of 17 mV after treatment with 100 μM H_2O_2. This maximum level of oxidation was about twice as high as that seen for the GSH redox couple. Analysis of the model system under the steady state peroxide condition (Table 5-3) suggests an unequal distribution of the anti-oxidative burden exists between the Trx1 and GSH redox couples in the intracellular cytosol; this unequal distribution offers one explanation for the unequal oxidation of the Trx1 and GSH redox couples described above. These results should be interpreted carefully as the flux distribution between the Trx1 and GSH redox couples may very well be compartment-specific and therefore altered in other subcellular compartments. Furthermore, Trx1 kinetics may change with hyperoxidation of the enzyme (Watson & Jones, 2003), and the kinetics of the G6PD enzyme are altered as a result of increasing levels of GSSG in the cell (Ursini et al, 1997). Future modeling efforts may need to account for these complex kinetic regulatory mechanisms to appropriately simulate more extreme oxidative conditions.

The steady-state concentration of H_2O_2 that develops within an individual cell as a result of a low (~ 9 μM), constant level of extracellular H_2O_2 was approximately 1 nM. From this steady state value, and using the respective rate constants of peroxide metabolism for each anti-oxidative branch (catalase, GPx/GSH, Prx/Trx1, Pr-SH, Pr-$(SH)_2$), in addition to the relative concentrations of the species in each branch, we were able to calculate the hydrogen peroxide flux (M/s) that passes through each anti-oxidative

branch (Table 5-3). These calculations reveal that the GPx and Prx enzyme systems were responsible for the majority of the peroxide metabolism at this steady-state condition, with calculated fluxes of 6.0×10^{-6} Ms^{-1} and 4.4×10^{-6} Ms^{-1}, respectively. In comparison, the flux through the catalase enzyme system was only 3.7×10^{-8} Ms^{-1}, approximately 0.6% of the flux through the GPx enzyme system. The contribution of catalase to the consumption of externally generated hydrogen peroxide is low compared to other antioxidant enzymes such as peroxiredoxin and glutathione peroxidase. This result reflects not only the low peroxisomal content of Jurkat cells, but also the inefficiency of intact peroxisomes in degrading externally generated hydrogen peroxide (Fritz et al, 2007). It must be noted that while catalase may be somewhat inefficient at degrading external hydrogen peroxide, it is highly efficient at degrading hydrogen peroxide generated within the peroxisomal matrix.

Table 5-3: Model-predicted steady-state hydrogen peroxide fluxes.

Branch	*Flux (M/s)*	*Flux (% of Total)*	*Flux (M/s)*	*Flux (% of Total)*
Prx	4.4×10^{-6}	32	5.6×10^{-6}	42
GPx	6.0×10^{-6}	44	7.7×10^{-6}	57
Catalase	3.7×10^{-8}	< 1	4.6×10^{-8}	< 1
Pr-SH	7.0×10^{-9}	< 1	1.1×10^{-8}	< 1
$Pr-(SH)_2$	3.1×10^{-6}	23	1.1×10^{-8}	< 1
	Fast Model		*Slow Model*	

Another prediction by the model flux analysis was the contribution of the protein dithiol pool to the steady-state peroxide consumption. The flux of hydrogen peroxide through the protein dithiol pool was 3.1×10^{-6} Ms^{-1}, approximately 23% of the total hydrogen peroxide consumption within the cell. Comparatively, the flux through the protein monothiol pool was less than 1%. These results are in line with previous predictions of protein thiol oxidation that suggest a majority of the proteins in the cell

react at relatively slow rates with hydrogen peroxide, whereas a few proteins, primarily those that form disulfide bonds, react with hydrogen peroxide at appreciably faster rates (Winterbourn & Hampton, 2008; Winterbourn & Metodiewa, 1999). This result offers another possible explanation for why the thioredoxin redox couple experienced more pronounced and sustained oxidation during times of oxidative stress as compared to its glutathione counterpart.

The current model advances our understanding of intracellular redox biology

Multiple advancements in knowledge have been gained by this modeling study. The question that motivated this study was whether the current knowledge in the redox biology field can explain experimental data, or if are there additional redox nodes, which have not yet been discovered, that may significantly contribute to peroxide clearance from the intracellular environment. This study has shown that the model topology - as it currently stands and with current parameter measurements available in the literature - is capable of describing the behavior of a particular cell line upon exposure to an external source of hydrogen peroxide if supplemented with the optimized estimates of unknown parameters. Although customized for Jurkat cells, the reactions that are described by the model can easily be adapted to other cell lines by inserting enzyme concentrations and reaction rate constants for the particular cell line of interest. The second contribution given by this model is its ability to provide predictions of the oxidation profiles of specific intracellular components that are not yet able to be quantified experimentally. The current model offers what can be called the first fully quantitative estimate for the concentration of intracellular hydrogen peroxide that results from an extracellular source in addition to the percentage of protein thiols that undergo both protein S-glutathionylation as well as protein disulfide formation. By including the contribution of the protein thiols to hydrogen peroxide clearance, the model explains why the glutathione and thioredoxin redox potentials are purported to be independent from one another; the

larger flux through the dithiol pool causes a capacitance in the thioredoxin branch that leads to a sustained oxidation of thioredoxin. Finally, the model is capable of simultaneously determining relative fluxes through each antioxidant branch, which would be extremely difficult to measure using traditional experimentation.

This framework used the controlled induction of oxidative stress to construct a kinetic model that is capable of describing the observed oxidation of redox couples as a function of time. As a tool for interrogation of a particular biochemical network, a bolus condition is extremely useful to "reverse-engineer" features. While the current model was fitted and validated with data based on the extracellular administration of hydrogen peroxide, this does not negate the ability of the model to simulate and predict the behavior of intracellular components as a result of endogenous generation of hydrogen peroxide. To validate these dynamics, however, advancements in the ability to quantitatively measure intracellular peroxide will need to be developed. Furthermore, while compartmentation was included, spatial gradients within the cell were not described by this model. With the network structure and kinetic description intact, future challenges to modeling efforts will involve the added complexity of intracellular H_2O_2 spatial gradients generated by NADPH oxidases, peroxisomes, and mitochondria.

CHAPTER 6

GLUTATHIONE REDOX BALANCE REGULATES DOX-INDUCED NF-KB ACTIVITY IN LEUKEMIC CELLS

Introduction

High concentrations of intracellular ROS can inflict irreparable damage to cellular biomolecules and cause subsequent cell death (Nordberg & Arnér, 2001). Low levels of ROS, however, are more likely to alter cellular signal transduction through the reversible modification of intracellular redox-sensitive proteins (Valko et al, 2007). The cellular protein modifications caused by low levels of ROS do not necessarily result in cell death, and may even promote cell viability in some instances (Oliveira-Marques et al, 2009). For this reason, increased understanding of the mechanisms through which low levels of ROS modify redox-sensitive signal transduction pathways can provide new insight into the intracellular networks that regulate cell growth and proliferation and help further understanding of how these networks are modified by changes to the intracellular redox environment.

The complex nature of the mammalian antioxidant network which stems from the interconnectivity of the many components that comprise the network (Adimora et al, 2010) makes the characterization and computational description of ROS-dependent signaling exceedingly challenging. In an attempt to address this complexity, a key question has emerged: Can redox-sensitive signaling pathways be somewhat insulated from one another, or are they all interconnected via the intracellular antioxidant network?

---

[*] Modified from Finn NA, Kemp ML "Pro-oxidant and antioxidant effects of N-acetylcysteine regulate doxorubicin-induced NF-kappaB activity in leukemic cells" *Submitted*

This will determine whether the accurate description of ROS-dependent signaling is contingent on the ability to model the entire antioxidant network as a whole, or whether a more simplified description of a portion of the antioxidant network suffice.

This investigation aimed to systematically analyze the biochemical mechanisms by which low levels of ROS induced by the redox recycling of Dox between its quinone and semiquinone forms potentially alter a redox-sensitive signal transduction pathway. The NF-κB signal transduction pathway was chosen for analysis because it is extremely well-characterized, and potential points of redox susceptibility have been reported to exist within the pathway. Moreover, the NF-κB signal transduction pathway is an oncogenic pathway believed to be involved in cellular growth, proliferation, and drug resistance development (Dolcet et al, 2005; Zhou et al, 2003b). The ability of chemotherapy to regulate NF-κB transcriptional activation has been shown previously (Lin et al, 2007), however, the mechanistic details behind this regulation are incompletely defined and extremely complex (Bednarski et al, 2009).

The glutathione antioxidant system has emerged as a potential mediator of the NF-κB activation pathway (Gallogly & Mieyal, 2007; Ghezzi, 2005; Peltoniemi et al, 2006). Furthermore, glutathione has been implicated in the drug resistance of hematological malignancies – most acute lymphoblastic leukemia (ALL) patients who are insensitive to Dox treatment show an increased expression of glutathione (Singh Ghalaut et al, 1999; Volm et al, 2002). Additionally, intracellular proteins that are involved in redox-dependent signaling can be susceptible to glutathione-dependent inactivation via protein S-glutathionylation (Reynaert et al, 2006). Because changes to the intracellular redox environment, as characterized by changes to the glutathione redox potential, can alter redox-sensitive signaling pathways, it was hypothesized that the intracellular redox environment likely modulates Dox-related NF-κB activation.

The use of the antioxidant N-acetylcysteine (NAC) to systematically alter intracellular GSH/GSSG redox potential during Dox treatment provided a mechanistic

framework for studying the manner in which a particular redox couple, acting independently of other intracellular redox couples, could potentially regulate chemotherapy-induced signaling. The objectives of this study, therefore, were to (a) determine which protein thiols in the NF-κB activation pathway are sensitive to ROS induced by clinically relevant concentrations of Dox, (b) determine how the glutathione/glutathione disulfide (GSH/GSSG) redox balance alters the redox sensitivity of the points identified in (a) and how this alteration affects Dox-induced NF-κB activity, and (c) develop a semi-quantitative computational model, based on the qualitative descriptions of individual redox-dependent reactions, that is capable of predicting the extent to which Dox treatment will affect NF-κB activity as a function of the varying GSH/GSSG redox potential. The results of this study provide evidence that the mechanistic description of a single redox couple, relatively isolated from the intracellular antioxidant network, is sufficient to accurately explain the ROS-dependent regulation of a redox-sensitive signal transduction pathway.

Materials and Methods

Materials, cell culture and treatment conditions

All reagents were from Sigma-Aldrich unless otherwise specified. A B-cell precursor ALL cell line derived from a pediatric patient (EU1-Res / EU1) has been previously characterized (Zhou et al, 2003a). EU1-Res cells were cultured in RPM1-1640 medium supplemented with 10% FBS and 100 U/ml of penicillin/streptomycin. For all experiments, unless otherwise stated, ALL cells were resuspended in fresh media (1×10^6 cells/ml) and treated with various concentrations of Dox (Enzo Life Sciences), the IKK-β inhibitor, SC-514 (Enzo Life Sciences), or NAC (Alfa Aesar, MA, USA), protected from light and incubated at 37°C in a humidified atmosphere of 5% CO_2. Phenol-red-free RPMI-1640 medium was supplemented with 10% FBS and 100 U/ml of penicillin/streptomycin. Antibodies: Mouse anti-IκB-α primary antibody (Genetex, CA, USA), rabbit anti-IKK-γ primary antibody (Cell Signaling, MA, USA), rabbit anti-IKK-β primary antibody (Santa Cruz Biotechnology, CA, USA) and rabbit anti-actin primary antibody (Sigma-Aldrich, MO, USA).

Luciferase transduction

EU1 cells were transduced with Cignal^{TM} lentiviral particles expressing Renilla (control) and Luciferase (NF-κB reporter) binding elements according to manufacturer's protocol (SA Biosciences, MD, USA). EU1 cells were seeded, in triplicate, in a 96-well plate format at a starting concentration of 1×10^5 cells/ml in 100 µl of RPMI-1640 media. Cells were allowed to incubate for 24 h. After 24 h, growth media was removed from the wells and Renilla and Luciferase lentiviral particles, diluted in a mixture of SureEntry Transduction Reagent and RPMI media without antibiotics, was added to the cells at a multiplicity of infection (MOI) of 25. Cells were incubated for 18 h, then the lentiviral-containing media was removed and 100 µl of fresh RPMI growth media was added to the cells. On day 4 of the transduction protocol, the growth media was removed

and replaced with 100 µl of fresh RPMI media containing 2 µg/ml of puromycin antibiotic. On day 7 of the transduction protocol, live cells were harvested and assayed for expression of the NF-κB reporter gene. Cells were maintained in culture using RPMI media supplemented with 2 µg/ml of puromycin antibiotic.

NF-κB activation (Luciferase Reporter Assay)

Luciferase reporter activity was quantified using the Dual-Luciferase Reporter Assay System (Promega, WI, USA) according to manufacturer's protocol. Transduced EU1 cells, suspended in 100 µl of RPMI-1640 media without puromycin antibiotic, were plated in 96-well plate format (1×10^6 cells/ml). Cells were treated with various treatment conditions (see below) for indicated times. After treatment, cells were lysed and luciferase protein expression was quantified using a Synergy 4 hybrid microplate reader (Biotek).

Intracellular ROS determination

EU1 cells were treated with (Dox/NAC samples) or without (Dox samples) 1 mM NAC in phenol red-free media (for Dox samples) for 30 min. After pretreatment, Dox, at a final concentration of 5 µM, was added to the cells and allowed to incubate for the indicated times. After Dox treatment, cells were spun down and the media removed. For determination of Dox-induced ROS formation, H_2DCFDA resuspended in DMSO was added to the cells after Dox treatment to a final concentration of 5 µM and cells were incubated for 15 min. After incubation, the cells were pelleted and resuspended in fresh PBS at room temperature and the plate was assayed for DCFDA fluorescence signal using the microplate reader (Ex = 500 nm, Em = 535 nm). Unstimulated cells, pre-incubated with and without H_2DCFDA dye, and phenol red-free media, pre-incubated with and without H_2DCFDA dye and Dox, respectively, were used as controls.

Cell fractionation

Cytoplasmic fractions were obtained by cell lysing in non-reducing 2% Triton X buffer containing 50 mM β-glycerophosphate, 10 mM NaPP, 30 mM NaF, 50 mM Tris-HCL, pH 7.5, 150 mM NaCl, 1 nM benzamidine, and 2 nM EGTA. Cells were lysed on ice for 1 h, followed by centrifugation for 10 min at 300 ×g.

Immunoprecipitation (IP)

Cytosolic lysates (150 µl) were incubated with 50 µl of magnetic protein A beads (Millipore, MA, USA) and placed on a rotating plate for 3 h at 4°C to minimize non-specific binding. After incubation, beads were removed and the supernatant transferred to a new tube. To the supernatant, 1 µl of anti-GSH antibody was added (Virogen, MA, USA) and the mixture was allowed to incubate overnight at 4°C. After overnight incubation, 50 µl of magnetic protein A beads were added to the sample mixture and allowed to incubate overnight at 4°C. After the secondary overnight incubation, samples were spun at 300 ×g and the supernatant was discarded. The pellet was washed 3 times with RIPA buffer. After the final wash step, the pellet was resuspended in 25 µl of resuspension buffer (a mixture of RIPA buffer and lysis buffer used for cell fractionation) then boiled for 10 min at 100 °C.

Western blotting

To analyze the redox state of IKK-γ, also known as NEMO, and to quantify S-glutathionylation of IKK-β and IκB-α, cytosolic and IP fractions were separated by native polyacrylamide gel electrophoresis and transferred to PVDF membranes. Primary antibodies were used at a dilution of 1:1000 in 10 ml of blocking buffer and incubated overnight at 4 °C, followed by three washes in TBS-T. Imaging and image analysis were conducted using the Li-Cor Odyssey Infrared Imaging System with the Odyssey 2.1 software. Where appropriate, β-actin was used as a loading control for normalization.

Intracellular GSH and GSSG quantification

Glutathione/glutathione disulfide assay (Oxford Biomedical, MI, USA) was used to measure GSH and GSSG levels in EU1 cytoplasmic lysate samples obtained after various Dox treatment conditions. GSH/GSSG quantification was achieved by the enzymatic recycling assay according to manufacturer's protocol.

Statistical Analysis

All values reported are the average of three or more independent biological replicates +/- standard error. Statistical significance is based upon the criteria of $p < 0.05$ for a Student's t-test (two-tailed, equal variance).

Computational modeling

To reconcile our experimental findings and to better understand the effect of the glutathione redox potential and the intracellular redox environment on chemotherapy-induced IKK-β S-glutathionylation, a biochemical model of pertinent reactions was constructed (Fig. 6-1). Previous models of ROS-induced protein thiol oxidation have characterized rate constants for the oxidation reactions that result in general protein thiol modification (Adimora et al, 2010; Antunes & Cadenas, 2000; Makino et al, 2004; Sasaki et al, 1998; Seaver & Imlay, 2001). The identification of oxidant targets based on the relative chemical reactivity of potential substrates (Winterbourn & Hampton, 2008), provided the quantitative basis by which a protein-specific S-glutathionylation model could be constructed.

A schematic diagram of the general framework of the model is shown in Figure 6-1. The model describes the relevant literature-reported processes that control oxidant-induced IKK-β S-glutathionylation. Upon Dox administration, intracellular enzymes convert the anthracycline drug into a semiquinone free radical (Bachur et al, 1979;

Cummings et al, 1992; Sinha et al, 1989). The differential equation describing the rate of change of intracellular semiquinone Dox as a function of time is modeled by the following equation:

$$\frac{d[Dox\ sq]}{dt} = 3.8 \times\ 10^{-7}\ \left(\frac{t}{60}\right) +\ 1.5 \times 10^{-5} \quad (6\text{-}1)$$

where t represents time in seconds. This equation was fit to the semiquinone Dox profile for a 500 nM Dox treatment condition, as predicted by a previous model of Dox bioactivation in EU1 cells (Chapter 4).

Reactions involving semiquinone Dox can also lead to the intracellular production of hydrogen peroxide (H_2O_2) and thiyl radicals ($RS^{\bullet}$) (Kostrzewa-Nowak et al, 2005; Menna et al, 2007; Ravi & Das, 2004). Molecular oxygen can react with semiquinone Dox to produce superoxide, which is converted to H_2O_2 by superoxide dismutase. Alternatively, intracellular proteins can react with the semiquinone Dox radical to produce the protein thiyl radical, $RS^{\bullet}$. The rate constants that describe the formation of H_2O_2 and $RS^{\bullet}$ from intracellular semiquinone Dox were estimated from the literature-reported reaction rates of molecular oxygen and protein thiols, respectively, with semiquinone Dox (Kalyanaraman et al, 1980; Winterbourn & Hampton, 2008).

The rate constants for the reactions used in the mathematical model for each treatment condition are shown in Table 6-1. Although these rates have units of inverse arbitrary unit × inverse time ($a.u.^{-1}s^{-1}$), the literature-reported proportionalities between the rate constants for the different reactions are conserved (Adimora et al, 2010; D'Autreaux & Toledano, 2007; Dalle-Donne et al, 2009; Winterbourn & Hampton, 2008). Correspondingly, the initial concentrations of the species utilized in the model (Table 6-2) also mirror the literature-reported proportionalities between each of the

components accounted for in the model (Adimora et al, 2010; Jones, 2008; Koshkin et al, 1997).

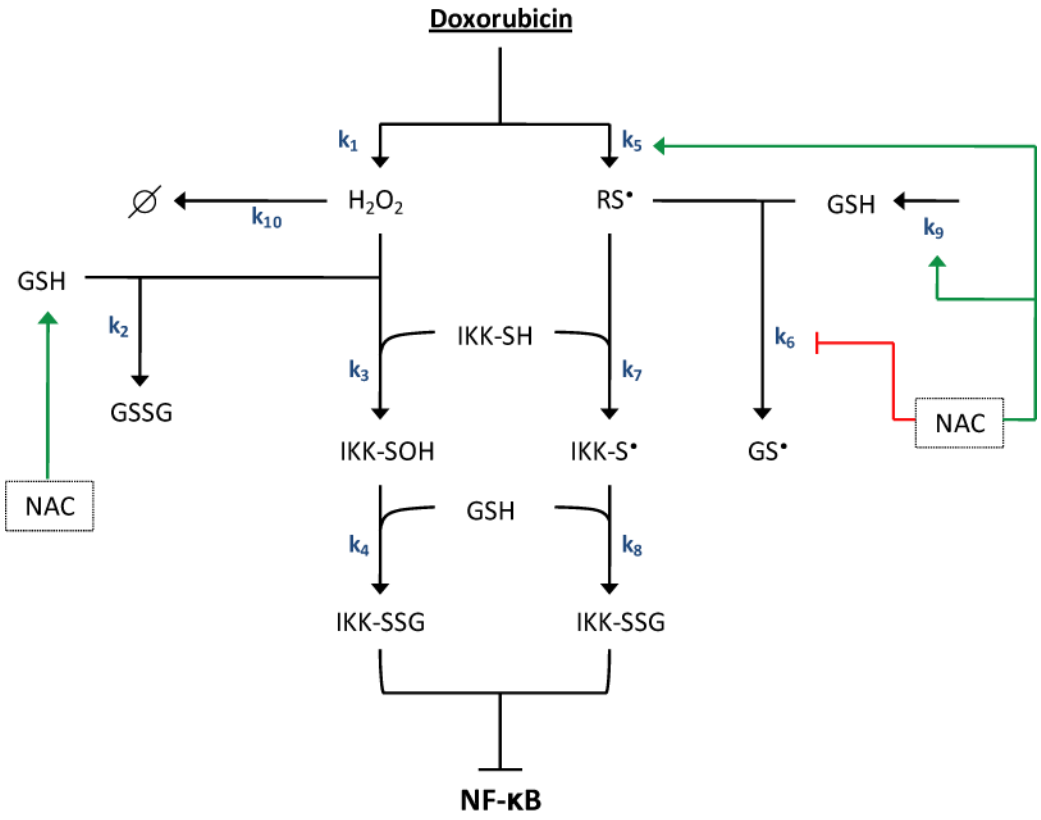

Figure 6-1. Mechanistic model of glutathione-dependent IKK-β S-glutathionylation. Schematic representation of the reactions involved in glutathione-dependent IKK-β S-glutathionylation. Dox treatment promotes the formation of hydrogen peroxide (H_2O_2) and protein thiyl radicals ($RS^{\bullet}$). Once formed, H_2O_2 mediates the S-glutathionylation of reduced IKK-β via the peroxide-dependent oxidation of IKK-β. Concurrently, Dox-induced $RS^{\bullet}$ formation induces IKK-β S-glutathionylation via the radical-dependent oxidation of IKK-β. However, increased thiyl radical levels simultaneously promote the radical oxidation of GSH into the glutathione thiyl radical ($GS^{\bullet}$) which serves to effectively diminish reduced GSH levels from the intracellular environment. NAC, the GSH precursor, regulates the peroxide-dependent and the radical-dependent mechanisms of IKK-β S-glutathionylation via its ability to promote glutathione synthesis as well as its ability to contribute to free-radical formation.

Table 6-1: Rate expressions and rate constants for the ODEs that comprise the mechanistic IKK-β S-glutathionylation model.

		Parameter Value at Various [NAC](mM)[*]			
Rxn	*Expression*	*0*	*0.5*	*1*	*5*
R_1	k_1 ([Dox sq]) → H_2O_2	$k_1 = 6.0 \times 10^{-3}$	6.0×10^{-3}	6.0×10^{-3}	6.0×10^{-3}
R_2	k_2 ([GSH]) ([H_2O_2]) → GSSG	$k_2 = 2.0 \times 10^{-3}$	2.0×10^{-3}	2.0×10^{-3}	2.0×10^{-3}
R_3	k_3 ([IKK-SH]) ([H_2O_2]) → IKK-SOH	$k_3 = 5.0 \times 10^{-5}$	5.0×10^{-5}	5.0×10^{-5}	5.0×10^{-5}
R_4	k_4 ([IKK-SOH]) ([GSH]) → IKK-SSG	$k_4 = 6.0 \times 10^{-3}$	6.0×10^{-3}	6.0×10^{-3}	6.0×10^{-3}
R_5	k_5 ([Dox sq]) → $RS^{\bullet}$	$k_5 = 1.2 \times 10^{-3}$	3.7×10^{-3}	3.7×10^{-3}	3.7×10^{-3}
R_6	k_6 ([GSH]) ([$RS^{\bullet}$]) → $GS^{\bullet}$	$k_6 = 5.0 \times 10^{-3}$	5.0×10^{-3}	5.0×10^{-3}	2.5×10^{-3}
R_7	k_7 ([IKK-SH]) ([$RS^{\bullet}$]) → IKK-$S^{\bullet}$	$k_7 = 5.0 \times 10^{-4}$	5.0×10^{-4}	5.0×10^{-4}	5.0×10^{-4}
R_8	k_8 ([GSH]) ([IKK-$S^{\bullet}$]) → IKK-SSG	$k_8 = 5.0 \times 10^{-3}$	5.0×10^{-3}	5.0×10^{-3}	5.0×10^{-3}
R_9	k_9 → [GSH]	$k_9 = 6.0 \times 10^{-2}$	1.8×10^{-1}	3.7×10^{-1}	6.0×10^{-1}
R_{10}	k_{10} ([H_2O_2]) → Null	$k_{10} = 5.2 \times 10^{-3}$	5.2×10^{-3}	5.2×10^{-3}	5.2×10^{-3}

[*]Reaction rate constants highlighted in red represent the rate constants that were fitted to experimentally-determined IKK-SSG behavior for the various NAC pretreatment conditions investigated. The rate constants are given in units of inverse a.u. × inverse time (a.u.$^{-1}$s^{-1})

Table 6-2: Initial concentration values of the components that comprise the mechanistic model of IKK-β S-glutathionylation.

Species	*Initial Condition (A.U.)*	*Reference*
[Dox sq]	6.5	Assigned
[H_2O_2]	0	Assigned
[$RS^{\bullet}$]	0	Assigned
[GSH]	500	(Schafer & Buettner, 2001)
[GSSG]	5	(Schafer & Buettner, 2001)
[$GS^{\bullet}$]	0	Assigned
[IKK-SH]	50	(Winterbourn & Hampton, 2008)
[IKK-SOH]	0	Assigned
[IKK-$S^{\bullet}$]	0	Assigned
[IKK-SSG]	0	Assigned

Major assumptions of the mechanistic model

The mechanistic model constructed for this study was based on the assumption that the GSH/GSSG redox couple is effectively insulated from the other major redox couples that comprise the mammalian antioxidant network (Adimora et al, 2010; Jones et al, 2004; Kemp et al, 2008). One of the main goals of this study was to evaluate whether variations in the redox potential of the GSH/GSSG redox couple can be significant enough to alter a redox-sensitive signaling process, the S-glutathionylation of IKK-β. Moreover, this study sought to determine whether qualitative observations regarding the directional effects of NAC pretreatment on particular redox-reaction rates could be effectively translated into accurate quantitative descriptions of IKK-β S-glutathionylation. To accomplish these tasks, it was necessary to develop a model for ROS-dependent IKK-β S-glutathionylation that explicitly described glutathione-dependent reactions only.

The next major assumption involved the effect of NAC pretreatment on the rates of formation of reduced glutathione (GSH), protein thiyl radical ($RS^{\bullet}$) and glutathione thiyl radical ($GS^{\bullet}$). NAC is well known for its ability to affect intracellular glutathione levels as it can be utilized as a substrate for glutathione synthesis (Raftos et al, 2010). However, because a molecule of NAC does not instantaneously transform into a molecule of GSH upon entrance into the cell, and because the kinetic characteristics of the enzymatic transformation of NAC into GSH are not well characterized (Raftos et al, 2010), it was deemed inappropriate to directly model the effect of NAC pretreatment as an instantaneous change to the initial level of reduced GSH in the model system. Instead, the effect of NAC pretreatment was modeled as a change to the synthesis rate of total free glutathione, as described previously (Raftos et al, 2010); NAC pretreatment was assumed to have no effect on the synthesis rates of the other molecular species that comprise the model.

The proposed model explicitly describes only a subset of the glutathione-dependent reactions that are assumed to take place within a given cell upon Dox administration. However, because other glutathione-dependent reactions occur during conditions of oxidative stress (Adimora et al, 2010) these additional reactions had to be implicitly taken into account by the model. Without the explicit inclusion of all GSH-dependent reduction reactions that involve intracellular proteins, an alternate technique was needed to accurately represent the competition over reduced GSH that exists across potential GSH targets *in vivo*. To prevent overestimation of GSH-dependent reduction in the model system, a viable modeling technique is to estimate the relative concentration of GSH that would be specifically available for reaction with oxidized IKK-β. This scaled GSH concentration was calculated from a previously published competition equation (Winterbourn & Hampton, 2008) that takes into account the ratio of [IKK-β] to [total protein] and the rate constant describing the GSH-dependent reduction of oxidized protein thiol (Adimora et al, 2010; Winterbourn & Hampton, 2008). Other assumptions made in the construction of the mechanistic model include the assumption that Dox degradation and efflux was negligible for the duration of the treatment (Ozols et al, 1979) and that all oxidation reactions occurred in the absence of target recycling.

Major assumptions utilized during mechanistic model fitting

Certain rules were utilized and assumptions made to determine the exact way in which NAC-dependent rate constant modulation was to be modeled and tested for its ability to explain experimental data. First, the reaction rates that were allowed to be modified by the presence of NAC were determined through an extensive literature search of the possible ways in which NAC can alter the intracellular redox environment. Preliminary searches indicated that a role for NAC, and other low molecular weight thiols, in the direct elimination of intracellular H_2O_2 is improbable due to low rate constant values for their reaction with hydrogen peroxide (D'Autreaux & Toledano, 2007;

Winterbourn & Hampton, 2008; Winterbourn & Metodiewa, 1999). The high proportion of GSH that is oxidized to GSSG by H_2O_2, as described by the model (Fig. 6-1), is representative of the GSH-dependent, GPx-catalyzed reduction of peroxide which occurs at a significantly fast rate (Ng et al, 2007). Based on this experimental detail, all peroxide-dependent reactions were excluded from explicit NAC-dependent alterations.

Next, the effect of NAC pretreatment on GSH-dependent reactions was investigated because NAC is known to modulate GSH synthesis. Since quantitative details of the effect of NAC pretreatment on GSH synthesis have been shown in the literature (Raftos et al, 2010), these quantitative effects were directly modeled for the various NAC pretreatment conditions considered. The fold-increases over the basal GSH synthesis rate that were experimentally reported for the various extracellular NAC treatment conditions being simulated were directly utilized in the mechanistic model, e.g. if 0.5 mM extracellular NAC was reported to result in a 2-fold increase in the rate of total free glutathione synthesis, then the basal rate of GSH synthesis in the model was automatically increased by 2-fold for the 0.5 mM [NAC] pretreatment condition. It was assumed that any additional modulation of non-radical, GSH-dependent reactions as a result of NAC pretreatment, through the explicit alteration of their respective rate constants, would overestimate the effect of increased GSH availability on the protein S-glutathionylation network being modeled. As a result, NAC-induced changes to the peroxide-dependent reactions that involve GSH were implicitly described by the literature reported effects of NAC pretreatment on GSH synthesis.

Lastly, the effect of NAC pretreatment on reactions involving thiyl radicals ($RS^{\bullet}$, $GS^{\bullet}$) was considered. A major goal of this study was to develop a mechanistic description of the effect of NAC pretreatment on a redox-sensitive process, namely IKK-β S-glutathionylation. Moreover, this goal was to be achieved without the explicit inclusion of all the details involved in the S-glutathionylation process. The following reactions were consulted to determine which, if any, of the radical-related reactions could

potentially be modified by NAC pretreatment *in vivo*, and the directionality of the proposed modifications (Nappi & Vass, 1997):

$$H_2O_2 + Fe^{2+} \rightarrow Fe^{3+} + OH^{\bullet} + HO^{-} \quad (6\text{-}2)$$

$$RSH\ (or\ NAC) + Fe^{3+} \rightarrow Fe^{2+} + RS^{\bullet} \quad (6\text{-}3)$$

Equation 6-2 represents the Fenton reaction of transition metals (Fe^{2+}) with H_2O_2 to produce Fe^{3+} and $OH^{\bullet}$ radical. Equation 6-3 represents the Haber-Weiss reaction of low molecular weight thiols or NAC with Fe^{3+} to produce protein thiyl radical species. Because iron is in excess in most mammalian cells (Kabat & Rohan, 2007), these two reactions, taken together, qualitatively illustrate that in the presence of peroxide, increased NAC availability will promote the formation of protein thiyl radicals.

The literature reports suggest that increased thiol availability, as a result of NAC administration, increases thiyl radical formation and thiyl-based oxidation by approximately 3-fold (O'Brien, 1988; Sagrista et al, 2002). Moreover, the systematic titration of various extracellular NAC concentrations, at various levels of initial [H_2O_2], yields a sigmoidal relationship between the extracellular NAC pretreatment concentration applied and the extracellular NAC concentration at which the 3-fold-change increase in thiyl radical formation was observed (Sagrista et al, 2002) (Fig. 6-2). From these literature-reported findings, it was concluded that the effect of NAC pretreatment could be modeled as a 3-fold increase in the rate of $RS^{\bullet}$ formation (k_5), for a given NAC pretreatment condition. Moreover, due to the sigmoid behavior of the effect of NAC pretreatment on thiyl radical formation, it was assumed that once the 3-fold increase in protein thiyl radical formation rate was fit to a particular NAC pretreatment condition, all subsequent NAC pretreatment conditions would maintain the same effect.

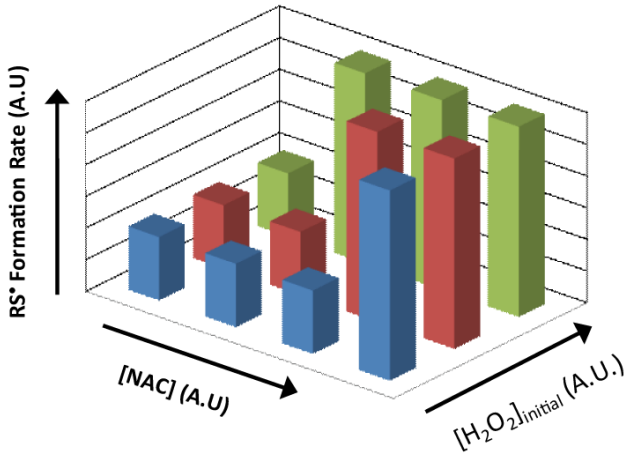

Figure 6-2. Effect of NAC thiols on peroxide-dependent protein thiyl ($RS^{\bullet}$) radical formation. The proposed extracellular [NAC]-dependent effects on protein thiyl radical formation rate as a function of initial H_2O_2 concentration. The rates of formation of protein thiyl radicals are not increased by NAC pretreatment until the concentration of NAC reaches a critical level. If [NAC] is at or above this threshold level, the rate of protein thiyl radical formation is increased by a factor of 3. Additionally, the threshold level of NAC at which this 3-fold increase in $RS^{\bullet}$ formation rate occurs is dependent on the initial concentration of H_2O_2 in the system. For lower levels of H_2O_2, the critical [NAC] is relatively high, whereas for higher levels of H_2O_2, the critical [NAC] is relatively low. Image adapted from the lipid peroxidation profiles described by (Sagrista et al, 2002).

The effect of NAC pretreatment on $GS^{\bullet}$ formation rate (k_6) was deduced using the same methodology that was employed to determine the effect of NAC pretreatment on $RS^{\bullet}$ formation rate (k_5). Consider the following radical-related reactions (Halliwell, 1991; O'Brien, 1988; Sagrista et al, 2002):

$$NAC + RS^{\bullet} \rightarrow NAC^{\bullet} + RSH \qquad (6\text{-}4)$$

$$GSH + RS^{\bullet} \rightarrow GS^{\bullet} + RSH \qquad (6\text{-}5)$$

Equations 6-4 and 6-5 represent the potential fates of the protein thiyl radical upon reaction with NAC or GSH thiols. In the absence of NAC, the rate of formation of $GS^{\bullet}$

(k_6) is larger than the rate of formation of $GS^{\bullet}$ in the presence of NAC. This occurs because NAC and GSH effectively compete over the limited pool of available intracellular radicals (Winterbourn & Hampton, 2008). Because this competition exists between NAC and GSH, as is illustrated by Equations 6-4 and 6-5, one can qualitatively conclude that increased NAC availability will decrease the formation of glutathione thiyl radicals.

Once the directionality of NAC-dependent modification was determined for the rate of formation of glutathione thiyl radicals, an appropriate quantitative estimate of the magnitude of this modification was needed. The rate at which NAC reacts with radicals is comparable to the rate at which GSH reacts with radicals (Winterbourn & Hampton, 2008; Winterbourn & Metodiewa, 1999). If it is assumed that the intracellular concentration of NAC at which NAC begins to compete with GSH for thiyl radicals is comparable to the intracellular concentration of GSH, then NAC pretreatment will decrease GSH thiyl radical formation by 2-fold according to the following equations (Winterbourn & Hampton, 2008):

$$\frac{-d[RS^{\bullet}]}{dt} = k_{GSH}[RS^{\bullet}][GSH] + k_{NAC}[RS^{\bullet}][NAC] \quad (6\text{-}6)$$

$$\frac{R_{GSH}}{R_{NAC}} = k_{GSH}[GSH]/k_{NAC}[NAC] \quad (6\text{-}7)$$

Equation 6-6 represents the rate equation for the second order $RS^{\bullet}$ reduction processes involving GSH and NAC, respectively. Equation 6-7 represents the flux ratio between the GSH-dependent and NAC-dependent $RS^{\bullet}$-reduction reactions. If [NAC] is equal to [GSH], as was previously assumed, and if k_{GSH} is equal to k_{NAC}, as has been previously reported (Winterbourn & Hampton, 2008; Winterbourn & Metodiewa, 1999), then a 1:1 flux ratio exists between the two competing reactions. Therefore in the

presence of NAC, it can be assumed that the rate of GSH thiyl radical formation will be decreased by a factor of 2.

Assuming that NAC pretreatment will only affect $GS^{\bullet}$ formation when the intracellular NAC concentration is at or above a certain threshold allows us to impose a sigmoidal type of relationship between NAC pretreatment and NAC-induced effects on $GS^{\bullet}$ formation rates. Moreover, because intracellular NAC is efficiently converted to GSH and cysteine (Cys) (Raftos et al, 2010), and because the levels of these species are regulated by transport mechanisms (Jones, 2008), the maximum levels of free intracellular NAC will most likely not exceed intracellular levels of GSH within the cell (Burgunder et al, 1989). Therefore, NAC pretreatment conditions above those that produce the threshold level of intracellular NAC at which the $GS^{\bullet}$ formation rates are affected will still result in a 2-fold decrease in the rate of $GS^{\bullet}$ formation. This type of sigmoidal behavior, as a function of NAC-pretreatment, is not unprecedented (Sagrista et al, 2002).

Results

Dox treatment induces ROS in EU1 cells that can be attenuated by NAC pretreatment

To characterize the capacity for Dox treatment to induce ROS generation in leukemia cells, the EU1 ALL cell line was treated with Dox (5 μM) for various time points, after which, Dox-induced ROS generation was quantified by plate reader measurement of H_2DCFDA fluorescence (Fig. 6-3). A significant increase in ROS production was seen at around 40 min of Dox treatment. This increase in ROS production was substantial with regards to its amplitude and its duration. After 40 min of Dox treatment, ROS levels had increased by 50% above baseline and the Dox-induced ROS levels continued to rise, almost reaching 2x its baseline value by 60 min of Dox treatment (Fig. 6-3).

Next, the ability of NAC to prevent Dox-induced ROS generation was assessed. EU1 cells were pretreated with NAC (1 mM) for 30 min followed by Dox administration (5 μM) for various time points up to 1 h (Fig. 6-3). Results show that NAC pretreatment was able to inhibit Dox-induced ROS in the EU1 cells. The deviation between the ROS profiles of EU1 cells with and without NAC pretreatment was evident by 30 min of Dox treatment and became more pronounced during the remainder of the treatment (Fig. 6-3). While the EU1 cells without NAC pretreatment experienced increased Dox-induced ROS levels up to 2x their baseline values, the NAC pretreated EU1 cells were able to maintain their baseline ROS levels for the majority of the treatment.

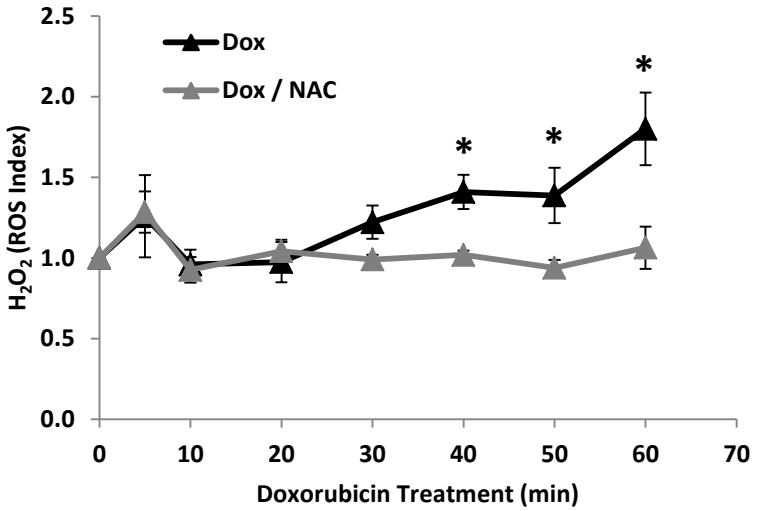

Figure 6-3. Dox treatment induces ROS in EU1 cells that can be attenuated by N-acetylecysteine (NAC) pre-treatment. Time-dependent Dox-induced H_2O_2 in EU1 cells, with and without NAC pre-treatment, quantified by plate reader measurement of H_2DCFDA fluorescence. ([NAC] = 1 mM, 30 min pre-treatment; [Dox] = 5 μM, 1 hr treatment; *$p < 0.05$)

NAC promotes Dox-induced NF-κB by selectively regulating ROS-induced IKK-β S-glutathionylation

The role that ROS play in regulating NF-κB activation has been addressed previously in the literature and multiple points of redox regulation have been reported, such as the disulfide-based dimerization of NEMO, the S-glutathionylation of IκB-α, and the S-glutathionylation of IKK-β (Oliveira-Marques et al, 2009). However, if a greater understanding of the mechanism by which Dox alters this pathway is to be achieved, it is necessary to determine the specific components in the pathway that are susceptible to Dox-induced ROS. To achieve this goal, luciferase-transduced EU1 cells were treated for 1 h with various combinations of NAC, Dox, and the IKK-β inhibitor, SC-514; the effects of these varied treatment conditions on NF-κB activation were quantified by plate reader

measurement of luciferase luminescence (Fig. 6-4 A). Dox treatment of luciferase-transduced EU1 cells led to a significant increase in NF-κB reporter activity. NAC pretreatment prior to Dox administration resulted in an even greater response in NF-κB reporter activity; luciferase luminescence values were almost 2x that of the Dox-only treatment group. However, when luciferase-transduced cells were pretreated with SC-514 (100 μM) prior to Dox administration, the Dox treatment regimen was no longer able to induce NF-κB reporter activity (Fig. 6-4 A). Moreover, when SC-514-pretreated cells were exposed to NAC, prior to Dox administration, the Dox treatment regimen was also unable to induce NF-κB reporter activity.

Having examined the general effects of NAC pretreatment on Dox-induced NF-κB activation, a more specific examination of the individual components of the NF-κB activation pathway was carried out. NEMO has been shown to undergo disulfide bond formation during periods of oxidative stress and this process is thought to positively contribute to NF-κB activation (Herscovitch et al, 2008). The effect of Dox treatment and NAC pretreatment on NEMO dimerization was assessed. Dox treatment did not result in any significant changes to the levels of disulfide bonded NEMO protein in EU1 cells; the same results were seen in the NAC-pretreated cells (Fig. 6-4 B).

Cys 179 of IKK-β (de Oliveira-Marques et al, 2007; Oliveira-Marques et al, 2009; Reynaert et al, 2006) and Cys 189 of IκB-α (Kil et al, 2008) have been reported as potential targets of protein S-glutathionylation with functional consequences on catalytic activity and protein-protein interactions; the addition of a glutathione moiety to an active cysteine residue of a protein can result in structural changes to the protein or blocked access to critical amino acid residues, two processes that can potentially inhibit DNA binding, enzyme attachment, or protein phosphorylation (Dalle-Donne et al, 2009). To assess the effect of Dox treatment on the S-glutathionylation of IKK-β and IκB-α, EU1 cells, with or without NAC pretreatment, were exposed to Dox for 1 h and then lysed. Protein-glutathione mixed disulfides were immunoprecipitated from cytoplasmic lysates

with an anti-GSH antibody then run on a western blot to quantify the relative amounts of IKK-β and IκB-α (Fig. 6-4 C, D). Doxorubicin treatment induced significant S-glutathionylation of IKK-β but insignificant S-glutathionylation of IκB-α. The basal level of S-glutathionylated IKK-β was significantly larger than that of S-glutathionylated IκB-α. NAC pretreatment was able to rescue the EU1 cells from Dox-induced IKK-β S-glutathionylation; however, NAC pretreatment had no effect on the low levels of Dox-induced IκB-α S-glutathionylation that were quantified (Fig. 6-4 C, D). NAC pretreatment was able to decrease the level of S-glutathionylated IKK-β independent of Dox administration.

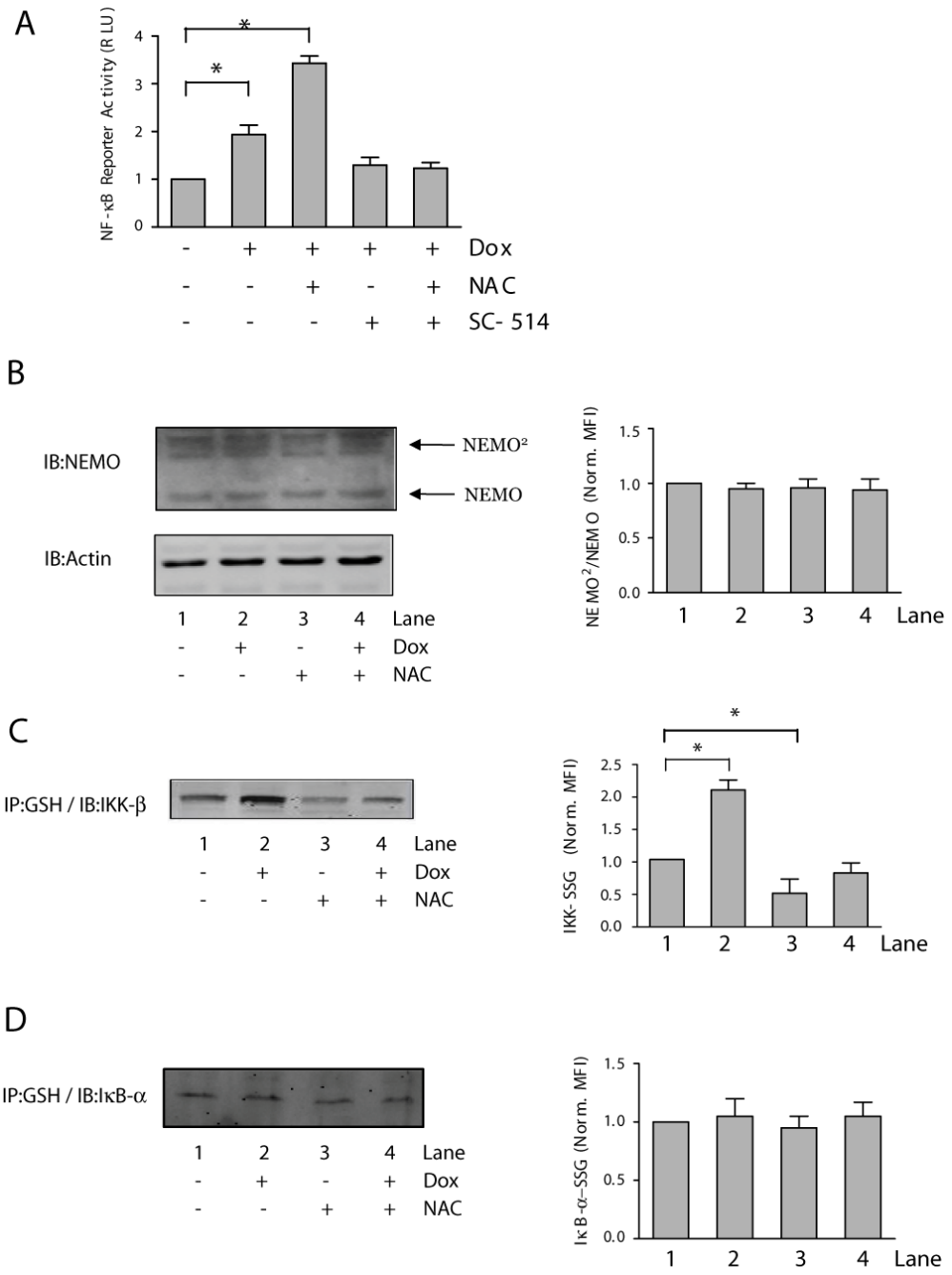

Figure 6-4. Dox-induced NFKB activity in EU1 cells is IKK-β dependent and promoted by NAC pre-treatment. (A) NF-κB activity, expressed as luciferase fold induction, in untreated and Dox-treated EU1 cells with and without pre-treatment with NAC or IKK-β inhibitor, SC-514. Representative immunoblot analysis, with accompanying densitometry quantification normalized to lane 1, of (B) Dox-induced NEMO dimerization, (C) Dox-induced IKK-β S-glutathionylation, and (D) Dox-induced IκB-α S-glutathionylation in EU1 cells, with and without NAC pretreatment. ([NAC] = 1 mM, 30 min pre-treatment; [SC-514] = 100 μM, 1hr pre-treatment; [Dox] = 5 μM, 4 hr treatment; *$p < 0.05$).

NAC modulates Dox-induced glutathione redox status, Dox-induced IKK-β S-glutathionylation and Dox-induced NF-κB activation

To examine the effect of NAC pretreatment on Dox-induced glutathione redox balance, EU1 cells were pretreated with various concentrations of NAC (0.5 – 5 mM) to alter the intracellular GSH/GSSG redox state prior to Dox treatment. The EU1 cells were pretreated with designated concentrations of NAC for 30 min followed by Dox (500 nM) administration for 1 h. A Dox concentration of 500 nM was utilized because a previous model of Dox bioactivation (Chapter 4) suggested a more substantial role for Dox-mediated signaling at low Dox concentrations. After Dox treatment, the intracellular glutathione redox balance was quantified (Fig. 6-5 A). NAC pretreatment prior to Dox administration promoted increased ratios of GSH/GSSG. The 0.5 mM NAC pretreatment condition resulted in GSH/GSSG values that were 3x higher than the GSH/GSSG values measured for the EU1 cells treated with Dox in the absence of NAC. The 5 mM NAC pretreatment group displayed similar GSH/GSSG values to the 0.5 mM NAC pretreatment group. Interestingly, however, the 1 mM NAC pretreatment condition, though it too resulted in increased GSH/GSSG values compared to the Dox-only controls, showed a slightly decreased GSH/GSSG compared to the 0.5 mM and 5 mM treatment groups (Fig. 6-5 A). Dox-induced ROS formation was also quantified as a function of NAC pretreatment condition (Fig. 6-5 B). The 0.5 mM NAC pretreatment group showed no significant difference in Dox-induced ROS formation compared to the Dox-only controls. Significant decreases in Dox-induced ROS, compared to the Dox-only controls, were seen only in the 1 mM and 5 mM NAC pretreatment groups.

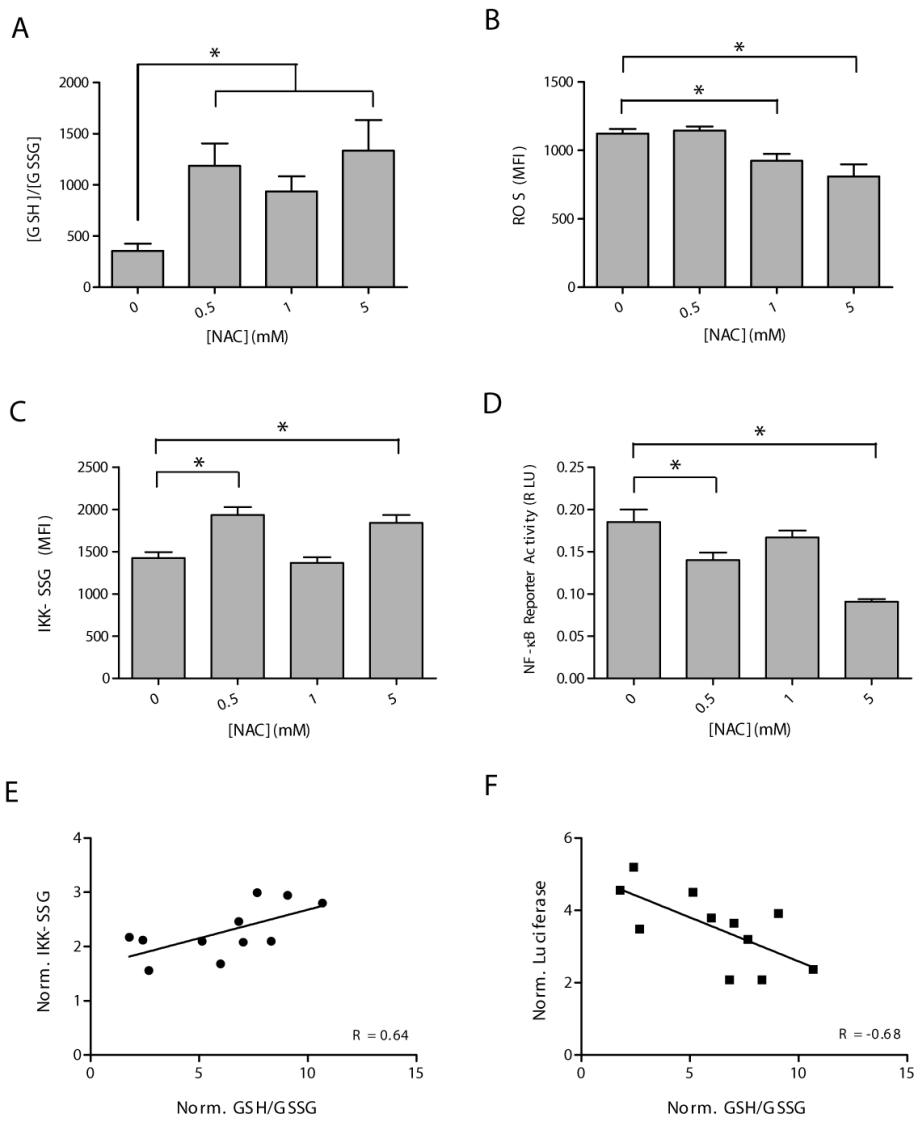

Figure 6-5. NAC controls Dox-induced IKK-β S-glutathionylation by modifying intracellular glutathione redox balance. EU1 cells were treated with various concentrations of NAC prior to Dox administration. After treatment, cells were harvested and lysed; (A) the intracellular GSH/GSSG ratio was quantified using an enzymatic recycling assay, and (B) the intracellular ROS was quantified using plate reader measurement of H_2DCFDA fluorescence. Luciferase-tranduced and non-tranduced EU1 cells, respectively, were pretreated with various concentrations of NAC prior to Dox administration and then lysed; (C) the intracellular levels of S-glutathionylated IKK-β were quantified by IP and western blot, and (D) the activity of NF-κB was quantified by plate reader measurement of luciferase luminescence. (E, F) Correlation plots of standardized Dox-induced IKK-β S-glutathionylation and standardized Dox-induced luciferase luminescence were plotted against standardized GSH/GSSG ratios. Pearson coefficients for the linear correlations are shown in each graph. (NAC = 30 min pre-treatment; [Dox] = 500 nM, 1 hr treatment; *$p < 0.05$)

To examine the effect of altered glutathione redox balance on Dox-induced NF-κB activity, non-transduced and luciferase-transduced EU1 cells were pretreated for 30 min with various concentrations of NAC (0.5 – 5 mM) prior to Dox (500 nM) administration for 1 h. After treatment, the intracellular concentration of S-glutathionylated IKK-β was quantified in the non-transduced EU1 cells, while Dox-induced NF-κB was quantified in the luciferase-transduced cells (Fig. 6-5 C, D). Surprisingly, none of the NAC pretreatment conditions were able to inhibit Dox-induced IKK-β S-glutathionylation at the 500 nM [Dox] condition (Fig. 6-5 C), as was previously seen for the 5 μM [Dox] treatment condition (Fig. 6-4 C). In fact, both the 0.5 mM and the 5 mM NAC pretreatment groups led to an increased level of Dox-induced IKK-β S-glutathionylation. The 1 mM NAC pretreatment group exhibited the same amount of Dox-induced IKK-β S-glutathionylation as the Dox-only treatment group (Fig. 6-5 C). Correspondingly, none of the NAC pretreatment groups were able to promote Dox-induced NF-κB activity to levels that were significantly higher than the Dox-only group (Fig. 6-5 D), a phenomenon that was exhibited at the 5 μM [Dox] treatment condition (Fig. 6-4 A). Both the 0.5 mM and the 5 mM NAC pretreatment groups experienced significantly less Dox-induced NF-κB activity compared to the Dox-only group. NAC pretreatment at the 1 mM level did not significantly affect Dox-induced NF-κB activity compared to the Dox-only controls (Fig. 6-5 D).

Linear correlation analyses were carried out to determine the degree to which the GSH/GSSG redox balance can be related to Dox-induced IKK-β S-glutathionylation and Dox-induced NF-κB activity. Results of this analysis reveal that the GSH/GSSG redox balance has a strong positive correlation to the level of Dox-induced IKK-β S-glutathionylation (Fig. 6-5 E). The Pearson's correlation value for this linear relationship was + 0.64. Interestingly, the GSH/GSSG redox balance has a strong negative correlation to the level of Dox-induced NF-κB activity (Fig. 6-5 F), with a Pearson's correlation value for this linear relationship of -0.68.

A Mechanistic model predicts dual roles for NAC in modulating glutathione-dependent IKK-β S-glutathionylation

The consistent biphasic trends we observed with NAC dosage required the development of biochemical models to test potential mechanisms by which NAC modulates IKK-β S-glutathionylation. Literature-reported effects of NAC treatment were systematically simulated and tested for their ability to reproduce the complex behavior of IKK-SSG levels under various NAC pretreatment conditions (Fig. 6-6). NAC treatment is known to induce GSH synthesis, so with increasing levels of NAC, the rate constant for GSH synthesis was proportionally increased according to published data on the effect of NAC treatment on the rate of GSH synthesis in the erythrocyte cell (Raftos et al, 2010). The rates of GSH synthesis for the four NAC treatment conditions are shown in Table 6-1. Literature-reported qualitative details related to NAC-dependent protein and GSH thiyl radical formation rates were translated into semi-quantitative rules that were used to determine the extracellular NAC pretreatment concentrations at which a 3-fold increase in protein thiyl radical formation rate and a 2-fold decrease in GSH thiyl radical formation would initially occur. The 3-fold and 2-fold effects of NAC pretreatment on the $RS^{\bullet}$ and $GS^{\bullet}$ formation rates were deduced from literature-published studies and the related redox-reactions that were derived from those studies (Halliwell, 1991; Nappi & Vass, 1997; O'Brien, 1988; Raftos et al, 2010; Sagrista et al, 2002; Winterbourn & Hampton, 2008). An illustration of the systematic process by which the model-fitting was carried out is shown in Figure 6-6.

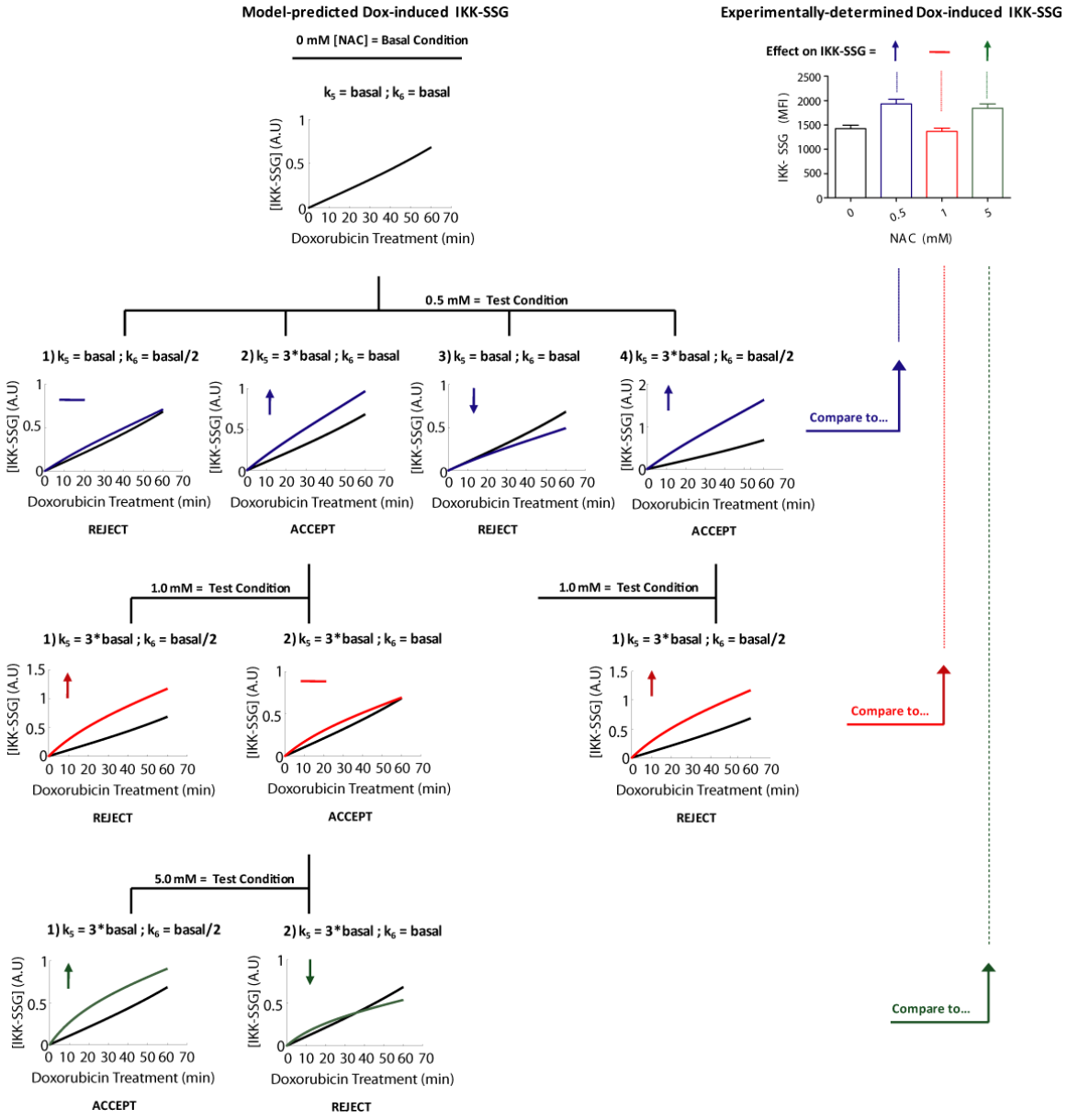

Figure 6-6. Schematic representation of the algorithm utilized to systematically predict the effect of NAC pretreatment on NAC-sensitive model parameters. Directional arrows represent the experimentally-measured effect of the NAC pretreatment, at various NAC concentrations, on IKK-SSG levels compared to control.

The systematic alteration of the rate constants describing the NAC-sensitive reactions (k_5, k_6) was carried out for the various NAC pretreatment conditions. The effect of NAC pretreatment on GSH synthesis was not considered to be a testable parameter in need of model fitting since the effect of NAC on GSH synthesis had already been quantitatively characterized in the literature (Raftos et al, 2010). The two NAC-dependent alterations that were tested were the threshold NAC concentrations at which the 3-fold NAC-dependent increase in $RS^{\bullet}$ formation rate (k_5) and the 2-fold NAC-dependent decrease in $GS^{\bullet}$ formation rate (k_6) occurs.

The 0.5 mM NAC pretreatment condition was analyzed first. For the 0.5 mM NAC pretreatment condition, all permutations of the two potential NAC-dependent effects were tested for their ability to replicate experimentally derived IKK-SSG levels (Fig. 6-6). The combinations that produced an increase in IKK-SSG levels compared to the 0 mM NAC pretreatment condition (basal), as was seen experimentally, were selected as potential candidates for further analysis. Those combinations that did not produce the experimentally-determined increase in IKK-SSG levels at the 0.5 mM condition were rejected; further analysis of these combinations at the 1 and 5 mM NAC pretreatment conditions were unnecessary due to the sigmoidal nature of the NAC-dependent effects (Fig. 6-2). This process was carried out consecutively for the 1 mM and 5 mM NAC pretreatment conditions to determine which of the possible combinations could effectively describe experimentally-determined Dox-induced IKK-SSG for all NAC pretreatment conditions (Fig. 6-6).

The results of the model-fitting simulations predict that the two processes susceptible to NAC modulation (apart from the well characterized GSH synthesis reactions (R_9)) exhibit their NAC-susceptibility at different extracellular NAC concentrations (Table 6-1). The model predicts that increasing concentrations of NAC result in a threshold-dependent decrease in the rate of GSH thiyl formation (R_6). The model confirms literature reports that show increasing concentrations of NAC result in a

threshold-dependent increase in the rate of protein thiyl radical formation (R_5) (Sagrista et al, 2002). The model predicts that the minimum [NAC] that produces the threshold-dependent decrease in the rate of GSH thiyl radical formation is higher than the minimum [NAC] that produces the threshold-dependent increase in the rate of protein thiyl radical formation (Table 6-1).

The mechanistic model behavior was fitted to the experimental dataset of Dox-induced IKK-β S-glutathionylation (Fig. 6-7 A). To test the universality of the model-predicted mechanism of IKK-β S-glutathionylation, the model-predicted step-like responses of (R_5) and (R_6) and the graded response of (R_9) to increasing NAC concentrations were tested in their ability to predict IKK-β S-glutathionylation as a result of a new experimental condition, NAC treatment only, independent of Dox. The mechanistic model was able to accurately predict NAC-dependent IKK-β S-glutathionylation in the absence of Dox treatment for a variety of NAC pretreatment conditions (Fig. 6-7 B) without any additional model fitting.

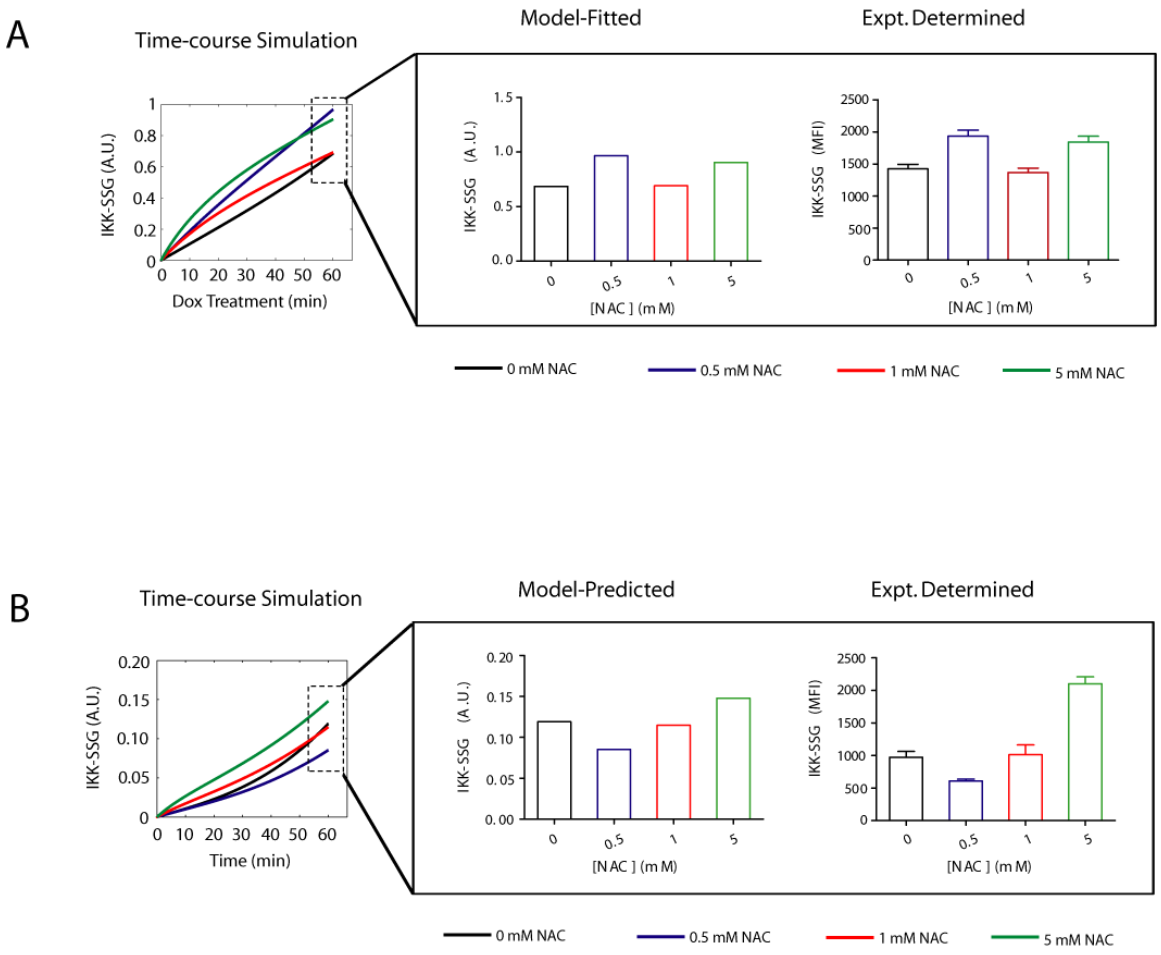

Figure 6-7. Mechanistic mathematical model of IKK-β S-glutathionylation predicts experimental behavior. (A) Model-fitted and experimentally-derived values for Dox-induced IKK-β S-glutathionylation after various NAC pretreatment regimens. (B) Model-predicted and experimentally-derived values for IKK-β S-glutathionylation after various NAC pretreatment regimens without Dox treatment.

Discussion

IKK-β, NEMO and IκB-α have differential sensitivities to chemotherapy-induced ROS

The NF-κB signal transduction pathway is a well-characterized redox sensitive pathway containing several proteins that are believed to be regulated by oxidative stress (Oliveira-Marques et al, 2009; Reynaert et al, 2006). In this study, the administration of clinically-relevant concentrations of Dox were utilized to decipher the points in the NF-κB activation pathway that are most sensitive to chemotherapy-induced ROS generation in a pediatric ALL cell line. Results suggest that in EU1 cells, NEMO dimerization is insensitive to ROS induced by Dox (Fig. 6-4 B). While it has been shown in the literature that NEMO dimerization does occur within mammalian cells (Herscovitch et al, 2008), and is a necessary step for some methods of NF-κB activation (Marienfeld et al, 2006), these results are consistent with reports that in some cell lines NEMO dimer formation remains unaltered upon stimulation (Marienfeld et al, 2006). This insensitivity could be the result of several factors. Primarily, the formation of disulfide bonds is a relatively fast process (Adimora et al, 2010; Winterbourn & Metodiewa, 1999) and is therefore highly sensitive to the intracellular redox environment. Cancer cells are well known to have higher than normal levels of oxidants and are considered to be under oxidative stress conditions even in the absence of external stimuli (Marnett, 2000; Mates et al, 1999). This basal oxidative condition could potentially induce substantial amounts of NEMO dimerization in the absence of external stimuli. If this is the case, then Dox treatment would result in little to no change in NEMO dimer levels. This dependency of NEMO dimerization on the intracellular redox environment is further supported by the fact that cells of different lineages exhibit significantly different levels of NEMO dimerization under basal conditions (Herscovitch et al, 2008).

The administration of Dox to the EU1 cells did not result in significant increases in the level of IκB-α-SSG, but did result in increases in the level of IKK-β-SSG (Fig. 6-4 C, D). While both of these processes involve protein-S glutathionylation (Kil et al, 2008),

it appears that the sensitivity of IKK-β to this modification is substantially greater than that of IκB-α. Differential sensitivity of cysteine residues is not an unprecedented idea; however, most of the studies that have provided insight into differential sensitivity have utilized the exogenous administration of oxidants in an *in vitro* system to accurately characterize the relative susceptibility of certain protein thiol species to oxidation (Winterbourn & Hampton, 2008; Winterbourn & Metodiewa, 1999). This study provides evidence that ROS induced endogenously by the metabolic bioactivation of Dox in a cellular system can also result in differential protein oxidation. Moreover, in EU1 cells, the S-glutathionylation process, compared to the protein disulfide formation process, may undergo differential regulation by other ROS-related enzymes, given the fact that Dox-treatment was able to induce higher levels of S-glutathionylated IKK-β which was attenuated by NAC treatment (Fig. 6-4 C). Correspondingly, protein S-glutathionylation has been considered in the literature to occur at a slower rate than protein disulfide formation (Adimora et al, 2010; Winterbourn & Hampton, 2008; Winterbourn & Metodiewa, 1999). IκB-α S-glutathionylation at Cys 189 has been proposed as a potential mechanism by which NF-κB is regulated (Kil et al, 2008), however, the results of our study suggest that this is not a relevant mechanism by which NF-κB is regulated in EU1 cells under the treatment conditions applied.

IKK-β S-glutathionylation occurs in the presence of multiple competing reactions

A schematic representation of the proposed reactions involved in glutathione-dependent IKK-β S-glutathionylation is presented in Figure 6-1. The protein S-glutathionylation mechanisms considered in the model include protein S-glutathionylation via peroxide-induced IKK-β sulfenic acid formation and via radical-induced IKK-β thiyl radical formation. The model was constructed after the systematic consideration of the literature-reported reactions that could potentially contribute to intracellular protein S-glutathionylation (Dalle-Donne et al, 2009; Mieyal et al, 2008).

This systematic consideration occurred in iterative steps. First, the literature reported rates of reactions and necessary conditions for the possible mechanisms of protein S-glutathionylation were utilized to rule out non-essential pathways of S-glutathionylation (Mieyal et al, 2008), pathways that would most likely not occur under the low level oxidative stress conditions induced by a 500 nM [Dox] treatment condition.

The results of this analysis immediately excluded thiol-disulfide exchange as a possible mechanism for IKK-β S-glutathionylation because the ratio of GSH/GSSG would have to decrease by over 100 fold (from 100/1 to 1/1) to drive 50% conversion of protein-SH to protein-SSG (Gilbert, 1990). For this reason, H_2O_2-induced GSSG formation was modeled as a GSH sink, rather than a source of IKK-β S-glutathionylation (Fig. 6-1). S-nitrosylation (protein-SNO) mechanisms of protein S-glutathionylation were disregarded, even though cysteine sulfhydryls do undergo nitrosylation *in vivo*, because protein-SNO is more prevalent in extracellular spaces (Meyer et al, 1994). Moreover, protein-SNO is a relatively stable sulfhydryl derivative with half-lives on the order of hours (Arnelle & Stamler, 1995; Park, 1988; Singh et al, 1996), making this mechanism of protein S-glutathionylation unlikely to be involved in the time frame of this study.

Sulfenylamide-dependent (protein-SNCO) protein S-glutathionylation was ignored in the model description because it has only been reported to occur for one protein, protein tyrosine phosphatase 1B, after treatment with H_2O_2, and is thought to develop from an initial protein sulfenic acid species (protein-SOH) (Salmeen et al, 2003; van Montfort et al, 2003). Thiolsulfinate mechanisms of protein S-glutathionylation (protein-SOS-protein) were not directly ruled out because thiolsulfinates are reported to be highly reactive with thiols and are very similar in characteristic to sulfenic acids. However, because it is difficult to distinguish between thiolsulfinate-dependent and sulfenic acid-dependent mechanisms of protein-S-glutathionylation, one can consider the thiolsulfinate-dependent mechanism of protein S-glutathionylation to be buried within the

sulfenic acid-dependent mechanism of protein S-glutathionylation that is accounted for by the model.

Thiyl radical-dependent IKK-β S-glutathionylation was considered in the model because production of thiyl radicals has been reported under *in vivo* conditions of redox signaling (Jourd'heuil et al, 2003; Karoui et al, 1996; Kwak et al, 1995; Maples et al, 1990). Although there are several mechanistic pathways for thiyl radical-dependent protein S-glutathionylation, only one pathway was taken into account by the model, the reaction of the IKK-β thiyl radical (IKK-β-S$^{\bullet}$) with reduced glutathione (GSH). The quenching of a glutathione thiyl radical (GS$^{\bullet}$) with IKK-β-S$^{\bullet}$ was deemed too improbable given the fact that thiyl radicals are the shortest-lived sulfhydryl derivatives (Schoneich, 1995; Wardman & von Sonntag, 1995; Winterbourn & Metodiewa, 1995) and the concentrations of IKK-β, and subsequently IKK-β-S$^{\bullet}$, are not significantly high enough to compete with the other intracellular thiols or thiyls that are capable of reacting with GS$^{\bullet}$ or GSH, respectively (Adimora et al, 2010). This was the same reasoning that was used to exclude the formation of S-glutathionylated IKK-β through the reaction of GS$^{\bullet}$ with reduced IKK-β. For the aforementioned reasons, RS$^{\bullet}$-induced GS$^{\bullet}$ formation was modeled as a GSH sink, rather than a source of IKK-β S-glutathionylation (Fig. 6-1).

The antioxidant and pro-oxidant effects of NAC modulate IKK-β-SSG

The results of the mechanistic modeling revealed that the three processes that are susceptible to NAC modulation, GSH synthesis (R_9), protein thiyl radical formation (R_5), and glutathione thiyl radical formation (R_6) (Table 6-1), are each affected in a different way by NAC pretreatment. The GSH synthesis rate increases in a graded manner as a result of increasing concentrations of extracellular NAC. The RS$^{\bullet}$ and GS$^{\bullet}$ radical formation rates revealed different threshold responses to increasing concentrations of extracellular NAC (Table 6-1). The model predicts that the NAC-dependent 3-fold increase in RS$^{\bullet}$ formation rate occurs at relatively low NAC pretreatment concentrations

(0.5 mM). Whereas, the NAC-dependent 2-fold decrease in $GS^{\bullet}$ formation rate occurs at relatively high NAC pretreatment concentrations (5 mM). The predicted behavior of the $RS^{\bullet}$ formation rate as a result of NAC pretreatment suggests that the level of H_2O_2 induced by a 500 nM Dox treatment regimen is significant enough to promote the Fenton and Haber-Weiss reactions, which lead to increased protein thiyl radical formation in the presence of NAC. The predicted behavior of the $GS^{\bullet}$ formation rate as a result of NAC pretreatment suggests that a relatively high extracellular concentration of NAC is needed to effectively compete with GSH for the quenching of intracellular thiyl radicals. This result offers some insight into the robust capacity of intracellular glutathione to deal with radical-induced oxidant assault.

Moreover, the ability of NAC to promote or hinder S-glutathionylation of IKK-β appears to be dependent on intracellular ROS levels. NAC addition to an intracellular environment with relatively low levels of H_2O_2 can effectively lower the amount of IKK-β S-glutathionylation (Fig. 6-7 B), a consequence that was not observed when NAC was administered in an intracellular environment with relatively high levels of H_2O_2 (Fig. 6-7 A). This discrepancy suggests that the intracellular ROS buffering capacity of leukemia cells may dictate the ability of NAC to alter Dox-induced NF-κB activation.

The intracellular redox environment dictates Dox-induced NF-κB activity by systematically regulating IKK-β S-glutathionylation

Exposure of cells to clinically relevant doses of Dox has the potential to regulate intracellular signal transduction pathways that are known to be redox-sensitive. The NF-κB signal transduction pathway was shown to be sensitive to Dox-induced ROS; the sensitivity of the NF-κB signal transduction pathway was regulated by NAC administration. Since NAC is a precursor to the antioxidant glutathione, it can effectively alter the intracellular redox environment by its ability to change the GSH/GSSG redox balance. The mechanistic model of Dox-induced IKK-β S-glutathionylation, therefore,

was utilized to predict the behavior of susceptible substrates (GSH and IKK-β) to varying doses of Dox for different NAC pretreatment conditions. This analysis was carried out to provide a qualitative description of the variability in Dox-induced IKK-β S-glutathionylation and ultimately NF-κB activation that can be realized in cancer cells with different intracellular redox environments (Fig. 6-8). This analysis reveals the importance of not only the intracellular redox environment, as modulated by NAC pretreatment, but also the concentration of Dox that is administered.

By necessity, these results are only approximations as the model contains only a few potential reactions, the concentrations of the species are not directly known, and the reactions are carried out in the absence of substrate recycling; however, the concept that variability in intracellular redox environment can promote variability in chemotherapy-induced intracellular signaling is wholly supported by this study.

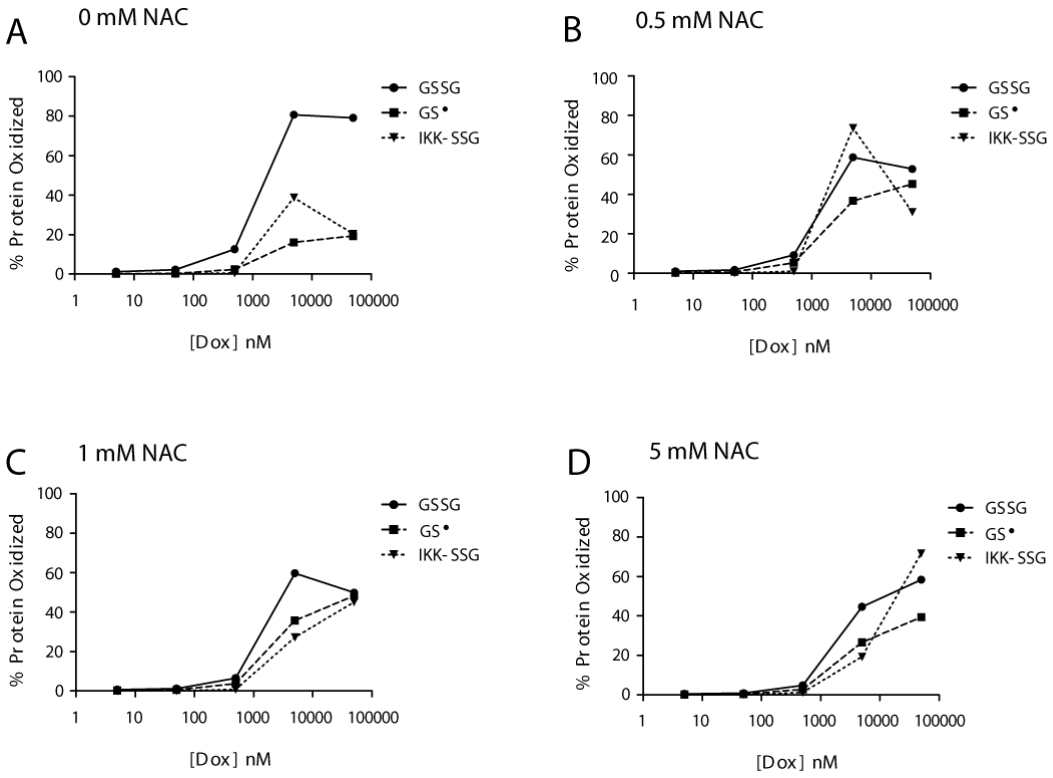

Figure 6-8. Quantitative simulation of GSH oxidation and IKK-β S-glutathionylation for varying NAC and Dox treatment conditions. Simulation of the oxidation of the thiol proteins IKK-β and GSH after treatment with increasing concentrations of Dox under various NAC pretreatment conditions: (A) 0 mM NAC pretreatment, (B) 0.5 mM NAC pretreatment, (C) 1 mM NAC pretreatment, and (D) 5 mM NAC pretreatment. Simulations of the kinetic traces were carried out using the proposed mechanistic model of IKK-β S-glutathionylation. The concentrations and rate constants used in the model for each treatment condition are shown in Table 6-2.

NAC-dependent modulation of the intracellular redox environment may affect clinical efficacy of Dox administration

During Dox treatment, cells are exposed to a variety of oxidants, some of which have the potential to alter redox sensitive signaling pathways that play a role in cell growth and proliferation and could potentially alter the efficacy of Dox treatment. Previous studies of Dox-induced toxicity in leukemia cells have revealed a possible role for Dox-induced ROS-mediated signaling (Chapter 4). Whether a particular redox-sensitive pathway is modified by Dox treatment or not, therefore, is dependent on the susceptibility to oxidation of the protein thiols that comprise the pathway.

The NF-κB activation pathway is a redox sensitive pathway that can be modified by chemotherapy-induced ROS via a variety of different mechanisms. The different sensitivities of protein cysteine residues to oxidative modification suggest that IKK S-glutathionylation is a primary mechanism by which Dox-induced ROS regulates the NF-κB activation pathway. Details of the mechanisms that drive Dox-induced IKK-β S-glutathionylation reveal the significance of protein thiyl and glutathione radical formation and the susceptibility of these reactions to the intracellular redox environment.

The results of this study provide a mechanistic rationale for the way in which intracellular glutathione levels, and ultimately the intracellular redox state, can regulate Dox-induced NF-κB signal transduction in ALL cells. If NF-κB activation is a mechanism by which cancer cells elude chemotherapy induced toxicity, then the systematic modulation of the glutathione redox balance through the controlled administration of NAC or other antioxidants, could potentially serve as a simple therapeutic measure to combat chemotherapy-induced drug resistance development.

The use of antioxidant supplements by patients with cancer is estimated between 13% and 87% (Block et al, 2007) and controversy over whether antioxidant supplementation alters the efficacy of cancer treatment still exists (Block et al, 2007). As NAC continues to be assessed for its cytoprotective capabilities during chemotherapy in

non-cancerous cell types (Shi et al, 2009), it is worth considering that the pro- and anti-oxidant effects of this molecule, induced by the competing reactions shown in this study, could prove to be deleterious in some cell types and beneficial or innocuous in others. This study shows the presence of NAC can either promote or hinder the activation of a redox-sensitive transcription factor whose actions may control the efficacy of Dox treatment; however, the ability of NAC to modify this redox-sensitive pathway is dependent on the intracellular environment into which it is introduced, a parameter that varies from one cancer cell type to the next. The directionality of this effect depends on the Dox dose to which the cells are exposed and the intracellular levels of ROS experienced by the cell. Therefore, the characterization of patient-specific intracellular redox capacity might inform the beneficial or harmful effects of NAC administration in conjunction with chemotherapy.

The current model advances our understanding of the independent behavior of particular redox systems

This study aimed to address issues related to the independent behavior of particular redox systems that comprise the mammalian antioxidant network and the ways in which these redox systems are computationally described. The modeling analysis carried out in this study demonstrates that the mathematical description of a particular redox-sensitive signaling pathway can be effectively carried out in isolation of the intracellular antioxidant network. More importantly, these modeling techniques highlighted the ability to translate qualitative descriptions of redox-dependent processes into semi-quantitative mathematical descriptions with the use of simple logical analysis. A simplified description of a portion of the antioxidant network was capable of accurately describing *in vivo* ROS-dependent signaling, as was evidenced by the ability of the model to predict IKK-β S-glutathionylation for various NAC pretreatment conditions (Fig. 6-7). In this modeling analysis, a detailed and highly complex signaling

network was simplified in description to reactions involving the GSH redox couple and IKK-β. Logical analysis based on simple redox-reactions was used to determine the possible effects of NAC treatment on a potentially important signaling pathway. Systematic comparisons of the possible NAC-dependent effects revealed intricacies of the redox signaling network with very little computational expense. This work has shown that the use of computational modeling in conjunction with traditional experimentation can effectively provide the framework necessary to "reverse-engineer" the features of the mammalian antioxidant system as they pertain to ROS-mediated signaling. Moreover, this study provides strong evidence that variations to the intracellular redox environment, as characterized by variations in GSH/GSSG redox balance, confers significant control over the extent to which Dox treatment can modify NF-κB signaling.

CHAPTER 7

CONCLUSIONS AND FUTURE WORK

The body of work presented in this dissertation advances knowledge of the role of redox systems in anthracycline chemotherapy administration. The redox dependence of Dox bioactivation (Chapter 4), the ability of cells to remove ROS (Chapter 5), and the ability of ROS to modulate signal transduction (Chapter 6), provide substantial evidence to the possibility that redox pathways modulate the efficacy of Dox treatment in cancer cells. The objective of this research was to investigate how the redox properties of the Dox bioactivation network influence Dox toxicity in acute lymphoblastic leukemia cells through the generation of toxic Dox metabolites and the induction of ROS. The central hypothesis behind this dissertation was that the Dox bioactivation pathway is regulated by intracellular levels of antioxidant components and metabolites that work collectively to generate toxic Dox metabolites or to generate intracellular ROS signals. Moreover, it was proposed that certain molecular conditions would lead to the preferential formation of toxic Dox metabolites at the expense of ROS generation, thereby promoting Dox-induced cell death. Lastly, because ROS can potentially affect redox-sensitive signaling pathways that regulate cell proliferation and growth, it was hypothesized that Dox-induced ROS could either promote cell death or cell viability, depending on the intracellular redox context in which the ROS signals are generated.

To test these hypotheses, a systems-based network of intracellular Dox bioactivation was developed (Chapter 4) and used to construct cell-specific models of cytosolic Dox bioactivation (Fig. 4-3, Fig. 4-5). This work helped to advance knowledge of how adaptation of the Dox bioactivation network to changes in Dox treatment or to patient-specific changes in network components could ultimately alter cellular sensitivity to Dox chemotherapy treatment. The importance of cell-specific protein levels to the

degree of Dox bioactivation that occurs *in vivo* supports the need for more personalized strategies in chemotherapy administration.

Secondly, a comprehensive network model of cellular ROS buffering was developed (Chapter 5) to predict changes to the intracellular redox environment that occur as a result of chemotherapy-induced oxidative stress (Fig. 5-1). This work helped to address the apparent paradox between the role of H_2O_2 as a cellular signaling molecule and its role as a cellular toxin. Through the development of a comprehensive model of H_2O_2 buffering in mammalian cells, this work provided quantitative and dynamic information regarding the antioxidant mechanisms that exert the most control over the removal of hydrogen peroxide from the cell, and how this control can be impacted by intervention.

Finally, a mechanistic model of chemotherapy-induced redox signaling was proposed (Chapter 6). This work set out to address the issue of redox-system isolation within the global context of the mammalian antioxidant network. The work highlighted in this study illustrated that redox-sensitive signaling pathways can be thought to exist somewhat in isolation of one another and the accurate description of ROS-dependent signaling was not contingent on the ability to describe the entire antioxidant network as a whole. Analyzing the redox-sensitivity of the NF-κB activation pathway, through the systemic modulation of the GSH/GSSG redox couple, demonstrates that knowledge of a particular redox-sensitive signaling pathway can be achieved through the mechanistic analysis of a single intracellular redox couple.

All three of the specific aims set out in this work utilized both computational and experimental approaches to further understand the role of redox systems in chemotherapy. The successful completion of the studies highlighted in this work has revealed some very unique challenges that exist in the development of kinetic models to help explain biological phenomena related to reduction and oxidation reactions. Intracellular redox reactions are highly regulated processes that are further complicated

by variations in susceptibility to oxidation of intracellular proteins and variations in availability of oxidants and reductants across different compartments of the intracellular milieu. For these reasons, many thiol-based redox couples are set and maintained at different redox potentials. The non-equilibrium redox potentials of intracellular redox couples make the computational modeling of signaling processes involving these redox couples somewhat difficult to accomplish.

This study offers one modeling approach to dealing with this issue: the driving force for electron transfer can be defined as a function of the difference between the homeostatic potential and the actual potential of the redox couple of interest (Equation 5-4) (Kemp et al, 2008). With this approach, the mathematical representation of a redox network can be used to accurately describe the dynamic response of the network to changes in intracellular [H_2O_2] without having to explicitly include the numerous steady-state fluxes that must within the network. This modeling technique allows for a more robust framework with which to investigate differences in chemotherapy-induced ROS buffering between cancer cell lines of different lineages of from different patients. Without having to explicitly define the numerous steady-state fluxes that will most likely be different across different cancer cell lines, the models can simply depend on the experimental determination of steady state concentrations in order to provide an accurate picture of the way in which individual cells eliminate chemotherapy-induced ROS from their intracellular environments.

The use of computational models to try to explain biological behavior is invaluable. Superior computational models, those that are based on validated and well established experimental data, are capable of providing meaningful insight into biological phenomena that would otherwise be difficult to interpret. However, because the construction of valid computational models relies on quantitative experimental data, the comprehensiveness of these models can sometimes be limited. Insufficient experimental techniques can sometimes be incapable of providing the depth of quantitative information

that is needed to construct valuable and useful computational models. This study has provided evidence that, when it comes to intracellular redox signaling, the need for a comprehensive model that takes into account all aspects of a particular signaling pathway may not be necessary to understand the important characteristics of the pathway (Chapter 6). Through the mechanistic modeling carried out for the S-glutathionylation of IKK-β, it was shown that an accurate description of glutathione-dependent reactions, somewhat independent of the rest of the intracellular antioxidant network, was sufficient enough to describe the signaling dynamics of the NF-κB activation pathway. This modeling effort provides precedent for the global understanding of a particular redox-sensitive signaling pathway using only a subset of the components that comprise the intracellular redox network.

The relative importance of the glutathione-dependent and thioredoxin-dependent antioxidant systems was also quantitatively characterized as a result of the studies highlighted in this work. The unequal anti-oxidative burden of intracellular redox enzymes and thiol-containing compounds was revealed. The Trx1 and GSH redox couples are often used as measures of the overall redox state of the cell (Schafer & Buettner, 2001) and a computational model was utilized to describe the dynamics of these two redox couples under conditions of oxidative stress. Analysis of the model system under the different peroxide generation conditions (Table 5-3) suggested an unequal distribution in anti-oxidative burden exists between the cytosolic Trx1 and GSH redox couples; this unequal distribution could help to inform potential therapeutic targets for the modulation of chemotherapy-induced ROS within cancer cells. Future modeling efforts will most likely be needed to accurately describe how changing oxidative conditions, perhaps as a result of changing doses of anthracycline chemotherapy, could potentially affect the oxidative burden distribution across the GSH-dependent and Trx-dependent intracellular antioxidant systems.

Interestingly, the role of NADPH, a metabolite that provides reducing equivalents for both the Trx- and GSH-dependent antioxidant systems, was shown to be extremely important in relation to the bioactivation of anthracyclines (Chapter 4). Modulation of NADPH availability in the EU1 and EU3 cell lines produced enough intracellular change to alter the bioactivation profile of Dox; DHEA-dependent alterations of NADPH availability were capable of modifying the sensitivity of ALL cells to Dox treatment. The importance of the NADPH metabolite is further exhibited in its ability to alter ROS-induced protein S-glutathionylation levels *in vivo*. An immortalized Jurkat T-cell line with decreased levels of the G6PD enzyme experiences a significantly different protein S-glutathionylation profile compared to Jurkat cells with normal levels of G6PD activity (Appendix A: Fig A-1).

The importance of NADPH availability to chemotherapy administration can be exhibited in multiple ways. NADPH has been shown to modulate anthracycline bioactivation in a manner that can potentially alter sensitivity to anthracycline treatment, but NADPH can also alter chemotherapy-induced redox signaling via its ability to modulate ROS-induced protein S-glutathionylation. These NADPH-dependencies should be further investigated given the fact that frequently-occurring somatic mutations in gliomas and leukemias can result in a directional change from NADPH production to NADPH consumption by isocitrate dehydrogenases (IDH1/2) resulting in lower intracellular NADPH levels (Dang et al, 2009; Ward et al, 2010). Whether these mutations promote chemotherapy drug resistance or not, is left to be investigated.

Chemotherapy administration is one way in which oxidative stress can be induced in mammalian cells. Previous discussions have highlighted the possibility that variations in ROS buffering components across different cancer cell lines can result in different levels of ROS being experienced by the cancer cells even for the same dosage of chemotherapy (Appendix B: Fig. B-1). This phenomenon becomes all the more important considering that ROS can potentially alter cellular signal transduction through the

reversible modification of intracellular redox-sensitive proteins (Valko et al, 2007); such alterations may serve to promote cell viability as a result of chemotherapy administration (Oliveira-Marques et al, 2009).

To address this issue, specific analysis of how low levels of ROS can modify redox-sensitive signal transduction pathways that regulate cell growth and proliferation was carried out in the EU1 acute lymphoblastic leukemia cell line (Chapter 6). This study aimed to characterize the importance of the intracellular redox environment in controlling the degree to which Dox-induced ROS modulates a redox-sensitive signal transduction pathway. The working hypothesis for this study was that the intracellular redox environment, as defined by the intracellular levels of the major antioxidant glutathione (GSH), determines the ability of Dox-induced ROS to modulate a redox-sensitive signal transduction pathway.

The role of the glutathione/glutathione disulfide (GSH/GSSG) redox balance in controlling Dox-induced NF-κB activity in ALL cells was investigated. The examination of Dox-induced NF-κB activation between two ALL cell lines with dissimilar antioxidant capacities (Appendix B: Fig. B-2), and the use of the antioxidant N-acetylcysteine (NAC) to systematically alter intracellular GSH/GSSG redox potential during Dox treatment, clearly illustrated how intracellular glutathione redox balance can regulate Dox-induced NF-κB signal transduction to potentially alter sensitivity ALL cell sensitivity to Dox treatment. A validated model of IKK-β S-glutathionylation was used to assess the antioxidant and pro-oxidant roles that NAC could potentially play during chemotherapy administration and, more importantly, how these roles ultimately affect the level of IKK-β S-glutathionylation that is induced by Dox treatment (Fig. 6-7, Fig. 6-8). The results of this study have shed some much needed light on the role that the intracellular redox environment can play in modulating chemotherapy-induced signal transduction. It has been shown previously that different cancer cells operate under distinctively different redox environments (Appendix B: Fig. B-1). Therefore, one cannot consider the capacity

for chemotherapy-induced ROS to alter a redox-sensitive signaling pathway to be a conserved parameter that is universally defined for all cancer cells. The capacity for chemotherapy-induced ROS to alter a redox-sensitive signaling pathway is a dynamic parameter that must be re-defined from one cell to the next, from patient to patient, and from dose to dose (Fig. 6-8).

Future Directions: A systems approach to cancer chemotherapy

Cancer is not a single disease but instead a collection of diseases that have distinct histopathological features, genetic and genome variability, and diverse prognostic outcomes (Vargo-Gogola & Rosen, 2007). If one understands cancer to be a heterogeneous disease, then perhaps the search for that mysterious "magic cancer bullet" should be substituted by a deeper understanding of cancer as a systems biology disease. With this understanding, one can begin to integrate quantitative experimental data through the use of comprehensive mathematical models to better understand the dynamics of chemotherapy-induced intracellular signaling. Advances in knowledge of how chemotherapy affects intracellular signaling pathways on a patient-to-patient basis will help not only in the understanding of chemotherapy-induced toxicity and drug resistance development, but also potentially in the discovery of more efficacious strategies to combat cancer cell growth and proliferation.

To help motivate this progress, future work can be conducted in all three areas of study highlighted in this dissertation. Aim 1 of this work focused on understanding the redox-dependent processes that contribute to Dox toxicity; however, the computational models generated in this study fall short in their dynamic description of some of the intracellular components involved in Dox bioactivation, e.g. the NADPH-dependent NOX4 enzymatic reaction that utilizes NADPH and molecular oxygen to produce superoxide. The importance of the NOX enzymes in Dox bioactivation requires a more in-depth characterization. Experiments that aim to decipher the exact mechanism by

which NOX activity is regulated by anthracycline treatment will add some much needed depth to the understanding of Dox bioactivation in cancer cells.

The Dox bioactivation models were also limited in scope due to the fact that they only considered cytosolic mechanisms of Dox bioactivation. There are multiple mechanisms for anthracycline bioactivation in mammalian cells: the mitochondria-dependent bioactivation of Dox by mitochondrial complex I and NADH (Davies & Doroshow, 1986; Doroshow & Davies, 1986), and the mitochondria-independent mechanisms of Dox bioactivation by CPR and NADPH (Bartoszek, 2002). Future work in this area could include the compartmentalization of Dox bioactivation. It was assumed that most of the Dox administered to the cells was metabolized in the cytosol, but this may not necessarily be the case. If nuclear-dependent or mitochondria-dependent bioactivation processes dominate in some cell lines, as opposed to others, then a computational model capable of describing these compartmentalized actions would increase the predictive power of such models.

Additionally, the *in vivo* Dox bioactivation network includes species that are involved in a variety of other intracellular reactions which are independent of Dox bioactivation, such as NADPH. NADPH is a metabolite that is used ubiquitously in cells for a variety of redox dependent reactions (Adimora et al, 2010). Moreover, NADPH-dependent thiol oxidation-based mechanisms may actually contribute to Dox-induced cell injury in some cells (Asmis et al, 2005), thereby providing a link between intracellular thiol-disulfide status and Dox-induced toxicity; a link that was unaccounted for by the model because of the qualitative nature of the findings.

The construction of computational models that take into account the spatial compartmentalization of intracellular components would go far in advancing knowledge of intracellular redox buffering. Aim 2 and Aim 3 of this work focused on understanding cellular capacity to deal with oxidative stress and how this oxidative stress could potentially regulate intracellular signal transduction during chemotherapy administration.

A limitation of the validated computational models offered in Aim 2 and Aim3 is that they dealt only with cytosolic, and in some instances, peroxisomal reactions. Spatially competent computational models could potentially provide insight into how the intracellular location of chemotherapy can have varying effects on chemotherapy-induced redox signaling and toxicity. Future experimental work could potentially focus on the systematic targeting of chemotherapy to particular subcellular locations and the analysis of how these varied targeting strategies affect degree of Dox bioactivation, ROS-induction, and signal transduction.

Results of this work provide strong evidence that variations to the intracellular redox environment, as characterized by variations in GSH/GSSG redox balance, confers significant control over the extent to which chemotherapy treatment can modify NF-κB signaling. If NF-κB activation is a mechanism by which cancer cells elude chemotherapy-induced toxicity, then the systematic modulation of the glutathione redox balance, perhaps through the controlled administration of NAC, could potentially serve as a simple therapeutic measure to combat chemotherapy-induced drug resistance development. It has been shown in the literature that oxidative activation and inactivation of NF-κB itself can occur and does play a role in NF-κB signal transduction (Oliveira-Marques et al, 2009). The work highlighted in this study did not investigate the mechanisms behind this possibility. Future work in this area could involve characterization of the extent to which variations in the redox balance of other intracellular redox couples, such as Trx-$(SH)_2$/Trx-SS, affects NF-κB signal transduction by the direct redox modification of the NF-κB transcription factor. The Prx enzyme system, which is dependent on the thioredoxin redox couple, contributes approximately 32% of the cell's redox buffering capacity. It would be interesting to see how variations in the Trx redox balance affects the ability of chemotherapy to alter cellular signaling pathways that control cell viability and proliferation.

It was mentioned that the comprehensive description of the intracellular redox network may not be necessary to accurately model intracellular signaling; however, it would be extremely powerful if the Dox bioactivation model could be coupled to the mechanistic S-glutathionylation model to provide some insight into the relative importance of the toxicity and signaling modules of Dox bioactivation for a particular treatment condition. As it stands, the work provided in this study successfully characterized the toxicity and signaling modules of Dox bioactivation, independently, yet in a patient, both of these modules most likely operate simultaneously. It would be extremely powerful to be able to take patient-specific protein levels, input them into a computational model, and predict the degree to which the toxicity-generating module of Dox dominates over the signal-generating module. Such a model would provide an invaluable tool for personalized medicine.

This study focused on the redox-mechanisms involved in anthracycline treatment of ALL, and in doing so revealed some possible biomarkers that could help inform the efficacy of said treatment. Future work in this area could involve the development of comprehensive models that incorporate the redox-dependence of anthracycline treatment with other signaling pathways that play a role in cancer cell proliferation and growth. It would be interesting to develop models of chemotherapy-induced cell death that incorporate the redox-sensitivity of apoptotic pathways. It has been shown in the literature that Trx1 mediates apoptosis via its redox-dependent association with ASK1 (Katagiri et al, 2010). Moreover, the redox-dependent translocation of thioredoxin into the nucleus is capable of modulating transcription factor binding (Wei et al, 2000). The use of the generalized model of cytosolic ROS buffering may help to inform the mechanisms by which these interactions and phenomena are regulated by chemotherapy-induced ROS.

Lastly, the inclusion of more cancer phenotypes and more chemotherapy drug alternatives for characterization is essential to understanding the variability that exists

across cancer cells for different chemotherapy treatment regimens. The research presented in this thesis aims to characterize the role of redox systems in chemotherapy metabolism and chemotherapy-mediated cell signaling. For this endeavor, the Dox anthracycline was utilized in the treatment of acute lymphoblastic leukemia cell lines to elucidate the redox-mechanisms that control chemotherapy-induced toxicity in cancer cells. The sum of these results allows for further understanding of the role of redox systems in overall cancer biology.

APPENDIX A

G6PD ACTIVITY REGULATES ROS-INDUCED PROTEIN S-GLUTATHIONYLATION

The NADPH/$NADP^+$ redox couple has been implicated in the metabolic conversion of Dox. Previous work (Chapter 4) revealed that the dual-nature of Dox metabolism is highly dependent on the availability of NADPH as evidenced by *in vivo* intervention strategies using the G6PD inhibitor DHEA. Furthermore, NADPH limitation at low Dox concentrations was shown to alter ALL-sensitivity to Dox treatment (Fig. 4-7 B, C) in an ROS-dependent manner. This finding suggested a role for NADPH in modulating not just the toxicity-generating module of Dox bioactivation, but also the ROS-generating module, which may be affiliated with intracellular signaling.

It has been shown previously that the S-glutathionylation of intracellular proteins upon induction of oxidative stress has the potential to alter intracellular signaling pathways (Chapter 6). To investigate whether changes to the intracellular availability of NADPH, characterized by G6PD activity, can alter the protein-S glutathionylation profile during conditions of oxidative stress, wild-type and G6PD-knockdown EU1 cells were treated with exogenous H_2O_2 to simulate the increased oxidative conditions that result from Dox administration. After treatment, the degree of protein S-glutathionylation was quantified by HPLC according to the previously described protocol (Chapter 5 Materials and Methods).

RNA interference

Stable knockdowns were created from Jurkat cells by targeting the expression levels of glucose-6-phosphate dehydrogenase using MISSION Lentiviral shRNA Transduction Particles according to manufacturer's protocol with puromycin selection (4

µg / ml). Jurkat cells tranduced with empty pLKO.1-puro lentiviral plasmids were used as controls to assess the effect of lentiviral transduction on ROS-induced protein S-glutathionylation. Lentiviral-tranduced cells were maintained in culture using the previously described culture conditions (Chapter 5 Materials and Methods) and Jurkat cell culture media supplemented with puromycin antibiotic at (4 µg / ml).

Results

Significant differences in level of protein S-glutathionylation were observed between WT and G6PD knockdown cells after treatment with 100 µM exogenous H_2O_2 (Fig. A-1). These differences occurred at 2 min and 5 min after peroxide addition. The WT cells experienced increased protein S-glutathionylation at 30 min of treatment and values returned to baseline by 1 h of treatment. Conversely, the G6PD cells experienced increased protein S-glutathionylation at earlier time points with a peak in protein S-glutathionylation exhibited at 5 min of peroxide treatment. By 10 min of treatment, Pr-SSG levels in the G6PD cells had returned to baseline and remained there for the remainder of the treatment duration. PLKO controls experienced no noticeable increase in Pr-SSG as a result of exogenous peroxide administration.

Conclusion

This experiment indicates that changes in G6PD expression, and thereby activity, can alter the Pr-SSG profile of Jurkat cells under conditions of oxidative stress. This experiment also indicates that the lentiviral transduction process can also lead to changes in the protein S-glutathionylation profile induced by oxidative stress.

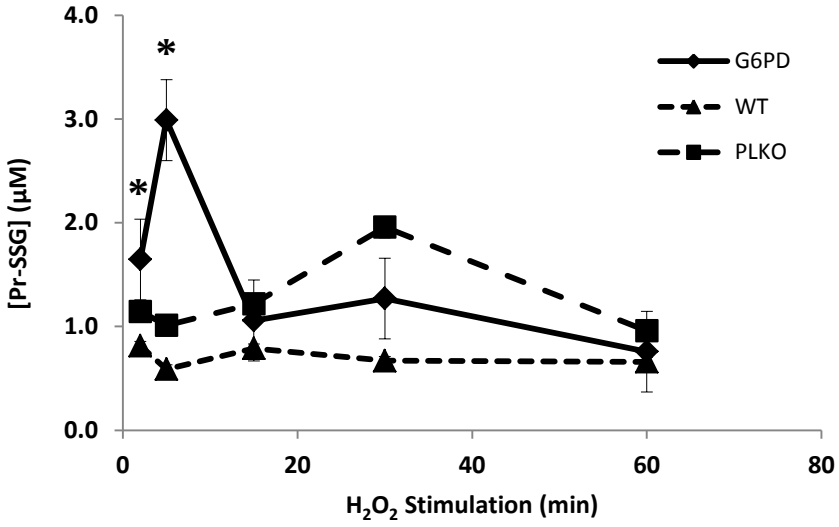

Figure A-1. Glucose-6-phosphate dehydrogenase controls ROS-induced protein S-glutathionylation in mammalian cells. G6PD-knockdown (G6PD), wild-type (WT), and empty-vector control (PLKO) Jurkat cells were treated with 100 µM H_2O_2 for 1 h and the level of ROS-induced protein S-glutathionylation was quantified by HPLC. (n = 3; *$p < 0.05$ between WT and G6PD Jurkat cells)

APPENDIX B

REDOX CAPACITY CONTROLS DOX-INDUCED ROS AND DOX-INDUCED NF-KB

The importance of the intracellular antioxidant network in dealing with exogenous and endogenous sources of ROS has been shown in the literature (Adimora et al, 2010). Dox-induced ROS has the capacity to alter intracellular signal transduction pathways and has been shown to affect the NF-κB signal transduction pathway via its ability to induce S-glutathionylation of IKK-β (Chapter 6). This process was revealed to be highly dependent on the intracellular redox balance of the GSH/GSSG redox couple. However, this dependency of dox-induced IKK-β S-glutathionylation on the intracellular redox network was revealed through the modification of intracellular GSH/GSSG redox balance by the external administration of NAC. In order to determine if inherent differences in ROS buffering capacity across ALL cell lines, as evidenced by the expression levels of select antioxidant enzymes, were enough to result in differences in dox-induced NF-κB activation, a comparative study of the EU1 and EU3 ALL cell lines was carried out. The antioxidant capacities of the dox-resistant EU1 cells and the dox-sensitive EU3 cells were characterized. Following this characterization, the level of dox-induced ROS and dox-induced NF-κB activation was assessed according to the previously described protocols (Chapter 6 Materials and Methods).

Antioxidant Enzyme Expression

The relative concentrations of the antioxidant proteins being investigated were determined via western blot (G6PD, Prx I, TR, Grx1, Trx1). Untreated EU1 and EU3 cells were lysed according to the previously described protocol (Chapter 6 Materials and Methods) and cytosolic lysates were analyzed for basal protein expression levels by

western blot using the following primary antibodies: anti-G6PD (AbCam); anti-Prx1 (Upstate, MA, USA); anti-TR (Upstate); anti-Grx1 (R&D Systems, MN, USA); anti-Trx1 (BD Pharmingen, NJ, USA). Basal GSH levels were quantified by HPLC according to the previously described protocol (Chapter 5 Materials and Methods). Protein levels were normalized to the EU3 cell line and results were expressed as fold change in comparison to the values obtained for the EU3 cell line.

Results

Significant differences in the basal levels of the antioxidant proteins chosen for analysis were seen between the EU1 and EU3 cell lines (Fig. B-1 A). The protein expression levels for all proteins except thioredoxin reductase (TR) were significantly lower in the EU1 cell line compared to the EU3 cell line. Correspondingly, the 5 μM Dox treatment condition resulted in significantly higher levels of dox-induced ROS in the EU1 cells compared to the EU3 cells (Fig. B-1 B). The level of dox-induced NF-κB, as quantified by luciferase luminescence, was significantly higher in the EU3 cells compared to the EU1 cells for the 5 μM Dox treatment condition (Fig. B-2).

Conclusion

This experiment indicates that inherent differences in antioxidant capacity across ALL cells lines can result in differential levels of Dox-induced ROS. This experiment also indicates that inherent differences in antioxidant capacity across ALL cells lines can result in differential levels of Dox-induced NF-κB activation, perhaps via the previously proposed mechanism of IKK-β S-glutathionylation (Chapter 6). The EU3 cells exhibit increased ROS buffering capacity which may help protect them from ROS-induced IKK-β S-glutathionylation, thereby promoting increased levels of dox-induced NF-κB activity compared to the EU1 cells.

A.

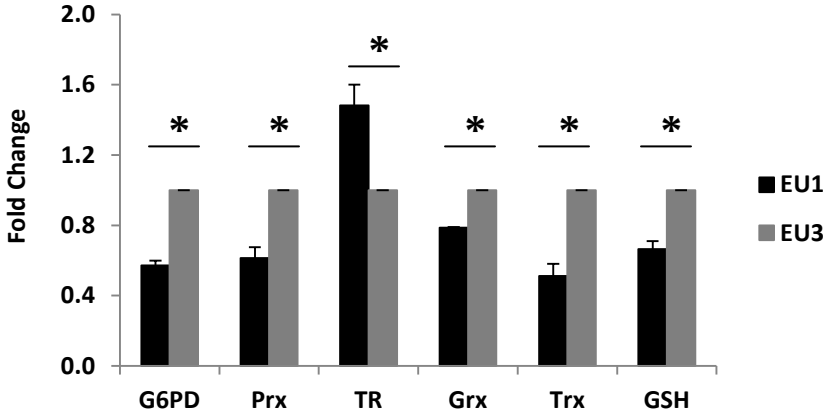

B.

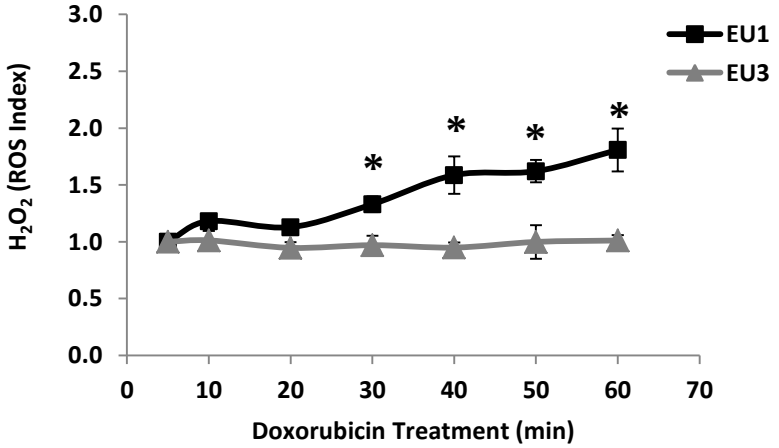

Figure B-1. ALL cells with altered redox capacities experience different levels of dox-induced ROS. (A) Relative expressions of antioxidant enzymes in EU1 and EU3 ALL cell lines. (B) Time-dependent Dox-induced H_2O_2 in EU1 and EU3 cells quantified by plate reader measurement of H_2DCFDA fluorescence. ([Dox] = 5 μM; n = 3; *$p < 0.05$)

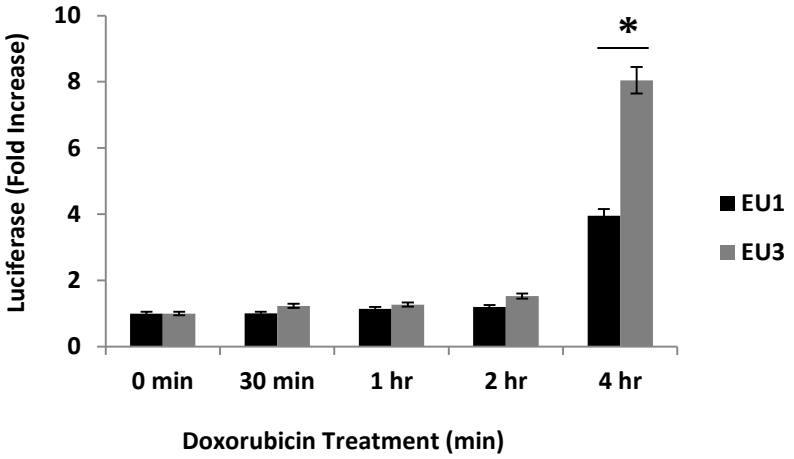

Figure B-2. ALL cells with altered redox capacities experience different levels of dox-induced NF-κB activation. Dox-induced NF-κB activity, as quantified by luciferase expression, in luciferase-tranduced ALL cells. ([Dox] = 5 μM; n = 3; *$p < 0.05$)

APPENDIX C

DOX BIOACTIVATION MODELS

Dox Bioactivation Model – *in vitro*

```
function out = Dox_Activation_in_vitro
    % model for in vitro Dox bioactivation
    % Solver Parameters
    ti = 0; % start time
    tf = 1200; % stop time
    step = 1;
    dt = step;
    tspan = ti:dt:tf;
    options=odeset('AbsTol',1E-10,'RelTol',1E-4,'maxstep',step);



%%%%%%%%%%%%%%%%%%%%%%%%%%%%%%%%%%%%%%%%%%%%%%%%%%%%%%%%%%%%%%%%%%%%%%%%%%%%%%%
%%%
        % Defining forward reaction rates ()
        % Defining the array, k, that will house reaction rates
        k = zeros(6,1);

        % CPR_reduced reacts with quinone Dox
        k(1) = 1.2e4;

        % CPR_oxidized reacts with reduced NADPH
        k(2) = k(1);

        % Molecular oxygen reacts with semi-quinone Dox
        k(3) = 3.0e8;

        % NADPH reacts with molecular oxygen
        k(4) = 2.9e1;

        % Superoxide reacts with quinone Dox
        k(5) = 5.5e7;

%         % Superoxide is removed by SOD
%         k(6) = 6.4e9;


%%%%%%%%%%%%%%%%%%%%%%%%%%%%%%%%%%%%%%%%%%%%%%%%%%%%%%%%%%%%%%%%%%%%%%%%%%%%%%%

        % Defining initial Conditions (Concentrations in M =
Moles/Liter)
        % Defining the array, x0, that will house initial
concentrations
```

```
        x0 = zeros(9,1);

        x0(1) = 1.0e-6; % CPR_reduced
        x0(2) = 0; % CPR_oxidized

        x0(3) = 1e-4; % DOX quinone
        x0(4) = 0;  % DOX semi-quinone

        x0(5) = 5e-4; % NADPH
        x0(6) = 0;     % NADP

        x0(7) = 2.73e-4; % Molecular oxygen
        x0(8) = 0; % Superoxide
        x0(9) = 0; % Hydrogen Peroxide


%%%%%%%%%%%%%%%%%%%%%%%%%%%%%%%%%%%%%%%%%%%%%%%%%%%%%%%%%%%%%%%%%%%%%%%%%%%%%%%
%%%%
        % integration
        tic
        [t x]=ode15s(@crank,tspan,x0,options,k);
        toc
        out = [t, x];


%%%%%%%%%%%%%%%%%%%%%%%%%%%%%%%%%%%%%%%%%%%%%%%%%%%%%%%%%%%%%%%%%%%%%%%%%%%%%%%
%%%%
        % description of derivatives

            function dxdt=crank(t, x, k);

                dxdt= x;  % setting up vector containing derivatives

                dxdt(1) = - k(1)*x(1)*x(3) + k(2)*x(2)*x(5); %
CPR_reduced

                dxdt(2) = k(1)*x(1)*x(3) - k(2)*x(2)*x(5); %
CPR_oxidized

                dxdt(3) = - k(1)*x(1)*x(3) + k(3)*x(4)*x(7) -
k(5)*x(3)*x(8); % DOX quinone

                dxdt(4) = k(1)*x(1)*x(3) - k(3)*x(4)*x(7) +
k(5)*x(3)*x(8); % DOX semi-quinone

                dxdt(5) = - k(2)*x(2)*x(5) - k(4)*x(5)*x(7); % NADPH

                dxdt(6) = k(2)*x(2)*x(5) + k(4)*x(5)*x(7); % NADP+

                dxdt(7) = - k(3)*x(4)*x(7) - k(4)*x(5)*x(7) +
k(5)*x(3)*x(8) + k(6)*x(8)*x(8); % Molecular oxygen

                dxdt(8) = k(3)*x(4)*x(7) + k(4)*x(5)*x(7) -
k(5)*x(3)*x(8) - k(6)*x(8)*x(8); % Superoxide
```

```
                dxdt(9) = k(6)*x(8)*x(8); % Hydrogen Peroxide

            end
end
```

Dox Bioactivation Model – EU1 cell line at 10 μM [Dox]

```
function out = Dox_Activation_EU1_HighDox
    % model for in vivo Dox bioactivation
    % Solver Parameters
    ti = 0; % start time
    tf = 3600; % stop time
    step = 1;
    dt = step;
    tspan = ti:dt:tf;
    options=odeset('AbsTol',1E-15,'RelTol',1E-7,'maxstep',step);


%%%%%%%%%%%%%%%%%%%%%%%%%%%%%%%%%%%%%%%%%%%%%%%%%%%%%%%%%%%%%%%%%%%%%%%%%%%%%%%
%%%
        % Defining forward reaction rates ()
        % Defining the array, k, that will house reaction rates
        k = zeros(10,1);

        % CPR_reduced reacts with quinone Dox
        k(1) = 1.2e4;

        % CPR_oxidized reacts with reduced NADPH
        k(2) = k(1);

        % Molecular oxygen reacts with semi-quinone Dox
        k(3) = 3.0e5;

        % NADPH reacts with molecular oxygen
        k(4) = 4.2e4;

        %Superoxide reacts with quinone Dox
        k(5) = 5.5e7;

        % Superoxide is removed by SOD
        k(6) = 6.4e9;

        % Permeability constant for Dox influx (plasma membrane)
        k(7) = 1.1e-6; % Permeability Constant value at High Dox
Concentration

        % Production of NADPH by G6PD
        k(8) = 1.8e-6;

        % Km of NADP+
        k(9) = 5.7e-5;

        % Oxygen Consumption from Environment
        k(10) = 1e-15;


%%%%%%%%%%%%%%%%%%%%%%%%%%%%%%%%%%%%%%%%%%%%%%%%%%%%%%%%%%%%%%%%%%%%%%%%%%%%%%%
```

```
        % Defining initial Conditions (Concentrations in M =
Moles/Liter)
        % Defining the array, x0, that will house initial
concentrations
        x0 = zeros(11,1);

        x0(1) = 1.3e-6; % CPR_reduced
        x0(2) = 0; % CPR_oxidized

        x0(3) = 0; % Intracellular DOX quinone
        x0(4) = 0;  % Intracellular DOX semi-quinone

        x0(5) = 3.0e-5; % NADPH
        x0(6) = 3.0e-7; % NADP+

        x0(7) = 1.5e-9; % Molecular oxygen
        x0(8) = 1.5e-11; % Superoxide
        x0(9) = 1.5e-11; % Hydrogen Peroxide

        x0(10) = 1e-5; % Extracellular DOX quinone 1.0e-5 = high

        x0(11) = 1.1e-6; % Permeability Coefficient for Dox influx
(Variable Parameter)


%%%%%%%%%%%%%%%%%%%%%%%%%%%%%%%%%%%%%%%%%%%%%%%%%%%%%%%%%%%%%%%%%%%%%%%%%%%%%%%
%%%%
        % integration
        tic
        [t x]=ode15s(@crank,tspan,x0,options,k);
        toc
        out = [t, x];


%%%%%%%%%%%%%%%%%%%%%%%%%%%%%%%%%%%%%%%%%%%%%%%%%%%%%%%%%%%%%%%%%%%%%%%%%%%%%%%
%%%%
        % description of derivatives

         function dxdt=crank(t, x, k);

                dxdt= x;  % setting up vector containing derivatives

                dxdt(1) = - k(1)*x(1)*x(3) + k(2)*(x(2)-x0(2))*x(5); %
CPR_reduced

                dxdt(2) = k(1)*x(1)*x(3) - k(2)*(x(2)-x0(2))*x(5); %
CPR_oxidized

                dxdt(3) = (x(11)*(x(10)*10e-3*6.15e-6)/(1.43e-12)) -
k(1)*x(1)*x(3) + k(3)*x(4)*x(7) - k(5)*x(3)*x(8); % Intracellular DOX
quinone
```

```
                dxdt(4) = k(1)*x(1)*x(3) - k(3)*x(4)*x(7) +
k(5)*x(3)*x(8); % Intracelluar DOX semi-quinone

                dxdt(5) = - k(2)*(x(2)-x0(2))*x(5) -
k(4)*x(5)*x(7)*(x(3)/(1e-5)) + k(8)*(x(6) - x0(6))/(k(9) + x(6)); %
NADPH

                dxdt(6) = k(2)*(x(2)-x0(2))*x(5) +
k(4)*x(5)*x(7)*(x(3)/(1e-5)) - k(8)*(x(6) - x0(6))/(k(9) + x(6)); %
NADP+

                dxdt(7) = - (x(4)*1e3)*k(3)*x(4)*x(7) -
k(4)*x(5)*x(7)*(x(3)/(1e-5)) + k(5)*x(3)*x(8) + k(6)*x(8)*x(8) + k(10);
% Molecular oxygen

                dxdt(8) = (x(4)*1e3)*k(3)*x(4)*x(7) +
k(4)*x(5)*x(7)*(x(3)/(1e-5)) - k(5)*x(3)*x(8) - k(6)*x(8)*x(8); %
Superoxide

                dxdt(9) = k(6)*x(8)*x(8); % Hydrogen Peroxide

                dxdt(10) = - x(11)*(x(10)*10e-3*6.15e-6*(1e9)); %
Extracellular Dox quinone

                if (x(10)) <= (8e-6)

                    dxdt(11) = x(11)*x(10);

                else

                    dxdt(11) = (x(11)/x(10))*(x(11))*5.5*(x(3) -
(x(10))); % PC ((x(11)/x(10)) - 0.11)*(x(11))*3*(x(3) - (x(10)))

                end

        end
end
```

Dox Bioactivation Model – EU3 cell line at 10 μM [Dox]

```
function out = Dox_Activation_EU3_HighDox
    % model for in vivo Dox bioactivation
    % Solver Parameters
    ti = 0; % start time
    tf = 3600; % stop time
    step = 1;
    dt = step;
    tspan = ti:dt:tf;
    options=odeset('AbsTol',1E-15,'RelTol',1E-7,'maxstep',step);


%%%%%%%%%%%%%%%%%%%%%%%%%%%%%%%%%%%%%%%%%%%%%%%%%%%%%%%%%%%%%%%%%%%%%%%%%%%%%%%%
%%%
        % Defining forward reaction rates ()
        % Defining the array, k, that will house reaction rates
        k = zeros(10,1);

        % CPR_reduced reacts with quinone Dox
        k(1) = 1.2e4;

        % CPR_oxidized reacts with reduced NADPH
        k(2) = k(1);

        % Molecular oxygen reacts with semi-quinone Dox
        k(3) = 3.0e5;

        % NADPH reacts with molecular oxygen
        k(4) = 9.7e3;

        %Superoxide reacts with quinone Dox
        k(5) = 5.5e7;

        % Superoxide is removed by SOD
        k(6) = 6.4e9;

        % Permeability constant for Dox influx (plasma membrane)
        k(7) = 1.1e-6; % Permeability Constant value at High Dox
Concentration

        % Production of NADPH by G6PD
        k(8) = 3.3e-6;

        % Km of NADP+
        k(9) = 5.7e-5;

        % Oxygen Consumption from Environment
        k(10) = 1e-15;


%%%%%%%%%%%%%%%%%%%%%%%%%%%%%%%%%%%%%%%%%%%%%%%%%%%%%%%%%%%%%%%%%%%%%%%%%%%%%%%%
```

```
        % Defining initial Conditions (Concentrations in M =
Moles/Liter)
        % Defining the array, x0, that will house initial
concentrations
        x0 = zeros(11,1);

        x0(1) = 8.9e-7; % CPR_reduced
        x0(2) = 0; % CPR_oxidized

        x0(3) = 0; % Intracellular DOX quinone
        x0(4) = 0;  % Intracellular DOX semi-quinone

        x0(5) = 5.4e-5; % NADPH
        x0(6) = 5.4e-7; % NADP+

        x0(7) = 1.5e-9; % Molecular oxygen
        x0(8) = 1.5e-11; % Superoxide
        x0(9) = 1.5e-11; % Hydrogen Peroxide

        x0(10) = 1e-5; % Extracellular DOX quinone 1.0e-5 = high

        x0(11) = 1.1e-6; % Permeability Coefficient for Dox influx
(Variable Parameter)


%%%%%%%%%%%%%%%%%%%%%%%%%%%%%%%%%%%%%%%%%%%%%%%%%%%%%%%%%%%%%%%%%%%%%%%%%%%%%%%
%%%%
        % integration
        tic
        [t x]=ode15s(@crank,tspan,x0,options,k);
        toc
        out = [t, x];


%%%%%%%%%%%%%%%%%%%%%%%%%%%%%%%%%%%%%%%%%%%%%%%%%%%%%%%%%%%%%%%%%%%%%%%%%%%%%%%
%%%%
        % description of derivatives

         function dxdt=crank(t, x, k);

                dxdt= x;  % setting up vector containing derivatives

                dxdt(1) = - k(1)*x(1)*x(3) + k(2)*(x(2)-x0(2))*x(5); %
CPR_reduced

                dxdt(2) = k(1)*x(1)*x(3) - k(2)*(x(2)-x0(2))*x(5); %
CPR_oxidized

                dxdt(3) = (x(11)*(x(10)*10e-3*6.15e-6)/(1.43e-12)) -
k(1)*x(1)*x(3) + k(3)*x(4)*x(7) - k(5)*x(3)*x(8); % Intracellular DOX
quinone

                dxdt(4) = k(1)*x(1)*x(3) - k(3)*x(4)*x(7) +
k(5)*x(3)*x(8); % Intracelluar DOX semi-quinone
```

```
                dxdt(5) = - k(2)*(x(2)-x0(2))*x(5) -
k(4)*x(5)*x(7)*(x(3)/(1e-5)) + k(8)*(x(6) - x0(6))/(k(9) + x(6)); %
NADPH

                dxdt(6) = k(2)*(x(2)-x0(2))*x(5) +
k(4)*x(5)*x(7)*(x(3)/(1e-5)) - k(8)*(x(6) - x0(6))/(k(9) + x(6)); %
NADP+

                dxdt(7) = - (x(4)*1e3)*k(3)*x(4)*x(7) -
k(4)*x(5)*x(7)*(x(3)/(1e-5)) + k(5)*x(3)*x(8) + k(6)*x(8)*x(8) + k(10);
% Molecular oxygen

                dxdt(8) = (x(4)*1e3)*k(3)*x(4)*x(7) +
k(4)*x(5)*x(7)*(x(3)/(1e-5)) - k(5)*x(3)*x(8) - k(6)*x(8)*x(8); %
Superoxide

                dxdt(9) = k(6)*x(8)*x(8); % Hydrogen Peroxide

                dxdt(10) = - x(11)*(x(10)*10e-3*6.15e-6*(1e9)); %
Extracellular Dox quinone

                if (x(10)) <= (8e-6)

                    dxdt(11) = x(11)*x(10);

                else

                    dxdt(11) = (x(11)/x(10))*(x(11))*5.5*(x(3) -
(x(10))); % PC ((x(11)/x(10)) - 0.11)*(x(11))*3*(x(3) - (x(10)))

                end

        end
end
```

Dox Bioactivation Model – EU1 cell line at 10 nM [Dox]

```
function out = Dox_Activation_EU1_LowDox
    % model for in vivo Dox bioactivation
    % Solver Parameters
    ti = 0; % start time
    tf = 3600; % stop time
    step = 1;
    dt = step;
    tspan = ti:dt:tf;
    options=odeset('AbsTol',1E-15,'RelTol',1E-7,'maxstep',step);


%%%%%%%%%%%%%%%%%%%%%%%%%%%%%%%%%%%%%%%%%%%%%%%%%%%%%%%%%%%%%%%%%%%%%%%%%%%%%%%
%%%
        % Defining forward reaction rates ()
        % Defining the array, k, that will house reaction rates
        k = zeros(10,1);

        % CPR_reduced reacts with quinone Dox
        k(1) = 1.2e4;

        % CPR_oxidized reacts with reduced NADPH
        k(2) = k(1);

        % Molecular oxygen reacts with semi-quinone Dox
        k(3) = 3.0e5;

        % NADPH reacts with molecular oxygen
        k(4) = 4.2e4;

        %Superoxide reacts with quinone Dox
        k(5) = 5.5e7;

        % Superoxide is removed by SOD
        k(6) = 6.4e9;

        % Permeability constant for Dox influx (plasma membrane)
        k(7) = 1.1e-5; % Permeability Constant value at Low Dox
Concentration

        % Production of NADPH by G6PD
        k(8) = 1.8e-6;

        % Km of NADP+
        k(9) = 5.7e-5;

        % Oxygen Consumption from Environment
        k(10) = 1e-15;


%%%%%%%%%%%%%%%%%%%%%%%%%%%%%%%%%%%%%%%%%%%%%%%%%%%%%%%%%%%%%%%%%%%%%%%%%%%%%%%
```

```
        % Defining initial Conditions (Concentrations in M =
Moles/Liter)
        % Defining the array, x0, that will house initial
concentrations
        x0 = zeros(11,1);

        x0(1) = 1.3e-6; % CPR_reduced
        x0(2) = 0; % CPR_oxidized

        x0(3) = 0; % Intracellular DOX quinone
        x0(4) = 0;  % Intracellular DOX semi-quinone

        x0(5) = 3.0e-5; % NADPH
        x0(6) = 3.0e-7; % NADP+

        x0(7) = 1.5e-9; % Molecular oxygen
        x0(8) = 1.5e-11; % Superoxide
        x0(9) = 1.5e-11; % Hydrogen Peroxide

        x0(10) = 1e-7; % Extracellular DOX quinone 1.0e-7 = low



%%%%%%%%%%%%%%%%%%%%%%%%%%%%%%%%%%%%%%%%%%%%%%%%%%%%%%%%%%%%%%%%%%%%%%%%%%%%%%%
%%%%
        % integration
        tic
        [t x]=ode15s(@crank,tspan,x0,options,k);
        toc
        out = [t, x];


%%%%%%%%%%%%%%%%%%%%%%%%%%%%%%%%%%%%%%%%%%%%%%%%%%%%%%%%%%%%%%%%%%%%%%%%%%%%%%%
%%%%
        % description of derivatives

         function dxdt=crank(t, x, k);

                dxdt= x;  % setting up vector containing derivatives

                dxdt(1) = - k(1)*x(1)*x(3) + k(2)*(x(2)-x0(2))*x(5); %
CPR_reduced

                dxdt(2) = k(1)*x(1)*x(3) - k(2)*(x(2)-x0(2))*x(5); %
CPR_oxidized

                dxdt(3) = (k(7)*(x(10)*10e-3*6.15e-6)/(1.43e-12)) -
k(1)*x(1)*x(3) + k(3)*x(4)*x(7) - k(5)*x(3)*x(8); % Intracellular DOX
quinone

                dxdt(4) = k(1)*x(1)*x(3) - k(3)*x(4)*x(7) +
k(5)*x(3)*x(8); % Intracelluar DOX semi-quinone
```

```
                dxdt(5) = - k(2)*(x(2)-x0(2))*x(5) -
k(4)*x(5)*x(7)*(x(3)/(1e-5)) + k(8)*(x(6) - x0(6))/(k(9) + x(6)); %
NADPH

                dxdt(6) = k(2)*(x(2)-x0(2))*x(5) +
k(4)*x(5)*x(7)*(x(3)/(1e-5)) - k(8)*(x(6) - x0(6))/(k(9) + x(6)); %
NADP+

                dxdt(7) = - (x(4)*1e3)*k(3)*x(4)*x(7) -
k(4)*x(5)*x(7)*(x(3)/(1e-5)) + k(5)*x(3)*x(8) + k(6)*x(8)*x(8) + k(10);
% Molecular oxygen

                dxdt(8) = (x(4)*1e3)*k(3)*x(4)*x(7) +
k(4)*x(5)*x(7)*(x(3)/(1e-5)) - k(5)*x(3)*x(8) - k(6)*x(8)*x(8); %
Superoxide

                dxdt(9) = k(6)*x(8)*x(8); % Hydrogen Peroxide

                dxdt(10) = - k(7)*(x(10)*10e-3*6.15e-6*(1e9)); %
Extracellular Dox quinone

        end
end
```

Dox Bioactivation Model – EU3 cell line at 10 nM [Dox]

```
function out = Dox_Activation_EU3_LowDox
    % model for in vivo Dox bioactivation
    % Solver Parameters
    ti = 0; % start time
    tf = 3600; % stop time
    step = 1;
    dt = step;
    tspan = ti:dt:tf;
    options=odeset('AbsTol',1E-15,'RelTol',1E-7,'maxstep',step);


%%%%%%%%%%%%%%%%%%%%%%%%%%%%%%%%%%%%%%%%%%%%%%%%%%%%%%%%%%%%%%%%%%%%%%%%%
%%%
        % Defining forward reaction rates ()
        % Defining the array, k, that will house reaction rates
        k = zeros(10,1);

        % CPR_reduced reacts with quinone Dox
        k(1) = 1.2e4;

        % CPR_oxidized reacts with reduced NADPH
        k(2) = k(1);

        % Molecular oxygen reacts with semi-quinone Dox
        k(3) = 3.0e5;

        % NADPH reacts with molecular oxygen
        k(4) = 9.7e3;

        %Superoxide reacts with quinone Dox
        k(5) = 5.5e7;

        % Superoxide is removed by SOD
        k(6) = 6.4e9;

        % Permeability constant for Dox influx (plasma membrane)
        k(7) = 1.1e-5; % Permeability Constant value at Low Dox
Concentration

        % Production of NADPH by G6PD
        k(8) = 3.3e-6;

        % Km of NADP+
        k(9) = 5.7e-5;

        % Oxygen Consumption from Environment
        k(10) = 1e-15;
```

```
%%%%%%%%%%%%%%%%%%%%%%%%%%%%%%%%%%%%%%%%%%%%%%%%%%%%%%%%%%%%%%%%%%%%%%%%%%%%

        % Defining initial Conditions (Concentrations in M =
Moles/Liter)
        % Defining the array, x0, that will house initial
concentrations
        x0 = zeros(11,1);

        x0(1) = 8.9e-7; % CPR_reduced
        x0(2) = 0; % CPR_oxidized

        x0(3) = 0; % Intracellular DOX quinone
        x0(4) = 0;  % Intracellular DOX semi-quinone

        x0(5) = 5.4e-5; % NADPH
        x0(6) = 5.4e-7; % NADP+

        x0(7) = 1.5e-9; % Molecular oxygen
        x0(8) = 1.5e-11; % Superoxide
        x0(9) = 1.5e-11; % Hydrogen Peroxide

        x0(10) = 1e-7; % Extracellular DOX quinone 1.0e-7 = low



%%%%%%%%%%%%%%%%%%%%%%%%%%%%%%%%%%%%%%%%%%%%%%%%%%%%%%%%%%%%%%%%%%%%%%%%%%%%
%%%%
        % integration
        tic
        [t x]=ode15s(@crank,tspan,x0,options,k);
        toc
        out = [t, x];


%%%%%%%%%%%%%%%%%%%%%%%%%%%%%%%%%%%%%%%%%%%%%%%%%%%%%%%%%%%%%%%%%%%%%%%%%%%%
%%%%
        % description of derivatives

         function dxdt=crank(t, x, k);

                dxdt= x;  % setting up vector containing derivatives

                dxdt(1) = - k(1)*x(1)*x(3) + k(2)*(x(2)-x0(2))*x(5); %
CPR_reduced

                dxdt(2) = k(1)*x(1)*x(3) - k(2)*(x(2)-x0(2))*x(5); %
CPR_oxidized

                dxdt(3) = (k(7)*(x(10)*10e-3*6.15e-6)/(1.43e-12)) -
k(1)*x(1)*x(3) + k(3)*x(4)*x(7) - k(5)*x(3)*x(8); % Intracellular DOX
quinone
```

```
                dxdt(4) = k(1)*x(1)*x(3) - k(3)*x(4)*x(7) +
k(5)*x(3)*x(8); % Intracelluar DOX semi-quinone

                dxdt(5) = - k(2)*(x(2)-x0(2))*x(5) -
k(4)*x(5)*x(7)*(x(3)/(1e-5)) + k(8)*(x(6) - x0(6))/(k(9) + x(6)); %
NADPH

                dxdt(6) = k(2)*(x(2)-x0(2))*x(5) +
k(4)*x(5)*x(7)*(x(3)/(1e-5)) - k(8)*(x(6) - x0(6))/(k(9) + x(6)); %
NADP+

                dxdt(7) = - (x(4)*1e3)*k(3)*x(4)*x(7) -
k(4)*x(5)*x(7)*(x(3)/(1e-5)) + k(5)*x(3)*x(8) + k(6)*x(8)*x(8) + k(10);
% Molecular oxygen

                dxdt(8) = (x(4)*1e3)*k(3)*x(4)*x(7) +
k(4)*x(5)*x(7)*(x(3)/(1e-5)) - k(5)*x(3)*x(8) - k(6)*x(8)*x(8); %
Superoxide

                dxdt(9) = k(6)*x(8)*x(8); % Hydrogen Peroxide

                dxdt(10) = - k(7)*(x(10)*10e-3*6.15e-6*(1e9)); %
Extracellular Dox quinone

        end
end
```

APPENDIX D

HYDROGEN PEROXIDE METABOLISM MODEL

```
function out = Adimora_PeroxideClearanceModel_2010
    % model for compartmentalized hydrogen peroxide consumption
    % Solver Parameters
    ti = 0; % start time
    tf = 3600; % stop time
    step = 1;
    dt = step;
    tspan = ti:dt:tf;
    options=odeset('AbsTol',1E-10,'RelTol',1E-4,'maxstep',step);


%%%%%%%%%%%%%%%%%%%%%%%%%%%%%%%%%%%%%%%%%%%%%%%%%%%%%%%%%%%%%%%%%%%%%%%%%%%%%%%
%%%
        % Defining forward reaction rates ()
        % Defining the array, k, that will house reaction rates
        k = zeros(28,1);

 %      Rxns (Cytosolic)

        % Permeability constant (plasma membrane)
        k(1) = 1.0e-5; % cm/s

        % Intracellular peroxide production
        k(2) = 1.1e-7; % M/s

        % GPx_red reacting with H2O2in
        k(3) = 2.1e7; % M-1*s-1

        % GPx_ox reacting with GSH
        k(4) = 4e4; % M-1*s-1

        % GPx-SSG reacting with GSH
        k(5) = 1e7; % M-1*s-1

        % Catalse reacts with H2O2 inside peroxisome
        k(6) = 3.4e7; % M-1*s-1

        % Km of NADP+
        k(7) = 5.7e-5; % M

        % Peroxiredoxin is oxidized by H2O2
        k(8) = 4e7; % M-1*s-1

        % Oxidized peroxiredoxin is over-oxidized by H2O2
        k(9) = 7.2e4; % M-1*s-1

        % Reduction of overoxidized Prx by Srx enzyme
```

```
k(10) = 3e-3; % s-1

% Self-catalyzed disulfide formation of Prx-SS from Prx-SOH
k(11) = 15; % s-1

% Peroxiredoxin is reduced by Thioredoxin
k(12) = 2.1e6; % M-1*s-1

% Auto-oxidation of GSH
k(13) = 7.4e-05; % s-1

% Protein monothiol oxidized by H2O2
k(14) = 1e4; % M-1*s-1

% Oxidized Protein monothiol glutathionylated by GSH
k(15) = 1.2e5; % M-1*s-1

% Grx-SH de-glutathionylates Protein-SSG
k(16) = 9.1e4; % M-1*s-1

% GSH de-glutathionylates Grx-SSG
k(17) = 3.7e4; % M-1*s-1

% Protein dithiol oxidized by H2O2
k(18) = 5e5; % M-1*s-1

% Protein disulfide reduced by Trx
k(19) = 1e5; % M-1*s-1

% GSSG reduced by GR
k(20) = 3.2e6; % M-1*s-1

% Oxidized Thioredoxin reduced by TrxR
k(21) = 2e7; % M-1*s-1

% Production of NADPH by G6P-DH
k(22) = 3.75e-04; % M/s

% Permeability constant (peroxisomal membrane)
k(23) = 3e-3; % cm/s

% GSH synthesis
k(24) = 4.1e-7; % M/s

% GSSG efflux
k(25) = 1.2e-8; % M/s

% GSH + GSSG efflux
k(26) = 1.2e-7; % M/s

% Trx_SH efflux
k(27) = 7.45e-10; % M/s
```

```
        % Trx_SH synthesis
        k(28) = 6.97e-10; % M/s



%%%%%%%%%%%%%%%%%%%%%%%%%%%%%%%%%%%%%%%%%%%%%%%%%%%%%%%%%%%%%%%%%%%%%%%%%%%%

        % Defining initial Conditions (Concentrations in M =
Moles/Liter)
        % Defining the array, x0, that will house initial
concentrations
        x0 = zeros(24,1);

        % Cytoplasm

        x0(1) = 1e-4;    % H2O2media
        x0(2) = 1.0e-9; % H2O2cytosol

        x0(3) = 5e-5;       % GPXr
        x0(4) = 1e-14;      % GPXo
        x0(5) = 1e-14;      % GPX-SG

        x0(6) = 3.68e-4;  % GSH
        x0(7) = 1.78e-6;  % GSSG

        x0(8) = 9e-7;      % Catalase
        x0(9) = 1.0e-10;  % H2O2peroxisome

        x0(10) = 1.92e-5;              % Prx-SH
        x0(11) = 1e-14;                % Prx-SOH
        x0(12) = 1e-14;                % Prx-SOOH
        x0(13) = x0(10)*(.5/100);      % Prx-SS

        x0(14) = 4.27e-7;    % Trx1-SH
        x0(15) = 7.54e-8;    % Trx1-SS

        x0(16) = 1.22e-4;            % Pr-SH
        x0(17) = x0(16)*(.5/100);   % Pr-SOH
        x0(18) = x0(16)*(.5/100);   % Pr-SSG

        x0(19) = 1.20e-6;           % Grx-SH
        x0(20) = x0(19)*(.5/100);   % Grx-SSG

        x0(21) = 1.09e-3;              % Pr-(SH)2
        x0(22) = x0(21)*(.5/100);     % Pr-SS

        x0(23) = 3.0e-5;  % NADPH
        x0(24) = 3.0e-7;  % NADP+



%%%%%%%%%%%%%%%%%%%%%%%%%%%%%%%%%%%%%%%%%%%%%%%%%%%%%%%%%%%%%%%%%%%%%%%%%%%%
%%%%
        % integration
```

```
        tic
        [t x]=ode15s(@crank,tspan,x0,options,k);
        toc
        out = [t, x];


%%%%%%%%%%%%%%%%%%%%%%%%%%%%%%%%%%%%%%%%%%%%%%%%%%%%%%%%%%%%%%%%%%%%%%%%%%%%%%%
%%%%
        % description of derivatives

            function dxdt=crank(t, x, k);

                dxdt= x;  % setting up vector containing derivatives

                %Cytosolic Dynamics

                dxdt(1) = k(1)*(x(2)- x(1))*10e-3*1.02e-5*(1e9); %
H2O2 out

                dxdt(2) = ((k(1)*(x(1))*10e-3*1.02e-5)/(9.16e-13)) -
((k(1)*(x(2))*10e-3*1.02e-5)/(9.16e-13)) - 2*(k(23)*x(2)*10e-3*2.98e-
9)/(1.53e-14) + k(2) - k(3)*x(3)*(x(2)- x0(2)) - k(6)*x(8)*(x(2)-
x0(2)) - k(8)*x(10)*(x(2)- x0(2)) - k(9)*x(11)*(x(2)- x0(2)) -
k(14)*x(16)*(x(2)- x0(2)) - k(18)*x(21)*(x(2)- x0(2)); % H2O2 cytosol

                dxdt(3) = - k(3)*x(3)*(x(2)- x0(2)) + k(5)*(x(5)-
x0(5))*x(6); % GPXr

                dxdt(4) = k(3)*x(3)*(x(2)- x0(2)) - k(4)*(x(4)-
x0(4))*x(6); % GPXo

                dxdt(5) = k(4)*(x(4)-x0(4))*x(6) - k(5)*(x(5)-
x0(5))*x(6); % GPX-SG

                dxdt(6) = - k(4)*(x(4)-x0(4))*x(6) - k(5)*(x(5)-
x0(5))*x(6) - 2*k(13)*x(6) - k(15)*(x(17)-x0(17))*x(6) - k(17)*(x(20)-
x0(20))*x(6) + 2*k(20)*(x(7)-x0(7))*x(23) + k(24) - k(26); % GSH

                dxdt(7) = k(5)*(x(5)-x0(5))*x(6) + k(13)*x(6) +
k(17)*(x(20)-x0(20))*x(6) - k(20)*(x(7)-x0(7))*x(23) - k(25) - k(26); %
GSSG

                dxdt(8) = 0; % FeCat

                dxdt(9) = (k(23)*x(2)*10e-3*2.98e-9)/(1.53e-14) -
k(6)*x(8)*(x(9)-x0(9)); % H2O2 peroxisome

                dxdt(10) = - k(8)*x(10)*(x(2)- x0(2)) + k(12)*(x(13)-
x0(13))*x(14); % Prx-SH

                dxdt(11) = k(8)*x(10)*(x(2)- x0(2)) -
k(9)*x(11)*(x(2)- x0(2)) + k(10)*(x(12)-x0(12)) - k(11)*x(11); % Prx-
SOH
```

```
                dxdt(12) = k(9)*x(11)*(x(2)- x0(2)) - k(10)*(x(12)-
x0(12)); % Prx-SOOH

                dxdt(13) = k(11)*x(11) - k(12)*(x(13)-x0(13))*x(14); %
Prx-SS

                dxdt(14) = - k(12)*(x(13)-x0(13))*x(14) -
k(19)*(x(22)-x0(22))*x(14) + k(21)*(x(15)-x0(15))*x(23) - k(27) +
k(28); % Trx-SH

                dxdt(15) = k(12)*(x(13)-x0(13))*x(14) + k(19)*(x(22)-
x0(22))*x(14) - k(21)*(x(15)-x0(15))*x(23); % Trx-SS

                dxdt(16) = - k(14)*x(16)*(x(2)- x0(2)) +
k(16)*x(19)*(x(18)-x0(18)); % Pr-SH

                dxdt(17) = k(14)*x(16)*(x(2)- x0(2)) - k(15)*(x(17)-
x0(17))*x(6); % Pr-SOH

                dxdt(18) = k(15)*(x(17)-x0(17))*x(6) -
k(16)*x(19)*(x(18)-x0(18)); % Pr-SSG

                dxdt(19) = k(17)*(x(20)-x0(20))*x(6) -
k(16)*x(19)*(x(18)-x0(18)); % Grx-SH

                dxdt(20) = k(16)*x(19)*(x(18)-x0(18)) - k(17)*(x(20)-
x0(20))*x(6); % Grx-SSG

                dxdt(21) = - k(18)*x(21)*(x(2)- x0(2)) + k(19)*(x(22)-
x0(22))*x(14); % Pr-(SH)2

                dxdt(22) = k(18)*x(21)*(x(2)- x0(2)) - k(19)*(x(22)-
x0(22))*x(14); % Pr-SS

                dxdt(23) = - k(20)*(x(7)-x0(7))*x(23) - k(21)*(x(15)-
x0(15))*x(23) + k(22)*(x(24)- x0(24))/(k(7) + x(24)); % NADPH

                dxdt(24) = k(20)*(x(7)-x0(7))*x(23) + k(21)*(x(15)-
x0(15))*x(23) - k(22)*(x(24)- x0(24))/(k(7) + x(24)); % NADP+



            end
end
```

APPENDIX E

IKK-BETA S-GLUTATHIONYLATION MODEL

```
function out = IKK_S_Glutathionylation
    % model for compartmentalized hydrogen peroxide consumption
    % Solver Parameters
    ti = 0; % start time
    tf = 3600; % stop time
    step = 1;
    dt = step;
    tspan = ti:dt:tf;
    options=odeset('AbsTol',1E-10,'RelTol',1E-4,'maxstep',step);


%%%%%%%%%%%%%%%%%%%%%%%%%%%%%%%%%%%%%%%%%%%%%%%%%%%%%%%%%%%%%%%%%%%%%%%%%%%%%%%
%%%
        % Defining forward reaction rates ()
        % Defining the array, k, that will house reaction rates
        k = zeros(9,1);

 %      Rxns (Cytosolic)

        % Peroxide Production Rate
        k(1) = 60e-4;

        % Peroxide Oxidation of GSH
        k(2) = 20e-4;

        % Peroxide Oxidation of IKK-SH
        k(3) = 0.5e-4;

        % Glutathionylation of IKK-SOH
        k(4) = 60e-4;

        % Radical Production Rate
        k(5) = 12.2e-4;

        % Radical-Induced GSH oxidation
        k(6) = 50e-4;

        % Radical-Induced IKK-SH oxidation
        k(7) = 5e-4;

        % GSH binds to IKK-Sdot
        k(8) = 50e-4;

        % GSH synthesis
        k(9) = 6e-2;

        % Peroxide Removal
```

```
        k(10) = 52e-4;


%%%%%%%%%%%%%%%%%%%%%%%%%%%%%%%%%%%%%%%%%%%%%%%%%%%%%%%%%%%%%%%%%%%%%%%%

        % Defining initial Conditions (Concentrations in M =
Moles/Liter)
        % Defining the array, x0, that will house initial
concentrations
        x0 = zeros(10,1);

        % Cytoplasm

        x0(1) = 6.5;  % Doxe-

        x0(2) = 0;    % Perox
        x0(3) = 0;    % RSdot

        x0(4) = 500;  % GSH
        x0(5) = 5;    % GSSG
        x0(6) = 0;    % GSdot

        x0(7) = 50;   % IKK-SH
        x0(8) = 0;    % IKK-SOH
        x0(9) = 0;    % IKK-Sdot
        x0(10) = 0;    % IKK-SSG

        x0(11) = 0; % NAC


%%%%%%%%%%%%%%%%%%%%%%%%%%%%%%%%%%%%%%%%%%%%%%%%%%%%%%%%%%%%%%%%%%%%%%%%
%%%%
        % integration
        tic
        [t x]=ode15s(@crank,tspan,x0,options,k);
        toc
        out = [t, x];


%%%%%%%%%%%%%%%%%%%%%%%%%%%%%%%%%%%%%%%%%%%%%%%%%%%%%%%%%%%%%%%%%%%%%%%%
%%%%
        % description of derivatives

            function dxdt=crank(t, x, k);

                dxdt= x;  % setting up vector containing derivatives

                %Cytosolic Dynamics

                dxdt(1) = (7.14e-6*(t/60) + 22.979*(t/60) + 15)*1e-6;
% Doxe-

                dxdt(2) = k(1)*x(1) - k(2)*x(4)*x(2) - k(3)*x(7)*x(2)
- k(10)*x(2); % Perox
```

```
                dxdt(3) = k(5)*x(1) - k(6)*x(4)*x(3) - k(7)*x(7)*x(3);
% RSdot

                dxdt(4) = - k(2)*x(4)*x(2) - k(6)*x(4)*x(3) -
k(4)*x(4)*x(8) - k(8)*x(4)*x(9) + k(9); % GSH

                dxdt(5) = k(2)*x(4)*x(2); % GSSG

                dxdt(6) = k(6)*x(4)*x(3); % GSdot

                dxdt(7) = - k(3)*x(7)*x(2) - k(7)*x(7)*x(3); % IKK-SH

                dxdt(8) = k(3)*x(7)*x(2) - k(4)*x(4)*x(8); % IKK-SOH

                dxdt(9) = k(7)*x(7)*x(3) - k(8)*x(4)*x(9); % IKK-Sdot

                dxdt(10) = k(4)*x(4)*x(8) + k(8)*x(4)*x(9); % IKK-SSG

            end
end
```

REFERENCES

Abdella BR, Fisher J (1985) A chemical perspective on the anthracycline antitumor antibiotics. *Environ Health Perspect* **64:** 4-18

Adimora NJ, Jones DP, Kemp ML (2010) A model of redox kinetics implicates the thiol proteome in cellular hydrogen peroxide responses. *Antioxid Redox Signal* **13:** 731-743

Aebi H (1984) Catalase in vitro. *Methods Enzymol* **105:** 121-126

Akerboom TP, Bilzer M, Sies H (1982) The relationship of biliary glutathione disulfide efflux and intracellular glutathione disulfide content in perfused rat liver. *J Biol Chem* **257:** 4248-4252

Akman SA, Forrest G, Chu FF, Esworthy RS, Doroshow JH (1990) Antioxidant and xenobiotic-metabolizing enzyme gene expression in Dox-resistant MCF-7 breast cancer cells. *Cancer Res* **50:** 1397-1402

Angermüller S, Islinger M, Völkl (2009) Peroxisomes and reactive oxygen species, a lasting challenge. *Histochem Cell Biol* **131:** 459-463

Annunziata CM, Stavnes HT, Kleinberg L, Berner A, Hernandez LF, Birrer MJ, Steinberg SM, Davidson B, Kohn EC (2010) Nuclear factor kappaB transcription factors are coexpressed and convey a poor outcome in ovarian cancer. *Cancer* **116:** 3276-3284

Antunes F, Cadenas E (2000) Estimation of H2O2 gradients across biomembranes. *FEBS Lett* **475:** 121-126

Armstrong RN (1997) Structure, catalytic mechanism, and evolution of the glutathione transferases. *Chem Res Toxicol* **10:** 2-18

Arnelle DR, Stamler JS (1995) NO+, NO, and NO- donation by S-nitrosothiols: implications for regulation of physiological functions by S-nitrosylation and acceleration of disulfide formation. *Arch Biochem Biophys* **318:** 279-285

Arner ES, Zhong L, Holmgren A (1999) Preparation and assay of mammalian thioredoxin and thioredoxin reductase. *Methods Enzymol* **300:** 226-239

Asmis R, Wang Y, Xu L, Kisgati M, Begley JG, Mieyal JJ (2005) A novel thiol oxidation-based mechanism for adriamycin-induced cell injury in human macrophages. *FASEB J* **19:** 1866-1868

Babior BM (1999) NADPH oxidase: an update. *Blood* **93:** 1464-1476

Bachur NR, Gordon SL, Gee MV, Kon H (1979) NADPH cytochrome P-450 reductase activation of quinone anticancer agents to free radicals. *Proc Natl Acad Sci U S A* **76:** 954-957

Bachur NR, Yu F, Johnson R, Hickey R, Wu Y, Malkas L (1992) Helicase inhibition by anthracycline anticancer agents. *Mol Pharmacol* **41:** 993-998

Balaban RS, Nemoto S, Finkel T (2005) Mitochondria, oxidants, and aging. *Cell* **120:** 483-495

Ban JO, Kwak DH, Oh JH, Park EJ, Cho MC, Song HS, Song MJ, Han SB, Moon DC, Kang KW, Hong JT (2010) Suppression of NF-kappaB and GSK-3beta is involved in colon cancer cell growth inhibition by the PPAR agonist troglitazone. *Chem Biol Interact* **188:** 75-85

Banfi B, Clark RA, Steger K, Krause KH (2003) Two novel proteins activate superoxide generation by the NADPH oxidase NOX1. *J Biol Chem* **278:** 3510-3513

Bannister JV, Bannister WH, Rotilio G (1987) Aspects of the structure, function, and applications of superoxide dismutase. *CRC Crit Rev Biochem* **22:** 111-180

Bannister WH (1988) From haemocuprein to copper-zinc superoxide dismutase: a history on the fiftieth anniversary of the discovery of haemocuprein and the twentieth anniversary of the discovery of superoxide dismutase. *Free Radic Res Commun* **5:** 35-42

Bao L, Haque A, Jackson K, Hazari S, Moroz K, Jetly R, Dash S (2011) Increased expression of P-glycoprotein is associated with Dox chemoresistance in the metastatic 4T1 breast cancer model. *Am J Pathol* **178:** 838-852

Bartoszek A (2002) Metabolic activation of adriamycin by NADPH-cytochrome P450 reductase; overview of its biological and biochemical effects. *Acta Biochim Pol* **49:** 323-331

Bartoszek A, Wolf CR (1992) Enhancement of Dox toxicity following activation by NADPH cytochrome P450 reductase. *Biochem Pharmacol* **43:** 1449-1457

Bates DA, Winterbourn CC (1982) Deoxyribose breakdown by the adriamycin semiquinone and H2O2: evidence for hydroxyl radical participation. *FEBS Lett* **145:** 137-142

Bayir H (2005) Reactive oxygen species. *Crit Care Med* **33:** S498-501

Beckman KB, Ames BN (1998) The free radical theory of aging matures. *Physiol Rev* **78:** 547-581

Bedard K, Krause K-H (2007) The NOX Family of ROS-Generating NADPH Oxidases: Physiology and Pathophysiology. *Physiological Reviews* **87:** 245-313

Bednarski BK, Baldwin AS, Jr., Kim HJ (2009) Addressing reported pro-apoptotic functions of NF-kappaB: targeted inhibition of canonical NF-kappaB enhances the apoptotic effects of Dox. *PLoS One* **4:** e6992

Benchekroun MN, Robert J (1992) Measurement of Dox-induced lipid peroxidation under the conditions that determine cytotoxicity in cultured tumor cells. *Anal Biochem* **201:** 326-330

Berggren MI, Husbeck B, Samulitis B, Baker AF, Gallegos A, Powis G (2001) Thioredoxin Peroxidase-1 (peroxiredoxin-1) Is Increased in Thioredoxin-1 Transfected Cells and Results in Enhanced Protection against Apoptosis Caused by Hydrogen Peroxide but Not by Other Agents Including Dexamethasone, Etoposide, and Dox. *Archives of Biochemistry and Biophysics* **392:** 103-109

Berlin V, Haseltine WA (1981) Reduction of adriamycin to a semiquinone-free radical by NADPH cytochrome P-450 reductase produces DNA cleavage in a reaction mediated by molecular oxygen. *J Biol Chem* **256:** 4747-4756

Berry CE, Hare JM (2004) Xanthine oxidoreductase and cardiovascular disease: molecular mechanisms and pathophysiological implications. *J Physiol* **555:** 589-606

Betteridge DJ (2000) What is oxidative stress? *Metabolism* **49:** 3-8

Bharti AC, Aggarwal BB (2002) Nuclear factor-kappa B and cancer: its role in prevention and therapy. *Biochemical Pharmacology* **64:** 883-888

Bienert GP, Schjoerring JK, Jahn TP (2006) Membrane transport of hydrogen peroxide. *Biochim Biophys Acta* **1758:** 994-1003

Bleyer WA (1990) The impact of childhood cancer on the United States and the world. *CA Cancer J Clin* **40:** 355-367

Block KI, Koch AC, Mead MN, Tothy PK, Newman RA, Gyllenhaal C (2007) Impact of antioxidant supplementation on chemotherapeutic efficacy: a systematic review of the evidence from randomized controlled trials. *Cancer Treat Rev* **33:** 407-418

Boveris A, Chance B (1973) The mitochondrial generation of hydrogen peroxide. General properties and effect of hyperbaric oxygen. *Biochemical Journal* **134:** 707-716

Broeckaert L, Moens J, Roos G, De Proft F, Geerlings P (2008) Intrinsic nucleofugality scale within the framework of density functional reactivity theory. *J Phys Chem A* **112:** 12164-12171

Butterfield DA, Koppal T, Howard B, Subramaniam R, Hall N, Hensley K, Yatin S, Allen K, Aksenov M, Aksenova M, Carney J (1998) Structural and functional changes in proteins induced by free radical-mediated oxidative stress and protective action of the antioxidants N-tert-butyl-alpha-phenylnitrone and vitamin E. *Ann N Y Acad Sci* **854:** 448-462

Calendi E, Dimarco A, Reggiani M, Scarpinato B, Valentini L (1965) On physico-chemical interactions between daunomycin and nucleic acids. *Biochim Biophys Acta* **103:** 25-49

Carney JM, Smith CD, Carney AM, Butterfield DA (1994) Aging- and oxygen-induced modifications in brain biochemistry and behavior. *Ann N Y Acad Sci* **738:** 44-53

Chae HZ, Kim HJ, Kang SW, Rhee SG (1999) Characterization of three isoforms of mammalian peroxiredoxin that reduce peroxides in the presence of thioredoxin. *Diabetes Research and Clinical Practice* **45:** 101-112

Chang TS, Jeong W, Woo HA, Lee SM, Park S, Rhee SG (2004) Characterization of mammalian sulfiredoxin and its reactivation of hyperoxidized peroxiredoxin through reduction of cysteine sulfinic acid in the active site to cysteine. *J Biol Chem* **279:** 50994-51001

Chapman ML, Rubin BR, Gracy RW (1989) Increased carbonyl content of proteins in synovial fluid from patients with rheumatoid arthritis. *J Rheumatol* **16:** 15-18

Chen WW, Schoeberl B, Jasper PJ, Niepel M, Nielsen UB, Lauffenburger DA, Sorger PK (2009) Input-output behavior of ErbB signaling pathways as revealed by a mass action model trained against dynamic data. *Mol Syst Biol* **5:** 239

Cullinane C, Phillips DR (1990) Induction of stable transcriptional blockage sites by adriamycin: GpC specificity of apparent adriamycin-DNA adducts and dependence on iron(III) ions. *Biochemistry* **29:** 5638-5646

Cummings J, Allan L, Willmott N, Riley R, Workman P, Smyth JF (1992) The enzymology of Dox quinone reduction in tumour tissue. *Biochem Pharmacol* **44:** 2175-2183

Cummings J, Bartoszek A, Smyth JF (1991) Determination of covalent binding to intact DNA, RNA, and oligonucleotides by intercalating anticancer drugs using high-performance liquid chromatography. Studies with Dox and NADPH cytochrome P-450 reductase. *Anal Biochem* **194:** 146-155

D'Autreaux B, Toledano MB (2007) ROS as signalling molecules: mechanisms that generate specificity in ROS homeostasis. *Nat Rev Mol Cell Biol* **8:** 813-824

Dalle-Donne I, Rossi R, Colombo G, Giustarini D, Milzani A (2009) Protein S-glutathionylation: a regulatory device from bacteria to humans. *Trends Biochem Sci* **34:** 85-96

Dalton TP, Shertzer HG, Puga A (1999) Regulation of gene expression by reactive oxygen. *Annu Rev Pharmacol Toxicol* **39:** 67-101

Dalton WS, Durie BG, Alberts DS, Gerlach JH, Cress AE (1986) Characterization of a new drug-resistant human myeloma cell line that expresses P-glycoprotein. *Cancer Res* **46:** 5125-5130

Dang L, White DW, Gross S, Bennett BD, Bittinger MA, Driggers EM, Fantin VR, Jang HG, Jin S, Keenan MC, Marks KM, Prins RM, Ward PS, Yen KE, Liau LM, Rabinowitz JD, Cantley LC, Thompson CB, Vander Heiden MG, Su SM (2009) Cancer-associated IDH1 mutations produce 2-hydroxyglutarate. *Nature* **462:** 739-744

Davies KJ, Doroshow JH (1986) Redox cycling of anthracyclines by cardiac mitochondria. I. Anthracycline radical formation by NADH dehydrogenase. *J Biol Chem* **261:** 3060-3067

de Haan JB, Bladier C, Griffiths P, Kelner M, O'Shea RD, Cheung NS, Bronson RT, Silvestro MJ, Wild S, Zheng SS, Beart PM, Hertzog PJ, Kola I (1998) Mice with a homozygous null mutation for the most abundant glutathione peroxidase, Gpx1, show increased susceptibility to the oxidative stress-inducing agents paraquat and hydrogen peroxide. *J Biol Chem* **273:** 22528-22536

de Oliveira-Marques V, Cyrne L, Marinho HS, Antunes F (2007) A quantitative study of NF-kappaB activation by H2O2: relevance in inflammation and synergy with TNF-alpha. *J Immunol* **178:** 3893-3902

Dhooge, De M, Laureys, Kint, Ferster, De B, Philippe, Benoit, Dhooge C (1999) P-glycoprotein is an independent prognostic factor predicting relapse in childhood acute lymphoblastic leukaemia: results of a 6-year prospective study. *British Journal of Haematology* **105:** 676-683

Di Marco A, Silvestrini R, Di Marco S, Dasdia T (1965) Inhibiting effect of the new cytotoxic antibiotic daunomycin on nucleic acids and mitotic activity of HeLa cells. *J Cell Biol* **27:** 545-550

Dolcet X, Llobet D, Pallares J, Matias-Guiu X (2005) NF-kB in development and progression of human cancer. *Virchows Archiv* **446:** 475-482

Doroshow JH, Akman S, Esworthy S, Chu FF, Burke T (1991) Dox resistance conferred by selective enhancement of intracellular glutathione peroxidase or superoxide dismutase content in human MCF-7 breast cancer cells. *Free Radic Res Commun* **12-13 Pt 2:** 779-781

Doroshow JH, Davies KJ (1986) Redox cycling of anthracyclines by cardiac mitochondria. II. Formation of superoxide anion, hydrogen peroxide, and hydroxyl radical. *J Biol Chem* **261:** 3068-3074

Dreher I, Schmutzler C, Jakob F, Kohrle J (1997) Expression of selenoproteins in various rat and human tissues and cell lines. *J Trace Elem Med Biol* **11:** 83-91

Egorin MJ, Hildebrand RC, Cimino EF, Bachur NR (1974) Cytofluorescence localization of adriamycin and daunorubicin. *Cancer Res* **34:** 2243-2245

El-Kareh AW, Secomb TW (2005) Two-mechanism peak concentration model for cellular pharmacodynamics of Dox. *Neoplasia* **7:** 705-713

Eliot H, Gianni L, Myers C (1984) Oxidative destruction of DNA by the adriamycin-iron complex. *Biochemistry* **23:** 928-936

Epp O, Ladenstein R, Wendel A (1983) The refined structure of the selenoenzyme glutathione peroxidase at 0.2-nm resolution. *Eur J Biochem* **133:** 51-69

Finkel T, Holbrook NJ (2000) Oxidants, oxidative stress and the biology of ageing. *Nature* **408:** 239-247

Fisher GA, Sikic BI (1995) Drug resistance in clinical oncology and hematology. Introduction. *Hematol Oncol Clin North Am* **9:** xi-xii

Fisher J, Ramakrishnan K, Becvar JE (1983) Direct enzyme-catalyzed reduction of anthracyclines by reduced nicotinamide adenine dinucleotide. *Biochemistry* **22:** 1347-1355

Fornari FA, Randolph JK, Yalowich JC, Ritke MK, Gewirtz DA (1994) Interference by Dox with DNA unwinding in MCF-7 breast tumor cells. *Mol Pharmacol* **45:** 649-656

Fridovich I (1997) Superoxide anion radical (O2-.), superoxide dismutases, and related matters. *J Biol Chem* **272:** 18515-18517

Fritz R, Bol J, Hebling U, Angermuller S, Volkl A, Fahimi HD, Mueller S (2007) Compartment-dependent management of H(2)O(2) by peroxisomes. *Free Radic Biol Med* **42:** 1119-1129

Gallogly MM, Mieyal JJ (2007) Mechanisms of reversible protein glutathionylation in redox signaling and oxidative stress. *Current Opinion in Pharmacology* **7:** 381-391

Garner AP, Paine MJ, Rodriguez-Crespo I, Chinje EC, Ortiz De Montellano P, Stratford IJ, Tew DG, Wolf CR (1999) Nitric oxide synthases catalyze the activation of redox cycling and bioreductive anticancer agents. *Cancer Res* **59:** 1929-1934

Gewirtz DA (1999) A critical evaluation of the mechanisms of action proposed for the antitumor effects of the anthracycline antibiotics adriamycin and daunorubicin. *Biochemical Pharmacology* **57:** 727-741

Ghezzi P (2005) Regulation of protein function by glutathionylation. *Free Radic Res* **39:** 573-580

Ghosh S, May MJ, Kopp EB (1998) NF-kappa B and Rel proteins: evolutionarily conserved mediators of immune responses. *Annu Rev Immunol* **16:** 225-260

Ghosn MG, Carbajal EF, Befrui NA, Tuchin VV, Larin KV (2008) Concentration effect on the diffusion of glucose in ocular tissues. *Optics and Lasers in Engineering* **46:** 911-914

Gilbert HF (1990) Molecular and cellular aspects of thiol-disulfide exchange. *Adv Enzymol Relat Areas Mol Biol* **63:** 69-172

Gilleron M, Marechal X, Montaigne D, Franczak J, Neviere R, Lancel S (2009a) NADPH oxidases participate to Dox-induced cardiac myocyte apoptosis. *Biochemical and Biophysical Research Communications* **388:** 727-731

Gray B, Carmichael AJ (1992) Kinetics of superoxide scavenging by dismutase enzymes and manganese mimics determined by electron spin resonance. *Biochem J* **281 (Pt 3):** 795-802

Grunwald V, DeGraffenried L, Russel D, Friedrichs WE, Ray RB, Hidalgo M (2002) Inhibitors of mTOR reverse Dox resistance conferred by PTEN status in prostate cancer cells. *Cancer Res* **62:** 6141-6145

Gu L, Findley HW, Zhou M (2002) MDM2 induces NF-kappaB/p65 expression transcriptionally through Sp1-binding sites: a novel, p53-independent role of MDM2 in Dox resistance in acute lymphoblastic leukemia. *Blood* **99:** 3367-3375

Guppy M (2002) The hypoxic core: a possible answer to the cancer paradox. *Biochemical and Biophysical Research Communications* **299:** 676-680

Gutteridge JM, Quinlan GJ (1985) Free radical damage to deoxyribose by anthracycline, aureolic acid and aminoquinone antitumour antibiotics. An essential requirement for iron, semiquinones and hydrogen peroxide. *Biochem Pharmacol* **34:** 4099-4103

Halliwell B (1991) Reactive oxygen species in living systems: Source, biochemistry, and role in human disease. *The American Journal of Medicine* **91:** S14-S22

Halvey PJ, Watson WH, Hansen JM, Go YM, Samali A, Jones DP (2005) Compartmental oxidation of thiol-disulphide redox couples during epidermal growth factor signalling. *Biochem J* **386:** 215-219

Hampton MB, Orrenius S (1997) Dual regulation of caspase activity by hydrogen peroxide: implications for apoptosis. *FEBS Lett* **414:** 552-556

Hansen JM, Go YM, Jones DP (2006) Nuclear and mitochondrial compartmentation of oxidative stress and redox signaling. *Annu Rev Pharmacol Toxicol* **46:** 215-234

Harris LR, Cake MH, Macey DJ (1994) Iron release from ferritin and its sensitivity to superoxide ions differs among vertebrates. *Biochem J* **301 (Pt 2):** 385-389

Hayashi T, Ueno Y, Okamoto T (1993) Oxidoreductive regulation of nuclear factor kappa B. Involvement of a cellular reducing catalyst thioredoxin. *J Biol Chem* **268:** 11380-11388

Henderson GB, Murgolo NJ, Kuriyan J, Osapay K, Kominos D, Berry A, Scrutton NS, Hinchliffe NW, Perham RN, Cerami A (1991) Engineering the substrate specificity of glutathione reductase toward that of trypanothione reduction. *Proc Natl Acad Sci U S A* **88:** 8769-8773

Herscovitch M, Comb W, Ennis T, Coleman K, Yong S, Armstead B, Kalaitzidis D, Chandani S, Gilmore TD (2008) Intermolecular disulfide bond formation in the NEMO dimer requires Cys54 and Cys347. *Biochem Biophys Res Commun* **367:** 103-108

Hilenski LL, Clempus RE, Quinn MT, Lambeth JD, Griendling KK (2004) Distinct subcellular localizations of Nox1 and Nox4 in vascular smooth muscle cells. *Arterioscler Thromb Vasc Biol* **24:** 677-683

Holmgren A (1976) Hydrogen donor system for Escherichia coli ribonucleoside-diphosphate reductase dependent upon glutathione. *Proc Natl Acad Sci U S A* **73:** 2275-2279

Holmgren A (1977) Bovine thioredoxin system. Purification of thioredoxin reductase from calf liver and thymus and studies of its function in disulfide reduction. *J Biol Chem* **252:** 4600-4606

Holmgren A (1985) Thioredoxin. *Annu Rev Biochem* **54:** 237-271

Holmgren A (1989) Thioredoxin and glutaredoxin systems. *J Biol Chem* **264:** 13963-13966

Holmgren A, Lu J (2010) Thioredoxin and thioredoxin reductase: current research with special reference to human disease. *Biochem Biophys Res Commun* **396:** 120-124

Hwang C, Sinskey AJ, Lodish HF (1992) Oxidized redox state of glutathione in the endoplasmic reticulum. *Science* **257:** 1496-1502

Ishizuka M, Toyama Y, Watanabe H, Fujiki Y, Takeuchi A, Yamasaki S, Yuasa S, Miyazaki M, Nakajima N, Taki S, Saito T (2004) Overexpression of human acyl-CoA thioesterase upregulates peroxisome biogenesis. *Exp Cell Res* **297:** 127-141

James PE, Grinberg OY, Swartz HM (1998) Superoxide production by phagocytosing macrophages in relation to the intracellular distribution of oxygen. *J Leukoc Biol* **64:** 78-84

Jani TS, DeVecchio J, Mazumdar T, Agyeman A, Houghton JA (2010) Inhibition of NF-kappaB signaling by quinacrine is cytotoxic to human colon carcinoma cell lines and is synergistic in combination with tumor necrosis factor-related apoptosis-inducing ligand (TRAIL) or oxaliplatin. *J Biol Chem* **285:** 19162-19172

Jones DP (2002) Redox potential of GSH/GSSG couple: assay and biological significance. *Methods Enzymol* **348:** 93-112

Jones DP (2008) Radical-free biology of oxidative stress. *Am J Physiol Cell Physiol* **295:** C849-C868

Jones DP, Go YM, Anderson CL, Ziegler TR, Kinkade JM, Jr., Kirlin WG (2004) Cysteine/cystine couple is a newly recognized node in the circuitry for biologic redox signaling and control. *FASEB J* **18:** 1246-1248

Jourd'heuil D, Jourd'heuil FL, Feelisch M (2003) Oxidation and nitrosation of thiols at low micromolar exposure to nitric oxide. Evidence for a free radical mechanism. *J Biol Chem* **278:** 15720-15726

Kabat GC, Rohan TE (2007) Does excess iron play a role in breast carcinogenesis? An unresolved hypothesis. *Cancer Causes Control* **18:** 1047-1053

Kabe Y, Ando K, Hirao S, Yoshida M, Handa H (2005) Redox regulation of NF-kappaB activation: distinct redox regulation between the cytoplasm and the nucleus. *Antioxid Redox Signal* **7:** 395-403

Kalyanaraman B, Perez-Reyes E, Mason RP (1980) Spin-trapping and direct electron spin resonance investigations of the redox metabolism of quinone anticancer drugs. *Biochimica et Biophysica Acta (BBA) - General Subjects* **630:** 119-130

Kamata H, Manabe T, Oka S, Kamata K, Hirata H (2002) Hydrogen peroxide activates IkappaB kinases through phosphorylation of serine residues in the activation loops. *FEBS Lett* **519:** 231-237

Karoui H, Hogg N, Frejaville C, Tordo P, Kalyanaraman B (1996) Characterization of sulfur-centered radical intermediates formed during the oxidation of thiols and sulfite by peroxynitrite. ESR-spin trapping and oxygen uptake studies. *J Biol Chem* **271:** 6000-6009

Katagiri K, Matsuzawa A, Ichijo H (2010) Regulation of apoptosis signal-regulating kinase 1 in redox signaling. *Methods Enzymol* **474:** 277-288

Kawahara T, Quinn MT, Lambeth JD (2007) Molecular evolution of the reactive oxygen-generating NADPH oxidase (Nox/Duox) family of enzymes. *BMC Evol Biol* **7:** 109

Kearns PR, Pieters R, Rottier MMA, Pearson ADJ, Hall AG (2001) Raised blast glutathione levels are associated with an increased risk of relapse in childhood acute lymphocytic leukemia. *Blood* **97:** 393-398

Kemp M, Go YM, Jones DP (2008) Nonequilibrium thermodynamics of thiol/disulfide redox systems: a perspective on redox systems biology. *Free Radic Biol Med* **44:** 921-937

Kievit FM, Wang FY, Fang C, Mok H, Wang K, Silber JR, Ellenbogen RG, Zhang M (2011) Dox loaded iron oxide nanoparticles overcome multidrug resistance in cancer in vitro. *J Control Release*

Kil IS, Kim SY, Park JW (2008) Glutathionylation regulates IkappaB. *Biochem Biophys Res Commun* **373:** 169-173

Kim HS, Lee TB, Choi CH (2001) Down-regulation of catalase gene expression in the Dox-resistant AML subline AML-2/DX100. *Biochem Biophys Res Commun* **281:** 109-114

Kirkman HN, Gaetani GF (1984) Catalase: a tetrameric enzyme with four tightly bound molecules of NADPH. *Proceedings of the National Academy of Sciences* **81:** 4343-4347

Kirkman HN, Rolfo M, Ferraris AM, Gaetani GF (1999) Mechanisms of Protection of Catalase by NADPH. *Journal of Biological Chemistry* **274:** 13908-13914

Kondo N, Ishii Y, Kwon YW, Tanito M, Horita H, Nishinaka Y, Nakamura H, Yodoi J (2004) Redox-sensing release of human thioredoxin from T lymphocytes with negative feedback loops. *J Immunol* **172:** 442-448

Kordes U, Krappmann D, Heissmeyer V, Ludwig WD, Scheidereit C (2000) Transcription factor NF-kappaB is constitutively activated in acute lymphoblastic leukemia cells. *Leukemia* **14:** 399-402

Korn SH, Wouters EF, Vos N, Janssen-Heininger YM (2001) Cytokine-induced activation of nuclear factor-kappa B is inhibited by hydrogen peroxide through oxidative inactivation of IkappaB kinase. *J Biol Chem* **276:** 35693-35700

Koshkin V, Lotan O, Pick E (1997) Electron transfer in the superoxide-generating NADPH oxidase complex reconstituted in vitro. *Biochimica et Biophysica Acta (BBA) - Bioenergetics* **1319:** 139-146

Kostrzewa-Nowak D, Paine MJ, Wolf CR, Tarasiuk J (2005) The role of bioreductive activation of Dox in cytotoxic activity against leukaemia HL60-sensitive cell line and its multidrug-resistant sublines. *Br J Cancer* **93:** 89-97

Kovacic P, Osuna JA, Jr. (2000) Mechanisms of anti-cancer agents: emphasis on oxidative stress and electron transfer. *Curr Pharm Des* **6:** 277-309

Kundu K, Knight SF, Willett N, Lee S, Taylor WR, Murthy N (2009) Hydrocyanines: a class of fluorescent sensors that can image reactive oxygen species in cell culture, tissue, and in vivo. *Angew Chem Int Ed Engl* **48:** 299-303

Kuppusamy P, Zweier JL (1989) Characterization of free radical generation by xanthine oxidase. Evidence for hydroxyl radical generation. *Journal of Biological Chemistry* **264:** 9880-9884

Kwak HS, Yim HS, Chock PB, Yim MB (1995) Endogenous intracellular glutathionyl radicals are generated in neuroblastoma cells under hydrogen peroxide oxidative stress. *Proc Natl Acad Sci U S A* **92:** 4582-4586

Lee TK, Hammond CL, Ballatori N (2001) Intracellular glutathione regulates taurocholate transport in HepG2 cells. *Toxicol Appl Pharmacol* **174:** 207-215

Liao BC, Hsieh CW, Lin YC, Wung BS (2010) The glutaredoxin/glutathione system modulates NF-kappaB activity by glutathionylation of p65 in cinnamaldehyde-treated endothelial cells. *Toxicol Sci* **116:** 151-163

Light DR, Walsh C, O'Callaghan AM, Goetzl EJ, Tauber AI (1981) Characteristics of the cofactor requirements for the superoxide-generating NADPH oxidase of human polymorphonuclear leukocytes. *Biochemistry* **20:** 1468-1476

Lillig CH, Berndt C, Holmgren A (2008) Glutaredoxin systems. *Biochim Biophys Acta* **1780:** 1304-1317

Lin TS, Teicher BA, Sartorelli AC (1980) 2-Methylanthraquinone derivatives as potential bioreductive alkylating agents. *J Med Chem* **23:** 1237-1242

Lin X, Li Q, Wang YJ, Ju YW, Chi ZQ, Wang MW, Liu JG (2007) Morphine inhibits Dox-induced reactive oxygen species generation and nuclear factor kappaB transcriptional activation in neuroblastoma SH-SY5Y cells. *Biochem J* **406:** 215-221

Liu H, Colavitti R, Rovira, II, Finkel T (2005) Redox-dependent transcriptional regulation. *Circ Res* **97:** 967-974

Lo HW, Antoun GR, Ali-Osman F (2004) The human glutathione S-transferase P1 protein is phosphorylated and its metabolic function enhanced by the Ser/Thr protein kinases, cAMP-dependent protein kinase and protein kinase C, in glioblastoma cells. *Cancer Res* **64:** 9131-9138

Loukili N, Rosenblatt-Velin N, Rolli J, Levrand S, Feihl F, Waeber B, Pacher P, Liaudet L (2010) Oxidants positively or negatively regulate nuclear factor kappaB in a context-dependent manner. *J Biol Chem* **285:** 15746-15752

Low FM, Hampton MB, Peskin AV, Winterbourn CC (2007) Peroxiredoxin 2 functions as a noncatalytic scavenger of low-level hydrogen peroxide in the erythrocyte. *Blood* **109:** 2611-2617

Lundberg M, Fernandes AP, Kumar S, Holmgren A (2004) Cellular and plasma levels of human glutaredoxin 1 and 2 detected by sensitive ELISA systems. *Biochem Biophys Res Commun* **319:** 801-809

Maioli E, Greci L, Soucek K, Hyzdalova M, Pecorelli A, Fortino V, Valacchi G (2009) Rottlerin inhibits ROS formation and prevents NFkappaB activation in MCF-7 and HT-29 cells. *J Biomed Biotechnol* **2009:** 742936

Makino N, Sasaki K, Hashida K, Sakakura Y (2004) A metabolic model describing the H2O2 elimination by mammalian cells including H2O2 permeation through cytoplasmic and peroxisomal membranes: comparison with experimental data. *Biochim Biophys Acta* **1673:** 149-159

Manta B, Hugo M, Ortiz C, Ferrer-Sueta G, Trujillo M, Denicola A (2009) The peroxidase and peroxynitrite reductase activity of human erythrocyte peroxiredoxin 2. *Archives of Biochemistry and Biophysics* **484:** 146-154

Maples KR, Kennedy CH, Jordan SJ, Mason RP (1990) In vivo thiyl free radical formation from hemoglobin following administration of hydroperoxides. *Arch Biochem Biophys* **277:** 402-409

Marienfeld RB, Palkowitsch L, Ghosh S (2006) Dimerization of the I kappa B kinase-binding domain of NEMO is required for tumor necrosis factor alpha-induced NF-kappa B activity. *Mol Cell Biol* **26:** 9209-9219

Marnett LJ (2000) Oxyradicals and DNA damage. *Carcinogenesis* **21:** 361-370

Martinovich G, Cherenkevich S, Sauer H (2005) Intracellular redox state: towards quantitative description. *Eur Biophys J* **34:** 937-942

Mates JM, Perez-Gomez C, Nunez de Castro I (1999) Antioxidant enzymes and human diseases. *Clin Biochem* **32:** 595-603

Matthews JR, Wakasugi N, Virelizier JL, Yodoi J, Hay RT (1992) Thioredoxin regulates the DNA binding activity of NF-kappa B by reduction of a disulphide bond involving cysteine 62. *Nucleic Acids Res* **20:** 3821-3830

Melov S, Schneider JA, Day BJ, Hinerfeld D, Coskun P, Mirra SS, Crapo JD, Wallace DC (1998) A novel neurological phenotype in mice lacking mitochondrial manganese superoxide dismutase. *Nat Genet* **18:** 159-163

Menna P, Recalcati S, Cairo G, Minotti G (2007) An introduction to the metabolic determinants of anthracycline cardiotoxicity. *Cardiovasc Toxicol* **7:** 80-85

Meyer DJ, Kramer H, Ozer N, Coles B, Ketterer B (1994) Kinetics and equilibria of S-nitrosothiol-thiol exchange between glutathione, cysteine, penicillamines and serum albumin. *FEBS Lett* **345:** 177-180

Mieyal JJ, Gallogly MM, Qanungo S, Sabens EA, Shelton MD (2008) Molecular mechanisms and clinical implications of reversible protein S-glutathionylation. *Antioxid Redox Signal* **10:** 1941-1988

Miller FJ, Jr., Filali M, Huss GJ, Stanic B, Chamseddine A, Barna TJ, Lamb FS (2007) Cytokine activation of nuclear factor kappa B in vascular smooth muscle cells requires signaling endosomes containing Nox1 and ClC-3. *Circ Res* **101:** 663-671

Miranda-Vizuete A, Ljung J, Damdimopoulos AE, Gustafsson JA, Oko R, Pelto-Huikko M, Spyrou G (2001) Characterization of Sptrx, a novel member of the thioredoxin family specifically expressed in human spermatozoa. *J Biol Chem* **276:** 31567-31574

Molavi B, Mehta JL (2004) Oxidative stress in cardiovascular disease: molecular basis of its deleterious effects, its detection, and therapeutic considerations. *Curr Opin Cardiol* **19:** 488-493

Montecucco A, Pedrali-Noy G, Spadari S, Zanolin E, Ciarrocchi G (1988) DNA unwinding and inhibition of T4 DNA ligase by anthracyclines. *Nucleic Acids Res* **16:** 3907-3918

Moore HW (1977) Bioactivation as a model for drug design bioreductive alkylation. *Science* **197:** 527-532

Moore HW, Czerniak R (1981) Naturally occurring quinones as potential bioreductive alkylating agents. *Med Res Rev* **1:** 249-280

Moore RB, Mankad MV, Shriver SK, Mankad VN, Plishker GA (1991) Reconstitution of Ca(2+)-dependent K+ transport in erythrocyte membrane vesicles requires a cytoplasmic protein. *J Biol Chem* **266:** 18964-18968

Mordente A, Meucci E, Martorana GE, Giardina B, Minotti G (2001) Human heart cytosolic reductases and anthracycline cardiotoxicity. *IUBMB Life* **52:** 83-88

Moreno-Sanchez R, Saavedra E, Rodriguez-Enriquez S, Gallardo-Perez JC, Quezada H, Westerhoff HV (2010) Metabolic control analysis indicates a change of strategy in the treatment of cancer. *Mitochondrion* **10:** 626-639

Mueller S, Riedel HD, Stremmel W (1997) Determination of catalase activity at physiological hydrogen peroxide concentrations. *Anal Biochem* **245:** 55-60

Muindi JR, Sinha BK, Gianni L, Myers CE (1984) Hydroxyl radical production and DNA damage induced by anthracycline-iron complex. *FEBS Lett* **172:** 226-230

Mulder KM (2000) Role of Ras and Mapks in TGFbeta signaling. *Cytokine Growth Factor Rev* **11:** 23-35

Munzert G, Kirchner D, Ottmann O, Bergmann L, Schmid RM (2004) Constitutive NF-kappab/Rel activation in philadelphia chromosome positive (Ph+) acute lymphoblastic leukemia (ALL). *Leuk Lymphoma* **45:** 1181-1184

Murdoch CE, Zhang M, Cave AC, Shah AM (2006) NADPH oxidase-dependent redox signalling in cardiac hypertrophy, remodelling and failure. *Cardiovasc Res* **71:** 208-215

Murphy ME, Kehrer JP (1989) Oxidation state of tissue thiol groups and content of protein carbonyl groups in chickens with inherited muscular dystrophy. *Biochem J* **260:** 359-364

Nakamura H, Nakamura K, Yodoi J (1997) Redox regulation of cellular activation. *Annu Rev Immunol* **15:** 351-369

Nappi AJ, Vass E (1997) Comparative studies of enhanced iron-mediated production of hydroxyl radical by glutathione, cysteine, ascorbic acid, and selected catechols. *Biochim Biophys Acta* **1336:** 295-302

Nauseef WM (1999) The NADPH-dependent oxidase of phagocytes. *Proc Assoc Am Physicians* **111:** 373-382

Nauser T, Pelling J, Schoneich C (2004) Thiyl radical reaction with amino acid side chains: rate constants for hydrogen transfer and relevance for posttranslational protein modification. *Chem Res Toxicol* **17:** 1323-1328

Neufeld G, Cohen T, Gengrinovitch S, Poltorak Z (1999) Vascular endothelial growth factor (VEGF) and its receptors. *FASEB J* **13:** 9-22

Ng CF, Schafer FQ, Buettner GR, Rodgers VG (2007) The rate of cellular hydrogen peroxide removal shows dependency on GSH: mathematical insight into in vivo H2O2 and GPx concentrations. *Free Radic Res* **41:** 1201-1211

Nicholson L, Hall AG, Redfern CP, Irving J (2010) NFkappaB modulators in a model of glucocorticoid resistant, childhood acute lymphoblastic leukemia. *Leuk Res* **34:** 1366-1373

Nordberg J, Arnér ESJ (2001) Reactive oxygen species, antioxidants, and the mammalian thioredoxin system. *Free Radical Biology and Medicine* **31:** 1287-1312

Nordstrom T, Mustelin T, Pessa-Morikawa T, Andersson LC (1992) Modulation of calcium fluxes in Jurkat T cells by myristic acid. Inhibition is independent of membrane potential and intracellular pH. *Biochem J* **283 (Pt 1):** 113-118

O'Brien PJ (1988) Radical formation during the peroxidase catalyzed metabolism of carcinogens and xenobiotics: the reactivity of these radicals with GSH, DNA, and unsaturated lipid. *Free Radical Biology and Medicine* **4:** 169-183

Oliveira-Marques V, Marinho HS, Cyrne L, Antunes F (2009) Role of hydrogen peroxide in NF-kappaB activation: from inducer to modulator. *Antioxid Redox Signal* **11:** 2223-2243

Ozols RF, Locker GY, Doroshow JH, Grotzinger KR, Myers CE, Young RC (1979) Pharmacokinetics of adriamycin and tissue penetration in murine ovarian cancer. *Cancer Res* **39:** 3209-3214

Pan SS, Pedersen L, Bachur NR (1981) Comparative flavoprotein catalysis of anthracycline antibiotic. Reductive cleavage and oxygen consumption. *Mol Pharmacol* **19:** 184-186

Park JW (1988) Reaction of S-nitrosoglutathione with sulfhydryl groups in protein. *Biochem Biophys Res Commun* **152:** 916-920

Pawlowska J, Tarasiuk J, Wolf CR, Paine MJ, Borowski E (2003) Differential ability of cytostatics from anthraquinone group to generate free radicals in three enzymatic systems: NADH dehydrogenase, NADPH cytochrome P450 reductase, and xanthine oxidase. *Oncol Res* **13:** 245-252

Peltoniemi MJ, Karala AR, Jurvansuu JK, Kinnula VL, Ruddock LW (2006) Insights into deglutathionylation reactions. Different intermediates in the glutaredoxin and protein disulfide isomerase catalyzed reactions are defined by the gamma-linkage present in glutathione. *J Biol Chem* **281:** 33107-33114

Peskin AV, Low FM, Paton LN, Maghzal GJ, Hampton MB, Winterbourn CC (2007) The high reactivity of peroxiredoxin 2 with H(2)O(2) is not reflected in its reaction with other oxidants and thiol reagents. *J Biol Chem* **282:** 11885-11892

Petry A, Weitnauer M, Gorlach A (2010) Receptor activation of NADPH oxidases. *Antioxid Redox Signal* **13:** 467-487

Pham LV, Fu L, Tamayo AT, Bueso-Ramos C, Drakos E, Vega F, Medeiros LJ, Ford RJ (2010) Constitutive BR3 receptor signaling in diffuse large B-cell lymphomas stabilizes NF-{kappa}B-inducing kinase, while activating both canonical and alternative NF-{kappa}B pathways. *Blood*

Pineda-Molina E, Klatt P, Vazquez J, Marina A, Garcia de Lacoba M, Perez-Sala D, Lamas S (2001) Glutathionylation of the p50 subunit of NF-kappaB: a mechanism for redox-induced inhibition of DNA binding. *Biochemistry* **40:** 14134-14142

Poli G, Leonarduzzi G, Biasi F, Chiarpotto E (2004) Oxidative stress and cell signalling. *Curr Med Chem* **11:** 1163-1182

Poole B (1975) Diffusion effects in the metabolism of hydrogen peroxide by rat liver peroxisomes. *J Theor Biol* **51:** 149-167

Raftos JE, Whillier S, Kuchel PW (2010) Glutathione synthesis and turnover in the human erythrocyte: alignment of a model based on detailed enzyme kinetics with experimental data. *J Biol Chem* **285:** 23557-23567

Ramji S, Lee C, Inaba T, Patterson AV, Riddick DS (2003) Human NADPH-cytochrome p450 reductase overexpression does not enhance the aerobic cytotoxicity of Dox in human breast cancer cell lines. *Cancer Res* **63:** 6914-6919

Ravi D, Das KC (2004) Redox-cycling of anthracyclines by thioredoxin system: increased superoxide generation and DNA damage. *Cancer Chemother Pharmacol* **54:** 449-458

Reynaert NL, van der Vliet A, Guala AS, McGovern T, Hristova M, Pantano C, Heintz NH, Heim J, Ho YS, Matthews DE, Wouters EF, Janssen-Heininger YM (2006) Dynamic redox control of NF-kappaB through glutaredoxin-regulated S-glutathionylation of inhibitory kappaB kinase beta. *Proc Natl Acad Sci U S A* **103:** 13086-13091

Rhee SG (2006) H2O2, a Necessary Evil for Cell Signaling. *Science* **312:** 1882-1883

Rhee SG, Kang SW, Chang TS, Jeong W, Kim K (2001) Peroxiredoxin, a novel family of peroxidases. *IUBMB Life* **52:** 35-41

Riley PA (1994) Free radicals in biology: oxidative stress and the effects of ionizing radiation. *Int J Radiat Biol* **65:** 27-33

Ross DD (2000) Novel mechanisms of drug resistance in leukemia. *Leukemia* **14:** 467-473

Rossi F, Bellavite P, Berton G, Grzeskowiak M, Papini E (1985) Mechanism of production of toxic oxygen radicals by granulocytes and macrophages and their function in the inflammatory process. *Pathol Res Pract* **180:** 136-142

Sagrista ML, Garcia AE, Africa De Madariaga M, Mora M (2002) Antioxidant and pro-oxidant effect of the thiolic compounds N-acetyl-L-cysteine and glutathione against free radical-induced lipid peroxidation. *Free Radic Res* **36:** 329-340

Salmeen A, Andersen JN, Myers MP, Meng TC, Hinks JA, Tonks NK, Barford D (2003) Redox regulation of protein tyrosine phosphatase 1B involves a sulphenyl-amide intermediate. *Nature* **423:** 769-773

Sasaki K, Bannai S, Makino N (1998) Kinetics of hydrogen peroxide elimination by human umbilical vein endothelial cells in culture. *Biochim Biophys Acta* **1380:** 275-288

Schafer FQ, Buettner GR (2001) Redox environment of the cell as viewed through the redox state of the glutathione disulfide/glutathione couple. *Free Radic Biol Med* **30:** 1191-1212

Schenk H, Klein M, Erdbrugger W, Droge W, Schulze-Osthoff K (1994) Distinct effects of thioredoxin and antioxidants on the activation of transcription factors NF-kappa B and AP-1. *Proc Natl Acad Sci U S A* **91:** 1672-1676

Schoneich C (1995) Kinetics of thiol reactions. *Methods Enzymol* **251:** 45-55

Seaver LC, Imlay JA (2001) Hydrogen peroxide fluxes and compartmentalization inside growing Escherichia coli. *J Bacteriol* **183:** 7182-7189

Serrander L, Cartier L, Bedard K, Banfi B, Lardy B, Plastre O, Sienkiewicz A, Fórró L, Schlegel W, Krause K-H (2007) NOX4 activity is determined by mRNA levels and reveals a unique pattern of ROS generation. *Biochem J* **406:** 105-114

Shi R, Huang C-C, Aronstam R, Ercal N, Martin A, Huang Y-W (2009) N-acetylcysteine amide decreases oxidative stress but not cell death induced by doxorubicin in H9c2 cardiomyocytes. *BMC Pharmacology* **9:** 7

Shuvaeva TM, Novoselov VI, Fesenko EE, Lipkin VM (2009) Peroxiredoxins, a new family of antioxidant proteins. *Bioorg Khim* **35:** 581-596

Singh Ghalaut V, Kharb S, Ghalaut PS, Rawal A (1999) Lymphocyte glutathione levels in acute leukemia. *Clin Chim Acta* **285:** 85-89

Singh SP, Wishnok JS, Keshive M, Deen WM, Tannenbaum SR (1996) The chemistry of the S-nitrosoglutathione/glutathione system. *Proc Natl Acad Sci U S A* **93:** 14428-14433

Sinha BK, Chignell CF (1979) Binding mode of chemically activated semiquinone free radicals from quinone anticancer agents to DNA. *Chem Biol Interact* **28:** 301-308

Sinha BK, Gregory JL (1981) Role of one-electron and two-electron reduction products of adriamycin and daunomycin in deoxyribonucleic acid binding. *Biochem Pharmacol* **30:** 2626-2629

Sinha BK, Mimnaugh EG, Rajagopalan S, Myers CE (1989) Adriamycin activation and oxygen free radical formation in human breast tumor cells: protective role of glutathione peroxidase in adriamycin resistance. *Cancer Res* **49:** 3844-3848

Sinha BK, Trush MA, Kennedy KA, Mimnaugh EG (1984) Enzymatic activation and binding of adriamycin to nuclear DNA. *Cancer Res* **44:** 2892-2896

Skladanowski A, Konopa J (1994) Interstrand DNA crosslinking induced by anthracyclines in tumour cells. *Biochem Pharmacol* **47:** 2269-2278

Srinivasan U, Mieyal PA, Mieyal JJ (1997) pH profiles indicative of rate-limiting nucleophilic displacement in thioltransferase catalysis. *Biochemistry* **36:** 3199-3206

Stadtman ER, Berlett BS (1998) Reactive oxygen-mediated protein oxidation in aging and disease. *Drug Metab Rev* **30:** 225-243

Steevels TA, Meyaard L (2011) Immune inhibitory receptors: essential regulators of phagocyte function. *Eur J Immunol* **41:** 575-587

Steinberg D (1997) Low density lipoprotein oxidation and its pathobiological significance. *J Biol Chem* **272:** 20963-20966

Supino R, Necco A, Dasdia T, Casazza AM, Di Marco A (1977) Relationship between effects on nucleic acid synthesis in cell cultures and cytotoxicity of 4-demethoxy derivatives of daunorubicin and adriamycin. *Cancer Res* **37:** 4523-4528

Taatjes DJ, Fenick DJ, Gaudiano G, Koch TH (1998) A redox pathway leading to the alkylation of nucleic acids by Dox and related anthracyclines: application to the design of antitumor drugs for resistant cancer. *Curr Pharm Des* **4:** 203-218

Tewey KM, Chen GL, Nelson EM, Liu LF (1984a) Intercalative antitumor drugs interfere with the breakage-reunion reaction of mammalian DNA topoisomerase II. *J Biol Chem* **259:** 9182-9187

Tewey KM, Rowe TC, Yang L, Halligan BD, Liu LF (1984b) Adriamycin-induced DNA damage mediated by mammalian DNA topoisomerase II. *Science* **226:** 466-468

Thannickal VJ, Fanburg BL (2000) Reactive oxygen species in cell signaling. *Am J Physiol Lung Cell Mol Physiol* **279:** L1005-1028

Tian W-N, Braunstein LD, Pang J, Stuhlmeier KM, Xi Q-C, Tian X, Stanton RC (1998) Importance of glucose-6-phosphate dehydrogenase activity for cell growth. *J Biol Chem* **273:** 10609-10617

Toledano MB, Leonard WJ (1991) Modulation of transcription factor NF-kappa B binding activity by oxidation-reduction in vitro. *Proc Natl Acad Sci U S A* **88:** 4328-4332

Tome ME, Johnson DB, Samulitis BK, Dorr RT, Briehl MM (2006) Glucose 6-phosphate dehydrogenase overexpression models glucose deprivation and sensitizes lymphoma cells to apoptosis. *Antioxid Redox Signal* **8:** 1315-1327

Tracey L, Streck CJ, Du Z, Williams RF, Pfeffer LM, Nathwani AC, Davidoff AM (2010) NF-kappaB activation mediates resistance to IFN beta in MLL-rearranged acute lymphoblastic leukemia. *Leukemia* **24:** 806-812

Trujillo M, Clippe A, Manta B, Ferrer-Sueta G, Smeets A, Declercq JP, Knoops B, Radi R (2007) Pre-steady state kinetic characterization of human peroxiredoxin 5: taking advantage of Trp84 fluorescence increase upon oxidation. *Arch Biochem Biophys* **467:** 95-106

Ursini F, Heim S, Kiess M, Maiorino M, Roveri A, Wissing J, Flohe L (1999) Dual function of the selenoprotein PHGPx during sperm maturation. *Science* **285:** 1393-1396

Ursini F, Maiorino M, Brigelius-Flohe R, Aumann KD, Roveri A, Schomburg D, Flohe L (1995) Diversity of glutathione peroxidases. *Methods Enzymol* **252:** 38-53

Ursini MV, Parrella A, Rosa G, Salzano S, Martini G (1997) Enhanced expression of glucose-6-phosphate dehydrogenase in human cells sustaining oxidative stress. *Biochem J* **323 (Pt 3):** 801-806

Valko M, Leibfritz D, Moncol J, Cronin MT, Mazur M, Telser J (2007) Free radicals and antioxidants in normal physiological functions and human disease. *Int J Biochem Cell Biol* **39:** 44-84

Valko M, Rhodes CJ, Moncol J, Izakovic M, Mazur M (2006) Free radicals, metals and antioxidants in oxidative stress-induced cancer. *Chem Biol Interact* **160:** 1-40

van Montfort RL, Congreve M, Tisi D, Carr R, Jhoti H (2003) Oxidation state of the active-site cysteine in protein tyrosine phosphatase 1B. *Nature* **423:** 773-777

Vargo-Gogola T, Rosen JM (2007) Modelling breast cancer: one size does not fit all. *Nat Rev Cancer* **7:** 659-672

Vasquez-Vivar J, Martasek P, Hogg N, Masters BS, Pritchard KA, Jr., Kalyanaraman B (1997) Endothelial nitric oxide synthase-dependent superoxide generation from adriamycin. *Biochemistry* **36:** 11293-11297

Vaupel P, Thews O, Kelleher DK, Hoeckel M (1998) Current status of knowledge and critical issues in tumor oxygenation. Results from 25 years research in tumor pathophysiology. *Adv Exp Med Biol* **454:** 591-602

Volm M, Sauerbrey A, Zintl F, Koomagi R, Efferth T (2002) Protein expression profile of newly diagnosed acute lymphoblastic leukemia in children developing relapses. *Oncol Rep* **9:** 965-969

Wang S, Konorev EA, Kotamraju S, Joseph J, Kalivendi S, Kalyanaraman B (2004) Dox Induces Apoptosis in Normal and Tumor Cells via Distinctly Different Mechanisms. *Journal of Biological Chemistry* **279:** 25535-25543

Wang Y, Blandino G, Givol D (1999) Induced p21waf expression in H1299 cell line promotes cell senescence and protects against cytotoxic effect of radiation and Dox. *Oncogene* **18:** 2643-2649

Ward PS, Patel J, Wise DR, Abdel-Wahab O, Bennett BD, Coller HA, Cross JR, Fantin VR, Hedvat CV, Perl AE, Rabinowitz JD, Carroll M, Su SM, Sharp KA, Levine RL, Thompson CB (2010) The common feature of leukemia-associated IDH1 and IDH2 mutations is a neomorphic enzyme activity converting alpha-ketoglutarate to 2-hydroxyglutarate. *Cancer Cell* **17:** 225-234

Wardman P, von Sonntag C (1995) Kinetic factors that control the fate of thiyl radicals in cells. *Methods Enzymol* **251:** 31-45

Watanabe J, Asaka Y, Tanaka T, Kanamura S (1994) Measurement of NADPH-cytochrome P-450 reductase content in rat liver sections by quantitative immunohistochemistry with a video image processor. *J Histochem Cytochem* **42:** 1161-1167

Watson WH, Jones DP (2003) Oxidation of nuclear thioredoxin during oxidative stress. *FEBS Lett* **543:** 144-147

Watson WH, Pohl J, Montfort WR, Stuchlik O, Reed MS, Powis G, Jones DP (2003) Redox potential of human thioredoxin 1 and identification of a second dithiol/disulfide motif. *J Biol Chem* **278:** 33408-33415

Watson WH, Yang X, Choi YE, Jones DP, Kehrer JP (2004) Thioredoxin and its role in toxicology. *Toxicol Sci* **78:** 3-14

Wei SJ, Botero A, Hirota K, Bradbury CM, Markovina S, Laszlo A, Spitz DR, Goswami PC, Yodoi J, Gius D (2000) Thioredoxin nuclear translocation and interaction with redox factor-1 activates the activator protein-1 transcription factor in response to ionizing radiation. *Cancer Res* **60:** 6688-6695

Winterbourn CC, Hampton MB (2008) Thiol chemistry and specificity in redox signaling. *Free Radic Biol Med* **45:** 549-561

Winterbourn CC, Metodiewa D (1995) Reaction of superoxide with glutathione and other thiols. *Methods Enzymol* **251:** 81-86

Winterbourn CC, Metodiewa D (1999) Reactivity of biologically important thiol compounds with superoxide and hydrogen peroxide. *Free Radic Biol Med* **27:** 322-328

Xu RH, Pelicano H, Zhou Y, Carew JS, Feng L, Bhalla KN, Keating MJ, Huang P (2005) Inhibition of glycolysis in cancer cells: a novel strategy to overcome drug resistance associated with mitochondrial respiratory defect and hypoxia. *Cancer Res* **65:** 613-621

Xue TY, Xu W, An Q, Wu Y, Xu CP, Zhang XY (2007) [Expression of nuclear transcription factor kappaB in childhood acute lymphoblastic leukemia and its significance]. *Zhongguo Shi Yan Xue Ye Xue Za Zhi* **15:** 767-771

Yang KS, Kang SW, Woo HA, Hwang SC, Chae HZ, Kim K, Rhee SG (2002) Inactivation of human peroxiredoxin I during catalysis as the result of the oxidation of the catalytic site cysteine to cysteine-sulfinic acid. *J Biol Chem* **277:** 38029-38036

Yeh GC, Occhipinti SJ, Cowan KH, Chabner BA, Myers CE (1987) Adriamycin resistance in human tumor cells associated with marked alteration in the regulation of the hexose monophosphate shunt and its response to oxidant stress. *Cancer Res* **47:** 5994-5999

Yeoh E-J, Ross ME, Shurtleff SA, Williams WK, Patel D, Mahfouz R, Behm FG, Raimondi SC, Relling MV, Patel A, Cheng C, Campana D, Wilkins D, Zhou X, Li J, Liu H, Pui C-H, Evans WE, Naeve C, Wong L et al (2002) Classification, subtype discovery, and prediction of outcome in pediatric acute lymphoblastic leukemia by gene expression profiling. *Cancer Cell* **1:** 133-143

Ying W (2008) NAD+/NADH and NADP+/NADPH in cellular functions and cell death: regulation and biological consequences. *Antioxid Redox Signal* **10:** 179-206

Yla-Herttuala S (1999) Oxidized LDL and atherogenesis. *Ann N Y Acad Sci* **874:** 134-137

Yue H, Brown M, Knowles J, Wang H, Broomhead DS, Kell DB (2006) Insights into the behaviour of systems biology models from dynamic sensitivity and identifiability analysis: a case study of an NF-kappaB signalling pathway. *Mol Biosyst* **2:** 640-649

Zhou M, Gu L, Findley HW, Jiang R, Woods WG (2003a) PTEN reverses MDM2-mediated chemotherapy resistance by interacting with p53 in acute lymphoblastic leukemia cells. *Cancer Res* **63:** 6357-6362

Zhou M, Gu L, Zhu N, Woods WG, Findley HW (2003b) Transfection of a dominant-negative mutant NF-kB inhibitor (IkBm) represses p53-dependent apoptosis in acute lymphoblastic leukemia cells: interaction of IkBm and p53. *Oncogene* **22:** 8137-8144

Zhou M, Zaki SR, Ragab AH, Findley HW (1994) Characterization of a myeloperoxidase mRNA(+) acute lymphoblastic leukemia cell line (EU-1/ALL) established from a child with an apparent case of ALL. *Leukemia* **8:** 659-663

Zunino F, Gambetta R, Di Marco A, Zaccara A (1972) Interaction of daunomycin and its derivatives with DNA. *Biochim Biophys Acta* **277:** 489-498

VITA

NNENNA A. FINN

Nnenna Adimora Finn was born in Lagos, Nigeria. When she was 7 years old, she and her family relocated to Scarsdale, New York, where she attended public school up until her graduation from Scarsdale High School in 2002. N.A. Finn received a B.S in Materials Science and Engineering, with a focus on biomaterials, from the University of Florida in 2006. Before coming to Georgia Tech to pursue a doctorate in biomedical engineering, N.A. Finn spent some time working for Shell Global Solutions in Houston TX, where she provided innovative technology solutions for the development, maintenance and characterization of materials used in the energy acquisition and energy management industry. When she is not working on her research, N.A. Finn enjoys making and buying one-of-a kind jewelry pieces, reading novels, and spending time with her family and friends.